A study of infra-red behaviour of gauge theories involving dark matter

By
Pritam Sen

PHYS10201305003

The Institute of Mathematical Sciences, Chennai

A thesis submitted to the

Board of Studies in Physical Sciences

In partial fulfillment of requirements

For the Degree of

DOCTOR OF PHILOSOPHY

of

HOMI BHABHA NATIONAL INSTITUTE

June, 2021

Homi Bhabha National Institute

Recommendations of the Viva Voce Board

As members of the Viva Voce Board, we certify that we have read the dissertation prepared by Pritam Sen entitled "A study of infra-red behaviour of gauge theories involving dark matter" and recommend that it may be accepted as fulfilling the dissertation requirement for the Degree of Doctor of Philosophy.

_____ Date: 15.11.21

Chair - Prof. RAHUL SINHA

_____ Date: 15.11.21

Guide/Convener - Prof. D. INDUMATHI

_____ Date: 15.11.21
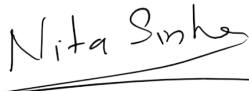
Examiner - Prof. SOURENDU GUPTA

_____ Date: 15.11.21

Member 1 - Prof. SANATAN DIGAL

_____ Date: 15.11.21

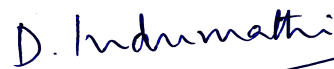Member 2 - Prof. R. SHANKAR

_____ Date: 15.11.21

Member 3 - Prof. NITA SINHA

     Final approval and acceptance of this dissertation is contingent upon the candidate's submission of the final copies of the dissertation to HBNI.

     I hereby certify that I have read this dissertation prepared under my direction and recommend that it may be accepted as fulfilling the dissertation requirement.

Date: 15.11.21   _____

Place: IMSc, Chennai.   **Guide** - Prof. D. INDUMATHI

i

STATEMENT BY AUTHOR

This dissertation has been submitted in partial fulfillment of requirements for an advanced degree at Homi Bhabha National Institute (HBNI) and is deposited in the Library to be made available to borrowers under rules of the HBNI.

Brief quotations from this dissertation are allowable without special permission, provided that accurate acknowledgement of source is made. Requests for permission for extended quotation from or reproduction of this manuscript in whole or in part may be granted by the Competent Authority of HBNI when in his or her judgment the proposed use of the material is in the interests of scholarship. In all other instances, however, permission must be obtained from the author.

Pritam Sen.

Pritam Sen

DECLARATION

I hereby declare that the investigation presented in the thesis has been carried out by me. The work is original and has not been submitted earlier as a whole or in part for a degree / diploma at this or any other Institution / University.

Pritam Sen.

_____

Pritam Sen

List of Publications arising from the thesis

Journal

1. "Infrared finiteness of a thermal theory of scalar electrodynamics to all orders",

   Pritam Sen, D. Indumathi and Debajyoti Choudhury,

   Eur. Phys. J. C **79** (2019) no.6, 532.

2. "Infrared finiteness of a complete theory of charged scalars and fermions at finite temperature",

   Pritam Sen, D. Indumathi and Debajyoti Choudhury,

   Eur. Phys. J. C **80** (2020) no.10, 972.

Conferences

1. "Infrared Finiteness of Theories with Bino-Like Dark Matter at $T = 0$",

   Pritam Sen, D. Indumathi and Debajyoti Choudhury,

   Springer Proceedings in Physics, vol **261** (2021), 351-356.

2. "IR Finiteness of Theories with Bino-Like Dark Matter at Finite Temperature",

   Pritam Sen, D. Indumathi and Debajyoti Choudhury,

   Springer Proceedings in Physics, vol **261** (2021), 375-381.

Pritam Sen.

Pritam Sen

Dedicated To,

The Loving Memory Of

My Father.

ACKNOWLEDGEMENTS

Contents

SUMMARY

This thesis concerns the demonstration of infrared (IR) finiteness of a thermal theory of neutrals interacting with charged fermions and scalars to all orders in perturbation theory specifically in the context of theories involving dark matter (DM). DM is predominantly conjectured to be thermally produced in the early Universe, staying in equilibrium with the background plasma until the occurrence of freeze-out. The thermal effects being of crucial importance can contribute appreciably while predicting the relic density of DM while trying to delineate the parameter space of models of viable DM candidates. The IR structure of the concerned theories are of great importance, playing a pivotal role while trying to predict the relic density reliably. The IR structure of theories is well known to become more intricate at finite temperature due to the presence of thermal fluctuations in addition to already present quantum fluctuations. In addition to this, at finite temperature, both the emission to and absorption of real particles from the heat bath also become feasible, making the situation more involved. To account for all these intricacies, the extension of the Grammer and Yennie (GY) technique [Phys. Rev. D 8 (1973), 4332] to finite temperature as was originally prescribed by Indumathi [Annals Phys. 263 (1998), 310] for the case of thermal purely fermionic QED, is implemented to unambiguously identify the correct IR divergent and finite pieces. As the theories of DM often involve charged scalars and fermions, we start by analyzing the IR structure of the thermal theory of scalar QED. The theory of charged scalars also involve quadrilinear seagull vertices in addition to usual trilinear interaction vertices. After applying the extension of GY technique, the IR divergent pieces of both the virtual and real photon contributions are found to factorize, leading to exponentiation and resummation. The quadrilinear seagull and tadpole diagrams play an indispensable role to obtain this neat IR factorization and resummation by exactly canceling out respectively the remnant IR finite linear and quadratic terms in photon momentum that would otherwise spoil the factorization, at all orders, of the purely IR divergent terms at finite temperature. The IR divergent pieces arising in the virtual and real contributions

are found to cancel among themselves, making the theory of thermal charged scalars IR finite to all orders in perturbation theory. We then focus our attention to a theory of DM involving interactions with charged scalars and charged fermions. The similar analysis of IR structure for this full theory having different kind of particles, after implementing the extension of GY technique becomes highly involved. We observe non-trivial double cancellations among terms after applying GY reduction. The IR divergent terms again factorize and get resummed into an exponential factor in both virtual and real photon contributions. The IR divergent pieces then cancel among the appropriate virtual and real contributions making the theory of DM to be IR finite to all orders in perturbation theory at finite temperature. The IR factorization, resummation and cancellation are found to be independent of the specific nature of the interaction term of neutrals, charged scalars and charged fermions making the proof and results of IR finiteness to be well applicable for a general thermal theory of neutrals interacting with charged fermions and scalars. This proof of IR finiteness was only possible after accounting for both the real photon emission to and absorption from the heat bath. Hence in this thesis, we establish, for the first time, the all-order proof of the infra-red finiteness of thermal field theories relevant to the study of dark matter. The effect of the heat bath is found to become perceptible at observable energy resolution giving rise to discernible temperature dependent finite corrections above soft limit. This finite contribution has been studied upto next-to-leading (NLO) order by Beneke and collaborators [JHEP 10 (2014), 045] but is beyond the scope of this thesis.

List of Figures

Chapter 1

Introduction

Quantum Field Theory (QFT) has emerged as one of the cornerstones of contemporary physics having its applicability in a wide range of physical phenomena. Perturbative quantum field theory has proved its predictive power regarding phenomena related to physics over a vast range of energy scales; even predicting extremely accurate theoretical predictions such as anomalous magnetic dipole moment of electron [1–3], which can be regarded as the epitome of predictable accuracy in the field of physics or rather in the field of empirical sciences. Often, when predicting these results from theoretical calculations one is riddled with divergent expression owing to Ultraviolet (UV) and Infrared (IR) divergences. The origin and the implication of these divergences has to be interpreted correctly and carefully to predict any sensible results in QFT. The origin and treatment of UV divergences are more readily discussed and understood in the literature.

The origin of UV divergences pertains to the fact that, while calculating higher order corrections to the related quantity of interest using QFT effects, all the possible quantum states[1] of the system have to be included as internal virtual states. These states also include some high momentum modes at the higher energy scale much beyond the low energy scale

---

[1]According to the framework of quantum mechanics while calculating higher order corrections in perturbation theory all possible feasible states, may it be all possible states in the Universe have to summed over as the internal states.

of the theory[2] at which calculations are being performed. The effect of inclusion of these high energy modes requires an understanding of high energy (small distance) physics much beyond the reach of the relevant theory, resulting in troubling divergences. For a sensibly written QFT at low energy scale, considering the QFT as an effective theory, these high energy modes can be integrated out, absorbing the effect of these modes by modifying the coupling constant, mass and field strength renormalization of the theory after performing matching calculations of deep IR quantities. The theory is then said to be UV renormalized and these renormalized theory can be used perturbatively to predict sensible results.

In the QFT having massless particles we often face another kind of divergences known as IR divergences. In the theories involving massless particles, those particles can simultaneously become both on-shell (or near on-shell) and soft carrying vanishing energy. In those scenarios those massless particles can propagate indefinitely carrying information at minuscule energy cost resulting in soft IR divergences. For theories involving interactions where *only* massless particles couple among themselves, there can be another kind of singularity which may arise. This kind of singularity arises (even with involved particles having finite momenta) when massless particles get converted into other massless ones while the momentum of both the initial and final particles are in the same (or opposite) direction, and is famously known as collinear singularities in the literature.

In practical scenarios, as any scattering experiment is performed during a finite time interval, hence emission of soft photons with vanishing momentum is highly non feasible, thus alleviating soft IR divergences in real experiments. It was initially shown by Bloch and Nordsieck [4] that *carefully constructed sufficiently inclusive observable cross sections in QED are free from any infrared divergences*. The subject of IR finiteness of QED has been also discussed by several authors in the literature, see Ref. [5–12]. A general theorem related to IR behaviour of field theories was proved by Kinoshita, Lee and Nauenberg (KLN) [13, 14] finding *IR divergences to cancel for any unitary theory when all the de-*

---

[2]Like any other theories of nature, QFT is also an effective theory with an inbuilt energy scale associated with it.

generate initial and final states are summed over. The KLN theorem turned out to be of formal interest, as in real settings one usually does not sum over initial states. In real situations one often manages to avoid IR singularities, understanding that a real detector has a finite energy and angular resolution.

The works of Weinberg [15] further shed light on the universal properties of leading soft structure of amplitudes for theories involving massless particles (generalized to gravity). Realization of the fact that scattered charged particles are always accompanied by a cloud of soft photons, has also led to reformulation of QED in terms of dressed coherent asymptotic states [16–24]. The seminal work of Faddeev and Kulish [24] then provided a prescription for construction of IR finite amplitudes for massive abelian gauge theories. This was followed by a similar construction for nonabelian gauge theory [25, 26] and gravitation [27] in literature. In recent times there have been important observations of 'asymptotic symmetries' [28–32] and 'memory effect' [33–36] related to the infrared dynamics of the field theory for both abelian and non-abelian gauge theories.

The IR structure plays a crucial role in the discussions of collider physics, Yang-Mills theories and field theories at finite temperature also. In this regard, IR behaviour of theories has been widely studied in the development of soft collinear effective theory (SCET) [37] which has been related in connection to soft theorems [38]. IR structure also plays a very important role in the studies of Quark Gluon Plasma (QGP) Ref. [39]. For field theories at finite temperature the IR divergent structure of the theories have been found to be more severe due to the presence of thermal fluctuations. The IR finiteness of the theory of thermal fermionic QED has been shown to all orders in perturbation theory, using *eikonal approximation* by Weldon [40] followed by an *exact* calculation by Indumathi [41].

In this thesis we discuss the proof and results of IR finiteness of theories of charged fermions and scalars interacting with neutrals at finite temperature, specifically in the context of gauge theories involving dark matter. We start by proving IR finiteness for scalar quantum electrodynamics [42] to all orders, and then generalizing to the case of theories

of dark matter [43] at finite temperature. The IR divergent structure was found to have an universal behaviour independent of the exact nature of the interaction terms.

1.1 Motivation

To explain the results of the observations ranging over a multitude of length-scales, starting with Zwicky's observations of Coma Cluster [44, 45], galactic rotation curves [46–48], gravitational lensing (strong lensing) [49], Microlensing [50, 51], observations of Bullet cluster [52], recent observations of galaxies and clusters of different sizes [53–55], to finally the observations of cosmic microwave background (CMB) [56–58] the existence of Dark Matter (DM) is necessitated [59], which overwhelms [58] the ordinary component of matter in the known Universe. Although the prominent evidences till now in favour of DM have arisen only from the gravitational effects, the theories simply trying to modify gravity (MOND) [60] or theories with cosmic fluid [61] have, so far, failed to successfully account for all the relevant observations.

The various non-baryonic and baryonic candidates such as WIMPs, Axions and axion-like particles (ALP), sterile neutrinos, particles from dark sectors, particles in universal extra dimensional theories to primordial black holes, can be feasible candidates for the DM, and details of the properties of these candidates have been extensively reviewed in literature [62–67]. Before moving to our particular model of interest, we will briefly discuss about some general properties concerning DM. As CMB is sensitive to the baryonic and the total matter densities respectively through the height of the first peak and through the ratio of the heights of the first and the second peaks, it can be inferred (from results of CMB) that not all matter in the Universe can be baryonic. In fact from the latest results of PLANCK [58] it has been noted that DM is dominated by non-baryonic component,

$$\sigma_m h^2 = 0.1430 \pm 0.0011 \,, \quad \sigma_c h^2 = 0.1200 \pm 0.0012 \,, \quad \sigma_b h^2 = 0.02237 \pm 0.00015 \,, \quad (1.1)$$

where σ_m, σ_c and σ_b are respectively the density of total matter, cold dark matter and baryonic matter; and h is the reduced Hubble's constant with $h = H_0/100 = 0.6736\pm0.0054$ [58]. The masses of the DM also can vary over a wide range of values. The lower bound of mass for the fermionic DM has resulted from Tremaine-Gunn limit [68] using results of the Fornax dwarf [69], to be 70 eV $< m_\mathcal{F}$. The lower bound for bosonic DM masses corresponds to a value 10^{-22}eV $\lesssim m_\mathcal{B}$ [70–74]. The upper limit of masses of DM have a bound of $5\text{M}_\odot$ [75, 76]. The DM candidate should be electrically neutral[3] and should not interact strongly, and must be stable on cosmological time scales [77].

DM particles can be classified in different ways. Depending on how relativistic DM candidates were when they decoupled from thermal plasma (falling out of thermal equilibrium in the early Universe), the DM candidates can be classified into three categories, *i.e.*, Hot dark Matter (HDM), Cold Dark Matter (CDM) and Warm Dark Matter (WDM). HDM and CDM were respectively relativistic and non-relativistic at the time of decoupling, and the WDM represents to a scenario in between HDM and CDM. The Large Scale Structure formation of the Universe strongly supports the dominant contribution to DM to be CDM in nature. The DM candidates also can be classified according to their formation mechanism, *i.e.*, thermal, non-thermal, freeze-in, asymmetric, primordial black hole formation etc.

In this thesis we will focus on the case of thermally produced CDM. The most natural and well studied production mechanism of CDM candidate to meet the current day abundance of DM is through the production of the CDM thermally in the post-inflation reheating phase. The relevant number density of CDM is then determined by coupled Boltzmann equations in the expanding Lemaitre-Friedmann-Robertson-Walker Universe [59]; until when due to the expansion of the Universe, the interaction rate of CDM falls below the Hubble expansion rate, resulting in the CDM component to fall out of equilibrium, and number density of CDM freezes out.

---

[3]Although some 'milli-charged' DM candidate (obtaining effective charge through kinetic mixing with a dark photon field, producing very suppressed coupling with photon field) can be feasible, it is severely constrained from the data.

In the current era of precision cosmology this relic density of DM is being measured with high precision [56–58]; and only an order of magnitude calculation of relic densities from theoretical point of view is not any more justifiable. Efforts to include higher order corrections to annihilation cross-section from theoretical calculations [78–85] have already been implemented, resulting in non-negligible contribution with respect to leading order at zero temperature. As the DM component was in thermal equilibrium with background plasma interacting with it until the freeze out, thus thermal effects become of crucial importance while performing relic density calculations. Hence, predictions of relic density at finite temperature including the higher order NLO corrections are highly preferable. The suitable efforts along this direction were taken in Refs. [86, 87]. Specifically in Ref. [86] Beneke et al. have implemented relic density calculations at NLO in thermal field theory obtaining finite thermal corrections. IR divergences related to the corresponding process were found to completely cancel at order NLO at finite temperature, when both absorption of particles and emission of them to the heat bath were allowed. This NLO result of Beneke et al. thus motivated us to look into an all order IR behaviour of the corresponding theory at finite temperature.

In this thesis, among various potential candidates of CDM, we will be interested in the discussions concerning weakly interacting massive particle (WIMP). Minimal Supersymmetric Standard Model (MSSM) [88–92] naturally has particle contents which can correspond to eligible candidates [93–99] related to the WIMP paradigm. We are interested in the neutralino particles as the Lightest Supersymmetric Particle (LSP) playing the role of WIMP CDM particle in the context of MSSM. Although the neutralino is a linear combination of the bino, the neutral wino and the two neutral higgsinos, we will be interested in the thesis regarding a simplified model of bino (bino-like) dark matter candidate.

The corresponding Lagrangian density related to the model is expressed as

$$\mathcal{L} = -\frac{1}{4}F_{\mu\nu}F^{\mu\nu} + \overline{f}\left(i\slashed{D} - m_f\right)f + \frac{1}{2}\overline{\chi}\left(i\slashed{\partial} - m_\chi\right)\chi$$
$$+ (D^\mu\phi)^\dagger (D_\mu\phi) - m_\phi^2\phi^\dagger\phi + \left(\lambda\overline{\chi}P_L f^-\phi^+ + \text{h.c.}\right), \qquad (1.2)$$

which has been extensively studied in the literature [100–103] at zero temperature. The model is an extension of Standard Model (SM) containing left handed SM fermion doublets $f = (f^0, f^-)^T$ along-with an additional scalar doublet $\phi = (\phi^+, \phi^0)^T$ which are super-partners of SM fermions f. Majorana fermion χ which is a $SU(2) \times U(1)$ singlet is also contained in the corresonding model as the concerned dark matter candidate, having a mass at TeV scale, $m_\chi \approx O$ (0.1–1 TeV), and mass of sfermion ϕ is $m_\phi > m_\chi$. As generically for CDM candidates freeze-out occurs at a temperature $T_{freeze-out} \approx m_\chi/20$, thus in this model freeze-out of DM occurs after the electro-weak transition, making only the electromagnetic interactions to be the relevant one at this scale, while having the discussion of IR behaviour of the corresponding theory. In the current model the DM candidate χ interacts with SM particles f via Yukawa interaction. In addition to interactions of charged components, there is the feasibility of the an interaction term coupling the neutral components as $\lambda\overline{\chi}P_L f^0\phi^0$. But, we have discounted writing such an expression in Eq. 1.2 as although the neutral particles play an important role in the calculation of inclusive cross-section they are not important in the analysis of IR behaviour of the theory being non-interacting to photon.

We would also note here that although the model Eq. 1.2 may look like too specific a choice but it fruitfully captures the spirit of a wide class of models. As it has been already explained, though neutralino can be an admixture of bino, neutral wino and two neutral higgsinos, for a very large class of supersymmetry breaking scenarios, we find the the higgsino mass parameter μ to be much larger than the soft terms ($M_{1,2}$) for the gauginos, suppressing the higgsino component to a negligible level. And as bino-wino mixing is also dependent on the value of μ, a large value of higgsino mass parameter also suppresses the

7

wino-component in the DM. The consideration of bino-like DM further simplifies the calculations as additional diagrams can be safely neglected, *e.g.*, with *s*-channel gauge bosons or Higgs[4]. Therefore restricting ourselves to the specific case of the bino (bino-like) DM does not represent the neglect of subtle issues while still allowing for considerable space for simplifications, both algebraic and in bookkeeping.

The IR structure of this theory of bino (bino-like) DM is then analyzed at finite temperature, starting with the proof of IR finiteness of the theory of scalar QED at finite temperature, and then generalizing to a full theory of DM with all the particle content. The final total cross-section for the theory of DM turns out to be IR finite to all orders in perturbation theory giving an *exact closed form* expression. The IR divergent pieces are found to be universal, and to be independent of the specific interaction terms, making the results useful for any complete theory for charged scalars, fermions and neutrals. The exact symbolic expression of the cross-section at finite temperature can be used order by order to calculate finite corrections. The calculation of such results of finite corrections are beyond the scope of the current thesis.

1.2   Outline of the thesis

The thesis has been organized as follows.

In Chapter 2 the basics of thermal field theory have been discussed. Starting with a brief discussion of general features of thermal field theory, we have quickly moved towards and discussed about the real time formulation of thermal field theory. Following the introduction of the Schwinger-Keldysh contour, we have found the thermal fields to be doubled, with thermal type-1 and type-2 fields correspondingly playing the role of respectively 'physical' and 'ghost' fields. The infrared structure of a field theory (especially involving massless bosons) at finite temperature is found to become more intricate and more

---

[4]Although for pure binos, such couplings only arise at the one-loop level, and are only of little consequence.

violently IR divergent. The leading IR divergence is found to be linear due to the effects of thermal fluctuations, in contrast to only logarithmic IR divergence present at zero temperature. In addition to leading linear IR divergence, the existence of an *additional* sub-leading logarithmic IR divergence arising due to thermal fluctuations is also found to be present at finite temperature.

The subject matter of Chapter 3 is to correctly identify and separate out the IR divergent and finite contributions for field theories. Identification and separation of IR finite and divergent contributions are performed using the technique of Grammer and Yennie (GY) [12]. The technique of GY is reviewed for zero temperature fermionic quantum electrodynamics (QED) to make readers familiar with the main features of it at zero temperature to start with, which will be generalized in the following chapters to field theories at finite temperature for more complicated theories. To achieve the goal of correctly separating out the IR divergent and finite pieces, the polarization sums of both the virtual and real photon contributions will be rearranged into modified polarization sums; respectively denoted by K and G polarization contributions (for virtual photons), and $\widetilde{K}$ and $\widetilde{G}$ polarization contributions (for real photons). All the IR divergent contributions are then found to be contained inside K and $\widetilde{K}$ terms; and the contributions of G and $\widetilde{G}$ terms are found to be IR finite. The notations regarding the use of GY rearrangement related to a general diagram having multiple photon interactions, is also set up in this chapter. These notations will be extensively used in the following chapters to fruitfully interpret the results arising from more general theories.

At finite temperature the IR structure of the field theories is more complicated due to the presence of additional leading linear and sub-leading logarithmically divergent terms due to the effects of thermal fluctuations. Thus a generalization of GY technique is required at finite temperature to correctly identify IR divergent and finite contributions. We start Chapter 4 by reviewing the generalization of GY technique at finite temperature as mentioned in Ref. [41]. After reviewing the technique for fermionic QED at finite temperature

we focus our attention on scalar QED at finite temperature. The original results and findings of the thesis begin at this section. To apply the GY rearrangements the generalized Feynman's Identities (Ward Identities) have been derived for scalar QED at finite temperature. In scalar QED in addition to trilinear (scalar-photon-scalar) interaction vertices (similar to fermionic QED) additional quadrilinear (scalar-scalar-photon-photon) seagull interaction vertices are also found to be present. To manage proliferating number of the Feynman diagrams, particular contributions from these set (trilinear and quadrilinear) of diagrams are clubbed together and are denoted by 'circled vertex'. These circled vertices will turn out to be of extreme importance to collect similar types of contributions while correctly identifying the IR divergent and finite contributions in discussions of the chapters following.

The proof technique and results regarding the IR finiteness of scalar QED at finite temperature is elaborately discussed in Chapter 5. Using the generalized Feynman identities all the IR divergences are found to be contained inside virtual K and real $\widetilde{K}$ polarization contributions. The IR divergent parts are found to factorize leading to resummation and exponentiation to all orders in thermal field theory. After including subtle arguments and proper phase space factors for real photon emission and absorption the virtual G and real $\widetilde{G}$ polarization contributions are found to be IR finite. The IR divergent factors are found to cancel between K and $\widetilde{K}$ contributions order by order to all orders in perturbation theory at finite temperature, resulting in a IR finite cross section. The presence of seagull and tadpole contributions is indispensable to achieve this result, canceling *exactly* remnant IR finite sub-contributions linear and quadratic in photon momentum, arising from GY rearrangement, making possible factorization and resummation of IR divergent pieces.

The proof and results of IR finiteness of the theories involving dark matter at finite temperature is the subject matter of Chapter 6. The particular theory inspected in this chapter is expressed by the Lagrangian of Eq. 1.2. Due to the presence of different species of particles (charged scalars, charged fermions, neutrals and photons) the applications of the

GY technique at finite temperature becomes an extremely involved one. Again all the IR divergences are found to be contained within virtual K and real $\widetilde{K}$ polarization contributions, and virtual G and real $\widetilde{G}$ polarization contributions are found to be IR finite. The IR divergent factors again get factorized leading to resummation for K and $\widetilde{K}$ contributions and then getting canceled among K and $\widetilde{K}$ terms. In contrast to all previous cases, the IR factorization in this case is rather non-trivial, which results due to non-trivial 'double-cancellation' of sub-contributions. This kind of non-trivial 'double-cancellation' could not in any way be speculated starting from individual thermal theories of either fermionic or scalar QED. The 'double-cancellation' leading to IR factorization and resummation was found to be independent of the particular interactions of charged particles and neutrals, implying the universality of the IR divergent structure at finite temperature. It should be also noted here, that the IR finite contributions are certainly model dependent and depend on the details of particular theories. Using all these we obtain a closed form exact expression for the IR finite cross section to all orders in perturbation theory at finite temperature.

The key findings of the thesis, future prospects and the concluding remarks have been summarized in Chapter 7.

Chapter 2

Introduction to thermal field theory

2.1 Prologue

Thermal field theory provides us a framework to discuss about the physics of systems comprising of multiple relativistic and quantum mechanical particles interacting among themselves. In addition to the quantum fluctuations, statistical fluctuations (arising due to the particles interacting among themselves and with the medium) also play crucial role in these scenarios. The effect of the medium (pertaining to statistical fluctuation) to a relevant process of interest is often non-negligible and brings out interesting physics. Most appropriate way to describe such system involving many degrees of freedom is through ensemble description. The ensemble consists of all the second quantized states belonging to the Fock space of the relevant system. The properties of the ensemble specifying the system, is suitably described by the density matrix (density operator) $\hat{\rho}$. The density matrix is defined as

$$\hat{\rho}(t_i) \equiv \sum_n p_n(t_i) \, |n(t_i)\rangle \, \langle n(t_i)| \; , \qquad (2.1)$$

where $|n\rangle$, $n = 1, 2, \ldots$ are the complete set of states belonging to the ensemble, and we are working in the Schrödinger picture. The probability of finding the quantum mechanical system in the state $|n\rangle$ at time t_i is given by $p_n(t_i)$, with $\sum_n p_n(t_i) = 1$. Hence, incorporating both effects of the quantum and statistical fluctuation, the expectation value (ensemble average) of an operator $\hat{O}$ at time t_i can be written as

$$\langle \hat{O}(t_i) \rangle = \sum_n p_n(t_i) \langle n(t_i)| \hat{O} |n(t_i)\rangle = \text{Tr} \left(p_n(t_i) |n(t_i)\rangle \langle n(t_i)| \hat{O}(t_i) \right) = \text{Tr} \, \hat{\rho}(t_i)\hat{O}(t_i) \, .$$

(2.2)

The expectation value of the same operator $\hat{O}$ at some later time t_f is given by

$$\langle \hat{O}(t_f) \rangle = \text{Tr} \, \hat{\rho}(t_f)\hat{O}(t_f) \, .$$ (2.3)

The ability to predict the expectation value of operator $\hat{O}$ at a time t_f given the expectation value of the same operator at some earlier time t_i, completely specifies the dynamics of the system. In the Schrödinger picture it is well known that the quantum states (describing the system) evolve with time (and the operators do not). Hence, the density matrix (encapsulating the properties of the states) evolve with time, and the time evolution of the density matrix is described by the Liouville-von Neumann equation written as,

$$i\frac{\partial \hat{\rho}(t)}{\partial t} = \left[\hat{H}, \hat{\rho}(t) \right] \, .$$ (2.4)

The *explicit solution* of the above Eq. 2.4 can be rather challenging for particular systems, where the Hamiltonian $\hat{H}$ is time dependent or even the Hamiltonian being time independent if that does not commute with the density matrix. The solution of the Eq. 2.4 can be generically (implicitly) given by,

$$\hat{\rho}(t_f) = U(t_f, t_i) \, \hat{\rho}(t_i) \, U^\dagger(t_f, t_i) = U(t_f, t_i) \, \hat{\rho}(t_i) \, U(t_i, t_f) \, ,$$ (2.5)

where $U(t_f, t_i)$ is the unitary time translation operator,

$$U(t_f, t_i) = T \exp\left[-i \int_{t_i}^{t_f} \hat{H}(t') \, dt'\right] . \tag{2.6}$$

In the above expression T represents the time ordering of the corresponding operator. Using the result of Eq. 2.5 in Eq. 2.3 the expectation value of operator $\hat{O}$ at some later time t_f is given by[1],

$$\langle \hat{O}(t_f) \rangle = \text{Tr} \left(U(t_f, t_i) \, \hat{\rho}(t_i) \, U(t_i, t_f) \, \hat{O}(t_f) \right) . \tag{2.7}$$

Evaluating the above expression by inserting complete set of states in the field basis[2] we obtain

$$\langle \hat{O}(t_f) \rangle = \sum_{a,b,c,d} \langle \varphi_a | U(t_f, t_i) | \varphi_b \rangle \langle \varphi_b | \hat{\rho}(t_i) | \varphi_c \rangle \langle \varphi_c | U(t_i, t_f) | \varphi_d \rangle \langle \varphi_d | \hat{O}(t_f) | \varphi_a \rangle$$

$$= \sum_{a,b,c,d} \langle \varphi_a | U(t_f, t_i) | \varphi_b \rangle \rho_{bc} \langle \varphi_c | U(t_i, t_f) | \varphi_d \rangle O_{da} . \tag{2.8}$$

The matrix element of the unitary time evolution operator can be represented using path integration formulation. The corresponding expression for time evolution operator thus reads as,

$$\langle \varphi_a | U(t_f, t_i) | \varphi_b \rangle = \left\langle \varphi_a \left| T \exp\left[-i \int_{t_i}^{t_f} \hat{H}(t') \, dt'\right] \right| \varphi_b \right\rangle$$

$$= \int_{\varphi_1(t_i) = \varphi_b}^{\varphi_1(t_f) = \varphi_a} \mathcal{D}\varphi_1 \, e^{iS(\varphi_1)} , \tag{2.9}$$

---

[1]Note that this expression is same and independent of different pictures used, *i.e.*, for Schrödinger, Heisenberg and Interaction picture. As, in the Heisenberg picture density matrix (states) does not evolve with time and operators evolve with full Hamiltonian; and in Interaction picture density matrix (states) evolve with interaction Hamiltonian and operators evolve with free Hamiltonian producing same result.

[2]We have applied φ to represent generic field in this discussion. For particular discussions relating to different fields (scalar ϕ, fermion ψ and gauge A^μ) we will use corresponding notations and use other related subtleties.

and,

$$\left\langle \varphi_c \left| U(t_i, t_f) \right| \varphi_d \right\rangle = \left\langle \varphi_c \left| T \exp\left[-i \int_{t_f}^{t_i} \hat{H}(t'') \, dt'' \right] \right| \varphi_d \right\rangle$$

$$= \int_{\varphi_2(t_i)=\varphi_c}^{\varphi_2(t_f)=\varphi_d} \mathcal{D}\varphi_2 \, e^{-iS(\varphi_2)} . \tag{2.10}$$

Using the results of Eq. 2.9 and Eq. 2.10 in the Eq. 2.8 we obtain the expectation value of the operator $\hat{O}$ to be,

$$\langle \hat{O}(t_f) \rangle = \sum_{a,b,c,d} \int_{\varphi_1(t_i)=\varphi_b}^{\varphi_1(t_f)=\varphi_a} \mathcal{D}\varphi_1 \int_{\varphi_2(t_i)=\varphi_c}^{\varphi_2(t_f)=\varphi_d} \mathcal{D}\varphi_2 \, e^{iS(\varphi_1)-iS(\varphi_2)} \rho_{bc} \, O_{da} . \tag{2.11}$$

In the above equation (unlike for pure states) the matrix elements of the density matrix is usually very hard to predict for an ensemble (mixed state), where multiple particles are interacting among themselves. For the special case of thermal equilibrium this problem can be mitigated. For a system in thermal equilibrium the density matrix takes up the form,

$$\hat{\rho}_{\text{eq}} = \frac{e^{-\beta\hat{\mathcal{H}}}}{Z}, \quad \text{where} \quad \hat{\mathcal{H}} = \begin{cases} \hat{H} & \text{for canonical ensemble .} \\ \hat{H} - \mu_i \hat{N}_i & \text{for grand canonical ensemble .} \end{cases} \tag{2.12}$$

In the above expression β corresponds to the inverse temperature of the system, $\beta = 1/T$ (where T corresponds to the temperature of the system and we are working in the natural unit so that Boltzmann constant $k_B = 1$). In Eq. 2.12 for the case of grand canonical ensemble, $\hat{N}_i$ corresponds to the operator related to conserved commuting Noether charge of the system, and μ_i refers to the chemical potential associated with the respective global conserved charge $\hat{N}_i$. In Eq. 2.12, Z refers to the partition function and is expressed as,

$$Z = \text{Tr} \, e^{-\beta\hat{\mathcal{H}}} = \begin{cases} \text{Tr} \, e^{-\beta\hat{H}} & \text{for canonical ensemble .} \\ \text{Tr} \, e^{-\beta(\hat{H}-\mu_i\hat{N}_i)} & \text{for grand canonical ensemble .} \end{cases} \tag{2.13}$$

We note here that the density matrix in the thermal equilibrium Eq. 2.12 has a formal analogy with the time evolution operator in Eq. 2.6, with time interval traded off with $-i\beta$. With this consideration, the matrix element of the equilibrium density matrix expressed in the path integral representation is written as

$$(\rho_{\text{eq}})_{bc} = \left\langle \varphi_b \left| \hat{\rho}_{\text{eq}} \right| \varphi_c \right\rangle = \left\langle \varphi_b \left| \frac{e^{-\beta(\hat{H} - \mu_i \hat{N}_i)}}{Z} \right| \varphi_c \right\rangle$$

$$= \frac{1}{Z} \int_{\varphi_E(t_i) = \varphi_c}^{\varphi_E(t_f - i\beta) = \pm \varphi_b} \mathcal{D}\varphi_E \, e^{-S_E(\varphi_E)} \,, \qquad (2.14)$$

where S_E corresponds to the Euclidean action,

$$S_E = \int_0^\beta \mathrm{d}\tau (L_E - \mu_i N_i) \,, \qquad (2.15)$$

where τ corresponds to imaginary time, $\tau = it$ and μ_i's vanishes for calculations in the canonical ensemble. In Eq. 2.14, $\varphi_E(t_f - i\beta)$ corresponds to the field at time $t_f - i\beta$, which is equal to $\pm\varphi_b$; where plus and minus sign respectively refer to the boundary conditions corresponding to bosonic and fermionic fields. Using the results of Eq. 2.14 with the results of Eq. 2.11 we find the partition function Z for the ensemble can be expressed in the path integral representation as

$$Z[\beta] = \int \mathcal{D}\varphi_E \, e^{-S_E(\varphi_E)} \int \mathcal{D}\varphi_1 \, \mathcal{D}\varphi_2 \, e^{iS(\varphi_1) - iS(\varphi_2)} \,. \qquad (2.16)$$

Let us spend a few moments appreciating the final expression of the partition function as obtained in the above expression. From the structure of the equilibrium density matrix Eq. 2.12 it is evident that it is time translation invariant (see Eq. 2.4); as it commutes with the Hamiltonian $\hat{H}$, $[\hat{\rho}_{\text{eq}}, \hat{H}] = 0$. Hence, for a system in equilibrium the choice of initial time t_i is completely arbitrary. Thus for a local operator in time, the final time t_f can be chosen to be $t_f = t_i$ (without loss of any generality). This renders the $\mathcal{D}\varphi_1$ and $\mathcal{D}\varphi_2$ integrals dropping out individually, leaving only the Euclidean $\mathcal{D}\varphi_E$ integral as the surviving one in Eq. 2.16. The above argument is also valid for a set of operators,

$\hat{O} = \hat{O}_1(\vec{x}_1)\dots\hat{O}_n(\vec{x}_n)$ having all the same time arguments (or if they are separated in spacelike intervals and are situated on a Cauchy surface). The above result is formally known as the *imaginary time formulation* [104–108] in literature.

For the case where the set of operators are separated in timelike intervals (in real time), $\hat{O} = \hat{O}_1(t_1, \vec{x}_1)\dots\hat{O}_n(t_n, \vec{x}_n)$ with $t_1 < t_2 < \dots < t_n$; then the first operator $\hat{O}_1(t_1, \vec{x}_1)$ acting on the equilibrium density matrix matrix $\hat{\rho}_{\text{eq}}$ creates a new density matrix $\hat{\rho}(t_1) = \hat{\rho}_{\text{eq}}\hat{O}_1(t_1, \vec{x}_1)$, which no longer commutes with $\hat{H}$ the Hamiltonian. Therefore the $\mathcal{D}\varphi_1$ and $\mathcal{D}\varphi_2$ integrals do not trivialize as before and gives non-vanishing contributions over the real branches of time integral in Eq. 2.16. This contour which is formed in the complex time plane having two real branches (C_1 and C_2) and imaginary branches (C_3 and C_4) is known as the Schwinger-Keldysh contour, and is shown in Fig. 2.1. The corresponding formalism is known as *real time formulation* [107–116] in literature.

The expectation value of set of operators separated in real time can be evaluated by defining the generating functional $Z[\beta, J_1, J_2]$ as

$$Z[\beta; J_1, J_2] = \int \mathcal{D}\varphi_E \, e^{-S_E(\varphi_E)} \int \mathcal{D}\varphi_1 \, \mathcal{D}\varphi_2 \, e^{i\left[S(\varphi_1) - S(\varphi_2) + \int \mathrm{d}^4x\left(J_1(x)\varphi_1(x) - J_2(x)\varphi_2(x)\right)\right]},$$
(2.17)

where J_1 and J_2 are the sources defined respectively on the C_1 and C_2 part of the contour in Fig. 2.1. The technique to evaluate (perturbatively) of the generating functional $Z[\beta, J_1, J_2]$ will be discussed in more details in the next Section 2.2.

There are mainly three formalisms which are widely used to study thermal systems in literature. These are respectively known as *imaginary time formalism* [104–108], *real time formalism* [107–116] and *thermo field dynamics* [117–121]. The imaginary time formalism is best suited to describe a system in thermal equilibrium, making it most suitable to calculate time independent bulk thermodynamic quantities (inherently Euclidean quantities). By analytically continuing the time into real domain, and after incorporating fluctuation-dissipation theorem using Kubo-Martin-Schwinger (KMS) relations [122, 123] few time

dependent quantities also can be evaluated in this formalism. But, imaginary time formulation is usually not well suited to calculate expectation values of operators which are well separated in real time, due to their inherent Minkowskian nature. This problem of evaluating expectation values of formally Minkowskian quantities is mitigated in the real time formulation. The real time formulation is well suited for estimating the quantities which are well separated in real time (inherently Minkowskian) and separates out the effect of the medium (thermal fluctuations) from the beginning. It is also applicable to describe non-equilibrium phenomena in real time formalism, which become crucial while estimating transport coefficients of thermodynamic systems. The other real time approach which is based on the operator field theory is known as the thermo field dynamics (TFD). This formulation is most suitable to describe the algebraic structure of thermal systems, including doubling of the Fock space involved. And being operator field theory approach, TFD is also extremely useful involving calculations related to the symmetry arguments of the systems.

In this thesis we are interested in the processes involving real time separations. Thus we will use the real time formulation in upcoming discussions. We will briefly review the aspects of the real time formulation in the next section, and will discuss only about the subtleties which will be of importance in the context of following chapters.

2.2 Introduction to real time formulation of thermal field theory

From the discussion of the previous sections, we have noticed that the Boltzmann operator in the density matrix Eq. 2.12 has a formal similarity with the unitary time evolution operator Eq. 2.6 identifying inverse temperature with imaginary time. Thus the allowed values of time can now have complex values, that is $t \in \mathbb{C}$. The formal quantities of interest for

the thermal system are the Green functions defined as,

$$G_C(x_1, \ldots, x_n) = \langle T_C(\hat{\varphi}(x_1), \ldots, \hat{\varphi}(x_n)) \rangle . \tag{2.18}$$

In the above equation $\langle \ldots \rangle$ refer to the thermal (ensemble) averaged quantities. The time arguments in the above equation can now have complex values. So to make sense of the time ordering, T_C is only defined along a path in complex time. The path can be parametrically defined as $t = z(w)$, where w is real and monotonically increasing parameter along the path, such that ordering in w corresponds to the ordering along the path. With this definition in mind, the step function θ and delta function δ along the path can be defined as

$$\theta_C(t - t') = \theta(w - w'), \quad \delta_C(t - t') = \left(\frac{\partial z}{\partial w}\right)^{-1} \delta(w - w') . \tag{2.19}$$

We can also generalize the notion of functional differentiation along the path as,

$$\frac{\delta J(x)}{\delta J(x')} = \delta_C(t - t')\delta(\vec{x} - \vec{x}') . \tag{2.20}$$

With the definitions of Eq. 2.19 and Eq. 2.20 we can define a generating functional $Z_C[\beta; J]$ to obtain the Green's functions,

$$G_C(x_1, \ldots, x_n) = \frac{1}{Z_C[\beta]} \frac{\delta^n Z_C[\beta; J]}{(i)^n \delta J(x_1) \ldots \delta J(x_n)}\bigg|_{J=0} . \tag{2.21}$$

The formal and obvious solution for the generating functional is given by

$$Z_C[\beta; J] = \text{Tr}\left[e^{-\beta \hat{\mathcal{H}}} T_C \exp\left(i \int_C d^4 x J(x)\hat{\varphi}(x)\right)\right]$$

$$= \int \mathcal{D}\varphi \exp\left[i \int_C d^4 x \left(\mathcal{L}(\varphi(x)) + J(x)\varphi(x)\right)\right] , \tag{2.22}$$

20

where the path C must pass through all the arguments of x_i in the relevant Green's function. In Eq. 2.22 the expression for the generating functional is finally expressed in terms of the path integral representation, such that the boundary conditions are given by $\varphi(t_i, \vec{x}) = \pm\varphi(t_i - i\beta, \vec{x})$, where plus and minus sign respectively refer to the bosonic and fermionic field.
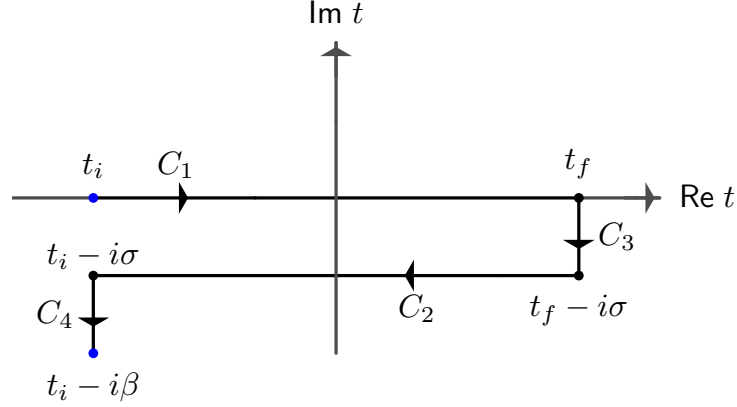
Figure 2.1: *Standard time path is shown for real time formulation of thermal field theory. The type-1 and type-2 thermal fields "live" on the C_1 and C_2 part of path of the full contour, and $0 \leq \sigma \leq \beta$. For symmetric choice of path, $\sigma = \beta/2$.*

Using the analytic properties of the Wightman functions along with the KMS relations [122, 123] (relating the Wightman functions in thermal equilibrium), it can be shown that the formal region of interest for evaluating the Green's functions lie in the strip of $-\beta \leq \text{Im}(t - t') \leq 0$ (we have already used this information to express the path integral representation in Eq. 2.22). Now, in this strip the path C must go through all the spacetime arguments. For drawing a path it has to be noted that the imaginary part of the time must have a non increasing dependence on the path parameter w, such that the path does not move upward in imaginary time. The path also must contain real time axis, as we are interested in Green's functions with real valued time arguments. These conditions provide us with many possibilities of path C, of which the usual standard choice is shown in Fig. 2.1.

The standard time path consist of four main parts,

1. C_1 : This part starts from a large negative real value of time t_i, $(t_i \to -\infty)$ following

the real time axis to a large positive real value of time t_f, $(t_i \to +\infty)$. The operators situated along this path are all time ordered.

2. C_3 : This part starts from t_f and goes to $t_f - i\sigma$, where $0 \le \sigma \le \beta$ along a vertical straight line along imaginary time.

3. C_2 : This part starts from $t_f - i\sigma$ and goes to $t_i - i\sigma$, along a horizontal straight line in the complex time plane. The operators situated along this path are all anti-time ordered.

4. C_4 : This part starts from $t_i - i\sigma$ and goes to $t_f - i\beta$, along a vertical straight line along imaginary time.

This path is famously known as Schwinger-Keldysh [111, 112] path in the literature.

Following the path the action now can be separated out in four distinct parts,

$$
\begin{aligned}
S &= \int_C dt \int d^3x\, \mathcal{L}(\varphi(x)) \\
&= \int_{t_i}^{t_f} dt \int d^3x\, \mathcal{L}(\varphi(t, \vec{x})) - i \int_0^\sigma d\tau \int d^3x\, \mathcal{L}(\varphi(t_f - i\tau, \vec{x})) \\
&\quad - \int_{t_i}^{t_f} dt \int d^3x\, \mathcal{L}(\varphi(t - i\sigma, \vec{x})) - i \int_\sigma^\beta d\tau \int d^3x\, \mathcal{L}(\varphi(t_i - i\tau, \vec{x})) .
\end{aligned}
\tag{2.23}
$$

In the above equation we have assumed that the Lagrangian does not contain any derivative expression for simplicity. Now we define the fields along the parts of the path C_1 and C_2 respectively as φ_1 and φ_2,

$$
\varphi_1(t, \vec{x}) \equiv \varphi(t, \vec{x}), \quad \varphi_2(t, \vec{x}) \equiv \varphi(t - i\sigma, \vec{x}) ,
\tag{2.24}
$$

and sources along parts of the path C_1 and C_2 respectively as J_1 and J_2,

$$
J_1(t, \vec{x}) \equiv J(t, \vec{x}), \quad J_2(t, \vec{x}) \equiv J(t - i\sigma, \vec{x}) .
\tag{2.25}
$$

22

Using the results of Eq. 2.23, Eq. 2.24, Eq. 2.25 in Eq. 2.22 we can separate out the generating functional into different parts. Using the Riemann–Lebesgue lemma for the (spatial Fourier transformed) Green's Function [116] it can be shown the generating functional can be factorized into two parts as in Eq. 2.26 when $t_i \to -\infty$ and $t_f \to \infty$,

$$
\begin{aligned}
Z_C[\beta, J] &= Z_{C_{34}}[\beta, J] Z_{C_{12}}[\beta, J] \\
&= \int \mathcal{D}\varphi_E \, e^{-S_E(\varphi_E)} \int \mathcal{D}\varphi_1 \, \mathcal{D}\varphi_2 \, e^{i\left[S(\varphi_1) - S(\varphi_2) + \int d^4 x \left(J_1(x)\varphi_1(x) - J_2(x)\varphi_2(x)\right)\right]} .
\end{aligned}
\tag{2.26}
$$

In the above expression, $Z_{C_{ij}}[\beta, J]$ corresponds to the respective contribution from the relevant part of the time path, where $C_{ij} = C_i \cup C_j$. See the similarity of Eq. 2.26 with Eq. 2.17.

Now to obtain a perturbative evaluation of Eq. 2.26 we remind ourselves,

$$
Z_C[\beta; J] = \exp\left[-i \int_C d^4 x \, \mathcal{V}\left(\frac{\delta}{i\delta J(x)}\right)\right] Z_C^F[\beta; J] .
\tag{2.27}
$$

In the above expression $Z_C^F[\beta; J]$ is the generating functional corresponding to free part of the Lagrangian,

$$
Z_C^F[\beta; J] = \int \mathcal{D}\varphi \exp\left[i \int_C d^4 x \left(\mathcal{L}_0(\varphi(x)) + J(x)\varphi(x)\right)\right] .
\tag{2.28}
$$

and the full Lagrangian is

$$
\mathcal{L}(\varphi(x)) = \mathcal{L}_0(\varphi(x)) + \mathcal{L}_{\text{int}}(\varphi(x)) = \mathcal{L}_0(\varphi(x)) - \mathcal{V}(\varphi(x)) ,
\tag{2.29}
$$

where for simplicity again we have considered that the Lagrangian does not contain any derivative interaction.

Using Eq. 2.29 in Eq. 2.26 and after noting that the effect of $Z_{C_{34}}[\beta, J]$ can be replaced by

an overall normalization factor $\mathcal{N}$, the expression for Eq. 2.26 can be written as,

$$Z_C[\beta; J] = \mathcal{N} \int \mathcal{D}\varphi_1 \, \mathcal{D}\varphi_2 \exp\left[i \int_{-\infty}^{\infty} d^4x \left(\mathcal{L}_0(\varphi_1(x)) - \mathcal{L}_0(\varphi_2(x))\right)\right.$$
$$-i \int_{-\infty}^{\infty} d^4x \left(\mathcal{V}(\varphi_1(x)) - \mathcal{V}(\varphi_2(x))\right)$$
$$\left. +i \int_{-\infty}^{\infty} d^4x \left(J_1(x)\varphi_1(x) - J_2(x)\varphi_2(x)\right)\right] . \quad (2.30)$$

The free part of the generating functional after integrating can be written as,

$$Z_C[\beta; J] = \mathcal{N} \int \mathcal{D}\varphi_1 \, \mathcal{D}\varphi_2 \exp\left[-\frac{1}{2} \int_{-\infty}^{\infty} d^4x \, d^4x' \varphi_a(x)(G_F^{-1})_{ab}(x-x')\varphi_b(x')\right.$$
$$-i \int_{-\infty}^{\infty} d^4x \left(\mathcal{V}(\varphi_1(x)) - \mathcal{V}(\varphi_2(x))\right)$$
$$\left. +i \int_{-\infty}^{\infty} d^4x \left(J_1(x)\varphi_1(x) - J_2(x)\varphi_2(x)\right)\right] , \quad (2.31)$$

where G_{ab}^F is the Green's function for the free theory. Now, using Eq. 2.27 into Eq. 2.31 we obtain the perturbative expansion of the generating functional as

$$Z_C[\beta; J] = \mathcal{N}' \exp\left[-i \int_{-\infty}^{\infty} d^4x \left(\mathcal{V}\left(\frac{\delta}{i\delta J_1(x)}\right) - \mathcal{V}\left(\frac{\delta}{i\delta J_2(x)}\right)\right)\right]$$
$$\exp\left[-\frac{1}{2} \int_{-\infty}^{\infty} d^4x \, d^4x' J_a(x)G_{ab}^F(x-x')J_b(x')\right] . \quad (2.32)$$

With the definitions of Eq. 2.20 and Eq. 2.25 the functional derivative can now be written down as

$$\frac{\delta J_a(x)}{\delta J_b(x')} = \delta_{ab} \delta^{(4)}(x-x') . \quad (2.33)$$

The Green's Function of the theory hence can be written down as,

$$G_{a,b}^F(x-y) = \frac{1}{Z_C[\beta; J]} \frac{\delta^2 Z_C[\beta; J]}{i^2 \, \delta J_a(x) \, \delta J_b(y)}\bigg|_{J_a, J_b=0} . \quad (2.34)$$

Now from above equation it can be seen that the thermal propagator takes a matrix form.

From Eq. 2.31 it can be noted that the doubling of field has happened. The φ_1 fields which live on the C_1 part of the contour are 'physical' fields, and can occur on both the internal and external lines of Green's function. Whereas φ_2 fields live on the C_2 part of the contour, and are to be interpreted as 'ghost' fields and can occur *only* on the internal lines of Green's function. The off-diagonal elements of the Green's function refer to the propagators related to different field types.

2.2.1   The propagators

Using the results of previous section, we express the Feynman rules for the propagators related to corresponding theories here. We will specify the Feynman rules in metric convention $g^{\mu\nu} = \eta^{\mu\nu} = diag(1, -1, -1, -1)$, and for symmetric choice $\sigma = \beta/2$ of the Schwinger-Keldysh contour. In our future discussions we will be interested in analysis of the structure of matrix elements involving multiple number of particles. We will use placeholders for characterizing vertex numbers in those general cases. Let two placeholders for the particular vertex numbers be i and j, with the thermal types t_i, t_j referring to the thermal types of particles at vertex i and j respectively; $t_i, t_j = (1, 2)$ depending on the particular thermal type. Hence, for those cases with zero chemical potential the Feynman rules in momentum space are specified as follows.

For a scalar having momentum p and mass m_ϕ, the Feynman rules for propagators are given by

$$iS^{t_i, t_j}(p, m_\phi) = \begin{pmatrix} \Delta(p) & 0 \\ 0 & \Delta^*(p) \end{pmatrix} + 2\pi\delta(p^2 - m_\phi^2) N_{\rm B}(|p^0|) \begin{pmatrix} 1 & e^{|p^0|/(2T)} \\ e^{|p^0|/(2T)} & 1 \end{pmatrix}, \quad (2.35)$$

where $\Delta(p) = i/(p^2 - m_\phi^2 + i\epsilon)$, and $N_{\rm B}(|p^0|)$ is the distribution function for bosons,

$$N_{\rm B}(|p^0|) \equiv \frac{1}{\exp\{|p^0|/T\} - 1} \quad . \quad (2.36)$$

25

After using the gauge fixing and then evaluating the Green's functions for photon having momentum k, the photon propagators in the Feynman gauge can be written down as,

$$i[D^{\mu\nu}]^{t_a,t_b}(k) = -g^{\mu\nu}iD^{t_a,t_b}(k) \tag{2.37}$$

where,

$$iD^{t_i,t_j}(k) = \begin{pmatrix} \Delta(k) & 0 \\ 0 & \Delta^*(k) \end{pmatrix} + 2\pi\delta(k^2)N_\text{B}(|k^0|)\begin{pmatrix} 1 & e^{|k^0|/(2T)} \\ e^{|k^0|/(2T)} & 1 \end{pmatrix}. \tag{2.38}$$

In the above equation $\Delta(k) = i/(k^2 + i\epsilon)$, which is written in accordance with Eq. 2.35 for massless photons, and $N_\text{B}(|k^0|)$ is the the distribution function for photons. Therefore,

$$i[D^{\mu\nu}]^{t_i,t_j}(k) = -g^{\mu\nu}iD^{t_i,t_j}(k) = -g^{\mu\nu}\,iS^{t_i,t_j}(k,0)\,. \tag{2.39}$$

After using the Grassmann algebra for fermions and then evaluating the Green's functions for fermions having momentum p and mass m_f, the fermionic propagators in real time formulation can be expressed as,

$$iF^{t_i,t_j}(p,m_f) = \begin{pmatrix} F & 0 \\ 0 & F^* \end{pmatrix} - 2\pi F'\delta(p^2 - m_f^2)N_\text{F}(|p^0|)\begin{pmatrix} 1 & \epsilon(p_0)e^{|p^0|/(2T)} \\ -\epsilon(p_0)e^{|p^0|/(2T)} & 1 \end{pmatrix},$$

$$\equiv (\not{p} + m_f)\begin{pmatrix} F_p^{-1} & G_p^{-1} \\ -G_p^{-1} & F_p^{*-1} \end{pmatrix}, \tag{2.40}$$

where $F = i/(\not{p} - m_f + i\epsilon)$, and $F' = (\not{p} + m_f)$. From the above expression it can be noted that the full fermion propagator is proportional to $(\not{p} + m_f)$. Here $N_\text{F}(|p^0|)$ corresponds to the distribution function of the fermion,

$$N_\text{F}(|p^0|) \equiv \frac{1}{\exp\{|p^0|/T\} + 1}\,. \tag{2.41}$$

In the above Eq. 2.35, Eq. 2.38 and Eq. 2.40, the first and second part respectively corre-

spond to the quantum fluctuation and the medium induced thermal parts for the relevant propagators $iS^{t_i,t_j}(p, m_\phi)$, $iD_{\mu\nu}^{t_a,t_b}(k)$ and $iF^{t_i,t_j}(p, m_f)$.

2.2.2   The interaction vertex factors

From the expression of Eq. 2.31 it is evident that the internal vertices in the perturbative expressions can be of two types. The first kind of vertex has all the particles with thermal type-1 and for the second kind the vertex has only thermal type-2 particles. It is also evident from Eq. 2.31 that a particular vertex has only the fields of one particular thermal type. The mixing of the fields only happen through the off-diagonal elements of the thermal propagators. It can be also realized from Eq. 2.31 that the contribution for the thermal type-1 and thermal type-2 vertices are opposite of each other.

In the upcoming discussions we will be interested in charged fermions and charged scalars interacting with photons. All possible allowed insertion vertices for a theory of fermions and scalars interacting with photons has been shown in Fig. 2.2 (where fermions, scalars and photons have been denoted by respectively single solid, dashed and wiggly lines). For the fermions only trilinear (fermion-photon-fermion) insertion is allowed. For the theories involving charged scalars, in addition to trilinear (scalar-photon-scalar) insertion vertices, quadrilinear seagull (scalar-scalar-photon-photon) insertion vertices are also allowed.

| a. Trilinear Fermionic Vertex | b. Trilinear Scalar Vertex | c. Quadrliniear Seagull Vertex |
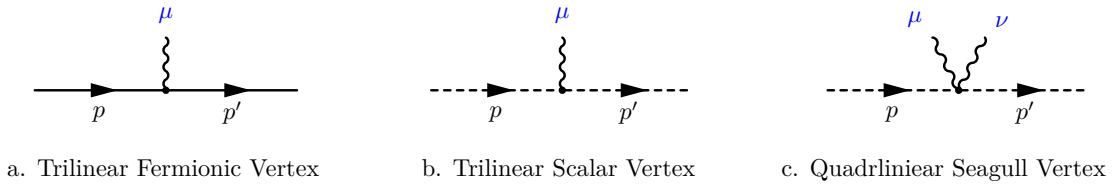
Figure 2.2: *All possible allowed insertion vertices for charged fermions and scalars interacting with photons.*

The fermion-photon-fermion trilinear insertion vertex has a contributing factor $(-ie\gamma_\mu)(-1)^{t_\mu+1}$, where $t_\mu = 1, 2$ according to the thermal type (type 1 or 2) of vertices.

The scalar-photon-scalar trilinear insertion vertex has a contributing factor $[-ie(p_\mu + p'_\mu)](-1)^{t_\mu+1}$, where p_μ and p'_μ are the four momenta of the scalar entering and leaving the insertion vertex.

The scalar-scalar-photon-photon quadrilinear seagull insertion vertex has a contributing factor of $[+2ie^2 g_{\mu\nu}](-1)^{t_\mu+1}$. It also has to be noted that the seagull vertices has an overall opposite relative sign with respect to trilinear scalar-photon-scalar insertion vertices. This sign, as well as the factor of 2, will play an important role in our calculations.

For the bino-scalar-fermion insertion vertex, the contributing factor at an insertion vertex V is denoted by Γ_V. The Feynman rules for Majorana particles at this kind of insertion vertex at zero temperature are given in Ref. [124,125]. These Feynman rules apply as well for type-1 thermal bino vertex; and for type-2 vertices we have to account for an overall negative sign.

All these Feynman rules are collected in the Appendix A for convenience.

2.3   Infrared structure of field theories at finite temperature

From Eq. 2.35, Eq. 2.38 and Eq. 2.40 it can be noticed that the medium induced thermal part of the propagators always accompany a distribution function in accordance to their spin, as expressed in Eq. 2.36 and Eq. 2.41. Now if the particles are nearly massless and their momenta are soft, then, for fermions the Infrared (IR) behaviour of the distribution function becomes

$$N_{\mathrm{F}}(|p^0|) \equiv \frac{1}{\exp\{|p^0|/T\} + 1} \xrightarrow{p^0 \to 0} \frac{1}{2} , \qquad (2.42)$$

which is finite and converges in the IR limit. But for the massless bosons such as photons the bosonic distribution function in the photon propagator in the soft limit contributes an

28

additional power of $|k^0|$ in the denominator

$$N_{\rm B}(|k^0|) \equiv \frac{1}{\exp\{|k^0|/T\} - 1} \xrightarrow{k^0 \to 0} \frac{T}{|k^0|} \; . \tag{2.43}$$

The contribution diverges in the IR limit. Thus it can be realized for the theories involving massless bosons such as photons, the leading IR divergence is linear due to thermal fluctuations in addition to logarithmic IR divergence which was already present due to quantum fluctuations Ref. [41, 126]. There is also residual sub-leading logarithmic IR divergence arising from the thermal fluctuations. Thus taming the IR divergences in the thermal field theory is much nontrivial and challenging than at zero temperature. The discussions of following chapters will focus on the issue of mitigating the apparent violent IR divergence problem.

We also note here that the distribution functions (both fermionic and bosonic) are well behaved in the Ultraviolet (UV) limit and act as a natural cut-off for any momentum p of the order of temperature T of the system. Thus the loop integrals involving fermions and bosons will have an effective cut-off at scale $O(T)$. As the medium does not invoke any new UV divergences in thermal field theory Ref. [127], thus the available tools related zero temperature UV renormalization is well applicable for thermal systems also.

2.4   Summary

Thermal field theory provides a framework for dealing with many body systems where particles are interacting among themselves. Due to this interaction in addition to quantum fluctuations, statistical fluctuations also become very important in thermal system. We briefly discuss the general properties of thermal systems and make a note that the Boltzmann operator in thermal equilibrium has a formal similarity with time evolution operator if inverse temperature can be identified with imaginary time argument. After that, we have focused our attention to real time formulation of thermal field theory, and have briefly pre-

sented the formulation of it arriving at the Schwinger-Keldysh contour. It has been found that field doubling has occurred, resulting in type-1 and type-2 fields. Whereas type-1 'physical' field can arise on both the internal and the external lines, the type-2 'ghost' fields can arise only on the internal lines. The propagators have taken 2×2 matrix form where the off-diagonal elements convert the fields of one type to another. The number of vertices also have doubled, having only similar type fields at a particular type of vertex. In the real time formulation the effect of the medium inducing thermal fluctuations are found to be separated out in the propagators. The part corresponding to the medium have been found to be proportional to distribution functions of the particle type (fermions or bosons) depending on their spin. The IR behaviour of the fermions were found to be well behaved in the soft limit, whereas the IR behaviour of massless bosons worsen in the soft limit. For massless bosons the leading IR behaviour turns out to be linear in thermal fluctuations in addition to already present logarithmic quantum fluctuations. There is also a sub-leading logarithmic IR divergence arising due to thermal fluctuation. Managing this violent IR structure will be our main motive of discussion in the following chapters.

Chapter 3

The technique of Grammer and Yennie to identify infrared structures

3.1 Prologue

The subject concerning Infrared (IR) structure of fermionic QED at zero temperature has a rich history. The conceptual intricacies related to the IR structure have been well understood in different formalisms. It has been well understood that, *a sufficiently inclusive observable cross-section* Ref. [4] in fermionic QED is free from any infrared divergences. There have been development of separate techniques and formalisms; involving summing over sets of diagrams (resulting sets of integrals) which when taken together is shown to be IR finite by Yennie, Frautschi and Suura (henceforth referred as YFS) Ref. [10], to reformulation of QED in terms of dressed coherent asymptotic states Ref. [16–24] . Although these techniques and reformulations have certainly increased the foundational insights about the subject; the results from these are often very hard to incorporate in practical calculations in perturbative theory. This difficulty has been resolved via a convenient technique formulated by Grammer Jr. and Yennie (henceforth referred as GY) in the classic paper Ref. [12] . GY in their technique have rewritten and rearranged the

photon polarization sums of both real and virtual photons to a sum of two modified photon polarizations; namely, K and G type polarization sums.

They have shown that, by construction, all the IR divergent terms are *only* contained in K type virtual and real polarization sums. When summed over all possible photon insertions, these IR divergent pieces factor out and can be exponentiated. Furthermore, the cancellation of those IR divergent pieces of K type polarization sums were shown to happen order by order to all orders in pertubation theory. The fascinating result that GY have also proved is, the G type polarization sums for both virtual and real photons *for every term* (*diagram*) are IR finite, which can be readily used in perturbation theory to get IR finite results. And, qualitatively to see the IR finiteness of these G type polarization sum terms, the actual momentum integrals need not to be performed; but the IR finiteness of these terms can be realized simply by gazing at the corresponding terms [1].

We will review the main features of GY technique at zero temperature in the next section, so that the generalization of this technique to finite temperature in Chapter 4 and then the use of those finite temperature techniques in Chapter 5 and Chapter 6 becomes convenient to follow.

3.2   Features of GY techniques and modification of polarization sums

We start with an overview of the basic technique of GY for correctly identifying the IR structure of a general process; beginning with an elastic scattering of a fermion due to an external local potential (need not be an electromagnetic potential) at leading order (in local potential) denoted by, $f(p)\gamma^*(q) \to f(p')$ shown pictorially in Fig. 3.1 .

---

[1]Obviously, to get the quantitative results from these IR finite terms, one has to explicitly perform momentum integrals.
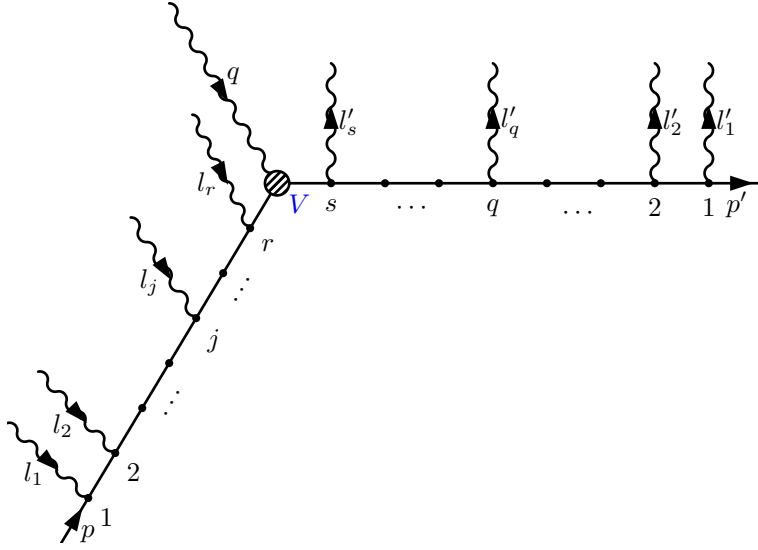
Figure 3.1: *A typical diagram of nth order for the process $f(p)\gamma^*(q) \to f(p')$, with particularly r and s photon vertices on respectively p and p' leg, with $r + s = m$.*

Fig. 3.1 corresponds to an nth order process [2] in electromagnetic interactions and leading order in local external potential (denoted by vertex V in Fig. 3.1). Here, in this chapter the external potential is explicitly an electromagnetic interaction (as we are speaking of process $f(p)\gamma^*(q) \to f(p')$), and that is denoted by wavy photon line bringing in *hard momentum q* at the vertex V. We will see in later chapters (Chap. 6) that, as the technique of GY does not depend on the specific nature of external potential, hence we will be provided the firm-base to use the technique consistently for the applications related to dark matter in Chap. 6.

We will examine the effect of adding an additional photon (be it virtual or real) in all possible ways to this n^{th} order process. We will find that after using symmetries (Feynman

---

[2] Here, we define the nth order process in a generic way, where by n^{th} order we mean that the corresponding matrix element should contribute at $O(e^{2n})$ or $O(\alpha^n)$ to the cross-section at the leading order, *i.e.*, if all the vertices on Fig. 3.1 should correspond to virtual photons then $\mathcal{M}_0^\dagger \mathcal{M}_n^{\text{all−virtual}} \approx O(e^{2n})$ (where $\mathcal{M}_0$ corresponds to the contribution from tree level diagrams) and if all the vertices correspond to the real photon insertions then $|\mathcal{M}_n^{\text{all−real}}|^2 \approx O(e^{2n})$, and accordingly generalizing this understanding for diagrams containing an admixture of arbitrary number of real and virtual photons. The bottom-line is that the diagrams corresponding to a particular order of α which are present in the squared matrix element have to be always considered together to find and see IR divergence cancellation. This fact will be of fundamental importance in succeeding chapters when charged scalars are also involved, as then we can have seagull insertions and tadpole diagrams (in addition to normal *fermion-photon-fermion* vertex); both of which will contribute a factor of e^2 per vertex to the matrix element.

identities) of the problem, the higher order matrix element (for K type polarization sums) will factorize to lower n^{th} order matrix element times IR divergent factors. These, IR divergent factors then can be resummed and will be shown to cancel order by order between K type virtual and real photon contributions.

Now, we will come to the notations related to Fig. 3.1. The fermion lines can be distinctively classified into two groups depending on whether that line comes *before or after* the interaction with external potential exchanging the *hard momenta q* . The fermion line which comes before the interaction with external potential at V is denoted as *incoming line* or p-leg (*to the left of the vertex V*) and the one which continues after the interaction with external potential at V is denoted as *outgoing line* or p'-leg (*to the right of the vertex V*). Henceforth, *any additional photon insertion* to this n^{th} order diagram will always be denoted and classified by the insertion on p or p' leg depending on whether the insertion is on respectively the *initial* or *final* fermion line.

The photons which are already present in the nth order diagram, see Fig. 3.1, leave the p' leg with momenta l'_q at vertices q, with $q = 1, \cdots, s$ and enter the p leg with momenta l_j at vertices j, with $j = 1, \cdots, r$ [3]. We have to also remind ourselves that this choice of photon momentum direction is just a convenient form of book-keeping without loss of any generality. According to this notation, the momentum of the fermion line to the *left* of the qth vertex on the p' leg becomes $(p' + \Sigma_{i=1}^{q} l'_i) \equiv (p' + \Sigma_q)$; and the momentum of the fermion line to the *right* of the jth vertex on the p leg reads $(p + \Sigma_{i=1}^{j} l_i) \equiv (p + \Sigma_j)$. Therefore, we will denote $F_{p+\Sigma_{j-1}}$ for a fermionic propagator on the p leg from vertex $j - 1$ to j having momentum $p + \Sigma_{i=1}^{j-1} l_i$; and $F_{p'+\Sigma_{q-1}}$ denotes a fermionic propagator from vertex $q - 1$ to vertex q, corresponding to a momentum flow[4] $p' + \Sigma_{i=1}^{q-1} l'_i$.

Now, if this n^{th} order diagram has one or more *virtual* photons, which rejoin at some vertex

---

[3] We will always use the same notation $l'(l)$ for photon momenta associated with particularly $p'(p)$ -leg *for all the upcoming chapters*.

[4] For the cases of scalar propagators in subsequent chapters F will be replaced by S; and for thermal cases these propagators will also carry additional thermal indices denoting thermal type of vertex (denoted in the superscripts) as F^{t_x,t_y} and S^{t_x,t_y} in addition to momentum identifier which will be always denoted in the subscripts of the propagators.

in the fermion line; then three possibilities may arise: virtual photon between p and p' leg, or virtual photon having both the end points on same leg, *i.e.*, both on p or both on p' leg. Now, supposing the virtual photon has k as its momentum, and is inserted at vertices x and y, the momentum k can be identified depending on the insertions being on the p' or p legs as,

- x belongs to p-leg and y belongs to p'-leg then, $k = l'_y = l_x$;

- x and y both belong to p'-leg then, $k = l'_y = -l'_x$;

- x and y both belong to p-leg then, $k = l_y = -l_x$;

where, in the above expression, the photon momenta k, l_x and l'_y correspond to four vectors and we have suppressed the Lorentz indices related to l (l')'s .
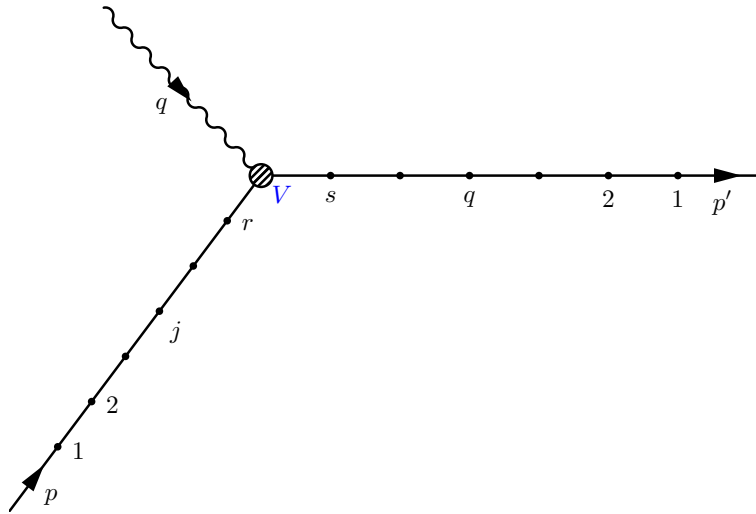
Figure 3.2: *Schematic diagram of an* n^{th} *order process* $f(p)\gamma^*(q) \rightarrow f(p')$*, which is exactly same as representing Fig. 3.1, but where* already present *photon lines have been suppressed to conveniently* focus only *on the all possible ways of new photon (real or virtual) insertions to* n^{th} *order diagram.*

All the notations which have been set up in last few paragraphs will be generically true and similar for the upcoming chapters. We now want to suppress all *already present* photon lines which were dangling in Fig. 3.1 to be newly represented as in Fig. 3.2 where all

the dots on the fermion line actually and *faithfully* represent *all already present* fermion-photon interaction vertices[5]. These suppression has been done to conveniently track all the possible ways of insertions of an *additional new* photon (real or virtual) to the nth order diagram. Moreover, whenever an nth order diagram of similar type appear in subsequent discussion, it should be understood that all the notations that have been set up in last few paragraphs *hold true* for those cases also.

3.2.1 Modification and rearrangement of polarization sums

To unambiguously and correctly identify the IR divergent and finite contributions arising from a virtual photon insertion, the polarization sum $-g^{\mu\nu}$ in the photon propagator will be modified to sum of two rearranged terms, such that all the IR divergent pieces are contained in one term, and the other term contains the IR finite pieces.

To attain this for the cases of virtual photons the photon propagator will be rearranged as,

$$-i\frac{g^{\mu\nu}}{k^2 + i\epsilon} = \frac{-i}{k^2 + i\epsilon} \left\{ \left[g^{\mu\nu} - b_k(p_f, p_i) \, k^\mu k^\nu \right] + \left[b_k(p_f, p_i) k^\mu k^\nu \right] \right\}$$

$$\equiv \frac{-i}{k^2 + i\epsilon} \left\{ [G] + [K] \right\} . \tag{3.1}$$

Here, $b_k(p_f, p_i)$ is defined as in the following expression, to separate out all the IR divergences correctly *only* at zero temperature [6],

$$b_k(p_f, p_i) = \begin{cases} \dfrac{(2p_f - k) \cdot (2p_i - k)}{(k^2 - 2p_f \cdot k)(k^2 - 2p_i \cdot k)} & , \text{ if } p_i \neq p_f . \\[4mm] \dfrac{1}{2} \left[\dfrac{(2p_f - k) \cdot (2p_i - k)}{(k^2 - 2p_f \cdot k)(k^2 - 2p_i \cdot k)} + (k \leftrightarrow -k) \right] & , \text{ if } p_i = p_f . \end{cases} \tag{3.2}$$

---

[5]In the above diagram Fig. 3.2 the dots refer to fermion-photon-fermion vertices. In the upcoming chapters, in the presence of charged scalars a particular dot will *either* refer to an *already present* trilinear scalar-photon-scalar vertex or to an *already present* quadrilinear seagull type scalar-scalar-photon-photon vertex of nth order diagram. Hence, in succeeding chapter we will specify how to tackle this kind of special situation.

[6]The definition of b_k has to be modified at finite temperature case to correctly identify the IR divergent pieces.

In the above expression, b_k depends on the relevant photon momentum k and also on the momenta, p_f, p_i. Here, p_i (p_f) refers to the momentum p or p' depending on whether the initial (final) vertex of the $(n+1)^{\text{th}}$ photon is inserted on the p or p'-leg.

In order to incorporate the effect of the rearrangement in Eq. 3.1, every new virtual photon insertion will now be re-expressed as sum of K and G terms (Henceforth, for convenience these will be referred to as K and G type photons). These K and G photons have to be inserted symmetrically, over already symmetrized n^{th} order diagrams. Consider the insertion of an additional virtual photon with momentum k at vertices μ, ν in an already symmetrised n^{th} order diagram. The factor $k^\mu k^\nu$ from the K photon insertion combines with the vertex factors that are proportional to $\gamma_\mu \gamma_\nu$ to give a factor of $\gamma_\rho k^\rho = \slashed{k}$ at *each* vertex. These vertex factors can be simplified using Feynman identities. It turns out that these contributions from a K photon insertion can be expressed as the *difference* of two terms. Insertion of K photons in all possible ways will then result in a *collection* of such terms. When contributions from all possible insertions of the virtual photon are included, these terms will have pair-wise cancellation among different contributions. This results in the higher $(n+1)^{\text{th}}$ order contribution arising due to K photon insertions to be proportional to the lower n^{th} order contribution times the *factored out* IR divergent contributions coming from the K photon insertions.

For real photon insertions an analogous rearrangement of polarization sums can be performed in the square of the matrix element. The polarization sums can be denoted as $\widetilde{K}$ and $\widetilde{G}$ (here tildes have been used to differentiate the real from the virtual photon contributions) which are identified through the following term arising in the *square* of the matrix element, viz.,

$$
\begin{aligned}
\sum_{\text{pol}} \epsilon_\mu^*(k)\, \epsilon_\nu(k) \;&=\; -g_{\mu\nu}\,, \\
&=\; -\left\{ \left[g_{\mu\nu} - \tilde{b}_k(p_f, p_i)k_\mu k_\nu \right] + \left[\tilde{b}_k(p_f, p_i)k_\mu k_\nu \right] \right\}, \\
&\equiv\; -\left\{ \left[\widetilde{G}_{\mu\nu} \right] + \left[\widetilde{K}_{\mu\nu} \right] \right\},
\end{aligned}
\qquad (3.3)
$$

where $\tilde{b}_k(p_f, p_i)$ is defined [12] to correctly identify IR divergent and finite pieces from real photon insertions:

$$\tilde{b}_k(p_f, p_i) = \frac{p_f \cdot p_i}{k \cdot p_f \; k \cdot p_i} \; . \tag{3.4}$$

Here, p_f (p_i) correspond to the momentum p' or p based on whether the real photon was inserted on the p' or p-leg of the matrix element $\mathcal{M}$ ($\mathcal{M}^\dagger$). With similarity to the virtual photon case it can be shown that the IR divergent pieces are all contained in the $\widetilde{K}$ photon contributions. GY have proved that the cross-section corresponding to the higher order $\widetilde{K}$ photon is proportional to the lower order cross-section times *factored out* IR divergent pieces. The IR finiteness of the cross section is then proven by showing that the IR divergent factors coming from virtual K and real $\widetilde{K}$ photons cancel among themselves order by order in perturbation theory.

The matrix element corresponding to virtual G photons, and the cross-section related to the real $\widetilde{G}$ photons are found to be IR finite for every separate diagram and hence can be used successfully in the context of perturbation theory.

3.2.2   Effect of rearranging matrix element in terms of $K, \widetilde{K}$ and $G, \widetilde{G}$ polarizations

We will consider the higher order corrections to the nth order process corresponding to $f(p)\gamma^*(q) \to f(p')$ (where, $p + q = p'$), which have been represented in both the Fig. 3.1 and Fig. 3.2. To understand the effect of separating the K and G photon polarizations, we will simply start with an nth order diagram, of which all the *already present* photon vertices correspond to virtual photons without loss of any generality (which can be easily extended to a process having arbitrary admixture of real and virtual photons).

The matrix element related to zeroth order (tree level) process denoting $f(p)\gamma^*(q) \to$

$f(p')$ is represented by the matrix element,

$$i\mathcal{M}_0^{\text{fermion}} = [\bar{u}_{p'}\,\Gamma_V\,u_p]\ ,\tag{3.5}$$

where $\Gamma_V = -ie\gamma_{\mu_V}$ for the case in which the external potential is the electromagnetic potential interacting with charged fermion f.

Now, consider the nth order diagram having n virtual photons with s number of vertices on the p'-leg and r number of vertices on the p-leg, such that $r + s = m = 2n$. The matrix element corresponding to this process can be expressed generically as,

$$\begin{aligned}
i\mathcal{M}_n^{\text{fermion}} &= (-ie)^{2n}(i)^m \times \left[\bar{u}_{p'}\gamma_{\mu_1}F_{p'+\Sigma_1}\,\gamma_{\mu_2}F_{p'+\Sigma_2}\,\cdots\,\gamma_{\mu_{s-1}}F_{p'+\Sigma_{s-1}}\,\gamma_{\mu_s}F_{p'+\Sigma_s}\right] \\
&\quad \times\ \Gamma_V \times \left[F_{p+\Sigma_r}\gamma_{\nu_r}F_{p+\Sigma_{r-1}}\gamma_{\nu_{r-1}}\cdots F_{p+\Sigma_1}\gamma_{\nu_1}u_p\right] \times \mathcal{D}^{\mu_1,\cdots,\mu_s;\nu_r,\cdots,\nu_1}\ , \\
&\equiv\ (-ie)^{2n}(i)^m \times \left[C_s^{p'}\right] \times \Gamma_V \times [C_r^p] \times \mathcal{D}_n\ .
\end{aligned}\tag{3.6}$$

In the above expression, C_r^p and $C_s^{p'}$ correspond to the contributions to the matrix element resulting from respectively p and p'-leg (which are denoted in the superscripts) and the subscripts on the C contributions denotes the exact number of vertices with photon insertions present on the related contribution (subdiagram) as pictorially represented in Fig. 3.2. Here, Γ_V factor again represents the contribution arising from interaction with external local potential. In Eq. 3.6 every vertex contributes a factor of $(-ie)$, and we have separated out a factor of (i) contributing from each propagator F [7].

While, writing Eq. 3.6 it was assumed all photon insertions were virtual photons[8], and

---

[7] Although, in this *particular* case, $m = 2n$, *i.e.*, the number of fermionic propagators and fermion-photon-fermion vertices are equal; but in a generic diagram these numbers can be quite different. For a case where charged scalars is involved, the number of vertices and propagators can be quite different even though all the vertices consist of virtual photons, due to the presence of seagull vertices and tadpole diagrams. Hence, the above notation has been chosen generically in accordance with what is to follow in succeeding chapters.

[8]If any real photon insertion was present in the nth order process, the analogous definition still holds, as the GY technique is performed at the *square* of matrix element level (in presence of any real photon), and therefore the number of vertices are still even, and generalisation of the above definition can be readily obtained in later discussions wherever applicable.

the contribution arising from photon propagators $\mathcal{D}_n$, is represented by a product over n terms,

$$\mathcal{D}_n \equiv \mathcal{D}^{\mu_1,\cdots,\mu_s;\nu_r,\cdots,\nu_1} = \prod_{\{\alpha\beta\}} \int \frac{\mathrm{d}^4 k_\alpha}{(2\pi)^4} \left[\frac{-i g^{\alpha\beta}}{k_\alpha^2 + i\epsilon} \right]. \tag{3.7}$$

Here, α, β denote any two among the dummy indices $\mu_1, \cdots, \mu_s; \nu_1, \cdots, \nu_r$, designating the vertices (whether on the p or the p'-legs) where the virtual photon is inserted, and the contribution is symmetrized over all possible allocations of α and β.

Effect of K photon insertion : A virtual K photon having momentum k is inserted on the nth order matrix element at vertices μ and ν (the notation μ, ν has to be understood according to the concerned discussion; it can be used as a placeholder denoting the vertices where the new photon is inserted; or μ and ν can be also used as Lorentz indices related to the four vectors (or tensors) such as J^μ, γ^μ, k^μ, $g^{\mu\nu}$ etc. denoting currents, photon momentum, polarization sum related to vertices with vertex number *placeholder μ and ν*. This same notation μ and ν has been used, as we do not want produce cumbersome over-complicated expressions in following chapters, and the notation should be understood sensibly depending on the particular situation). The photon is inserted in a way so that momentum k *leaves* at the vertex μ and *enters* back at the vertex ν. The new K photon can be inserted in three possible ways; such that the endpoints of K photon is each on (different) p and p'-leg, or the other two cases, where the endpoints are on same (both on p or both on p') leg. We will start with the first case when the inserted new K photon vertices are on different legs[9].

If the ν vertex is inserted to the *left* of vertex j on the p leg and μ vertex is inserted to the *right* of vertex q on the p' leg, then the photon momenta flows though all the fermion propagators in between and all the other propagator momenta are unchanged. That is, all

---

[9]Since, it is the simplest of three possibilities, and hence to understand the basic technique involved. As in other two cases (both the vertices are on same leg) we have to be cautious not to double count the new vertices, and will discuss about this in upcoming chapters.

the fermion propagators to the left of vertex ν has unchanged momenta, but all the fermion propagators to the right of vertex ν are shifted by an amount $+k_\nu$, *i.e.*, the momenta of the propagators to the right of vertex a on p-leg is given by $p + \sum_{i=1}^{a} l_i + k$, for $a \geq j$. And, similarly all the fermion propagators to the right of vertex μ has unchanged momenta, but all the fermion propagators to the left of vertex μ are shifted by an amount $+k_\mu$; *i.e.*, the propagator momenta for the left of vertex b on p'-leg is given by $p' + \sum_{i=1}^{b} l'_i + k$, for $b \geq q$. With this understanding, the matrix element after attaching new photon is represented by,

$$
i\mathcal{M}_{n+1}^{\text{fermion};p',p} = (-ie)^{2n+2}(i)^{m+2} \times
$$

$$
\left[\bar{u}_{p'} \gamma_{\mu_1} F_{p'+\Sigma_1} \cdots \gamma_{\mu_{q-1}} F_{p'+\Sigma_{q-1}} \gamma_\mu F_{p'+\Sigma_{q-1}+k} \gamma_{\mu_q} \cdots F_{p'+\Sigma_{s-1}+k} \gamma_{\mu_s} F_{p'+\Sigma_s+k} \right]
$$

$$
\times \Gamma_V \times \left[F_{p+\Sigma_r+k} \gamma_{\nu_r} \cdots \gamma_{\nu_j} F_{p+\Sigma_{j-1}+k} \gamma_\nu F_{p+\Sigma_{j-1}} \gamma_{\nu_{j-1}} \cdots F_{p+\Sigma_1} \gamma_{\nu_1} u_p \right]
$$

$$
\times \mathcal{D}^{\mu,\nu;\mu_1,\cdots,\mu_s;\nu_r,\cdots,\nu_1} ,
$$

$$
= (-ie)^{2n+2}(i)^{m+2} \times \left[C_{s+1}^{p';\mu} \right] \times \Gamma_V \times \left[C_{r+1}^{p;\nu} \right] \times \mathcal{D}_{n+1}^{\mu\nu} , \tag{3.8}
$$

Here, $C_{s+1}^{p';\mu}$ ($C_{r+1}^{p;\nu}$) represents corresponding contributions arising from $p'(p)$-leg, on which there are now '$s + 1$' ('$r + 1$') number of vertices, and the new vertex μ (ν) insertion of photon is on $p'(p)$-leg.

The contribution from the newly inserted photon propagator is

$$
\mathcal{D}_{n+1}^{\mu\nu} \equiv \mathcal{D}^{\mu,\nu;\mu_1,\cdots,\mu_s;\nu_r,\cdots,\nu_1} = \int \frac{\mathrm{d}^4k}{(2\pi)^4} \left[\frac{-ig^{\mu\nu}}{k^2 + i\epsilon} \right] \times \mathcal{D}^{\mu_1,\cdots,\mu_s;\nu_r,\cdots,\nu_1} ,
$$

$$
= \int \frac{\mathrm{d}^4k}{(2\pi)^4} \left[\frac{-ig^{\mu\nu}}{k^2 + i\epsilon} \right] \times \mathcal{D}_n , \tag{3.9}
$$

where $\mathcal{D}_n$ represents the contribution of the photon propagators from the underlying n^{th} order matrix element and only the contribution of the $(n+1)^{\text{th}}$ photon is explicitly shown. Using the definition of the K and G photon propagator from Eq. 3.1, the corresponding K

photon contribution from the Eq. 3.9 reads,

$$\left[\frac{-ig^{\mu\nu}}{k^2 + i\epsilon}\right]^K = \left[(-ib_k(p',p)k^\mu k^\nu) \times \frac{1}{k^2 + i\epsilon}\right].\tag{3.10}$$

Inserting the corresponding contribution of K photon from Eq. 3.10 to Eq. 3.8 we see the contribution to the matrix element for the two legs get factorized and hence can be evaluated independently of each other,

$$\mathcal{M}_{n+1}^{\text{fermion};p',p} \sim b_k(p',p)\left[k_\mu C_{s+1}^{p';\mu}\right] \times \Gamma_V \times \left[k_\nu C_{r+1}^{p;\nu}\right] \times \left[-i\frac{1}{k^2 + i\epsilon}\right] \times \mathcal{D}_n.\tag{3.11}$$

K photon insertion: contribution from the p'-leg : We will now focus on the effect of the K photon insertion on the p'-leg represented by $k_\mu C_{s+1}^{p';\mu}$ in Eq. 3.11. All possible ways of insertions of μ vertex on the p'-leg will contribute $(s+1)$ number of diagrams, which are represented schematically in Fig. 3.3. The first diagram corresponds to the new photon being inserted to the right of vertex '1'. The others correspond to the insertion of vertex μ to the right of vertex 2, 3, $\cdots$, s, V respectively, giving $s+1$ number of diagrams in all.
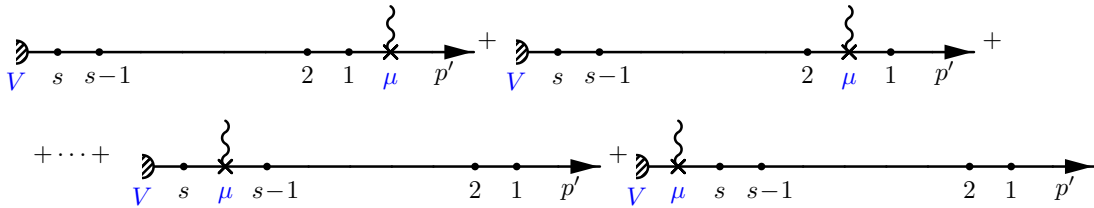
Figure 3.3: *All possible ways of insertions of a virtual K photon at vertex μ on p'-leg of a fermion of an nth order diagram, which on its p'-leg already has s vertices. The shaded (left most) vertex correspond to vertex V, and the p leg of the diagram is not shown.*

Before venturing to calculate the contribution of the whole set of diagrams, let us see the structure of a generic diagram of the set as schematically represented in Fig. 3.4.
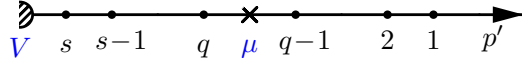
Figure 3.4: *A generic diagram of K photon insertion on the p′-leg, where μ vertex is between vertices q and q − 1 .*

The contribution of the diagram when μ is inserted to the left of vertex number $q - 1$ in Fig. 3.4 can be expressed as,

$$k_\mu \, C_{s+1}^{p';\,\mu\,\text{right of}\,q} = \bar{u}_{p'} \gamma_{\mu_1} \cdots \gamma_{\mu_{q-1}} \Big[F_{p'+\Sigma_{q-1}} \slashed{k} \, F_{p'+\Sigma_{q-1}+k} \Big] \cdots ,$$

$$= \bar{u}_{p'} \gamma_{\mu_1} \cdots \gamma_{\mu_{q-1}} \Big[F_{p'+\Sigma_{q-1}} - F_{p'+\Sigma_{q-1}+k} \Big] \cdots ,$$

$$\equiv M'_q - M'_{q-1} , \tag{3.12}$$

where in the Eq. 3.12 the term in the squared bracket turns into the difference of two terms using 'Feynman's Identity' [128–130], which reduces the term into a difference of two propagators as follows,

$$F_{p'+\Sigma_{q-1}} \, (\slashed{k}) \, F_{p'+\Sigma_{q-1}+k} = \left[\frac{1}{\slashed{p}' + \sum_{i=1}^{q-1} \slashed{l}_i - m_f} \, \slashed{k} \, \frac{1}{\slashed{p}' + \sum_{i=1}^{q-1} \slashed{l}_i + \slashed{k} - m_f} \right]$$

$$= \left[\frac{1}{\slashed{p}' + \sum_{i=1}^{q-1} \slashed{l}_i - m_f} - \frac{1}{\slashed{p}' + \sum_{i=1}^{q-1} \slashed{l}_i + \slashed{k} - m_f} \right]$$

$$= F_{p'+\Sigma_{q-1}} - F_{p'+\Sigma_{q-1}+k} . \tag{3.13}$$

Looking at the Eq. 3.12 we find that the particular contribution becomes the difference of two terms. A similar procedure can be performed for other terms also. Hence, the contribution of the diagrams for which μ vertex is inserted to immediate right of $q = 2$ to $q = V$ (last s diagrams of Fig. 3.3) is expressed as,

$$\sum_{q=2}^{V} k_\mu \, C_{s+1}^{p';\,\mu\,\text{right of}\,q} \equiv (M'_2 - M'_1) + (M'_3 - M'_2) + \cdots + (M'_{s+1} - M'_s) ,$$

$$\equiv - M'_1 + M'_{s+1} , \tag{3.14}$$

43

where in Eq. 3.14 'V' is the vertex (corresponding interaction with local external potential) to the immediate left of vertex number s. And, the contribution of the first diagram in Fig. 3.3 is,

$$k_\mu C_{s+1}^{p';\mu \, \text{right of 1}} = \bar{u}_{p'} \, \slashed{k} \, F_{p'+k} \gamma_{\mu_1} F_{p'+\Sigma_1 + k} \cdots \, ,$$

$$= \bar{u}_{p'} \gamma_{\mu_1} F_{p'+\Sigma_1 + k} \cdots \gamma_{\mu_{q-1}} F_{p'+\Sigma_{q-1}+k} \cdots \, ,$$

$$\equiv M_1' \, , \tag{3.15}$$

where we have used the fact that external fermion line is on-shell. This fact gives rise to a single term in Eq. 3.15 opposed to difference of two terms in Eq. 3.12. With the help of Eq. 3.14 and Eq. 3.15 we find the total contribution of the K photon insertion in the p'-leg is reduced to,

$$k_\mu C_{s+1}^{p';\mu} = (-M_1' + M_{s+1}') + M_1' \; = M_{s+1}' \, ,$$

$$= \left[\bar{u}_{p'} \, \gamma_{\mu_1} \cdots \gamma_{\mu_{q-1}} F_{p'+\Sigma_{q-1}} \cdots F_{p'+\Sigma_s} \right] \, ,$$

$$= C_s^{p'} \, , \tag{3.16}$$

Hence, after adding all the possible contributions of K photon insertion on the p'-leg, the result turns out to be proportional (apart from factors of $b_k(p', p)$ and e^2) to the lower order contribution $C_s^{p'}$. A similar exercise can be done for the p-leg, finding then that all the possible contributions of K photon insertion on the p-leg turns out to be proportional to the lower order contribution C_r^p.

$$k_\nu C_{r+1}^{p;\nu} = (M_V - M_r) + (M_r - M_{r-1}) + \cdots + (M_1 - M_0) = M_V \, ,$$

$$= \left[F_{p+\Sigma_r} \, \gamma_{\nu_r} \cdots F_{p+\Sigma_{j-1}} \, \gamma_{\nu_{j-1}} \cdots u(p) \right] \, ,$$

$$= C_r^p \, . \tag{3.17}$$

Hence, the total contribution of all possible K photon insertions in between p and p'-leg

turns out to be,

$$\mathcal{M}_{n+1}^{K\gamma;\,p'\,p} = -ie^2 \int \frac{\mathrm{d}^4k}{(2\pi)^4}\, b_k(p',p)\,\mathcal{M}_n \,. \tag{3.18}$$

After performing a similar exercise when both the insertions are on same leg (for when both the K photon vertex are on either p or p'-leg) we can write the total contribution Ref. [12] due to the insertion of K photon as,

$$\begin{aligned}
\mathcal{M}_{n+1}^{K\gamma,\mathrm{tot}} &= \frac{ie^2}{2} \int \frac{\mathrm{d}^4k}{(2\pi)^4} \left[b_k(p',p') - 2b_k(p',p) + b_k(p,p) \right] \mathcal{M}_n \,, \\
&\equiv \frac{ie^2}{2} \int \frac{\mathrm{d}^4k}{(2\pi)^4} \left[J^2(k) \right] \mathcal{M}_n \equiv [B]\,\mathcal{M}_n \,,
\end{aligned} \tag{3.19}$$

where all the IR divergences are now contained in the factored out B, which solely represents the contribution of inserted K photon contribution (which is logarithmically divergent for zero temperature case).

Effect of $\widetilde{K}$ photon insertion :   The contribution from insertions of real $\widetilde{K}$ photons to the nth order diagram can be similarly be factorized using the Feynman's identity in the square of the matrix element, giving rise to an expression,

$$\begin{aligned}
\left|\mathcal{M}_{n+1}^{\widetilde{K}\gamma,\mathrm{tot}}\right|^2 &\propto -e^2 \left[\tilde{b}_k(p,p) - 2\tilde{b}_k(p',p) + \tilde{b}_k(p',p') \right] \times \left|\mathcal{M}_n\right|^2 \\
&\equiv -e^2 \widetilde{J}^2(k) \left|\mathcal{M}_n\right|^2 \,,
\end{aligned} \tag{3.20}$$

where all the IR divergences have been now factored out into $\widetilde{J}^2(k)$. Now, it can be shown the IR divergent pieces arising from K and $\widetilde{K}$ cancel among themselves order by order in perturbation theory [12].

Effect of virtual G and real $\widetilde{G}$ photon insertions :   In the above discussions we have shown that the K and $\widetilde{K}$ photon contributions have IR divergent pieces. Now it is the time to show that the G and $\widetilde{G}$ tilde photons contributions do not have any IR divergent pieces

and are all IR finite.

GY have shown that, for the insertion of G photon to the nth order matrix element, when the μ vertex is inserted on p_f-leg and the ν vertex is inserted on the p_i-leg (where p_f, p_i belong to either p', p as in earlier discussion), as $k \to 0$, the dominant part of the the corresponding contribution reduces to terms in the numerator proportional to,

$$\mathcal{M}_{n+1}^{G\gamma, p_f, p_i} \sim \int \frac{\mathrm{d}^4 k}{(2\pi)^4} \frac{\left\{ g_{\mu\nu} - b(p_f, p_i) k_\mu k_\nu \right\} \left\{ \cdots p_f^\mu \cdots p_i^\nu \cdots \right\}}{(k^2)(p_f.k)(p_i.k)} \ . \tag{3.21}$$

Hence, the G photon contributions at zero temperature turn out to be proportional to,

$$\mathcal{M}_{n+1}^{G\gamma; \text{fermion}} \sim \left\{ g_{\mu\nu} - b(p_f, p_i) k_\mu k_\nu \right\} \times p_f^\mu p_i^\nu \ ,$$
$$= 0 + \mathcal{O}(k) + \text{higher order in } k \ , \tag{3.22}$$

where the leading IR divergence behaviour of the lower n^{th} order diagram was already known to be logarithmic, and can be easily relatable from Eq.3.21. After addition of virtual G-photon contribution the leading IR divergent term has become zero, as has been shown in Eq. 3.22. The next important term in numerator is $\mathcal{O}(k)$, which is IR finite (as at zero temperature the original divergence was *only* logarithmic making G photon contributions IR finite). The argument presented here only proves the fact that there are no leading IR divergences related to G photons, but there can be divergent subgraphs present in a Feynman diagram. GY have shown in Ref. [12] that the result of IR finiteness of G photons can be fruitfully extended to those cases also by looking at controlling set of momenta in skeletal graphs Ref. [12]. Hence, the G photon contributions are IR finite.

A similar exercise can be carried out to show that the real $\widetilde{G}$ photon contributions are also IR finite.

3.2.3 Final remarks

It has to be noted that, while rearranging the photon polarizations according to the technique of GY, we have not worsened the ultraviolet (UV) structure of the propagators. It should noted that in UV limit when photon momenta $k \gg p(p')$ the G photon propagators resembles the form of the photon propagator in Landau gauge. The K photon propagator then resembles a gauge transformation leading to zero contribution, after using Feynman's Identity Ref. [128].

We also have to note that, here we have only spoken about the simplest scattering due to external potential at a single vertex. The GY technique is well applicable to the processes involving multiple scattering from local external potential, to processes where charged fermionic loops are present and fermion to fermion scattering etc. The interested readers may look into Ref. [12] to find out that GY technique is well applied for these cases also.

We have presented the technique of GY in detail since we will adapt this technique to prove the IR finiteness of theories at finite temperature. We will show this systematically for different theories in the succeeding chapters.

3.3 Summary

The conceptual complexities related to infrared structure of fermionic QED at zero temperature have been understood quite well using different formalisms. In this chapter we were interested in the technique prescribed by Grammer and Yennie to identify the correct IR structure of fermionic QED. To identify the IR divergent and finite contributions unambiguously, the contributions of both the virtual and real photons have been rearranged into two terms. The effects of virtual photons were rearranged into K and G contribution terms in matrix element level. The effects of real photons were rearranged into $\widetilde{K}$ and $\widetilde{G}$ contribution terms in the cross section level. All the IR divergences were found to be

contained inside K and $\widetilde{K}$ terms, and G and $\widetilde{G}$ contributions were found to be IR finite. It has been also mentioned that the IR divergent pieces of K and $\widetilde{K}$ contribution terms cancel in the cross-section in the soft limit, making the theory of fermionic QED IR finite at zero temperature.

Chapter 4

Extension of technique of Grammer and Yennie to finite temperature

4.1 Prologue

In the previous chapter we have discussed about the prescription of the rearrangement of the polarization sum of the photon due to Grammer Jr. and Yennie [12], which produced a clear way of identifying IR divergent and finite pieces related to a process involving fermionic QED in perturbation theory at zero temperature. We have already discussed in Chapter 2 that the infrared structure of a theory at finite temperature is much more rich and complicated than the same theory at zero temperature. The complication is due to presence of *thermal fluctuations* in addition to the already present *quantum fluctuations*. The presence of the thermal fluctuation is manifested by the presence of adequate statistical factors in both the propagators and in phase space integrals, in the form of distribution functions (number operator) for bosons (obeying Bose-Einstein statistics) and fermions (obeying Fermi-Dirac statistics). Although the number operator related to fermions are

49

well behaved in the infrared limit,

$$N_{\text{F}}(|p^0|) \equiv \frac{1}{\exp\{|p^0|/T\} + 1} \xrightarrow{p^0 \to 0} \frac{1}{2} \, , \tag{4.1}$$

but, the number operator of the bosons (particularly for massless bosons) diverge in the infrared limit,

$$N_{\text{B}}(|k^0|) \equiv \frac{1}{\exp\{|k^0|/T\} - 1} \xrightarrow{k^0 \to 0} \frac{T}{|k^0|} \, . \tag{4.2}$$

This divergence is the source of the non-trivial structure of the IR divergence of theories of bosons and the theories where the bosons are interacting with fermions and/or bosons at finite temperature.

Usually, for the theories at zero temperature, if a Feynman diagram related to some process does not have any divergent subgraphs, then the diagram is known to diverge logarithmically in IR (in photon momenta for QED). But as seen from Eq. 4.2 in the IR limit, the number operator of massless bosons diverges as $T/|k^0|$ as $k^0 \to 0$. Therefore, it can be easily realized from the Feynman rules of the theories at finite temperature, as mentioned in Chapter 2 and Appendix A, that now in the IR limit we have *linear* superficial degree of divergences from thermal fluctuations, in addition to *logarithmic* divergence from quantum fluctuations and *additional* (in finite temperature) *logarithmic* sub-divergence arising from thermal fluctuations.

Hence, the IR structure is very much non-trivial at finite temperature. Not only the theories (involving massless bosons) diverge much more severely, *i.e.*, linearly as opposed to logarithmically as in zero temperature case; but it also has an additional logarithmic sub-leading divergence from thermal fluctuations which also needs to be tamed.

Apart from all these, as the system is inside a heat bath now and is interacting with it; hence in addition to the real particle emission the absorption of real particles from the heat bath is also perfectly feasible. We have to take account of all such possibilities with correct weight factors. And, it will be shown in upcoming discussions that *only* with the

inclusion of absorption of particles from heat bath the IR divergent terms will be shown to have canceled and perturbation theory can be fruitfully be applied.

We will be interested in the processes involving electrodynamics (involving charged scalars or fermions) in upcoming discussions. From the discussions of the last few paragraphs, we understand that correct identification of the IR divergent and finite pieces related to photon polarization is going to be our main focus. Hence, we have to generalize and extend the technique of GY to the case of finite temperature such that this identification of IR finite and divergent pieces at finite temperature becomes unambiguous. This can be done by rearranging and modifying the polarization sum of the photons accordingly, as mentioned below.

4.2 Extension of the GY technique to finite temperature

To correctly identify the IR divergent and finite pieces arising from the photon insertions at finite temperature, an extension of GY technique is performed as below. This minimal extension of GY technique has been shown to correctly identify the relevant IR finite and divergent contribution initially for thermal fermionic QED in Ref. [41] giving rise to correct eikonal currents, as was mentioned in Ref. [40]. Later, it was also shown that the same extension of GY technique also works successfully for theories of thermal scalar QED in Ref. [42] and for a full theory of charged scalars and fermions at finite temperature in Ref. [43]. The proof of IR finiteness of these field theories at finite temperature, and the isolation and exponentiation of the IR divergent terms to all orders using the GY technique constitute the main results of this thesis. In particular, due to the presence of quadrilinear vertices, the case of thermal field theories with scalars becomes much more complicated. However, it will be seen that the proof of IR finiteness is generic and applies to an entire class of such thermal field theories.

The fact that the factor of $-g^{\mu\nu}$ representing photon polarization factor which is used in

GY rearrangement, is present in all the components of the thermal photon propagator (see Appendix A), enables us to correctly rearrange photon polarization sum into sum of two terms in the finite temperature case as well. This is the key step in obtaining the factorization of IR divergences in the thermal theories.

To correctly obtain and distinguish the IR finite and divergent pieces arising due to virtual photons, the polarization sum of photons at finite temperature are rearranged as,

$$-ig^{\mu\nu}D^{t_a,t_b}(k) = -iD^{t_a,t_b}(k) \left\{ \left[g^{\mu\nu} - b_k(p_f, p_i) \, k^\mu k^\nu \right] + \left[b_k(p_f, p_i)k^\mu k^\nu \right] \right\}$$

$$\equiv -iD^{t_a,t_b}(k) \left\{ [G] + [K] \right\}, \tag{4.3}$$

where $iD^{t_a,t_b}(k)$ is the part of the thermal photon propagator which remains after separating out the $-g^{\mu\nu}$ part (see Eq. 2.37, and Eq. 2.38). In Eq. 4.3 $b_k(p_f, p_i)$ is defined so as to contain all the IR divergences *only* in the K-photon contribution (henceforth called K photon term) at finite temperature,

$$b_k(p_f, p_i) = \frac{1}{2} \left[\frac{(2p_f - k) \cdot (2p_i - k)}{(k^2 - 2p_f \cdot k)(k^2 - 2p_i \cdot k)} + (k \leftrightarrow -k) \right] \ \forall \text{ choices of } p_i, \ p_f. \tag{4.4}$$

In contrast to Eq. 3.2, it is to be noted that $b_k(p_f, p_i)$ is now always symmetric in the exchange of $(k \leftrightarrow -k)$ for all choices of p_i and p_f (whether that be related to p and/or p'-leg). This modification of definition of $b_k(p_f, p_i)$ is sufficient to correctly separate out all the linear leading and logarithmic sub-leading divergence to only virtual K photon terms, leaving G-photon polarization sum (henceforth called G photon term) at finite temperature IR finite.

For the real photons a similar rearrangement of polarization sums can be obtained in the square of the matrix element at finite temperature. These new polarization sums are denoted as $\widetilde{K}$ and $\widetilde{G}$ (here tildes have been used to differentiate the real polarization sums rearrangements from the virtual photons, and these will be referred as $\widetilde{K}$ and $\widetilde{G}$ photons in

all upcoming discussions); which are identified through the following equation,

$$\begin{aligned}
\sum_{\text{pol}} \epsilon_\mu^*(k)\, \epsilon_\nu(k) &= -g_{\mu\nu}\,, \\
&= -\left\{ \left[g_{\mu\nu} - \tilde{b}_k(p_f, p_i)k_\mu k_\nu \right] + \left[\tilde{b}_k(p_f, p_i)k_\mu k_\nu \right] \right\}\,, \\
&\equiv -\left\{ \left[\widetilde{G}_{\mu\nu} \right] + \left[\widetilde{K}_{\mu\nu} \right] \right\}\,,
\end{aligned} \tag{4.5}$$

In the above expression $\tilde{b}_k(p_f, p_i)$ is related to $b_k(p_f, p_i)$ as photons become on-shell with $k^2 = 0$ (real), and is expressed as,

$$\tilde{b}_k(p_f, p_i) = b_k(p_f, p_i)\Big|_{k^2=0} = \frac{p_f \cdot p_i}{k \cdot p_f\ k \cdot p_i}\,. \tag{4.6}$$

It is also to be noted that, as the real photons are physical; hence whether real photons are emitted or absorbed, the real photons will correspond to thermal type 1 only. Therefore, any insertion vertex due to real photons is only of type 1. Hence, the cancellation of IR divergence between virtual and soft real photons can only take place, if contributions due to virtual photons also come out to be proportional to D^{11}. We find that this is indeed the case in the thermal theories that we consider.

Along with this we also have to note that, the real photon brings in or takes out physical momentum. In Chapter 5 it will be mentioned in detail, how to tackle this issue. Apart from this, in thermal field theory the phase space corresponding to emission or absorption of photons is not symmetric with respect to photon momenta and is expressed as,

$$d\phi_i = \frac{d^4 k_i}{(2\pi)^4}\, 2\pi\delta(k_i^2) \left[\theta(k_i^0) + N_{\text{B}}(|k_i^0|) \right]\,. \tag{4.7}$$

Where, '$k_i^0 > 0$' refers to the photon emission, and '$k_i^0 < 0$' refers to the absorption of the photon with photon momentum k_i. Thus, the real photon emission is proportional to a factor of $(1 + N_{\text{B}}(|k_i^0|))$, and the absorption is proportional to a factor $N_{\text{B}}(|k_i^0|)$. Although the whole phase space is not symmetric in $k_i \leftrightarrow -k_i$ but the concerned part which is appearing

due to the effect of finite temperature, *i.e.*, $N_{\mathrm{B}}(|k_i^0|)$, is symmetric under $k_i \leftrightarrow -k_i$. *Only after including both the emission and absorption of real photons, and taking into account the symmetric nature of $N_{\mathrm{B}}(|k_i^0|)$ it will be shown that all the leading linear and sub-leading logarithmic IR divergences are contained in $\widetilde{K}$ photon contributions, leaving $\widetilde{G}$ photon contributions IR finite.*

4.3 Application of extension of GY technique to thermal fermionic QED
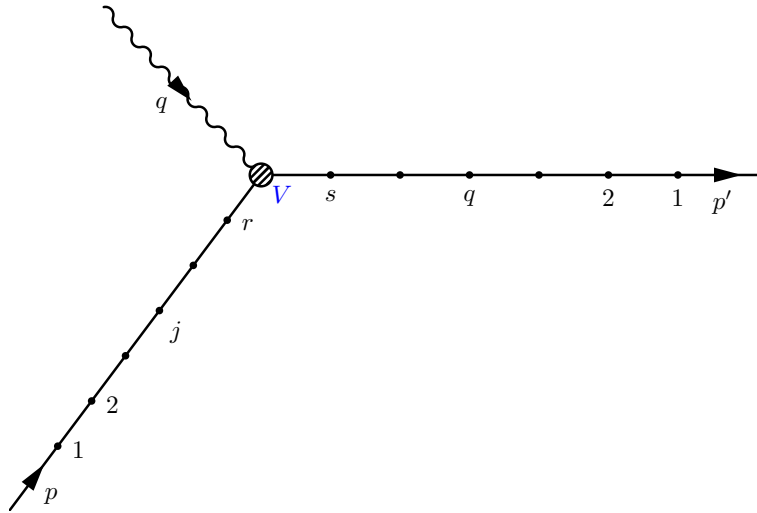
Figure 4.1: *Schematic diagram of an nth order process $f(p)\gamma^*(q) \to f(p')$ at finite temperature, where the every virtual photon interaction vertices can have both the thermal types (type-1, type-2) of vertices, except the ones which are just next to the physically observable particles. Here solid lines represent fermions and the wavy line represents the photon.*

We will start again with an nth order process corresponding to the $f(p)\gamma^*(q) \to f(p')$ (where, $p + q = p'$) as in Chapter 3, but now in thermal field theory[1]. The higher order

---

[1] The IR finiteness of thermal fermionic QED has been shown in Ref. [41] and is reproduced here for completeness (since it is the simplest thermal case without the complication of quadrilinear vertices as for scalar QED). In addition, these results for fermionic QED will be used in Chapter 6 when we deal with the full interacting thermal theory of fermions and scalars.

corrections to it will generate a similar set of diagrams with some changes due to presence of finite temperature. To emphasize on the differences between zero and finite temperature cases, (and also for completeness and convenience of readability) we will again represent the schematics of the nth order contribution to the process $f(p)\gamma^*(q) \rightarrow f(p')$ Fig. 4.1, which naively and schematically looks similar to Fig. 3.2; but we will stress on the differences. Now, in this n^{th} order diagram the virtual photons can have both the types of thermal vertex type (*i.e.*, both type-1, type-2), except the ones which are immediately next to physically observable particles which bring in *hard* momenta. Hence the thermal type of vertex immediately adjacent to the in/out states (*i.e.*, vertex number 1) on both p and p'-leg, and thermal type of vertex V can be only of type-1, *i.e.*, $t_1(\text{p}-leg) = t_1(\text{p}'-leg) = t_V = 1$ (as always for physical processes involving *hard* observable photons, the photon being observable imply $t_V = 1$). With this understanding, and taking the same notation discussed in Chapter 3 (*i.e.*, already present photon momenta on p' (p)-leg is taken to be outgoing (incoming), and is represented by l'_i (l_i) at the i-th vertex on that particular leg), the nth order matrix element for process $f(p)\gamma^*(q) \rightarrow f(p')$, with $m = r + s = 2n$ number of virtual photon vertices (the involvement of any finite number of real photons will not change any argument) can be written as,

$$
\begin{aligned}
i\mathcal{M}_n^{\text{fermion}} &= (-ie)^{2n}(-1)^{\sum_{i=1}^{m}(t_i+1)}(i)^m \times \left[\bar{u}_{p'}\gamma_{\mu_1} F_{p'+\Sigma_1}^{t_1,t_2} \gamma_{\mu_2} F_{p'+\Sigma_2}^{t_2,t_3} \cdots \gamma_{\mu_{s-1}} F_{p'+\Sigma_{s-1}}^{t_{s-1},t_s} \gamma_{\mu_s} F_{p'+\Sigma_s}^{t_s,t_V} \right] \\
&\quad \times \Gamma_V \times \left[F_{p+\Sigma_r}^{t_V,t_r} \gamma_{\nu_r} F_{p+\Sigma_{r-1}}^{t_r,t_{r-1}} \gamma_{\nu_{r-1}} \cdots F_{p+\Sigma_1}^{t_2,t_1} \gamma_{\nu_1} u_p \right] \times \mathcal{D}_{\{t_i\}}^{\mu_1,\cdots,\mu_s;\nu_r,\cdots,\nu_1}, \\
&= (-ie)^{2n}(-1)^{\sum_{i=1}^{m}(t_i+1)}(i)^m \times \left[C_s^{p'} \right] \times \Gamma_V \times [C_r^p] \times \mathcal{D}_n. \quad\quad (4.8)
\end{aligned}
$$

In the expression above, $\Gamma_V = -ie\gamma_V$; $C_s^{p'}$ and C_r^p correspond to the contributions to the matrix element resulting from respectively p' and p-leg. Fermion propagators now have thermal indices (where we represent the thermal type at vertex i by t_i. If the thermal vertex type at vertex number i is of type 1, then $t_i = 1$; and if that is of type 2, then $t_i = 2$) on their superscripts in addition to momenta being denoted in their subscripts (accroding to the notations defined in Chapter 3). Here, the factors of $(-ie \times (-1)^{(t_q+1)})$ are related to

vertex factors at interaction vertex q, and all factors of $(i)^m$ from propagators have been separated. And here,

$$\mathcal{D}_n \equiv \mathcal{D}_{\{t_i\}}^{\mu_1,\cdots,\mu_s;\nu_r,\cdots,\nu_1} = \prod_{\{\alpha\beta\}} \int \frac{\mathrm{d}^4 k_\alpha}{(2\pi)^4} \left[-ig^{\alpha\beta} D^{t_\alpha,t_\beta} \right] , \tag{4.9}$$

In the above expression, α, β denote any two amidst the dummy indices $\mu_1, \cdots, \mu_s; \nu_1, \cdots, \nu_r$, referring to the vertices (can be present on either p and/or the p'-legs) where the ends of the virtual photon are inserted and then symmetrized over all possible values of α and β.

4.3.1 Effect of virtual K, G photon insertion at finite temperature

Now, let us insert an additional virtual photon having momentum k, on the nth order matrix element. The direction of the momenta k is outgoing at the new insertion vertex μ and incoming at the new insertion vertex ν. Among the three possibilities (first two possibilities: both insertion vertices are on same leg, third possibility:insertion vertices are on different legs), in which new vertex μ and ν can be added we will start with the possibility where the insertion vertices are on different leg; *i.e.*, μ is inserted on the final p'-leg just right to the vertex q and ν is inserted on the initial p-leg just left to the vertex j. Hence, the matrix element after attaching the new virtual photon reads,

$$i\mathcal{M}_{n+1}^{\text{fermion}; p', p} = (-ie)^{2n+2}(-1)^{\sum_{i=1}^{m}(t_i+1)}(-1)^{(t_\mu+1)}(-1)^{(t_\nu+1)}(i)^{m+2}\times$$

$$\left[\bar{u}_{p'}\gamma_{\mu_1} F_{p'+\Sigma_1}^{t_1,t_2} \cdots \gamma_{\mu_{q-1}} F_{p'+\Sigma_{q-1}}^{t_{q-1},t_\mu} \gamma_\mu F_{p'+\Sigma_{q-1}+k}^{t_\mu,t_q} \gamma_{\mu_q} \cdots F_{p'+\Sigma_{s-1}+k}^{t_{s-1},t_s} \gamma_{\mu_s} F_{p'+\Sigma_s+k}^{t_s,t_\nu} \right]$$

$$\times \Gamma_V \times \left[F_{p+\Sigma_r+k}^{t_\nu,t_r} \gamma_{\nu_r} \cdots \gamma_{\nu_j} F_{p+\Sigma_{j-1}+k}^{t_j,t_\nu} \gamma_\nu F_{p+\Sigma_{j-1}}^{t_\nu,t_{j-1}} \gamma_{\nu_{j-1}} \cdots F_{p+\Sigma_1}^{t_2,t_1} \gamma_{\nu_1} u_p \right]$$

$$\times \mathcal{D}_{t_\mu,t_\nu;\{t_i\}}^{\mu,\nu;\mu_1,\cdots,\mu_s;\nu_r,\cdots,\nu_1} ,$$

$$= (-ie)^{2n+2}(-1)^{\sum_{i=1}^{m}(t_i+1)}(-1)^{(t_\mu+1)}(-1)^{(t_\nu+1)}(i)^{m+2}\times$$

$$\left[C_{s+1}^{p';\mu} \right] \times \Gamma_V \times \left[C_{r+1}^{p;\nu} \right] \times \mathcal{D}_{n+1}^{\mu\nu} , \tag{4.10}$$

56

where the notation and contribution of $C_{r+1}^{p;\nu}$ and $C_{s+1}^{p';\mu}$ are in accordance with the notation defined just below Eq. 3.8. And $\mathcal{D}_{n+1}^{\mu\nu}$ is,

$$\mathcal{D}_{n+1}^{\mu\nu} \equiv \mathcal{D}_{t_\mu,t_\nu;\{t_i\}}^{\mu,\nu;\mu_1,\cdots,\mu_s;\nu_r,\cdots,\nu_1} = \int \frac{\mathrm{d}^4k}{(2\pi)^4} \left[-ig^{\mu\nu}D^{t_\mu,t_\nu}\right] \times \mathcal{D}_{\{t_i\}}^{\mu_1,\cdots,\mu_s;\nu_r,\cdots,\nu_1},$$

$$= \int \frac{\mathrm{d}^4k}{(2\pi)^4} \left[-ig^{\mu\nu}D^{t_\mu,t_\nu}\right] \times \mathcal{D}_n . \qquad (4.11)$$

Here we are particularly interested in K and G photon rearrangements, and corresponding contributions of those from $\mathcal{D}_{n+1}^{\mu\nu}$ is obtained after rearranging the appropriate parts of thermal photon propagator as mentioned below. The virtual K photon contribution in Eq. 4.11 can be obtained as

$$\left[-ig^{\mu\nu}D^{t_\mu,t_\nu}\right]^K = \left[-iD^{t_\mu,t_\nu}\right]\left[b_k(p',p)k^\mu k^\nu\right] , \qquad (4.12)$$

and for virtual G photon polarization sum contribution,

$$\left[-ig^{\mu\nu}D^{t_\mu,t_\nu}\right]^G = \left[-iD^{t_\mu,t_\nu}\right]\left[g^{\mu\nu} - b_k(p',p)k^\mu k^\nu\right] . \qquad (4.13)$$

We have to replace $-ig^{\mu\nu}D^{t_\mu,t_\nu}$ via the the corresponding virtual K and G polarization sums in accordance with respectively Eq. 4.12 and Eq. 4.13 while talking in terms of particular polarization sum. Keeping aside G photon contribution momentarily, let us at first focus on the K photon contributions. The contribution due to insertion of a K photon to the nth order matrix element hence yields,

$$i\mathcal{M}_{n+1}^{\text{fermion};p',p} = (-ie)^{2n+2}(-1)^{\sum_{i=1}^m(t_i+1)}(-1)^{(t_\mu+1)}(-1)^{(t_\nu+1)}(i)^{m+2}\times$$

$$\int \frac{\mathrm{d}^4k}{(2\pi)^4} b_k(p',p) \left[k_\mu C_{s+1}^{p';\mu}\right] \times \Gamma_V \times \left[k_\nu C_{r+1}^{p;\nu}\right] \times \left[-iD^{t_\mu,t_\nu}\right] \times \mathcal{D}_n .$$

$$(4.14)$$

From Eq. 4.14 it is seen that the contribution to the matrix element for the p and p'-legs get factorized in this case, and hence can be evaluated independently of each other.

Effect of virtual K photon insertion : We will start by observing the effect of K photon insertion on the p'-leg, $k_\mu C_{s+1}^{p';\mu}$ at first. The insertion of the K photon in this case exactly produces $(s+1)$ number of diagrams. These diagrams when schematically drawn, look to be exactly same as what was mentioned in Fig. 3.3, except that the vertices now can have both the types of thermal vertices. The set of diagrams is again presented in Fig. 4.2 for sake of completeness and readability.
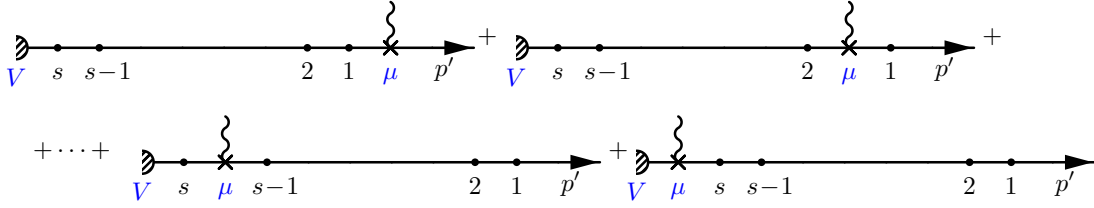
Figure 4.2: *All possible ways of insertions of a virtual K photon at vertex μ on p'-leg of an nth order diagram in thermal fermionic QED, which already had s number of vertices on p'-leg.*

A typical diagram when μ vertex is situated in between vertices q and $q-1$ is shown Eq. 4.3 and will be calculated first to emphasize the structure of GY factorization at finite temperature.
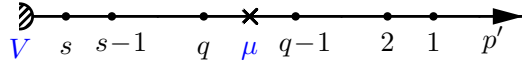
Figure 4.3: *A generic diagram of K photon insertion on the p'-leg from Fig. 4.2 in thermal fermionic QED, where μ vertex is situated in between vertices q and $q-1$.*

The contribution of Fig. 4.3 can be expressed as,

$$
\begin{aligned}
k_\mu C_{s+1}^{p';\mu \text{ right of } q} &= \bar{u}_{p'} \gamma_{\mu_1} \cdots \gamma_{\mu_{q-1}} \left[F_{p'+\Sigma_{q-1}}^{t_{q-1},t_\mu} \slashed{k} F_{p'+\Sigma_{q-1}+k}^{t_\mu,t_q} \right] \cdots , \\
&= (-1)^{(t_\mu+1)} \bar{u}_{p'} \gamma_{\mu_1} \cdots \gamma_{\mu_{q-1}} \left[\delta_{t_\mu,t_q} F_{p'+\Sigma_{q-1}}^{t_{q-1},t_q} - \delta_{t_\mu,t_{q-1}} F_{p'+\Sigma_{q-1}+k}^{t_{q-1},t_q} \right] \cdots , \\
&\equiv M'_q - M'_{q-1} ,
\end{aligned}
\tag{4.15}
$$

where the rearrangement (which looks quite similar to its zero temperature counterpart

58

Eq. 3.12) of the part of the matrix element in the square bracket is due to application of the 'Generalized Feynman's Identity' at finite temperature (see Eq. B.3), which are mentioned in Appendix B. We also want to mention that the factor $(-1)^{(t_\mu+1)}$ highlighted in the above equation is also a result of the Grammer and Yennie (GY) reduction after using 'Generalized Feynman's Identity'. This is an extra factor what we have obtained after performing the GY reduction, and has no source related to already present overall factor of $(-ie)^{2n+2}(-1)^{\sum_{i=1}^{m}(t_i+1)}(-1)^{(t_\mu+1)}(-1)^{(t_\nu+1)}(i)^{m+2}$ which was factored out, see Eq. 4.14.

From Eq. 4.15 we find that the typical term reduces to difference of two terms; this procedure can be performed for each diagram of Fig. 4.2 which will result in series of 'difference of two terms' which will cancel in pairs among themselves. Similar to the zero temperature case (see Eq. 3.14), the contribution of the diagrams excluding the first one, as shown in Fig. 4.2 is given by

$$\sum_{q=2}^{V} k_\mu\, C_{s+1}^{p';\mu\,\text{right of}\,q} \equiv (M_2' - M_1') + (M_3' - M_2') + \cdots + (M_{s+1}' - M_s')\,,$$

$$\equiv -M_1' + M_{s+1}'\,, \tag{4.16}$$

Where in above equation 'V' is the vertex which is situated at the immediate left of vertex s (of p'-leg). The contribution corresponding to the first diagram of Fig. 4.2 will look little bit different, as p'-leg is on-shell and one of the term will become zero, giving the contribution as

$$k_\mu\, C_{s+1}^{p';\mu\,\text{right of}\,1} = \bar{u}_{p'}\,\slashed{k}\, F_{p'+k}^{t_\mu,t_1}\gamma_{\mu_1} F_{p'+\Sigma_1+k}^{t_1,t_2}\cdots\,,$$

$$= (-1)^{(t_\mu+1)}\delta_{t_\mu,t_1}\,\bar{u}_{p'}\gamma_{\mu_1} F_{p'+\Sigma_1+k}^{t_1,t_2}\cdots\gamma_{\mu_{q-1}} F_{p'+\Sigma_{q-1}+k}^{t_{q-1},t_q}\cdots\,,$$

$$\equiv M_1'\,, \tag{4.17}$$

where we have used the 'Generalized Feynman's Identity' as mentioned in Appendix B. Using Eq. 4.16 and Eq. 4.16 we can write the total contribution of K photon insertion on

p'-leg as,

$$k_\mu C_{s+1}^{p';\mu} = (-M'_1 + M'_{s+1}) + M'_1 = M'_{s+1} ,$$

$$= (-1)^{(t_\mu+1)}\delta_{t_\mu,t_V} \left[\bar{u}_{p'} \, \gamma_{\mu_1} \cdots \gamma_{\mu_{q-1}} F_{p'+\Sigma_{q-1}}^{t_{q-1},t_q} \cdots F_{p'+\Sigma_s}^{t_s,t_V} \right] ,$$

$$= (-1)^{(t_\mu+1)}\delta_{t_\mu,t_V} C_s^{p'} . \tag{4.18}$$

Hence, the term $k_\mu C_{s+1}^{p';\mu}$ becomes equal to the lower order contribution $C_s^{p'}$ times the multiplicative $(-1)^{(t_\mu+1)}\delta_{t_\mu,t_V}$ factor.

Similarly, the contribution $k_v C_{r+1}^{p;v}$ from Eq. 4.14 can also be independently calculated. A similar calculation for K photon insertion on p-leg will produce $(r+1)$ number of terms. A typical diagram of that set when v has been inserted in between $j-1$ and j has been schematically shown below.
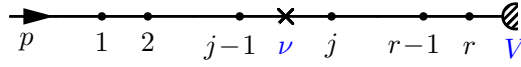
Figure 4.4: *A generic diagram of K photon insertion on the p-leg in thermal fermionic QED, where the new vertex v is situated in between vertices $j-1$ and j .*

This particular contribution can be again simplified by the use of 'Generalized Feynman Identity' (see Eq. B.2) as

$$k_v C_{r+1}^{p;\,v\,\text{left of }j} = F_{p+\Sigma_r+k}^{t_V,t_r} \cdots \gamma_{v_j} \left[F_{p+\Sigma_{j-1}+k}^{t_j,t_v} \not{k} F_{p+\Sigma_{j-1}}^{t_v,t_{j-1}} \right] \gamma_{v_{j-1}} \cdots u(p) ,$$

$$= (-1)^{(t_v+1)} F_{p+\Sigma_r+k}^{t_V,t_r} \cdots \gamma_{v_j} \left[\delta_{t_v,t_j} F_{p+\Sigma_{j-1}}^{t_j,t_{j-1}} - \delta_{t_v,t_{j-1}} F_{p+\Sigma_{j-1}+k}^{t_j,t_{j-1}} \right] \times$$

$$\gamma_{v_{j-1}} \cdots u(p) ,$$

$$\equiv M_j - M_{j-1} , \tag{4.19}$$

where now the GY reduction yields an overall factor of $(-1)^{(t_v+1)}$ in place of $(-1)^{(t_\mu+1)}$ when compared to Eq. 4.15 as the reduction now occurs at the v vertex. Now, performing a similar analysis for other terms of p-leg and after remembering that the contribution

$M_{j-1} = 0$ for $j = 1$ due to the on-shell nature of p-leg we find that the whole K photon contribution from the p-leg now simplifies to,

$$k_v C_{r+1}^{p;\,v} = (M_V - M_r) + (M_r - M_{r-1}) + \cdots + (M_1 - M_0) = M_V\,,$$

$$= (-1)^{(t_v+1)} \delta_{t_v, t_V} \left[F_{p+\Sigma_r}^{t_V, t_r} \gamma_{v_r} \cdots F_{p+\Sigma_{j-1}}^{t_j, t_{j-1}} \gamma_{v_{j-1}} \cdots u(p) \right]\,,$$

$$= (-1)^{(t_v+1)} \delta_{t_v, t_V} C_r^p\,. \tag{4.20}$$

From the above equation we find again that $k_v C_{r+1}^{p;\,v}$ reduces to the lower order contribution C_r^p times the multiplicative $(-1)^{(t_v+1)} \delta_{t_v, t_V}$ factor.

Hence, the matrix element $\mathcal{M}_{n+1}^{\text{fermion};\,K\gamma,\,p',\,p}$ after taking all possible K photon insertion contribution in between p and p'-leg evaluates to

$$\mathcal{M}_{n+1}^{\text{fermion};\,K\gamma,\,p',\,p} = -ie^2 \int \frac{\mathrm{d}^4 k}{(2\pi)^4}\, b_k(p', p)\, \delta_{t_\mu, t_V}\, \delta_{t_v, t_V}\, D^{t_\mu, t_v}(k)\, \mathcal{M}_n^{\text{fermion};\,p',\,p}\,. \tag{4.21}$$

The contributions due to other legs also factorize in a similar manner. The effect of all the contributions of K photon factorize as shown in Ref. [41]:

$$\mathcal{M}_{n+1}^{\text{fermion};\,K\gamma,\,\text{tot}} = \frac{ie^2}{2} \int \frac{\mathrm{d}^4 k}{(2\pi)^4} \left\{ \delta_{t_\mu, t_1}\, \delta_{t_v, t_1}\, D^{t_\mu, t_v}(k) \left[b_k(p', p') + b_k(p, p) \right] \right.$$

$$\left. + \delta_{t_\mu, t_V}\, \delta_{t_v, t_V}\, D^{t_\mu, t_v}(k) \left[-2 b_k(p', p) \right] \right\} \mathcal{M}_n^{\text{fermion}}\,,$$

$$\equiv [B]\, \mathcal{M}_n\,, \tag{4.22}$$

where

$$B = \frac{ie^2}{2} \int \frac{\mathrm{d}^4 k}{(2\pi)^4}\, D^{11}(k) \left[b_k(p', p') - 2 b_k(p', p) + b_k(p, p) \right]\,,$$

$$\equiv \frac{ie^2}{2} \int \frac{\mathrm{d}^4 k}{(2\pi)^4}\, D^{11}(k) \left[J^2(k) \right]\,. \tag{4.23}$$

In Eq. 4.22 it was considered that the hard and/or external vertices can be only of type-1 thermal type; *i.e.*, $t_1 = t_V = 1$. From Eq. 4.23 it is evident that B has both leading

linear and sub-leading logarithmic divergences, and this prescription of extension of GY technique to finite temperature has separated out IR divergences into the contributions due to K-photon terms, and is manifested inside B.

Effect of virtual G photon insertion : A similar analysis can be performed for the all the virtual G photons insertions to n^{th} order process in fermionic thermal QED. The objective here is then to show that the G photons do not contain any IR divergent terms, and *all* the IR divergent terms are contained and separated out in virtual K photon contributions.

After using the Dirac algebra, the G photon contributions for fermionic QED at finite temperature in the soft limit (irrespective of the choice of final p_f and initial p_i-leg) turn out as,

$$
\mathcal{M}_{n+1}^{G\gamma} \sim \int d^4k \left[\frac{i}{k^2 + i\epsilon} \delta_{t_\mu, t_\nu} \pm 2\pi\delta(k^2) N_B(|k|) D^{t_\mu, t_\nu} \right] \times \left[\frac{\{g_{\mu\nu} - b_k(p_f, p_i)k_\mu k_\nu\} \times p_f^\mu p_i^\nu}{O(k^2)} \right] .
$$

(4.24)

Looking at Eq. 4.24 naively it seem that the corresponding matrix element has both the linear leading and logharithmic sub-leading divergence. We have to prove that G photon contributions are actually IR finite. The proof of IR finiteness of these contributions are quite complicated and was shown for the case of thermal fermionic QED in Ref. [41].

At this juncture, we simply point out that the proof of IR finiteness of the thermal field theory thus comprises two parts. One is to prove that the G photon insertions (and so also the real $\widetilde{G}$ photon insertions) are IR finite. The second is to show that the IR divergences, which are completely contained in the K and $\widetilde{K}$ photon contributions, cancel against each other, order by order in perturbation theory. This then constitutes an all-order proof for the IR safety of the corresponding thermal field theory.

4.3.2 Effect of real $\widetilde{K}$, $\widetilde{G}$ photon contributions at finite temperature

In order to compute the contributions arising from the real $\widetilde{K}$ and $\widetilde{G}$ photons for the thermal fermionic QED, we have to rearrange the polarization sum in the square of matrix element as mentioned in Eq. 4.5. We also have to make note of the fact that, in addition to photon emission to the heat bath the absorption of photon from the heat bath is also perfectly feasible (which is not the case in vacuum field theory). And, it has been shown in Ref. [41] that, *only* with the inclusion of the photon absorption the IR divergent pieces cancel between real and virtual cross-sections. The phase space related to the photon absorption and emission comes with different weight factor and has been discussed in Eq. 4.7.

Hence, taking into account these facts it was shown in Ref. [41] that the square of the matrix element for the $\widetilde{K}$ photon contribution factorize and become,

$$
\begin{aligned}
\left| \mathcal{M}_{n+1}^{\text{fermion};\,\widetilde{K}\gamma,\,\text{tot}} \right|^2 &\propto - e^2 \left[\tilde{b}_k(p,p) - 2\tilde{b}_k(p',p) + \tilde{b}_k(p',p') \right] \times \left| \mathcal{M}_n^{\text{fermion}} \right|^2 \\
&\equiv - e^2 \widetilde{J}^{\,2}(k) \left| \mathcal{M}_n^{\text{fermion}} \right|^2 ,
\end{aligned}
\tag{4.25}
$$

apart from the relevant phase space factors which contain the number operator for the photon; see Eq. 4.7. It can be shown in accordance with Ref. [41] that, all the leading linear; and leading and sub-leading logarithmic IR divergence contributions are now completely contained in these real $\widetilde{K}$ photon terms. These IR divergent contributions will cancel with virtual K photon contributions order by order, while the $\widetilde{G}$ photon contributions turn out to be IR finite.

We have used this section to record the already available results for thermal fermionic QED, as well as highlighted how the Generalized Feynman identities can be used to simplify the K photon contributions resulting a factorization of the IR divergent part. We now proceed to address the same problem, but for a thermal theory of charged scalars interacting with an electromagnetic field.

4.4 Application of extension of GY technique to thermal scalar QED

As in the thermal fermionic QED case, to identify and separate out the relevant IR finite and divergent contributions in thermal scalar QED, we have to the consider effects of adding virtual/real photon expressed in new polarization sums $(K, G, \widetilde{K}, \widetilde{G})$, in all possible ways to the nth order diagram related to the process, $\phi(p)\gamma^*(q) \to \phi(p')$, where ϕ is the charged scalar.
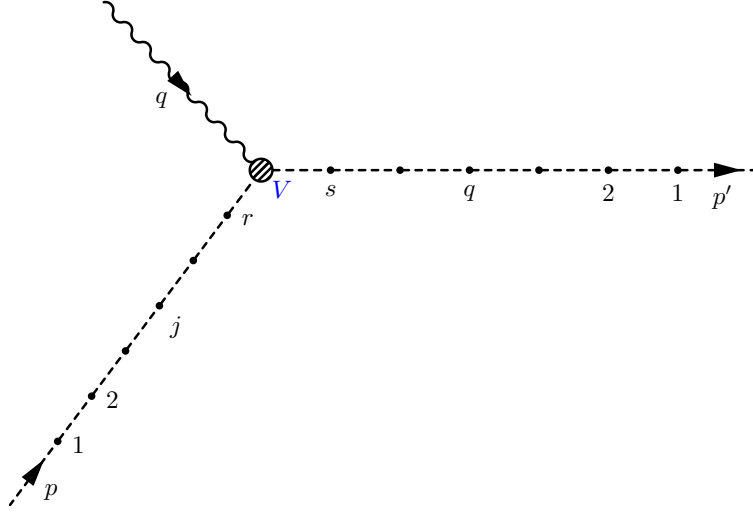
Figure 4.5: *Schematic diagram of an nth order process $\phi(p)\gamma^*(q) \to \phi(p')$ in scalar QED at finite temperature. ϕ is the charged scalar, represented by dashed lines. Here, any dotted vertex can now represent either a seagull or a trilinear vertex; hence even for an nth order diagram with all virtual photon vertices, $n \le s + r = m \le 2n$.*

The nth order diagram related to the process $\phi(p)\gamma^*(q) \to \phi(p')$ at finite temperature scalar QED has been expressed schematically in Fig. 4.5. Here, now the difference is, in scalar QED, in addition to normal trilinear scalar-photon-scalar interaction vertex, the quadrilinear (seagull) scalar-scalar-photon-photon interaction vertices are also possible. The immediate contrast from fermionic case due to the presence of seagull vertices is that, in the schematic Feynman diagram (as shown in Fig. 4.5) related to n^{th} order process $\phi(p)\gamma^*(q) \to \phi(p')$ in scalar QED, the dots can represent *either* a trilinear or a quadrilinear

(seagull) vertex. In previous schematic diagrams of nth order in fermionic QED (as in Fig. 4.1 and Fig. 3.2); if the dotted vertices were all virtual, then the number of vertices $m = 2n$ (where n is the order of the diagram). But, in the case of scalar QED (whether at finite or zero temperature) a seagull vertex contributes 'e^2' factor to matrix element and a trilinear vertex contributes a factor of 'e' to matrix element. Hence, as the nth order *all-virtual* matrix element should contribute at order e^{2n} (as in the definition of Footnote 2 of Chap. 3); hence the number of vertices (represented by dots in schematic diagram) for an all-virtual n^{th} order diagram can vary from n (implying that all the dotted vertices are seagull) to a number $2n$ (implying that all the dotted vertices are trilinear). For an admixture of already present trilinear and seagull vertex m can be any number in between n to $2n$, *i.e.*, generically for an nth order all-virtual diagram $n \leq s + r = m \leq 2n$ as shown in Fig. 4.5. Taking this into account, matrix element for an nth order all-virtual diagram for process $\phi(p)\gamma^*(q) \rightarrow \phi(p')$ at finite temperature, which have all trilinear vertices (these can be generalized to an arbitrary mixture of seagull and trilinear vertices and will be discussed elaborately in Chapter 5) can be represented by the following expression,

$$
\begin{aligned}
i\mathcal{M}_n^{\text{scalar}} =&(e)^{2n}(-i)^m(-1)^{\sum_{i=1}^m(t_i+1)}(i)^m \times \Big[(2p'+l'_1)_{\mu_1} S^{t_1,t_2}_{p'+\Sigma_1} \cdots \times \\
&(2p'+2\Sigma_{s-2}+l'_{s-1})_{\mu_{s-1}} S^{t_{s-1},t_s}_{p'+\Sigma_{s-1}}(2p'+2\Sigma_{s-1}+l'_s)_{\mu_s} S^{t_s,t_V}_{p'+\Sigma_s}\Big] \times \Gamma_V \times \\
&\Big[S^{t_V,t_r}_{p+\Sigma_r}(2p+2\Sigma_{r-1}+l_r)_{\nu_r} S^{t_r,t_{r-1}}_{p+\Sigma_{r-1}} \cdots S^{t_2,t_1}_{p+\Sigma_1}(2p+l_1)_{\nu_1}\Big] \times \mathcal{D}^{\mu_1,\cdots,\mu_s;\nu_r,\cdots,\nu_1}_{\{t_i\}} \\
=&(e)^{2n}(-i)^m(-1)^{\sum_{i=1}^m(t_i+1)}(i)^m \times \Big[C_s^{\text{scalar } p'}\Big] \times \Gamma_V \times \Big[C_r^{\text{scalar } p}\Big] \times \mathcal{D}_n ,\qquad (4.26)
\end{aligned}
$$

where the matrix element has been written in accordance with all previously defined notations, *i.e.*, the photon momenta at the vertices on the $p'(p)$-leg are always outgoing(incoming) (without loss of any generality), and are denoted by $l'_i(l_i)$. And for notational convenience the momenta of scalar propagators on respectively p' and p-leg are written as, $(p'+\Sigma_{i=1}^q l'_i) \equiv (p'+\Sigma_q)$; $(p+\Sigma_{i=1}^j l_i) \equiv (p+\Sigma_j)$ which is in accordance with all the notation used previously (for more details on notations see Chapter 3). $\Gamma_V = -ie\gamma_V$ in Eq. 4.26; and $C_s^{\text{scalar } p'}$ and $C_r^{\text{scalar } p}$ respectively correspond to the contributions to the

matrix element of scalar QED resulting from p' and p-leg. Here, S corresponds to the scalar propagator.

Now, let us focus on the similarities and the differences between Eq. 4.26 with similar expressions written for thermal fermionic QED as in Eq. 4.8. As both the expressions correspond to n^{th} order all-virtual matrix element hence, both have correct number of 'e^{2n}' in their expression. But, as the number of vertices, m (in general) varies in scalar QED case, thus we have separately written the factors of i's coming from vertices in this case as $(-i)^m$ in Eq. 4.26. In this case if the schematic diagram has 'm' number of vertices, then there are m number of internal scalar propagators, and we have separately written the $(i)^m$ factors coming out of them in the expression of matrix element.

4.4.1   Effect of insertion of K, G photon contributions

We will examine now the effect of insertion of an additional virtual photon having momentum k to the nth order matrix element. The virtual photon can be inserted in three possible ways, corresponding to *both* the insertion vertices being inserted on the same leg (two cases), and the other possibility (third case) where the new insertion vertices are on separate legs. The first two cases, where both the insertion vertices of photon are inserted on the same leg is far more complicated than the fermionic QED case; as there can be tadpole diagrams arising from seagull insertions. The full fledged discussion of that is worth a separate chapter. We will discuss in detail on this issue in Chapter 5, which comprises one of the main results of this thesis. Therefore, to be able to recognize the basic technology involved in the GY factorization in thermal scalar QED we will start with the third case where the new insertion vertices are inserted on separate legs. We will only present the basic GY rearrangement and the notations used for this case in this section, and will reserve the main results for Chapter 5.

To instruct the basic technology involved, we will begin with an nth order diagram, where

all the already present dotted vertices represent trilinear ones. The matrix element after adding a new virtual photon between p and p'-leg is written symbolically below in Eq. 4.27. The explicit expression for it (which is analogous to explicit expression Eq. 4.10 for fermionic QED) is very cumbersome; as the new vertices can be trilinear one, or the new photon can add to an already present trilinear vertex making it a seagull one. Hence, we have presented only an symbolic expression here, and will confront the particular cases separately in subsequent discussion.

$$
iM_{n+1}^{\text{scalar}; p', p} = (e)^{2n+2}(-i)^{m+2}(-1)^{\sum_{i=1}^{m}(t_i+1)}(-1)^{(t_\mu+1)}(-1)^{(t_\nu+1)}(i)^{m+2}\times
$$
$$
\left[C_{s+1}^{\text{scalar } p'; \mu}\right] \times \Gamma_V \times \left[C_{r+1}^{\text{scalar } p; \nu}\right] \times \mathcal{D}_{n+1}^{\mu\nu} . \tag{4.27}
$$

We will explain on the notation used in the above equation, before moving to further discussions. Although it may naively seem as if the above expression only considers the insertions of trilinear diagrams (after counting of overall factors of (i) and (e)), but it is not actually the case. It also contains information about the diagrams with quadrilinear (seagull) insertion vertices, corresponding to the cases when the new additional photon is inserted at an already existing trilinear vertex.

If the new insertion vertex on either of p or p'-leg correspond to seagull insertion then, on that leg we have one less number of insertion vertex, and one less number of scalar propagator. Suppose for now, if the leg is the p'-leg, and if the new insertion vertex μ was a trilinear vertex inserted between vertex number $(q-1)$ and q then, corresponding overall charge and thermal factors would be

$$
\left[(-1)^{\sum_{i=1}^{s}(t_i+1)}(-ie)^s\right]\left[i^{s+1}\right]\left[-ie(-1)^{(t_\mu+1)}\right] = (-1)^{\sum_{i=1}^{s}(t_i+1)} (-1)^{(t_\mu+1)} (e)^{s+1} , \tag{4.28}
$$

for the contribution corresponding to that leg (p'-leg). The exact factor corresponds to factors arising from [s numbers of already present trilinear vertex] times [$(s+1)$ number of scalar propagators on p'-leg] times [vertex factor coming due to new μ trilinear insertion].

Now, if the new μ insertion vertex becomes a seagull vertex at already present vertex number q on p'-leg then, the corresponding overall factor coming due to that case is,

$$
\begin{aligned}
\left[(-1)^{\sum_{i=1,i\neq q}^{s}(t_i+1)}(-ie)^{s-1}\right]\left[i^s\right]&\left[2ie^2(-1)^{(t_\mu+1)}\delta_{t_\mu,t_q}\,g_{\mu\mu_q}\right]\\
&=(-1)^{\sum_{i=1}^{s}(t_i+1)}\,(-1)^{(t_\mu+1)}\,(e)^{s+1}\times\left[(-1)^{(t_\mu+1)}\delta_{t_\mu,t_q}\left(-2g_{\mu\mu_q}\right)\right]\,.
\end{aligned}
$$
(4.29)

The above factor correspond to $[(s-1)$ numbers of trilinear vertices] times [s number of scalar propagators on p'-leg] times [the vertex contribution of $\mu=q$ seagull vertex on the p'-leg]. We have also manipulated the delta function as,

$$
\delta_{t_\mu,t_q}=(1)\times\delta_{t_\mu,t_q}=(-1)^{(t_\mu+1)}(-1)^{(t_\mu+1)}\times\delta_{t_\mu,t_q}=(-1)^{(t_\mu+1)}(-1)^{(t_q+1)}\times\delta_{t_\mu,t_q}\quad(4.30)
$$

in Eq. 4.29. Therefore we find presence of a $[(-1)^{(t_\mu+1)}\delta_{t_\mu,t_q}(-2g_{\mu\mu_q})]$ extra factor for the case of seagull insertion at $q=\mu$ with respect to new trilinear insertion between $(q-1)$ and q , which will be absorbed inside $C_{s+1}^{\text{scalar }p';\mu}$ contribution in Eq. 4.27 when written symbolically, making the *separated out* overall factors arising due to new insertion vertex to be similar for the both cases, corresponding to seagull and trilinear vertex.

By convention, the contribution $C_{s+1}^{\text{scalar }p';\mu}$ in Eq. 4.27 now suggest that this refers to the contribution of p'-leg in scalar QED, when new insertion vertex μ has been inserted on the p'-leg. The $(s+1)$ factor in subscript is to correctly track the factors of electron charge e coming out of this higher order contribution with respect to $C_s^{\text{scalar }p'}$. In any case, whether the new vertex is trilinear or seagull the $C_{s+1}^{\text{scalar }p';\mu}$ *always* contributes an extra factor of electric charge, e with respect to $C_s^{\text{scalar }p'}$; and hence suggesting the notation $(s+1)$ in subscript. It should be also noted that $(s+1)$ does not always represent the number of dotted vertices on a higher order *schematic diagram* truthfully for *scalar QED* ; as now both seagull and trilinear vertices are possible. A trilinear new vertex will certainly increase the number of vertices on p'-leg to $(s+1)$; but if the new vertex is of seagull type then number of vertices on p'-leg will not increase and will be 's' (but the number

68

of electron charge factors will be same for both the cases, as seagull vertex contributes a factor of e^2 in contrast to a trilinear vertex that contributes a factor of e). Hence, in the subscript, the number $(s+1)$ for $C_{s+1}^{\text{scalar } p';\mu}$ have to be taken with a pinch of salt. The difference between fermionic and scalar case hence is that in fermionic case $C_{s+1}^{\text{fermion } p';\mu}$ contribution suggest that there are *exactly* $(s+1)$ number of dotted vertices on the p'-leg, but in scalar case $C_{s+1}^{\text{scalar } p';\mu}$ contribution does not always imply $(s+1)$ numbers of dotted vertices on the p'-leg. For scalar QED there are some diagrams (where every dotted vertices are trilinear), where there are *exactly* $(s+1)$ number of dotted vertices on the schematic diagram; but then in that contribution $C_{s+1}^{\text{scalar } p';\mu}$ there also exist such diagrams (where seagull vertices are present) for which the number of vertices are less than $(s+1)$. Hence, for the scalar case it should be understood that the *maximum number* of dotted vertices on schematic diagram for contribution $C_{s+1}^{\text{scalar } p';\mu}$ can be $(s+1)$; but then each diagram which belongs to this contribution $C_{s+1}^{\text{scalar } p';\mu}$, contributes a factor of e^{s+1} (which has exactly one more charge 'e' factor than $C_s^{\text{scalar } p'}$) to the matrix element, and this notation is a matter of book-keeping. A similar argument can also be spoken about $C_{r+1}^{\text{scalar } p;\nu}$ in Eq. 4.27 .

With the understanding of the all the above discussion and with the help of Eq. 4.12, the relevant part of the higher order matrix element corresponding to the virtual K photon insertion in the Eq. 4.27 can be written symbolically as

$$
\begin{aligned}
i\mathcal{M}_{n+1}^{\text{scalar}; K\gamma, p', p} &= (e)^{2n+2}(-1)^{\sum_{i=1}^{m}(t_i+1)}(-1)^{(t_\mu+1)}(-1)^{(t_\nu+1)}\times \\
&\int \frac{\mathrm{d}^4 k}{(2\pi)^4}\left[k_\mu C_{s+1}^{\text{scalar } p';\mu}\right]\times \Gamma_V \times \left[k_\nu C_{r+1}^{\text{scalar } p;\nu}\right]\times [b_k(p',p)\times -iD^{t_\mu,t_\nu}]\times \mathcal{D}_n .
\end{aligned}
$$
(4.31)

where the effect from K photon insertions has been separated out. From the above expression we can see that, now $k_\mu C_{s+1}^{\text{scalar } p';\mu}$ and $k_\nu C_{r+1}^{\text{scalar } p;\nu}$ contributions can be evaluated independently of each other.

Effect of virtual K photon insertion : We will discuss about the fundamentals of the $k_\mu C_{s+1}^{\text{scalar } p';\mu}$ contribution here (the full sophisticated discussion[2] about K photon insertion for thermal scalar QED is mentioned in detail in Chapter 5) at first, and then will discuss about $k_\nu C_{r+1}^{\text{scalar } p;\nu}$ contribution.

The $k_\mu C_{s+1}^{\text{scalar } p';\mu}$ contribution comprises of two distinct sets of diagrams shown respectively in Fig. 4.6 and Fig. 4.7 below.
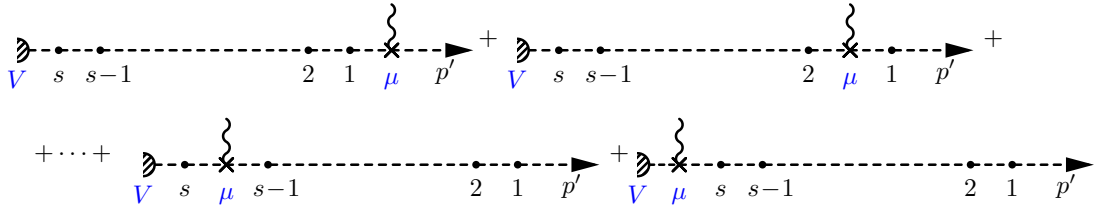
Figure 4.6: $(s + 1)$ *number of diagrams, which are schematically representing all the possible trilinear insertions of a virtual K photon at vertex μ on the p′ leg in thermal scalar QED. These figure is analogue of Fig. 4.2 of thermal fermionic QED.*

These diagrams in the Fig. 4.6 above correspond to the, new trilinear insertion vertices. All possible ways of inserting the trilinear vertices on the p'-leg (which already had s number of vertices) in thermal scalar QED generates $(s + 1)$ number of diagrams which are exactly the analogue of similar diagrams in Fig. 4.2 of thermal fermionic QED.

In addition to these diagrams, there are also a set of (s) number of diagrams arising due to seagull insertions of a virtual K photon at vertex μ to one of the already existing vertices on p'-leg. Those set of diagrams[3] are unique to this scalar QED and have been schematically drawn in Fig. 4.7.

---

[2]We have restricted the discussions here, to a point where the Generalized Feynman Identities (Appendix B) for scalars are used to reduce the expressions of particular K photon diagrams producing difference of two terms (similar to the thermal fermionic QED case of Eq. 4.19).

[3]Note that we have assumed all vertices of the underlying n^{th} order graph are trilinear so that an additional photon can be inserted at each one. We will relax this assumption later when we perform the complete calculation in Chapter 5.
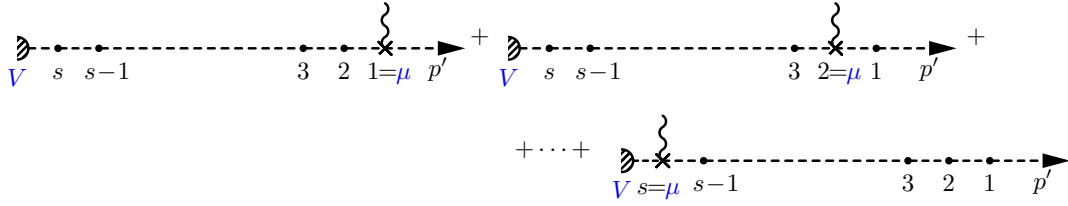
Figure 4.7: *s number of diagrams, which are schematically representing all the possible seagull insertions of a virtual K photon at vertex μ to one of the already existing vertex, on the p′-leg in thermal scalar QED. These are extra contributions for scalar QED case, analogue of which does not exist in fermionic QED.*

We will schematically define now the circled vertex, which will be a convenient group of typical diagrams from the set of trilinear diagrams from Fig. 4.6, and from the set of seagull (quadrilinear) diagrams from Fig. 4.7. On the p'-leg for a new K photon insertion at vertex μ we will combine the insertion of trilinear μ vertex to the *right* of a generic vertex number q, with the seagull μ vertex *at* the vertex number q. These two generic diagrams are schematically shown in Fig. 4.8. Contribution from the addition of these two diagram is also shown in Fig. 4.8, and is schematically pictured by a circled vertex, which is denoted and labeled by notation $_q\mu$.
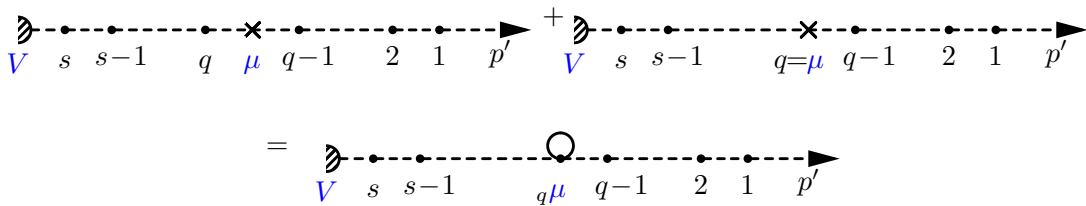
Figure 4.8: *A generic diagram having trilinear new μ insertion located to the immediate right of vertex number q from Fig. 4.6, and new seagull μ insertion at vertex number q from Fig. 4.7; is combined together to produce a single* circled vertex, *which is denoted and labeled by $_q\mu$. The photon lines have been suppressed in above diagram for the clarity.*

This definition of circled vertices will help us a lot in upcoming discussion, to schematically represent of higher order diagrams, when the number of these diagrams proliferate considerably.

The contribution of trilinear diagram shown in Fig. 4.8 can be written as,

$$
\begin{aligned}
k_\mu\, C_{s+1}^{\text{scalar } p';\mu\,\text{right of } q} &= (2p'+l_1')_{\mu_1} S_{p'+\Sigma_1}^{t_1,t_2}\cdots (2p'+2\Sigma_{q-2}+l_q')_{\mu_{q-1}} \Bigg[S_{p'+\Sigma_{q-1}}^{t_{q-1},t_\mu} \\
&\quad (2p'+2\Sigma_{q-1}+k)\cdot k\, S_{p'+\Sigma_{q-1}+k}^{t_\mu,t_q} (2p'+2\Sigma_{q-1}+2k+l_q')_{\mu_q}\Bigg]\times \\
&\quad S_{p'+\Sigma_q+k}^{t_q,t_{q+1}}\cdots, \\
&= (-1)^{(t_\mu+1)}(2p'+l_1')_{\mu_1} S_{p'+\Sigma_1}^{t_1,t_2}\cdots (2p'+2\Sigma_{q-2}+l_q')_{\mu_{q-1}}\Bigg[\Big\{\delta_{t_\mu,t_q} S_{p'+\Sigma_{q-1}}^{t_{q-1},t_q} - \\
&\quad \delta_{t_\mu,t_{q-1}} S_{p'+\Sigma_{q-1}+k}^{t_{q-1},t_q}\Big\} (2p'+2\Sigma_{q-1}+2k+l_q')_{\mu_q}\Bigg] S_{p'+\Sigma_q+k}^{t_q,t_{q+1}}\cdots,
\end{aligned}
$$

$$(4.32)$$

where the separation of the bracketed term is the result of application of 'Generalized Feynman Identity' (see Eq. B.6) as mentioned in Appendix B . And, again $(-1)^{(t_\mu+1)}$ factor arises here as a result of GY reduction.

With the understanding of the overall factors mentioned in Eq. 4.29, the contribution of seagull diagram as shown in Fig. 4.8 can be expressed as,

$$
\begin{aligned}
k_\mu\, C_{s+1}^{\text{scalar } p';\mu\,\text{at } q} &= (-1)^{(t_\mu+1)}(2p'+l_1')_{\mu_1} S_{p'+\Sigma_1}^{t_1,t_2}\cdots (2p'+2\Sigma_{q-2}+l_q')_{\mu_{q-1}} \\
&\quad \Big[S_{p'+\Sigma_{q-1}}^{t_{q-1},t_\mu}\, \delta_{t_\mu,t_q}(-2g_{\mu\mu_q})k^\mu\Big]\times S_{p'+\Sigma_q+k}^{t_q,t_{q+1}}\cdots.
\end{aligned}
$$

$$(4.33)$$

We have to note here that the contribution of this diagram also produces a factor of $(-1)^{(t_\mu+1)}$. This exact same factor was also produced in Eq. 4.32 after using Feynman's identity. This same overall factor gives us freedom to club together Eq. 4.32 and Eq. 4.33 as a circled vertex as shown in Fig. 4.8.

The square bracketed term in Eq. 4.33 will produce a factor $(-2g_{\mu\mu_q})k^\mu = -2k_{\mu_q}$ and will cancel against a similar term from Eq. 4.32, when adding together the contributions as circled vertex. Therefore, the contribution of the circled vertex which is shown in Fig. 4.8

and is given by the sum of Eq. 4.32 Eq. 4.33 evaluates to,

$$
\begin{aligned}
k_\mu\, C_{s+1}^{\text{scalar }p';\,q\mu} &\equiv k_\mu\left(C_{s+1}^{\text{scalar }p';\,\mu\,\text{right of }q} + C_{s+1}^{\text{scalar }p';\,\mu\,\text{at }q}\right), \\
&= (-1)^{(t_\mu+1)}(2p'+l_1')_{\mu_1} S_{p'+\Sigma_1}^{t_1,t_2} \cdots \left[S_{p'+\Sigma_{q-1}}^{t_{q-1},t_q}\,\delta_{t_\mu,t_q}\left(2p'+2\Sigma_{q-1}+l_q'\right)_{\mu_q} \right. \\
&\qquad \left. - S_{p'+\Sigma_{q-1}+k}^{t_{q-1},t_q}\,\delta_{t_\mu,t_{q-1}}\left(2p'+2\Sigma_{q-1}+2k+l_q'\right)_{\mu_q} \right] S_{p'+\Sigma_q+k}^{t_q,t_{q+1}} \cdots, \\
&\equiv M_q - M_{q-1}.
\end{aligned}
\tag{4.34}
$$

The term having a factor proportional to $(2k_{\mu_q})$ in Eq. 4.32 has canceled with an opposite contribution from seagull insertion in Eq. 4.33, in the parentheses of the first squared bracketed term in expression above. Eq. 4.34 is the analogue of the fermionic QED result as mentioned in Eq. 4.15 to the scalar QED case, but looks little cumbersome and is not so clean.

A similar redefinition of circled vertex can be done for $k_\nu\, C_{r+1}^{\text{scalar }p;\,\nu}$ contribution term (defined as in Eq. 4.31) for the insertions on the p-leg. A typical diagrams for this case is shown below in Fig. 4.9.
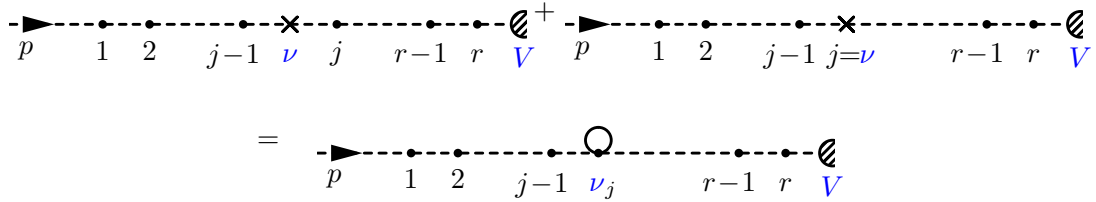
Figure 4.9: *A generic diagram having trilinear new ν insertion to the immediate* left *of vertex number j, and new seagull ν insertion at vertex number j on p-leg is combined together to produce a single* circled vertex*, which is denoted and labeled by* ν_j.

In contrast to Fig. 4.8, here in Fig. 4.9, the new vertex insertion ν when placed immediately *left* to vertex j, is added together with ν at j seagull insertion to form a circled vertex. Such a clubbing of diagrams is done because, as per our notation the momenta of K photon enters at vertex ν and thus flows through the vertex j. Hence, to have a similar cancellation of $(2k_{\nu_j})$ term as in Eq. 4.34, the above grouping of diagrams is done.

With this consideration the contribution of the v_j circled vertex is expressed as below,

$$
\begin{aligned}
k_v C_{s+1}^{\text{scalar}; v_j} &\equiv k_v \left(C_{r+1}^{\text{scalar } p; \, v \text{ left of } j} + C_{r+1}^{\text{scalar } p; \, v \text{ at } j} \right) , \\
&= (-1)^{(t_v+1)} \cdots S_{P+\Sigma_j+k}^{t_{j+1}, t_j} \times \\
&\quad \left[\delta_{t_v, t_j} \left(2P + 2\Sigma_{j-1} + l_j \right)_{v_j} S_{P+\Sigma_{j-1}}^{t_j, t_{j-1}} - \delta_{t_v, t_{j-1}} \left(2P + 2\Sigma_{j-1} + 2k + l_j \right)_{v_j} S_{P+\Sigma_{j-1}+k}^{t_j, t_{j-1}} \right] \times \\
&\quad \left(2P + 2\Sigma_{j-2} + l_{j-1} \right)_{v_{j-1}} \cdots \left(2P + l_1 \right)_{v_1} , \\
&\equiv N_j - N_{j-1} .
\end{aligned}
\tag{4.35}
$$

The things to note here is that, this contribution is proportional to an overall factor $(-1)^{(t_v+1)}$ as this is related to the insertion of v vertex. And, in the first parentheses of the square bracketed term a similar $(2k_{v_j})$ term has vanished. Actually, Eq. 4.35 is an exact analogue of Eq. 4.34, which will be used in greater detail in Chapter 5 .

Now, before moving onto further discussion; let us take time to say a few words regarding the notations of circled vertices. There are three cases related to the insertion of K of G photons; corresponding to when μ and v vertices are inserted on different legs, or the cases where both of them are inserted on the same leg (two cases). Now, to avoid double-counting of the vertices, we will always place v vertex to the left of μ vertex, irrespective of whether both the vertices are on same leg of different legs. And, we will always consider photon momentum k leaving at vertex μ and entering at vertex v without loss of any generality (as this momenta is anyway integrated over all possible values ranging from $-\infty$ to $+\infty$). Hence, this photon momentum now flows through all the scalar (or fermion, as appropriate) propagators which are in between vertex v and μ , and all the other outside propagator momenta remain unchanged. Hence, from this perspective as v can be the leftmost vertex from where the photon momentum k starts to flow and ends at the rightmost vertex μ, all the internal scalar vertices now have extra factors depending on the photon momentum according to the Feynman rules of scalar QED. To counteract this extra momentum factor of $(2k)$ at trilinear vertex corresponding to v/μ insertion, they have been grouped together with adjacent seagull vertex arising due to insertion of v/μ vertex,

justifying the definition of Fig. 4.8 and Fig. 4.9.

Therefore, irrespective of the choice of legs it should be understood[4].

- $_q\mu$ contribution

  $\equiv$ contribution of (trilinear μ to the right of q) + (seagull μ insertion at q);

- ν_j contribution

  $\equiv$ contribution of (trilinear ν to the left of j) + (seagull ν insertion at j).

For the case where both the insertion vertices of new photon are on the same scalar leg, there can be a circled vertex denoted by $_\nu\mu$ (as to avoid double count ν is always placed left to μ insertion). This circled vertex should be understood as follows,

- $_\nu\mu$ contribution $\equiv \nu_\mu$ contribution

  $\equiv$ contribution of (trilinear ν to the left of trilinear μ) + (seagull ν, μ vertex contribution, which is actually a tadpole).

With this understanding, and with all the results of Eq. 4.34 and Eq. 4.35 it can be shown the K photon contribution factorizes and contains all the leading linear and logarithmic, and sub-leading logarithmic divergences. The proof of this is rather intricate and involved, and hence is the discussion material of Chapter 5.

Effect of virtual G photon insertion **:** The contribution of virtual G photon after incorporating correct factors from Eq. 4.3 and Eq. 4.13 can be shown to have superficial leading linear and sub-leading logarithmic divergences pertaining to thermal fluctuations, and leading logarithmic divergences due to quantum fluctuations.

---

[4] In special cases, due to the requirement and for convenience related to particular calculation there may be a need to define μ_q and $_j\nu$ contributions; and these have to be understood according to the defined notations; *i.e.*, **1.** μ_q contribution $\equiv$ contribution of (trilinear μ to the left of q) + (seagull μ insertion at q), and **2.** $_j\nu$ contribution $\equiv$ contribution of (trilinear ν to the right of j) + (seagull ν insertion at j).

It will be shown in Chapter 5 that all those divergences in G photon contributions for the theory thermal scalar QED vanishes, making the G photon contributions IR finite.

4.4.2 Effect of insertion of $\widetilde{K}, \widetilde{G}$ photon contributions

The effects of contributions arising from the real $\widetilde{K}$ and $\widetilde{G}$ photons for thermal scalar QED can be computed in the square of matrix element level by noting the effects of Eq. 4.5. Here in this case, we also have to consider the fact that, in addition to photon emission to the heat bath, the absorption of photons from the heat bath is also perfectly feasible with different phase space weight factors as mentioned in Eq. 4.7 . And, *only* with the inclusion of the photon absorption the IR divergent pieces cancel between real and virtual cross-sections.

Considering correct phase space factors, it can be shown (and will be shown in Chapter 5) that all the leading and sub-leading IR divergences is contained in real $\widetilde{K}$ photon contributions. These IR divergences will cancel with virtual K photon contributions order by order to all orders in perturbation theory.

The $\widetilde{G}$ contributions turn out to be IR finite (Chapter 5), after noting that the phase space factor related to finite temperature is symmetric in photon momenta.

4.5 Summary

The IR structure of a thermal field theory is far more intricate than for the similar theory at zero temperature due to the presence of thermal fluctuations. Particularly, for the theories involving bosons the IR structure is much more complicated to tackle as the distribution function of massless bosons diverge at IR limit. In addition to that, for a thermal field theory, particles can be both emitted to and absorbed from the heat bath. And, *only* with the inclusion of the absorption of particles the cross-section turns out to be IR finite.

This knowledge was applied fruitfully, to generalize the GY technique to thermal field theories in Section. 4.2 . We have then applied this generalized GY technique for thermal fermionic QED and thermal scalar QED to show the validity of the technique. The thermal theory of the charged scalars are complicated to discuss as in addition to normal trilinear vertices, quadrilinear seagull vertices are also allowed. We define circled vertex in Section. 4.4 to systematically include this effect. It has been mentioned that all the IR divergences of thermal scalar QED are contained in virtual K and real $\widetilde{K}$ photon contributions, while the G and $\widetilde{G}$ photon contributions are finite. The IR divergences cancel among virtual K and real $\widetilde{K}$ photon contributions.

The cross-section related to thermal scalar QED turns out to be IR finite and the intricate details of that proof is discussed in details in next chapter, *i.e.*, Chapter 5.

Chapter 5

Infrared safety of scalar QED at finite temperature

5.1 Prologue

The enhancement of the complexity of the Infrared (IR) structure due to the presence of thermal fluctuations has been a main topic of discussion in Chapter 4. We have discussed the effects of the finite temperature in the IR structure particularly in fermionic and scalar QED. Just like fermionic QED, the IR structure of scalar QED at zero temperature has been a matter of extreme interest in literature and has been discussed in several of them using different formulations and techniques.

At zero temperature, Low showed that [7] the IR divergence structure of the soft photons for processes involving bremsstrahlung has a general structure as given by expression below,

$$\sigma_{\text{brems}} = \frac{\sigma_0}{k} + \sigma_1 + k\sigma_2 + \dots , \tag{5.1}$$

where all the σ_i have appropriate dimensions; and energy of the photon is denoted by k. Low has showed that this structure is independent of the spin of the charged particle as long

as the particle is massive. A generalization of this theorem was proved by Weinberg [15], showing the leading IR structure to be independent of the spin structure, even for the theories involving gravitation. To understand and interpret the IR structure of fermionic QED at zero temperature clearly, a reformulation of fermionic QED in terms of dressed coherent asymptotic states was performed in Ref. [24]. A similar reformulation was also performed for scalar QED at zero temperature, using velocity super-selection rules motivated by heavy quark effective theories to obtain on-shell IR finite Green's functions to all orders in perturbation theory in Ref. [132,133] . They have also shown that due to spin structure of scalar QED the asymptotic dynamics becomes more rich, as the charged scalar particles go massless, turning on the collinear divergences. A more recent discussion on this rich asymptotic dynamics, and on the phase space of scalar QED at zero temperature can be found in Ref. [32] .

There have also been discussions regarding the IR finite pieces of scalar QED at zero temperature, in Ref. [134–136] where factorizing and exponentiation of IR divergent contributions are proved in a translation and gauge invariant fashion. They achieved this IR factorization after incorporating an order by order agreement with Operator Product Expansion (OPE). Then, after generalizing Low's theorem to all orders (which involve both soft and hard photon term calculations) they were able to produce IR finite contributions in terms of correlations relating to the photon momentum in the integrands.

Although all these developments have been immensely helpful to understand the foundation of the IR structure of scalar QED at zero temperature, the actual calculation of IR finite pieces in scalar QED order by order (at even zero temperature) in perturbation theory is still quite troublesome (often the calculations depend on imposing an IR cut-off by hand). Hence, inspired by the technique of GY at zero temperature (which does not require IR cut-off to predict IR finite pieces) for fermionic QED [12] we examine the IR structure of scalar QED at finite temperature in this chapter using the extension of GY technique to finite temperature [41–43] . While identifying the intricate IR structure of scalar QED

80

at finite temperature, we also consequently prove the IR finiteness of the scalar QED at zero temperature ($T \rightarrow 0$ limit). The identification of correct IR finite contributions order by order in scalar QED at finite temperature is more difficult due to the presence of both the trilinear (3-point) scalar-photon-scalar vertices and quadrilinear (4-point) seagull scalar-scalar-photon-photon vertices; along with the presence of additional leading linear and sub-leading logarithmic IR divergences present at finite temperature. This identification and prediction of IR finite pieces will be of fundamental importance in many different scenarios involving different physics. We in our future discussions, in Chapter 6 will be interested in models of Dark Matter (DM), Ref. [86, 103] where heavy charged scalars are involved. The finite temperature higher order corrections to such models of DM are extremely important to predict the temperature corrections to relic densities of DM. Hence, a thorough understanding of the thermal scalar QED is indispensable for these calculations.

The relevant Lagrangian for our analysis of scalar QED is,

$$\mathcal{L}_{\text{sQED}} = (\mathcal{D}_\mu \phi)^\dagger (\mathcal{D}_\mu \phi) - m_\phi^2 \phi^\dagger \phi - \frac{1}{4} F_{\mu\nu} F^{\mu\nu} \,. \tag{5.2}$$

In the above expression covariant derivative is, $\mathcal{D}_\mu = \partial_\mu + ieA_\mu$; and ϕ is the charged scalar. In Eq. 5.2 we have dropped a quartic scalar self coupling which will be generically present in theories of charged scalars (like theories involving squarks, sleptons). But, those quartic couplings does not give us any further new insight regarding GY procedure involved and therefore has been simply dropped here without loss of any generality of the upcoming discussions.

From the Lagrangian we can see that in addition to normal trilinear interaction vertex, in theories of scalar QED we also have presence of quadrilinear seagull vertex as shown in Fig. 5.1. The presence of these seagull vertices plays a crucial role in the identification of IR structure. And, it will be seen in upcoming discussions, that only in the presence of these seagull vertices and tadpole diagrams is an *exact* and clean IR factorization and resummation possible.

81
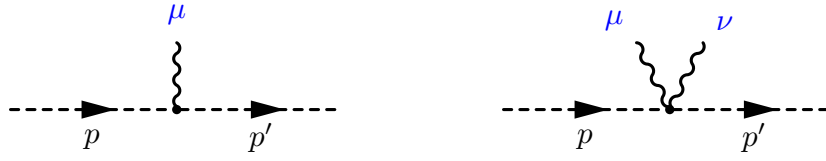
a. Trilinear Interaction Vertex   b. Quadrilinear Seagull Vertex

Figure 5.1: *Allowed vertices for scalar-photon interactions. Here dashed lines represent scalars.*

5.2 Insertion of virtual K photons

To identify and separate out the relevant IR divergent pieces, the effect of insertion of virtual K photons have to be taken into account. We will start with inclusion of virtual K photon to an nth order process corresponding to $\phi(p)\gamma^*(q) \rightarrow \phi(p')$ in scalar QED at finite temperature as was shown in Fig. 4.5. For completeness and convenience of the readers we again present the schematic diagram related to above process here in Fig. 5.2.
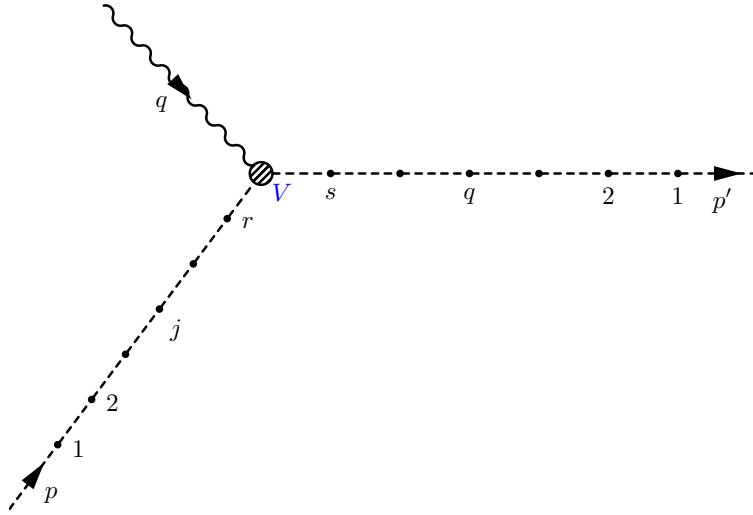
Figure 5.2: *The schematic diagram of a nth order process $\phi(p)\gamma^*(q) \rightarrow \phi(p')$ in thermal scalar QED, which was also shown in Fig. 4.5. Here, any dotted vertex can represent a seagull or a trilinear vertex. Therefore, even for a nth order diagram with all virtual photon vertices, $n \leq s + r = m \leq 2n$.*

In Fig. 5.2 and in upcoming discussions, all the previously mentioned notations which were defined in paragraphs below Fig. 4.5 and Eq. 4.26 hold true. Therefore, with the understanding that the already existing photon momenta at the $p'(p)$-leg are always outgoing(incoming) (without loss of any generality), and are denoted by $l'_i(l_i)$, we can write down the matrix element corresponding to the nth order matrix element.

A single dotted vertex in Fig. 4.5 can either represent a trilinear or a seagull insertion vertex. Here, we will start with a nth order diagram, where all the existing dotted vertices represent virtual photon trilinear insertions. We will relax the constraints one by one in the following discussion; *i.e.*, will include seagull and real photons successively.

So, for an nth order diagram with all the already existing vertices representing trilinear virtual photon insertion the matrix element can be written as,

$$
\begin{aligned}
i\mathcal{M}_n^{\text{scalar}} =& (e)^{2n}(-i)^m(-1)^{\sum_{i=1}^{m}(t_i+1)}(i)^m \times \Big[(2p' + l'_1)_{\mu_1} S^{t_1,t_2}_{p'+\Sigma_1} \cdots \times \\
& (2p' + 2\Sigma_{s-2} + l'_{s-1})_{\mu_{s-1}} S^{t_{s-1},t_s}_{p'+\Sigma_{s-1}} (2p' + 2\Sigma_{s-1} + l'_s)_{\mu_s} S^{t_s,t_V}_{p'+\Sigma_s} \Big] \times \Gamma_V \times \\
& \Big[S^{t_V,t_r}_{p+\Sigma_r} (2p + 2\Sigma_{r-1} + l_r)_{\nu_r} S^{t_r,t_{r-1}}_{p+\Sigma_{r-1}} \cdots S^{t_2,t_1}_{p+\Sigma_1} (2p + l_1)_{\nu_1} \Big] \times \mathcal{D}^{\mu_1,\cdots,\mu_s;\nu_r,\cdots,\nu_1}_{\{t_i\}} \\
=& (e)^{2n}(-i)^m(-1)^{\sum_{i=1}^{m}(t_i+1)}(i)^m \times \Big[\mathcal{C}_s^{\text{scalar }p'} \Big] \times \Gamma_V \times \Big[\mathcal{C}_r^{\text{scalar }p} \Big] \times \mathcal{D}_n ,
\end{aligned} \tag{5.3}
$$

which is the same expression which was expressed in Eq. 4.26, and we have mentioned it here again for completeness and convenience of readability. The new virtual photon can be added in exactly three ways to this diagram. The first way, where the new insertion vertices are on different legs; and in other two cases the ends of photon insertions will be on the same leg. Let us start with the first case.

5.2.1 K photon insertion between p and p'-leg

Let us start with adding a virtual photon in all possible ways in an nth order diagram between p and p'-leg. The resulting expression can be written down symbolically as,

$$i\mathcal{M}_{n+1}^{\text{scalar};p',p} = (e)^{2n+2}(-i)^{m+2}(-1)^{\sum_{i=1}^{m}(t_i+1)}(-1)^{(t_\mu+1)}(-1)^{(t_\nu+1)}(i)^{m+2}\times$$

$$\left[C_{s+1}^{\text{scalar }p';\mu}\right]\times\Gamma_V\times\left[C_{r+1}^{\text{scalar }p;\nu}\right]\times\mathcal{D}_{n+1}^{\mu\nu}. \tag{5.4}$$

As the new insertion can be trilinear or seagull, the above expression has been only expressed symbolically. It contains both the trilinear and seagull insertion contributions. The reader is referred to the discussions below Eqs. 4.27, 4.28 and 4.29 to fully understand the notation related to Eq. 5.4 .

The relevant virtual K photon insertion from this term is specified in Eq. 5.5, which is repetition of Eq. 4.31 and the readers are referred to the discussion below Eq. 4.31 for notational clarity. We have

$$i\mathcal{M}_{n+1}^{\text{scalar};K\gamma,p',p} = (e)^{2n+2}(-1)^{\sum_{i=1}^{m}(t_i+1)}(-1)^{(t_\mu+1)}(-1)^{(t_\nu+1)}\times$$

$$\int\frac{\mathrm{d}^4k}{(2\pi)^4}\left[k_\mu C_{s+1}^{\text{scalar }p';\mu}\right]\times\Gamma_V\times\left[k_\nu C_{r+1}^{\text{scalar }p;\nu}\right]\times\left[b_k(p',p)\times -iD^{t_\mu,t_\nu}\right]\times\mathcal{D}_n.$$

$$\tag{5.5}$$

From the above expression we can find that, now $k_\mu C_{s+1}^{\text{scalar }p';\mu}$ and $k_\nu C_{r+1}^{\text{scalar }p;\nu}$ contributions can be evaluated independently of each other.

The contribution of the p'-leg, $i.e.$, $k_\mu C_{s+1}^{\text{scalar }p';\mu}$ consist of two distinct sets of diagrams; shown in Fig. 4.6 and Fig. 4.7. Fig. 4.6 denotes all new possible trilinear insertions on the p'-leg and Fig. 4.7 refers to all the new insertion vertices being seagull insertions. For the sake of convenience a trilinear vertex 'μ to the right of vertex number q' and a seagull vertex 'μ at the vertex number q' on p'-leg were grouped together in Fig. 4.8 resulting in a circled vertex denoted by '$_q\mu$' contribution of which is expressed in Eq. 4.34.

Hence, using the convention of circled vertices on p'-leg, the (s) seagull insertion diagrams of Fig. 4.7 can be grouped together with the first (s) number of the trilinear insertion diagrams of Fig. 4.6. The last trilinear contribution of Fig. 4.6 is left un-grouped. The resulting diagram after this regrouping is shown in Fig. 5.3.
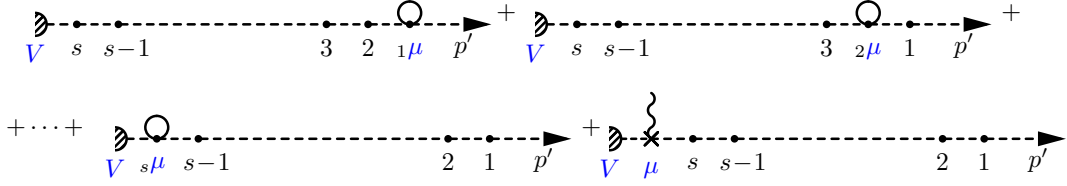
Figure 5.3: *The sets of diagrams in Figs. 4.6 and 4.7 are grouped to form the s circled vertices and one leftover $(s+1)^{th}$ trilinear diagram (where the new μ vertex is inserted to the left of vertex number s on the p'-leg).*

The corresponding contribution $k_\mu C_{s+1}^{\text{scalar } p';\mu}$ can be written down symbolically as,

$$k_\mu C_{s+1}^{\text{scalar } p';\mu} = \left[\sum_{q=1}^{s} k_\mu C_{s+1}^{\text{scalar } p';q\mu} \right] + \left[k_\mu C_{s+1}^{\text{scalar } p';\mu \text{ left of } s} \right]. \tag{5.6}$$

The terms in the first square bracket in Eq. 5.6 represent the (s) number of circled vertex diagrams. The contribution of these terms after using Eq. 4.34 can be expressed as

$$
\begin{aligned}
\sum_{q=1}^{s} k_\mu C_{s+1}^{\text{scalar } p';q\mu} &= (-1)^{(t_\mu+1)} \times \Bigg(\Big\{ 0 + \delta_{t_\mu,t_1}(2p'+l'_1)_{\mu_1} S_{p'+\Sigma_1+k}^{t_1,t_2} \times \\
&\quad (2p'+2\Sigma_1+2k+l'_2)_{\mu_2} \cdots S_{p'+\Sigma_s+k}^{t_s,t_V} \Big\} \\
&\quad + \Big\{ (2p'+l'_1)_{\mu_1} \Big[S_{p'+\Sigma_1}^{t_1,t_2} \delta_{t_\mu,t_2}(2p'+2\Sigma_1+l'_2)_{\mu_2} \\
&\quad - S_{p'+\Sigma_1+k}^{t_1,t_2} \delta_{t_\mu,t_1}(2p'+2\Sigma_1+2k+l'_2)_{\mu_2} \Big] \cdots S_{p'+\Sigma_s+k}^{t_s,t_V} \Big\} \\
&\quad + \{ \cdots \} \\
&\quad + \Big\{ (2p'+l'_1)_{\mu_1} S_{p'+\Sigma_1}^{t_1,t_2} \cdots \Big[S_{p'+\Sigma_{s-1}}^{t_{s-1},t_s} \delta_{t_\mu,t_s}(2p'+2\Sigma_{s-1}+l'_s)_{\mu_s} \\
&\quad - S_{p'+\Sigma_{s-1}+k}^{t_{s-1},t_s} \delta_{t_\mu,t_{s-1}}(2p'+2\Sigma_{s-1}+2k+l'_s)_{\mu_s} \Big] S_{p'+\Sigma_s+k}^{t_s,t_V} \Big\} \Bigg), \\
&= \Big(\{0+M_1\} + \{M_2-M_1\} + \{\cdots\} + \{M_s-M_{s-1}\} \Big). \tag{5.7}
\end{aligned}
$$

In Eq. 5.7 each circled vertex gives rise to difference of two terms in accordance with Eq. 4.34 and the first contribution vanishes as scalar p'-leg is on-shell. The terms cancels among themselves in pairs.

The singled out trilinear contribution (last diagram of Fig. 5.3), which is expressed symbolically as in the second squared bracketed term in Eq. 5.6, can also be expressed as difference of two terms after using Eq. 4.32 as,

$$k_\mu C_{s+1}^{\text{scalar } p';\, \mu \text{ left of } s} = (-1)^{(t_\mu+1)} \left\{ (2p' + l_1')_{\mu_1} S_{p'+\Sigma_1}^{t_1,t_2} \cdots (2p' + 2\Sigma_{s-1} + l_s')_{\mu_s} \times \right.$$
$$\left. \left[S_{p'+\Sigma_s}^{t_s,t_V} \delta_{t_\mu,t_V} - S_{p'+\Sigma_s+k}^{t_s,t_V} \delta_{t_\mu,t_s} \right] \right\},$$
$$= \{ M_{s+1} - M_s \} . \tag{5.8}$$

Here, the contribution M_s of Eq. 5.8 cancels with a similar remnant term from Eq. 5.7, giving rise to the total contribution $k_\mu C_{s+1}^{\text{scalar } p';\, \mu}$ to be proportional to the lower order contribution $C_s^{\text{scalar } p'}$ times the delta function δ_{t_μ,t_V} which resulted due to GY reduction,

$$k_\mu C_{s+1}^{\text{scalar } p';\, \mu} = (-1)^{(t_\mu+1)} \left\{ (2p' + l_1')_{\mu_1} S_{p'+\Sigma_1}^{t_1,t_2} \cdots S_{p'+\Sigma_s}^{t_s,t_V} \left[\delta_{t_\mu,t_V} \right] \right\}$$
$$= (-1)^{(t_\mu+1)} \delta_{t_\mu,t_V} C_s^{\text{scalar } p'} . \tag{5.9}$$

In Eq. 5.9 the external hard photon being physically observable, the thermal type of vertex V is of type-1, *i.e.*, $t_V = 1$. And, hence, the delta function in above expression constrains $t_\mu = 1$ also.

A similar regrouping of the terms can be performed on the p-leg also regarding the $k_\nu C_{r+1}^{\text{scalar } p;\, \nu}$ term of Eq. 5.5. The sets of diagrams after using the notation of circled vertices as in Fig. 4.9 can be schematically represented as in Fig. 5.4. The terms regroup to become r number of circled vertex diagrams and one leftover $(r + 1)^{\text{th}}$ trilinear diagram (resulting from trilinear ν vertex being inserted to the right of vertex number r on the p-leg).
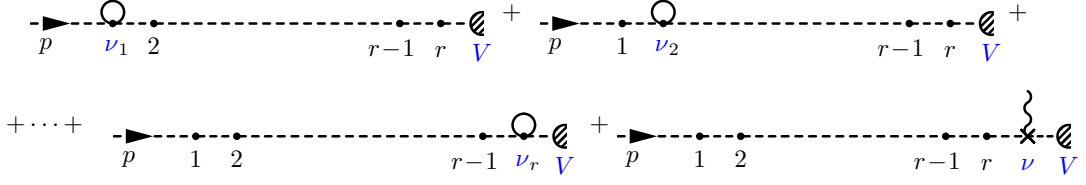
Figure 5.4: *The set of diagrams representing K photon contribution of p-leg after using the convention of Fig. 4.9. There are r circled vertex diagrams and one leftover $(r+1)^{\text{th}}$ trilinear diagram (where the new ν vertex is inserted to the right of vertex number r on the p-leg).*

The corresponding contribution of Fig. 5.4 is expressed in Eq. 5.10 as,

$$k_\nu C_{r+1}^{\text{scalar } p;\nu} = \left[\sum_{j=1}^{r} k_\nu C_{r+1}^{\text{scalar } p;\nu_j} \right] + \left[k_\nu C_{r+1}^{\text{scalar } p;\nu \text{ right of } r} \right]. \tag{5.10}$$

After using the contributions arising from circled vertices on p-leg, as was expressed in Eq. 4.35 and also using the 'Generalized Feynman's Identity' for p-leg as mentioned in Appendix B, we can write the contribution $k_\nu C_{r+1}^{\text{scalar } p;\nu}$ to be proportional to lower order contribution $C_r^{\text{scalar } p}$ times the delta function δ_{t_ν,t_V} which resulted due to GY reduction,

$$k_\nu C_{r+1}^{\text{scalar } p;\nu} = (-1)^{(t_\nu+1)} \left\{ [\delta_{t_\nu,t_V}] S_{p+\Sigma_r}^{t_V,t_r} \cdots S_{p+\Sigma_1}^{t_2,t_1} (2p+l_1)_{\nu_1} \right\}$$

$$= (-1)^{(t_\nu+1)} \delta_{t_\nu,t_V} C_r^{\text{scalar } p} . \tag{5.11}$$

Again the thermal type of vertex V being type-1, *i.e.*, $t_V = 1$, the delta function in above expression constrains $t_\nu = 1$.

Hence, after using the results of Eq. 5.9 and Eq. 5.11 with Eq. 5.5 and Eq. 5.3 the total contribution of K photon insertion between p and p'-leg becomes,

$$iM_{n+1}^{\text{scalar}; K\gamma, p', p} = e^2 (-1)^{(t_\mu+1)} (-1)^{(t_\nu+1)} (-1)^{(t_\mu+1)} (-1)^{(t_\nu+1)} \times$$

$$\int \frac{d^4k}{(2\pi)^4} \delta_{t_\mu,t_V} \delta_{t_\nu,t_V} b_k(p',p) \left[-iD^{t_\mu,t_\nu}(k) \right] \times iM_n^{\text{scalar}} , \tag{5.12}$$

which after simplification can be written as,

$$\mathcal{M}_{n+1}^{\text{scalar}; K\gamma, p', p} = -ie^2 \int \frac{\mathrm{d}^4 k}{(2\pi)^4} \, \delta_{t_\mu, t_V} \, \delta_{t_\nu, t_V} \, b_k(p', p) D^{t_\mu, t_\nu}(k) \times \mathcal{M}_n^{\text{scalar}}. \qquad (5.13)$$

The total matrix element as in Eq. 5.13 turns out to be proportional to the lower order matrix element with all the contribution due to K photon insertions factored out.

5.2.2 Inclusion of already existing seagull interaction vertices

The calculation of the K photon insertion in between p and p'-leg can be also extended to the case, when some of the already existing dotted vertices in Fig. 5.2 correspond to the seagull vertices. If x number of dotted vertices refer to the seagull vertices, and rest of the vertices refer to the trilinear vertices, then the total number of existing dotted vertices in the schematic n^{th} order (all virtual photon) diagram will be equal to '$m = (2n - x)$', where $x \in [0, n]$.

Now, suppose in the nth order diagram on p'-leg, at vertex numbers $(q - 1)$ and q no separate trilinear vertices were present. But, rather there is a single seagull vertex in place of these two trilinear vertices, from which photons with momenta l'_{q-1} and l'_q are coming out. The vertex element then would have been proportional to a term '$\delta_{t_{q-1}, t_q}(-2g_{\mu_{q-1}\mu_q})$' (apart from some overall factors). Now, a new K photon cannot get inserted at this seagull vertex, making this vertex an inert one. The new K photon can be inserted on the scalar propagators, which are present on both the sides of this already existing seagull vertex. The momenta k of the new photon does not alter the seagull vertex contribution of '$\delta_{t_{q-1}, t_q}(-2g_{\mu_{q-1}\mu_q})$'. And, it can be shown using simple algebra using 'Generalized Feynman's Identity' (Appendix B) that the pairwise cancellation of terms still holds, from those two trilinear insertions, which are on each side of already existing seagull vertices.

Therefore, the factor proportional to '$\delta_{t_{q-1}, t_q}(-2g_{\mu_{q-1}\mu_q})$' gets carried along like an inert factor, and GY reduction still holds. This is also true, if more than one seagull vertices are

88

present on a particular leg. In those cases, we will obtain more than one inert factors carried along. And, the argument does not depend on, whether the new K photon is inserted between different legs, or if it is inserted on same leg. Hence, the presence of already present seagull vertices in n^{th} order diagram, does not create trouble; and all the above and following results holds true, after just including the inert factors due to seagull vertices.

5.2.3 Both the K photon insertion vertices being on p'-leg

After discussing the effects of the K photon insertion in between different legs; now we turn our attention to the cases where both the virtual photon insertion vertices are on the same leg. We will at first consider the case, where both the photon vertices are inserted on the p'-leg.

Now, as both the vertices are on the p'-legs; hence by the virtue of seagull insertions, the tadpole diagrams are also possible. To avoid the double counting of the newly inserted vertices, we will always insert vertex ν to the left of vertex μ. The new photon momenta k will be leaving(entering) at vertex $\mu(\nu)$ without loss of any generality (as four momenta of virtual photons will anyway be integrated for all possible values of momenta).

We will again start with an nth photon diagram as shown in Fig. 5.2, where all already existing dotted vertices correspond to the trilinear virtual photon vertices. Therefore, the contribution of adding both the K photon insertion vertices to p'-leg can be expressed as in following expression (with the understanding of notation used in Eq. 5.3 and Eq. 5.5),

$$i\mathcal{M}_{n+1}^{\text{scalar};\,K\gamma,p',p'} = (e)^{2n+2}(-1)^{\sum_{i=1}^{m}(t_i+1)}(-1)^{(t_\mu+1)}(-1)^{(t_\nu+1)}\times$$
$$\int \frac{\mathrm{d}^4 k}{(2\pi)^4}\left[k_\mu\, k_\nu\, C_{s+2}^{\text{scalar}\; p';\mu,\nu}\right]\times \Gamma_V \times \left[C_r^{\text{scalar}\; p}\right]\times [b_k(p',p)\times -iD^{t_\mu,t_\nu}]\times \mathcal{D}_n\,,$$

(5.14)

where the $k_\mu\, k_\nu\, C_{s+2}^{\text{scalar}\; p';\mu,\nu}$ is the relevant part of the matrix element; and the notation has to be understood in accordance with the discussion of paragraphs below Eq. 4.29.
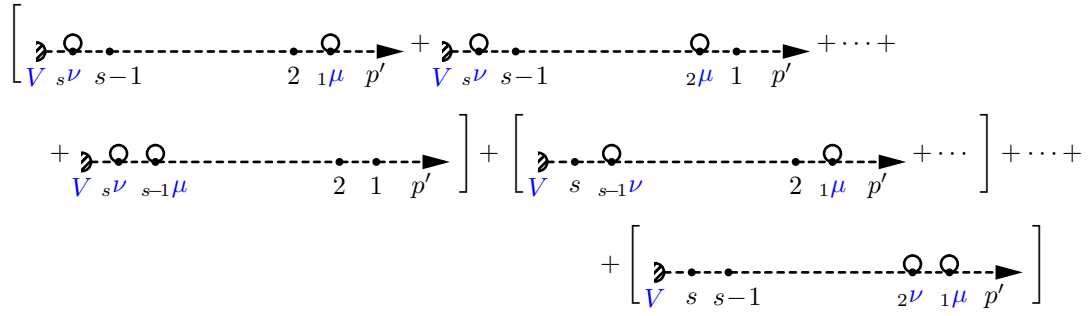
Figure 5.5: *Set I: Diagrams where at both the μ and ν insertions all are circled vertices.*
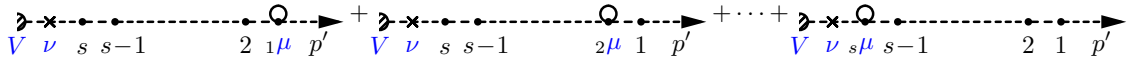
Figure 5.6: *Set II: Diagrams where at only μ insertions all are circled vertices, and ν insertion is kept fixed.*
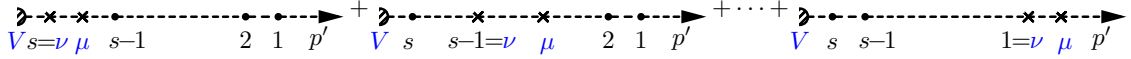
Figure 5.7: *Set III: Diagrams where at q = ν are all seagull insertions; and trilinear μ insertion is at immediate right to all possible ν insertions.*

Figure 5.8: *Set IV: Diagrams where all $_\nu\mu$ circled vertices are present. The last diagram corresponds to the outermost self energy contribution and to avoid double counting, is to be omitted on similar set of diagram on the p-leg.*
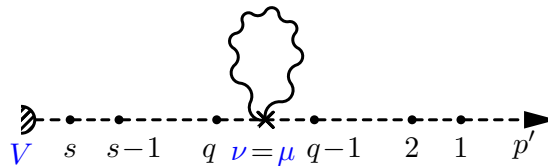
Figure 5.9: *A typical tadpole diagram on p′-leg, where the insertion vertices μ, ν due the new K photon have been inserted in between the vertex number q − 1 and q. These diagrams are sub-contributions of Set IV of Fig. 5.8.*

90

Due to the presence of the seagull vertices and tadpole diagrams the concerned numbers of diagrams contributing to the $k_\mu k_\nu C_{s+2}^{\text{scalar } p';\mu,\nu}$ proliferate in numbers. To easily see the nature of factorization, we regroup these diagrams into 4 sets of diagrams; as shown in the figures above. The Set-I of Fig. 5.5 consist of diagrams, where at both the μ and ν insertions all are circled vertices. The Set-II of Fig. 5.6 consist of diagrams, where at only μ insertions all are circled vertices, and ν insertion is kept fixed to the right of vertex V. The Set-III of Fig. 5.7 consist of diagrams, where at $q = \nu$ are all seagull insertions; and trilinear μ insertion is at immediate right to all possible ν insertions. And Set-IV of Fig. 5.8 consist of diagrams, where all the possible $_\nu\mu$ circled vertices are present. Fig. 5.8 has sub-contributions from tadpole diagrams. A typical tadpole diagram is shown in Fig. 5.9. All these Sets of diagrams can be evaluated using Eq. 4.34, Eq. 4.35 and the 'Generalized Feynman Identities' of Appendix B.

The contribution of Set-I of the diagrams of Fig. 5.5 can be expressed as,

$$
\begin{aligned}
k_\mu k_\nu\, C_{s+2}^{\text{scalar } p';\mu,\nu,I} &= (-1)^{(t_\mu+1)}(-1)^{(t_\nu+1)}\times \\
&\Bigg(\Big\{ (2p'+l_1')_{\mu_1} S_{p'+\Sigma_1}^{t_1,t_2}(2p'+2\Sigma_1+l_2')_{\mu_2}\cdots\Big[S_{p'+\Sigma_{s-1}}^{t_{s-1},t_s}(2p'+2\Sigma_{s-1}+l_s')_{\mu_s}\delta_{t_\nu,t_{s-1}}\delta_{t_\mu,t_{s-1}} \\
&\qquad -S_{p'+\Sigma_{s-1}+k}^{t_{s-1},t_s}(2p'+2\Sigma_{s-1}+2k+l_s')_{\mu_s}\delta_{t_\nu,t_s}\delta_{t_\mu,t_{s-1}}\Big] S_{p'+\Sigma_s}^{t_s,t_V}\Big\} \\
&+ \Big\{ (2p'+l_1')_{\mu_1} S_{p'+\Sigma_1}^{t_1,t_2}(2p'+2\Sigma_1+l_2')_{\mu_2}\cdots\Big[S_{p'+\Sigma_{s-2}}^{t_{s-2},t_{s-1}}(2p'+2\Sigma_{s-2}+l_{s-1}')_{\mu_{s-1}}\delta_{t_\nu,t_{s-2}} \\
&\qquad -S_{p'+\Sigma_{s-2}+k}^{t_{s-2},t_{s-1}}(2p'+2\Sigma_{s-2}+2k+l_{s-1}')_{\mu_{s-1}}\delta_{t_\nu,t_{s-1}}\Big]\delta_{t_\mu,t_{s-2}}\cdots S_{p'+\Sigma_s}^{t_s,t_V}\Big\} \\
&+ \{\cdots\} \\
&+ \Big\{ (2p'+l_1')_{\mu_1}\Big[S_{p'+\Sigma_1}^{t_1,t_2}(2p'+2\Sigma_1+l_2')_{\mu_2}\delta_{t_\nu,t_1}\delta_{t_\mu,t_1}- \\
&\qquad S_{p'+\Sigma_1+k}^{t_1,t_2}(2p'+2\Sigma_1+2k+l_2')_{\mu_2}\delta_{t_\nu,t_2}\delta_{t_\mu,t_1}\Big] S_{p'+\Sigma_2}^{t_2,t_3}\cdots S_{p'+\Sigma_s}^{t_s,t_V}\Big\}\Bigg).
\end{aligned}
$$

$$(5.15)$$

For Set-II of diagrams as seen in Fig. 5.6, pairwise cancellation happens between typical

terms, leaving us with single contributing expression,

$$k_\mu k_\nu C_{s+2}^{\text{scalar } p';\mu,\nu,II} = (-1)^{(t_\mu+1)}(-1)^{(t_\nu+1)} \times$$

$$\left(\left\{ (2p'+l_1')_{\mu_1} S_{p'+\Sigma_1}^{t_1,t_2} (2p'+2\Sigma_1+l_2')_{\mu_2} \cdots S_{p'+\Sigma_{s-1}}^{t_{s-1},t_s} \delta_{t_\mu,t_s}(2p'+2\Sigma_{s-1}+l_s')_{\mu_s} \times \right. \right.$$

$$\left. \left. \left[S_{p'+\Sigma_s}^{t_s,t_V} \delta_{t_\nu,t_s} - S_{p'+\Sigma_s+k}^{t_s,t_V} \delta_{t_\nu,t_V} \right] \right\} \right). \quad (5.16)$$

Now, the contributions Set-III of diagrams of Fig. 5.7 can be expressed as,

$$k_\mu k_\nu C_{s+2}^{\text{scalar } p';\mu,\nu,III} = (-1)^{(t_\mu+1)}(-1)^{(t_\nu+1)} \times$$

$$\left(\left\{ (2p'+l_1')_{\mu_1} S_{p'+\Sigma_1}^{t_1,t_2} (2p'+2\Sigma_1+l_2')_{\mu_2} \cdots \left[S_{p'+\Sigma_{s-1}}^{t_{s-1},t_s} \delta_{t_\mu,t_s} \right. \right. \right.$$

$$\left. \left. -S_{p'+\Sigma_{s-1}+k}^{t_{s-1},t_s} \delta_{t_\mu,t_{s-1}} \right] \delta_{t_\nu,t_s}(-2k)_{\mu_s} \right\}$$

$$+\left\{ (2p'+l_1')_{\mu_1} S_{p'+\Sigma_1}^{t_1,t_2} (2p'+2\Sigma_1-2k+l_2')_{\mu_2} \cdots \left[S_{p'+\Sigma_{s-2}}^{t_{s-2},t_{s-1}} \delta_{t_\mu,t_{s-1}} \right. \right.$$

$$\left. \left. -S_{p'+\Sigma_{s-2}+k}^{t_{s-2},t_{s-1}} \delta_{t_\mu,t_{s-2}} \right] \delta_{t_\nu,t_{s-1}}(-2k)_{\mu_{s-1}} S_{p'+\Sigma_s}^{t_s,t_V} \right\} + \left\{ \cdots \right\}$$

$$+\left\{ (2p'+l_1')_{\mu_1} \left[S_{p'+\Sigma_1}^{t_1,t_2} \delta_{t_\mu,t_2} - \right. \right.$$

$$\left. \left. S_{p'+\Sigma_1+k}^{t_1,t_2} \delta_{t_\mu,t_1} \right] \delta_{t_\nu,t_2}(-2k)_{\mu_2} S_{p'+\Sigma_2}^{t_2,t_3} \cdots S_{p'+\Sigma_s}^{t_s,t_V} \right\}$$

$$+ \left\{ \delta_{t_\mu,t_1}(-2k)_{\mu_1} \delta_{t_\nu,t_1} S_{p'+\Sigma_1}^{t_1,t_2}(2p'+2\Sigma_1+l_2')_{\mu_2} \cdots \right\} \right). \quad (5.17)$$

We have to note that the contribution of Eq. 5.17 has a similar structure like Set-I of diagrams of Eq. 5.15. But, it is also to be noted that all the terms of Eq. 5.17 are *linearly dependent* in the K photon momenta via the factors of $(-2k)_{\mu_i}$. All the particular contributing diagrams of Fig. 5.7 can be written down after applying 'Generalized Feynman Identity' as a difference of two terms. Only the last diagram of Fig. 5.7 contributes a single term as p'-leg is on-shell, represented by the last curly bracketed term in Eq. 5.17. It is to be noted that this term does not have any other dependence on K photon momenta k expect via the factor $(-2k)_{\mu_1}$.

Before calculating the full contribution of Set-IV of diagrams Fig. 5.8, let us observe the contribution due to a particular diagram of that set. Let that particular diagram be the

one where the $_\nu\mu$ circled vertex is placed in between vertex number $(q-1)$ and q on the p' leg. The $_\nu\mu$ circled vertex insertion consist of two sub-diagrams, the first where 'trilinear ν insertion is at immediate left to trilinear μ insertion', and the one where 'μ and ν insertion make a tadpole diagram' (shown in Fig. 5.9). The contribution of first subgraph is expressed inside first square bracketed terms in Eq. 5.18; and the contribution of the tadpole diagram is expressed in the second square bracketed term in Eq. 5.18. Note that any typical tadpole contribution has a symmetry factor of $1/2$, nullifying the factor of (-2) coming from seagull vertex.

$$
\begin{aligned}
k_\mu k_\nu C_{s+2}^{\text{scalar }p';\mu,\nu,IV,q} = {} & (-1)^{(t_\mu+1)}(-1)^{(t_\nu+1)}\times \\
& \left((2p'+l_1')_{\mu_1} S_{p'+\Sigma_1}^{t_1,t_2}(2p'+2\Sigma_1+l_2')_{\mu_2}\cdots\left\{\left[S_{p'+\Sigma_{q-1}+k}^{t_{q-1},t_q}\delta_{t_\mu,t_{q-1}}\delta_{t_\nu,t_q} \right.\right. \right. \\
& \left. -S_{p'+\Sigma_{q-1}}^{t_{q-1},t_q}\delta_{t_\mu,t_{q-1}}\delta_{t_\nu,t_{q-1}} + S_{p'+\Sigma_{q-1}}^{t_{q-1},t_\mu}(2p+2\Sigma_{q-1}+k)\cdot k\,\delta_{t_\mu,t_\nu}S_{p'+\Sigma_{q-1}}^{t_\nu,t_q}\right] \\
& \left.\left.\left. + \left[S_{p'+\Sigma_{q-1}}^{t_{q-1},t_\mu}(-k^2)\delta_{t_\mu,t_\nu}S_{p'+\Sigma_{q-1}}^{t_\nu,t_q}\right]\right\}\right)\right. . \quad (5.18)
\end{aligned}
$$

In the expression of Eq. 5.18, the $O(k^2)$ contributions coming from trilinear self energy corrections and the tadpole contributions cancel *exactly* among themselves. Although any $O(k^2)$ contributions in the numerator is IR finite at finite temperature (as the leading IR divergence is linear in denominator), but without the exact cancellation of these finite $O(k^2)$ terms, the IR factorization and resummation would be impossible. Hence, the tadpole contributions are *indispensable* to achieve the IR factorization and resummation.

With this understanding, the total contribution of Set-IV of diagrams of Fig. 5.8 can be expressed in detail in Eq. 5.20, and schematically in Eq. 5.19 below,

$$
k_\mu k_\nu C_{s+2}^{\text{scalar }p';\mu,\nu,IV} = \left[\sum_{q=1}^{s} A_q - \sum_{q=0}^{s} B_q + \sum_{q=0}^{s} C_q \right], \quad (5.19)
$$

where to identify A_q, B_q, C_q clearly with convenience, the contributing terms in Eq. 5.20 have been coloured with same colours. In Eq. 5.20 the last term $\{[-B_0+C_0]\}$ arises from

the outermost self-energy contribution on the p' leg. All the B_q terms are proportional to $C_s^{\text{scalar }p'}$, and all the C_q terms are odd in photon momenta k.

$$k_\mu k_\nu C_{s+2}^{\text{scalar }p';\mu,\nu,IV} = (-1)^{(t_\mu+1)}(-1)^{(t_\nu+1)} \times$$

$$\Bigg(\Big\{ (2p'+l'_1)_{\mu_1} S_{p'+\Sigma_1}^{t_1,t_2} (2p'+2\Sigma_1+l'_2)_{\mu_2} \cdots \Big[S_{p'+\Sigma_s+k}^{t_s,t_V} \delta_{t_\mu,t_s} \delta_{t_\nu,t_V}$$

$$-S_{p'+\Sigma_s}^{t_s,t_V} \delta_{t_\mu,t_s} \delta_{t_\nu,t_s} + S_{p'+\Sigma_s}^{t_s,t_\mu} (2p'+2\Sigma_s)\cdot k\, \delta_{t_\mu,t_\nu} S_{p'+\Sigma_s}^{t_\nu,t_V} \Big] \Big\}$$

$$+\Big\{ (2p'+l'_1)_{\mu_1} S_{p'+\Sigma_1}^{t_1,t_2} (2p'+2\Sigma_1+l'_2)_{\mu_2} \cdots \Big[S_{p'+\Sigma_{s-1}+k}^{t_{s-1},t_s} \delta_{t_\mu,t_{s-1}} \delta_{t_\nu,t_s}$$

$$-S_{p'+\Sigma_{s-1}}^{t_{s-1},t_s} \delta_{t_\mu,t_{s-1}} \delta_{t_\nu,t_{s-1}} + S_{p'+\Sigma_{s-1}}^{t_{s-1},t_\mu} (2p'+2\Sigma_{s-1})\cdot k\, \delta_{t_\mu,t_\nu} S_{p'+\Sigma_{s-1}}^{t_\nu,t_s} \Big] \cdots \Big\} + \Big\{ \cdots \Big\}$$

$$+\Big\{ (2p'+l'_1)_{\mu_1} \Big[S_{p'+\Sigma_1+k}^{t_1,t_2} \delta_{t_\mu,t_1} \delta_{t_\nu,t_2} - S_{p'+\Sigma_1}^{t_1,t_2} \delta_{t_\mu,t_1} \delta_{t_\nu,t_1}$$

$$+S_{p'+\Sigma_1}^{t_1,t_\mu} (2p'+2\Sigma_1)\cdot k\, \delta_{t_\mu,t_\nu} S_{p'+\Sigma_1}^{t_\nu,t_2} \Big] \cdots \Big\}$$

$$+\Big\{ -\delta_{t_\mu,t_1} \delta_{t_\nu,t_1} (2p'+l'_1)_{\mu_1} S_{p'+\Sigma_1}^{t_1,t_2} (2p'+2\Sigma_1+l'_2)_{\mu_2} \cdots$$

$$+(2p')\cdot k\, S_{p'}^{t_\mu,t_1} \delta_{t_\mu,t_\nu} (2p'+l'_1)_{\mu_1} S_{p'+\Sigma_1}^{t_1,t_2} (2p'+2\Sigma_1+l'_2)_{\mu_2} \cdots \Big\} \Bigg),$$

$$\equiv \{[A_s - B_s + C_s]\} + \{\cdots\} + \{[A_1 - B_1 + C_1]\} + \{[-B_0 + C_0]\}. \tag{5.20}$$

$$k_\mu k_\nu C_{s+2}^{\text{scalar }p';\mu,\nu,I+II+III} = k_\mu k_\nu C_{s+2}^{\text{scalar }p';\mu,\nu,I} + k_\mu k_\nu C_{s+2}^{\text{scalar }p';\mu,\nu,II} + k_\mu k_\nu C_{s+2}^{\text{scalar }p';\mu,\nu,III}$$

$$= (-1)^{(t_\mu+1)}(-1)^{(t_\nu+1)} \times \Bigg(\Big\{ (2p'+l'_1)_{\mu_1} S_{p'+\Sigma_1}^{t_1,t_2} (2p'+2\Sigma_1+l'_2)_{\mu_2} \cdots S_{p'+\Sigma_s}^{t_s,t_V} \cdots \times$$

$$\Big[\delta_{t_\mu,t_1} \delta_{t_\nu,t_1} + \delta_{t_\mu,t_2} \delta_{t_\nu,t_2} + \cdots + \delta_{t_\mu,t_s} \delta_{t_\nu,t_s} \Big] \Big\}$$

$$+\Big\{ \Big[(-2k)_{\mu_1} \delta_{t_\mu,t_1} \delta_{t_\nu,t_1} \Big] S_{p'+\Sigma_1}^{t_1,t_2} (2p'+2\Sigma_1+l'_2)_{\mu_2} \cdots +$$

$$+(2p'+l'_1)_{\mu_1} S_{p'+\Sigma_1}^{t_1,t_2} \Big[(-2k)_{\mu_2} \delta_{t_\mu,t_2} \delta_{t_\nu,t_2} \Big] (2p'+2\Sigma_1+l'_2)_{\mu_2} \cdots + \cdots$$

$$+(2p'+l'_1)_{\mu_1} S_{p'+\Sigma_1}^{t_1,t_2} \cdots S_{p'+\Sigma_{s-1}}^{t_{s-1},t_s} \Big[(-2k)_{\mu_s} \delta_{t_\mu,t_s} \delta_{t_\nu,t_s} \Big] \cdots \Big\}$$

$$-\Big\{ (2p'+l'_1)_{\mu_1} S_{p'+\Sigma_1}^{t_1,t_2} (2p'+2\Sigma_1+l'_2)_{\mu_2} \cdots \Big[S_{p'+\Sigma_s+k}^{t_s,t_V} \delta_{t_\mu,t_s} \delta_{t_\nu,t_V} \Big] \cdots$$

$$+(2p'+l'_1)_{\mu_1} S_{p'+\Sigma_1}^{t_1,t_2} (2p'+2\Sigma_1+l'_2)_{\mu_2} \cdots \Big[S_{p'+\Sigma_{s-1}+k}^{t_{s-1},t_s} \delta_{t_\mu,t_{s-1}} \delta_{t_\nu,t_s} \Big] \cdots + \cdots$$

$$+(2p'+l'_1)_{\mu_1} \Big[S_{p'+\Sigma_1+k}^{t_1,t_2} \delta_{t_\mu,t_1} \delta_{t_\nu,t_2} \Big] (2p'+2\Sigma_1+l'_2)_{\mu_2} \cdots \Big\} \Bigg)$$

$$\equiv \{X\} + \{Y\} - \{Z\}. \tag{5.21}$$

The Set-I, Set-II and Set-III contributions from Eq. 5.15, Eq. 5.16 and Eq. 5.16 can be

added together. These result in mutual cancellation of terms within themselves, producing a final expression as in Eq. 5.21 above, where again the contributing terms have been colour coded in Eq. 5.21 to correctly identify the X, Y, Z, sets of terms conveniently.

Now, to obtain the $k_\mu k_\nu C_{s+2}^{\text{scalar } p';\mu,\nu}$ the expressions of Eq. 5.20 and Eq. 5.21 have to be added together. By observing those equations it can be easily noted that the same colour coded terms of Eq. 5.20 and Eq. 5.21 are of same structure. Hence, the s number of A_q terms of Eq. 5.20 (or Eq. 5.19) exactly cancels with s number of Z terms from Eq. 5.21. The C_q terms of Eq. 5.20 (or Eq. 5.19) and Y terms from Eq. 5.21 are *odd* in photon momenta k (with no other photon momenta dependence anywhere); hence vanishing upon integrating photon momenta $\int \mathrm{d}^4 k$. And, s number of X terms of Eq. 5.21 cancels exactly with s number of B_q terms of Eq. 5.20 (or Eq. 5.19); leaving only a single term from Eq. 5.20 which corresponds to $(-B_0)$ which resulted from outermost self energy correction on p'-leg. Therefore the total contribution of all the Sets of diagrams on p'-leg reduces to,

$$
\begin{aligned}
k_\mu k_\nu C_{s+2}^{\text{scalar } p';\mu,\nu} &= k_\mu k_\nu C_{s+2}^{\text{scalar } p';\mu,\nu,\,I+II+III} + k_\mu k_\nu C_{s+2}^{\text{scalar } p';\mu,\nu,\,IV} \\
&= (-1)^{(t_\mu+1)}(-1)^{(t_\nu+1)} \left\{ \left[-\delta_{t_\mu,t_1}\delta_{t_\nu,t_1} \right](2p'+l_1')_{\mu_1} S_{p'+\Sigma_1}^{t_1,t_2} (2p'+2\Sigma_1+l_2')_{\mu_2} \cdots S_{p'+\Sigma_s}^{t_s,t_V} \right\} \\
&= (-1)^{(t_\mu+1)}(-1)^{(t_\nu+1)} \left[-\delta_{t_\mu,t_1}\delta_{t_\nu,t_1} \right] C_s^{\text{scalar } p'} \ .
\end{aligned}
\tag{5.22}
$$

The contribution of K photon insertion on p'-leg, $k_\mu k_\nu C_{s+2}^{\text{scalar } p';\mu,\nu}$ becomes proportional to the lower order contribution $C_s^{\text{scalar } p'}$ times the delta function $\left[-\delta_{t_\mu,t_1}\delta_{t_\nu,t_1} \right]$. Note, the presence of a minus sign (which resulted from Eq. 5.20) in contrast to a similar expression for the insertion between different legs in Eq. 5.9 and Eq. 5.11. The external scalar being physical and observable, the thermal type of vertex number '1' can be of type-1 only, *i.e.*, $t_1 = 1$. The delta function in Eq. 5.22 hence constrains $t_\mu = t_\nu = t_1 = 1$ only.

With this understanding and using Eq. 5.14 the effect of adding a virtual K photon to only

p'-leg can be written as,

$$i\mathcal{M}_{n+1}^{\text{scalar};\,K\gamma,p',p'} = e^2(-1)^{(t_\mu+1)}(-1)^{(t_\nu+1)}(-1)^{(t_\mu+1)}(-1)^{(t_\nu+1)} \times$$

$$\int \frac{\mathrm{d}^4k}{(2\pi)^4}\left[-\delta_{t_\mu,t_1}\,\delta_{t_\nu,t_1}\right]b_k(p',p')\left[-iD^{t_\mu,t_\nu}(k)\right]\times i\mathcal{M}_n^{\text{scalar}}. \quad (5.23)$$

which after simplification becomes,

$$\mathcal{M}_{n+1}^{\text{scalar};\,K\gamma,p',p'} = +ie^2\int\frac{\mathrm{d}^4k}{(2\pi)^4}\,\delta_{t_\mu,t_1}\,\delta_{t_\nu,t_1}\,b_k(p',p')D^{t_\mu,t_\nu}(k)\times\mathcal{M}_n^{\text{scalar}}. \quad (5.24)$$

Note the 'plus' sign in the above expression in contrast to 'minus' sign in Eq. 5.13 (which resulted from extra 'minus' sign from Eq. 5.22).

5.2.4 Schematic discussion of K photon factorization on p'-leg

In the above section we have discussed in detail the effects of the K photon insertion, when both the insertion vertices are on p'-leg. Due to presence of seagull diagrams, there arose the possibility of tadpole diagrams on p'-leg. We have discussed about the technique to avoid double-counting of insertion vertices, by always placing the ν insertion vertex to the left-side of insertion vertex μ. Due to presence of seagull and tadpole diagrams, the number of relevant diagrams proliferate; and we have to regroup the diagrams in terms of four distinct classes, *i.e.*, Set-I, II, III and IV.

Although we have exhibited the full technical details of the calculation, it is instructive to understand the *nature of the cancellation* through a schematic discussion on the effect of K photon insertion with both vertices on the p' leg. The matrix element, after insertion of the K photon, can be schematically expressed as

$$\mathcal{M}_{n+1}^{\text{scalar};\,K\gamma,p',p'} \propto \int\frac{\mathrm{d}^4k}{(2\pi)^4}\left[\left\{O(k)_d + \text{Seagull}\right\} + O(k)_{no\,d} + \left\{O(k^2)_{no\,d} + \text{tadpole}\right\} + \mathcal{M}_n^{\text{scalar}}\right]$$

$$\propto \int\frac{\mathrm{d}^4k}{(2\pi)^4}\mathcal{M}_n^{\text{scalar}}. \quad (5.25)$$

In Eq. 5.25, $O(k)$ and $O(k^2)$ respectively denote the remainder linear and quadratic in k terms in addition to $\mathcal{M}_n^{\text{scalar}}$. The suffixes, '$d$' and '$no\ d$' respectively reflect the dependence and absence of photon momentum (k) in the denominators of particular terms . The '$O(k)_d$' terms exactly cancels against the 'Seagull' contributions. The '$O(k^2)_{no\ d}$' terms though finite, cancels exactly against 'tadpole terms'. And, there are some terms which are represented by '$O(k)_{no\ d}$' they being odd under the momentum integral vanishes to zero. Hence, the '$\mathcal{M}_{n+1}^{\text{scalar};\, K\gamma,\, p',\, p'}$' becomes proportional to the lower order matrix element '$\mathcal{M}_n^{\text{scalar}}$'; and the exact result is shown in Eq. 5.24.

Now, from this discussion we see that, without the incorporation of seagull and tadpole contributions the $O(k)_d$ and $O(k^2)_{no\ d}$ terms would not have cancelled; and we would not have got such a clean factorization as in Eq. 5.24. Hence, seagull and tadpole contributions are *indispensable* to achieve this clean factorization.

5.2.5 Both the K photon insertion vertices being on p-leg

Analogous to both the K photon insertion vertices being inserted on the p'-leg, a similar analysis can be performed when both the K photon insertion vertices are inserted on the p-leg. The resulting diagrams can again be grouped into four classes of sets of diagrams. After adding all of them we find analogous cancellation between the contributions leaving us with a similar expression of $(-B_0)$ as in Eq. 5.20 for the p-leg. The origin of this $(-B_0)$ term was the outermost self energy correction. But, according to the method of the GY this outermost self energy contribution has to be discounted in favour of wave function renormalization [137]. Hence, on dropping the similar term of $(-B_0)$ for the K photon insertion on the p-leg the total contribution vanishes.

But there is nothing special about the p or p'-leg, as this compensation for wave function renormalization could have been included in either of the legs. Therefore we symmetrize the result of K photon insertion with both vertices on the same leg over the two possibilities

related to different legs. The contributions then can be expressed as,

$$\mathcal{M}_{n+1}^{\text{scalar}; K\gamma, p', p'} = +ie^2 \frac{1}{2} \int \frac{\mathrm{d}^4 k}{(2\pi)^4} \, \delta_{t_\mu, t_1} \, \delta_{t_\nu, t_1} \, b_k(p', p') D^{t_\mu, t_\nu}(k) \times \mathcal{M}_n^{\text{scalar}},$$

$$\mathcal{M}_{n+1}^{\text{scalar}; K\gamma, p, p} = +ie^2 \frac{1}{2} \int \frac{\mathrm{d}^4 k}{(2\pi)^4} \, \delta_{t_\mu, t_1} \, \delta_{t_\nu, t_1} \, b_k(p, p) D^{t_\mu, t_\nu}(k) \times \mathcal{M}_n^{\text{scalar}}. \tag{5.26}$$

5.2.6 Including the disallowed diagrams
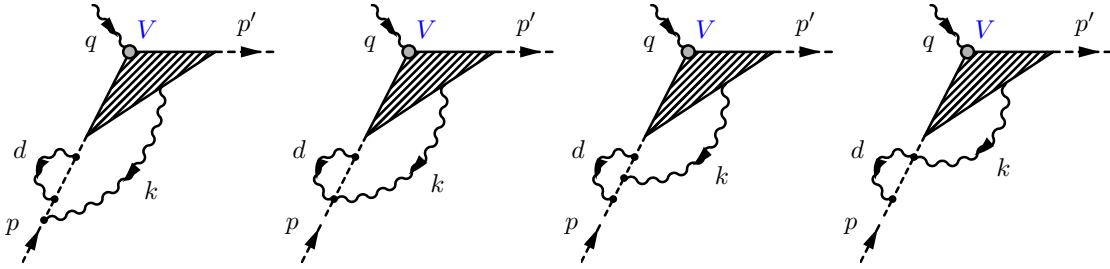
Figure 5.10: *Disallowed diagrams related to* n^{th} *order diagrams; which becomes possible allowed diagrams at the* $(n+1)^{\text{th}}$ *order while inserting virtual photons.*

There were certain diagrams which were disallowed at an nth order process to account for the correct wave function renormalization prescription in GY technique Ref. [12]. These diagrams refer to the outermost self energy diagrams which were discounted to compensate for the wave function renormalization. However, when we add a virtual photon to the nth order diagrams by either insertion of K or G photons, these diagrams become allowed in the $(n+1)^{\text{th}}$ order diagrams. Therefore, the contributions of these terms must be taken into account at higher orders. Now, as we are performing the calculation at finite temperature the insertion vertices of *some* (not every diagram) of these disallowed diagrams (represented by momenta d in Fig. 5.10) can *sometimes* (not always) have both the thermal types of insertion vertices at both insertions. As in the first picture of the disallowed diagram in Fig. 5.10 both the insertion vertices related to the photon momenta 'd' can be of either be thermal type-1 or type-2. Hence, in those cases of *particular* (n^{th} order disallowed but at $(n+1)^{\text{th}}$ order allowed) diagrams at the $(n+1)^{\text{th}}$ order the thermal type of vertex number '1' can be of type-2 thermal type also, *i.e.*, '$t_1 = 2$' also. But, the

thermal type of vertex t_ν related to the new photon momenta k when inserted on outermost leg is always of thermal type-1 (as this is the inserted on outermost physical p-leg), *i.e.,* '$t_\nu = 1$' *always for outermost insertion.* Therefore, taking into account of all these disallowed diagrams with all possible thermal vertices; we find that, with the addition of mass counterterm all the contribution of disallowed diagrams vanish to zero, as in zero temperature GY case. Therefore, the disallowed diagrams does not create any trouble for the calculation.

5.2.7 The total contribution due to K photon insertions

The total contribution for the K photon insertion to an nth order diagram can be expressed as,

$$
\begin{aligned}
\mathcal{M}^{\text{scalar};\, K\gamma,\, \text{tot}}_{n+1} =\ & \frac{ie^2}{2} \int \frac{\mathrm{d}^4 k}{(2\pi)^4} \left\{ \delta_{t_\mu, t_1}\, \delta_{t_\nu, t_1}\, D^{t_\mu, t_\nu}(k) \left[b_k(p', p') + b_k(p, p) \right] \right. \\
& \left. +\ \delta_{t_\mu, t_V}\, \delta_{t_\nu, t_V}\, D^{t_\mu, t_\nu}(k) \left[- 2 b_k(p', p) \right] \right\} \mathcal{M}^{\text{scalar}}_n\,, \\
\equiv\ & [B]\, \mathcal{M}^{\text{scalar}}_n\,.
\end{aligned}
\tag{5.27}
$$

Here,

$$
\begin{aligned}
B =\ & \frac{ie^2}{2} \int \frac{\mathrm{d}^4 k}{(2\pi)^4}\, D^{11}(k) \left[b_k(p', p') - 2 b_k(p', p) + b_k(p, p) \right]\,, \\
\equiv\ & \frac{ie^2}{2} \int \frac{\mathrm{d}^4 k}{(2\pi)^4}\, D^{11}(k) \left[J^2(k) \right]\,.
\end{aligned}
\tag{5.28}
$$

In Eq. 5.28 the fact that the thermal type of vertices related to external/hard physically observable particles must be of type-1, constrains '$t_V = t_1 = 1$'. With this consideration B becomes proportional to the '(11)' component of thermal photon propagator. This result of being proportional to the $D^{11}(k)$ type thermal photon propagator will be of prime importance while cancelling the the IR divergent pieces in between virtual and real soft photon contributions.

99

It is also to be noted that, by observing the structure of $D^{11}(k)$ in Eq. 5.28 that, the leading linear and sub-leading logarithmic divergence are contained in B which has been factored out from n^{th} order matrix element in Eq. 5.27. Both these leading and sub-leading divergences will cancel against real photon contributions as will be shown in upcoming discussion.

5.3   Insertion of virtual G photons

As we have already discussed, in thermal field theory due to the presence of thermal fluctuations the IR behaviour diverge more violently; *i.e.*, at leading behaviour linearly (as opposed to leading logarithmic behaviour at zero temperate) and at sub-leading behaviour logarithmically. We have already proved in Eq. 5.27 that K photon contributions have both leading linear and sub-leading logarithmic divergence. Now, we have to correctly identify all the IR finite pieces related to a particular process. It has been already seen in Chapter 3 and in Chapter 4 that the G photon contributions are completely IR finite. We know that at zero temperature the contribution of G photon contribution behaves like,

$$\mathcal{M}_{n+1}^{G\gamma;T=0} \propto \left\{ g_{\mu\nu} - b_k(p_f, p_i)k_\mu k_\nu \right\} \times p_f^\mu p_i^\nu \,,$$
$$= 0 + \mathcal{O}(k) \,. \tag{5.29}$$

The leading divergence for the zero temperature theory (both in fermionic and scalar QED) was logarithmic in nature and hence any power of photon momenta k in the numerator will make the corresponding G photon contribution IR finite.

Now in the thermal field theory due to the presence of bosonic number operator, there are mainly two issues which we have to focus on. These are inclusion of thermal photons and thermal scalar. Keeping aside the issue of thermal scalar for the moment (we will return to this issue) we can see that the leading thermal behaviour due to the thermal part of the

photon propagators for all the components is proportional to,

$$2\pi\delta(k^2)N(|k^0|) \equiv 2\pi\delta(k^2)\frac{1}{\exp^{|k^0|/T}-1} \ . \tag{5.30}$$

This makes the leading IR divergence to be linear and also produces additional sub-leading logarithmic IR divergence from any $O(k)$ term in the numerator.

As the zero temperature structure of G photon insertion is well known, we proceed by focusing on finite temperature part. As thermal part of the photon propagators contain $\delta(k^2)$ part hence, there are mainly two modification that happen. First, the $b_k(p_f, p_i)$ modifies to,

$$b_k^{T\neq0}(p_f, p_i) = \frac{p_f \cdot p_i}{p_f \cdot k \ \ p_i \cdot k} \ . \tag{5.31}$$

And then we can drop off any (k^2) terms, whether in the scalar propagators or in the numerators of the matrix element. With this understanding a generic insertion of the G photon to an nth order matrix element can be written as,

$$\mathcal{M}_{n+1}^{scalar; G\gamma} \sim \int \frac{\mathrm{d}^4k}{(2\pi)^4}\left[\frac{i}{k^2+i\epsilon}\delta_{t_\mu,t_\nu} \pm 2\pi\delta(k^2)N(|k|)D_T^{t_\mu,t_\nu}\right]\left[g^{\mu\nu} - b_k k^\mu k^\nu\right]\left[\text{scalar}\right]_{\mu\nu},$$
$$\tag{5.32}$$

where the first square bracketed term comes from the photon propagator (the relative $\pm$ sign is due to different components of the propagators). The second square bracketed term represents the rearranged polarization sum of G photon and the third square bracketed term corresponds to the matrix element part of charged scalar (with scalar vertices, scalar propagator, and already existing photons).

The relevant portion of the scalar matrix element is the part, where the new G photon is inserted at vertex μ and ν. Hence, contracting the G photon polarization sum with the relevant vertex factors of scalar matrix element contribution at *only* the μ and ν vertices

(assuming μ, ν insertion to be trilinear at first), we obtain from Eq. 5.32,

$$[g^{\mu\nu} - b_k k^\mu k^\nu] \left\{ S^{t_{q-1},t_\mu}_{p_f+\Sigma_{q-1}} \left[(2p_f + 2\Sigma_{q-1} + k)_\mu S^{t_\mu,t_q}_{p_f+\Sigma_{q-1}+k}(2p_f + 2\Sigma_{q-1} + 2k + l'_q)_{\mu_q} \right] \right\} \times$$

$$\left\{ S^{t_{j+1},t_\nu}_{p_i+\Sigma_j+k} \left[(2p_i + 2\Sigma_j + k)_\nu S^{t_\nu,t_j}_{p_f+\Sigma_j}(2p_i + 2\Sigma_{j-1} + l_j)_{\nu_j} \right] \right\}$$

$$= \left[4P_f \cdot P_i + 2(P_f + P_i) \cdot k - 4b_k P_f \cdot k\, P_i \cdot k \right] \left[S^{t_{q-1},t_\mu} S^{t_\mu,t_q} S^{t_{j+1},t_\nu} S^{t_\nu,t_j}(\cdots)_{\mu_q}(\cdots)_{\nu_j} \right],$$

$$= \left[0(p_f \cdot p_i) + 2(p_f + p_i) \cdot k \right] \left[\text{scalar} \right]_{\slashed{\mu}\slashed{\nu}}, \tag{5.33}$$

In the above expression, we have used $P_i = p_i + \sum_{i=1}^{j-1} l_i$, and $P_f = p_f + \sum_{i=1}^{q-1} l'_i$. In the IR limit, we have replaced $P_i \to p_i$ and $P_f \to p_f$, and have also used Eq. 5.31 to substitute the expression for b_k, to obtain the final expression of Eq. 5.33. We find due to the construction of b_k the leading $(p_f \cdot p_i)$ term vanishes to zero. The $[\text{scalar}]_{\slashed{\mu}\slashed{\nu}}$ refer to the remaining scalar matrix element contribution due to the other vertices and propagators. The $\slashed{\mu}$ and $\slashed{\nu}$ in the subscript has been used to remind us that the contribution of μ and ν insertion vertices have been contracted with G photon polarization sum. As the momenta of G photon flows through all the propagators and the vertices which are in between ν and μ (here ν vertex is always situated to the left of μ) insertion vertices, the $[\text{scalar}]_{\slashed{\mu}\slashed{\nu}}$ term can be expressed in a power series expansion of photon momenta k in the soft limit as,

$$[\text{scalar}]_{\slashed{\mu}\slashed{\nu}} \sim \left[\frac{O(1) + O(k) + O(k^2) + \cdots}{(p_i.k)(p_f.k)} \right] \sim \left[\frac{O(1) + O(k) + O(k^2) + \cdots}{O(k^2)} \right] \tag{5.34}$$

Hence, using the results of Eq. 5.33 and Eq. 5.34 in the Eq. 5.32 we obtain the following expression,

$$\mathcal{M}^{scalar;G\gamma}_{n+1} \sim \int \frac{\mathrm{d}^4 k}{(2\pi)^4} \left[\frac{i}{k^2 + i\epsilon} \delta_{t_\mu,t_\nu} \pm 2\pi\delta(k^2)N(|k|)D_T^{t_\mu,t_\nu} \right] \times$$

$$\left[0(p_f \cdot p_i) + 2(p_f + p_i) \cdot k \right] \left[\frac{O(1) + O(k) + O(k^2) + \cdots}{O(k^2)} \right] \tag{5.35}$$

Here we see the leading linear divergence '$2\pi\delta(k^2)N(|k|) \times (0(p_f \cdot p_i)) \times O(1)$' coming from finite temperature ($T \neq 0$) part, and the leading logarithmic divergence coming from

zero temperature $(T = 0)$ part '$(1/(k^2 + i\epsilon)) \times (0(p_f \cdot p_i)) \times O(1)$' vanishes to zero due to the construction of b_k (as b_k was constructed such that the coefficient of $(p_f \cdot p_i)$ *vanishes*).

At finite temperature $(T \neq 0)$ there are also other potential logarithmic sub-divergent contributions due to the term '$2\pi\delta(k^2)N(|k|) \times (0(p_f \cdot p_i)) \times O(k)$' which also vanishes as the coefficient of $(p_f \cdot p_i)$ term is *zero*. There is also other potential logarithmic sub-divergence at finite temperature $(T \neq 0)$ due to the term, '$2\pi\delta(k^2)N(|k|) \times (2(p_f + p_i) \cdot k) \times O(1)$'. This term is odd under the photon momenta (k), *i.e.*, $(k \leftrightarrow -k)$, and hence vanishes upon the momentum integral. Hence, all the sub-divergences also vanishes.

Therefore, the contribution of the G photon is free of any IR divergences and is completely IR finite. Here, it was assumed that there were no IR divergences associated with already existing photon momenta (l'_i/l_i). In reality, IR divergence can arise due to any of these photon momenta going soft. We also have not discussed about the effects of inclusion of thermal scalars. We will discuss about these cases in more details in following subsection. It will be found that after inclusion of all these generalities also G photon contributions are IR finite.

5.3.1   Insertion of thermal scalars and other subtleties

In the above discussion we had considered many simplifications to show the fundamental aspects of G photon insertion. We relax those simplifications here, one by one to finally find again, the G photon contributions to be IR finite.

1. **IR divergence due to any of the already existing photon momenta l'_i/l_i :**

   In the previous discussion we have presumed that there were no IR divergences associated with the photon momenta $l_i(l'_i)$ of the already existing photons in an nth order diagram, which is not necessarily the case. A potential IR divergence can be produced from any of the already existing photons becoming soft in a particular diagram. Hence, according to GY, we have to identify the sets of momenta l_i which

controls the IR divergence of a particular diagram. If $l_i, i = 1, \cdots, m$ photon momenta have been identified as the controlling set of momenta for IR divergence, then it is also known that there is not any divergence related to any subset of these controlling momenta [12]. In literature [12,41] the diagrams with controlling momenta are often referred to as 'Skeletal Diagram'.

Now, it has been shown for fermionic QED at zero [12] and finite [41] temperature that the skeletal diagram cannot create any IR divergence when *all* of the controlling momenta correspond to G photon polarization.

This argument can easily be generalized to the case of thermal scalar QED here as the basic structure due to any of the controlling momenta being G photon is same as of the structure of Eq. 5.35. Hence, it can be shown that, any single momentum factor l_i among the set $l_i, i = 1, \cdots, m$ in numerator will make the whole contribution of skeletal diagram IR finite as all the controlling momenta being G photon, correspond to all of them being virtual photons (as G photon is a rearrangement of virtual polarization). Thus we have the freedom to symmetrize the skeletal diagram with respect to all virtual G photon controlling momenta $(l_i \rightarrow -l_i)$ (photon propagators $-iD^{t_a,t_b}(l_i)$ are anyway symmetric in l_i's). It was shown in Ref. [41] (for fermionic QED), and also can be shown here with simple algebra that this symmetrization brings in one or more factors of momenta l_i from controlling set $l_i, i = 1, \cdots, m$, to the numerator of the corresponding expression. As the leading linear and subleading logarithmic divergence has already been shown to have cancelled from the construction of G photons in Eq. 5.35; hence any extra powers of l_i from the controlling set $l_i, i = 1, \cdots, m$ due to this symmetrization procedure softens and removes any asociated sub-divergences, making the skeletal diagram with all the G photons again IR finite.

2. **Presence of already existing real photon vertices on n^{th} order diagram**: If some of the dotted vertices in the nth order diagram correspond to the real photon vertices,

then the diagram is not symmetric in the real photon emission/absorption (absorption is also possible in finite temperature) due to the presence of weighted phase space factor (but is symmetric in thermal part $N_B(k^0)$ of phase space factor) as shown in Eq. 4.7. But, the diagram has to be *only* symmetrized in virtual G photon controlling momenta; hence this does to pose any problem. Symmetrizing in virtual photons again renders skeletal diagram IR finite.

3. **The inclusion of thermal scalars**: Now the inclusion of thermal scalars can potentially bring in additional divergence due to the presence of the thermal propagators; which are proportional to 'delta function times bosonic number operator for scalars'. Now, if scalars go thermal, for p-leg (for p'-leg also we get an analogous result) we get additional $\delta((p + \sum_j + k)^2 - m^2)$ factors from scalar propagators. Using the properties of the delta functions the new photon momenta k can be constrained in terms of the controlling set of momenta $l_i, i = 1, \cdots, m$; for skeletal diagram. And, as we have already seen that there is no IR divergence related to skeletal diagram, when all the controlling momenta correspond to G photons, hence the inclusion of thermal scalars does not worsen the IR structure of matrix element, and the matrix elements are IR finite.

4. *G photon is inserted on a trilinear vertex making that a seagull vertex*: Till now we have only discussed about G photon insertion, where they have been inserted to make new trilinear μ and ν vertices. But, this is not always true; any one or both of μ and ν vertices can be inserted at an already existing trilinear vertex making it a seagull vertex. These kind of insertions produce additional factors such as,

$$\left\{ S\,{}^{t_{q-1},t_\mu}_{p_f + \Sigma_{q-1}} \left[-2g_{\mu,\mu_q} \right] \right\} \text{ and } \left\{ S\,{}^{t_{j+1},t_\nu}_{p_i + \Sigma_j + k} \left[-2g_{\nu,\nu_j} \right] \right\} . \tag{5.36}$$

In the above expression of Eq. 5.36 the terms in the curly brackets replaces similar terms in curly braces in Eq. 5.33 if the new insertion were to be seagull ones.

At zero temperature it can be shown that the G photon contributions due to seagull

diagrams have an extra term linearly dependent on the photon momentum k than a corresponding trilinear insertion.

This can be very easily seen from looking at the circled vertex analogue of G photon insertion from Fig. 4.8 where a trilinear μ insertion vertex is inserted at the immediate right vertex number q, and in a different contribution at vertex number q making a seagull vertex on p'-leg.

We will concentrate on the zero temperature part at first, before moving to the finite temperature analogue. The relevant contribution of the analogous 'Circled G Photon' combined expression has the form, (for sake of clarity after dropping the part of G photon polarization and loop integrations):

$$M_{n+1,q}^{\mu,G\gamma} \sim \cdots \frac{1}{(p' + \Sigma_{q-1})^2 - m^2}\left[(2p' + 2\Sigma_{q-1} + k)_\mu \frac{1}{(p' + \Sigma_{q-1} +k)^2 - m^2}\times \right.$$
$$\left. \times(2p' + 2\Sigma_{q-1} + 2k + l'_q)_{\mu_q} - 2g_{\mu\mu_q}\right] \times \frac{1}{(p' + \Sigma_q +k)^2 - m^2} \cdots . \quad (5.37)$$

In the above expression the photon momentum of the already existing trilinear vertex at q is denoted by l'_q. A similar contribution can be written down for a similar G photon insertion at the v vertex insertion (which will be the analogous diagram of Fig. 4.9) at vertex j. Factoring out the scalar propagator contribution $1/((p' + \Sigma_{q-1} +k)^2 - m^2)$ and multiplying with $-2g_{\mu q}$ contribution of the seagull insertion, we get the term to be reducing to $(2p' \cdot k + k^2)$. We note that the leading power of IR divergence in G photon insertion arises when all the controlling sets of momenta goes soft *together* in skeletal diagrams. Thus we have put all $l'_i = 0$ and and have used the on-shellness of p'-leg in the above expression of Eq. 5.37.

The contribution of the seagull insertion becoming proportional to $(2p' \cdot k + k^2)$, implies that at the leading order it will contribute linearly in k at zero temperature and hence is IR finite according to previously mentioned discussions.

Now, for the case when the scalars are thermal then, extra thermal part (delta func-

tion times number operator) of scalar propagators are also present in the discussion. The relevant part of the matrix element again looks like $[g^{\mu\nu} - b_k k^\mu k^\nu][\text{scalar}]_{\mu\nu}$. Where, in $[\text{scalar}]_{\mu\nu}$ now one or both of the μ, ν insertion can be trilinear/seagull insertion. A similar analysis analogous to Eq. 5.37 can be performed for both μ and ν insertions now, but with presence of thermal scalar propagators. The final results are very messy and we will not write down the explicit expression here.

But, we will point out the main results. The contribution when both the μ and ν vertices are trilinear has leading linear and sub-leading logarithmic divergence (as already seen from Eq. 5.35). The contribution when one of the insertion vertices among μ or ν is seagull and other one is trilinear have *only* logarithmic divergences. The contribution where both the μ and ν insertion correspond to seagull insertion has an overall factor $O(k)$ in the numerator, *i.e.*, it is linear in numerator and hence is IR finite. The term when μ and ν are identified (a tadpole diagram) is $O(k^2)$ in the numerator and also is IR finite.

The leading linear and sub-leading logarithmic divergence, when both the μ and ν insertion are trilinear have already been found to vanish according to Eq. 5.35. The other sub-divergence, arising from one of the insertions μ or ν being trilinear and the other one being quadrilinear is logarithmic and also vanishes after symmetrizing with respect to photon momenta G photon momenta k. And, when there are more than one controlling momenta $l_i, i = 1, \cdots, m$; controlling the divergences then, symmetrising over all of them, at-least bring one or more additional powers of l_i's in the numerator cancelling any logarithmic sub-divergence.

It is also to be noted that, this argument does not depend on whether the vertices where the new G photon is inserted, corresponded to already existing K or G photon insertion. Hence, all the contribution which refer to seagull type due to insertions of new G photons are IR finite.

5. **If there were already existing seagull vertices in n^{th} order diagram**: Till now we have only considered the nth order diagrams which have trilinear insertions. If there were already existing seagull diagrams in the nth order diagram, then this does not complicate the concerned scenario. As, no new photons (whether G or K) can be inserted on those seagull insertions; hence they behave like some inert vertices. The contributions due to those already existing seagull insertion vertices just get carried along and does not spoil any of the above analysis.

6. **If there were already existing K photons in n^{th} order diagram**: If there were already existing K photon insertions present in the nth order diagram, then we have already seen that those contributions can be factored out as in Eq. 5.27 to a multiplicative factor. If more than one K photons were present then the procedure should be repeated multiple times untill all the factors related to K photons are factorized and the diagram only contain G photon contributions. Then all the above results can be again applied.

It is also to be noted that, "fleshing out" skeletal diagrams and adding self-energy or vertex insertions does not complicate the situation as all those insertions contribute linear term in photon momentum k in the numerator and thus become IR finite. This can be proved using a generic argument as in GY [12] after rationalizing the denominator factors and then applying the concerned equation of motion. Also, the inclusion of charged scalar loops or photon loops also do not spoil the IR finiteness. Due to the mass terms of charged scalars, the scalar loops cannot contribute any IR divergence; and the photon loops which are tadpole diagrams are already shown to be IR finite. Therefore, the result of the fleshing out of skeletal diagrams are unchanged in scalar QED at finite temperature.

5.4 The total matrix element for the virtual photon insertions

We have found that the K photon insertions contain all the IR divergences, and these IR divergent terms gets factored out. The higher order K photon contribution becomes proportional to the lower order matrix element as in Eq. 5.27. The G photon contributions turned out to be IR finite from previous discussions and using Eq. 5.35. As a fully virtual n^{th} order graph contributes a factor of 'e^{2n}' charge factor to the leading order, hence for a fully virtual diagram there are always n number of virtual photons present. But, according to the prescription of GY all the virtual photon polarization sums should be re-written in terms of K and G photon polarization sums. Hence, if in an nth order diagram there are n_K number of virtual K photons and n_G number of virtual G photons present, such that $n = n_K + n_G$, due to the Bose symmetry related to n number of photons, each distinct class of diagram can arise in $n!/(n_K!\, n_G!)$ ways. Therefore, the full matrix element for virtual photon insertions has to be expressed as a summation of all possible individual terms,

$$\frac{1}{n!}\,\mathcal{M}_n^{\text{scalar}} = \sum_{n_K=0}^{n} \frac{1}{n_K!}\frac{1}{n - n_K!}\mathcal{M}_{n_G,n_K} \ . \tag{5.38}$$

Therefore, summing over to all orders the expression becomes,

$$\sum_{n=0}^{\infty} \frac{1}{n!}\mathcal{M}_n^{\text{scalar}} = \sum_{n=0}^{\infty}\sum_{n_K=0}^{n} \frac{1}{n_K!}\frac{1}{n - n_K!}\mathcal{M}_{n_G,n_K}^{\text{scalar}} \ ,$$

$$= \sum_{n_K=0}^{\infty}\sum_{n_G=0}^{\infty} \frac{1}{n_K!}\frac{1}{n_G!}\mathcal{M}_{n_G,n_K}^{\text{scalar}} \ . \tag{5.39}$$

Using the result of Eq. 5.27 that the K photon higher order contribution is proportional to lower order matrix element we find,

$$\mathcal{M}_{n_G,n_K}^{\text{scalar}} = (B)^{n_K}\mathcal{M}_{n_G,0}^{\text{scalar}} \equiv (B)^{n_K}\mathcal{M}_{n_G}^{\text{scalar}} \ . \tag{5.40}$$

In the above expression, B is defined as in Eq. 5.28. Therefore, all the K-photon insertion contributions can be factored out, separating out the IR finite G-photon insertion contribution, $\mathcal{M}^{\text{scalar}}_{n_G}$. After manipulating and re-sorting the K photon terms, it can be expressed and resummed as an IR divergent exponential term:

$$\sum_{n=0}^{\infty} \frac{1}{n!} \mathcal{M}^{\text{scalar}}_n = \sum_{n_K=0}^{\infty} \frac{(B)^{n_K}}{n_K!} \sum_{n_G=0}^{\infty} \frac{1}{n_G!} \mathcal{M}^{\text{scalar}}_{n_G} ,$$
$$= \mathrm{e}^B \sum_{n_G=0}^{\infty} \frac{1}{n_G!} \mathcal{M}^{\text{scalar}}_{n_G} . \tag{5.41}$$

This neat factorization and the exponentiation was only possible due to the presence of seagull and tadpole contributions, which cancelled all the finite $O(k)$ and $O(k^2)$ terms resulting in the higher order K photon contribution to be proportional to a single lower order term. Therefore, the relevant part of the cross section, which incorporates only the virtual photon contributions to all orders can be written as,

$$\sigma^{\text{virtual}} \propto \int \mathrm{d}\phi_{p'} (2\pi)^4 \delta^4(p + q - p') \left| \sum_{n=0}^{\infty} \frac{1}{n!} \mathcal{M}^{\text{scalar}}_n \right|^2 ,$$
$$= \int \mathrm{d}\phi_{p'} (2\pi)^4 \delta^4(p + q - p') \, |Z|^2 \, \sigma^{\text{virtual}}_G . \tag{5.42}$$

In the above expression we have suppressed flux factors, and $\mathrm{d}\phi_{p'}$ correspond to the phase space factors related to the final state charged scalar with momentum p'. The IR finite part is denoted by $\sigma^{\text{virtual}}_G$ in Eq. 5.42 and both the linear and logarithmic IR divergent contributions are contained in the term in the exponent,

$$|Z|^2 \equiv \exp\left(B + B^*\right) . \tag{5.43}$$

The IR divergent contribution will be shown in following discussions to cancel against similar IR divergent contributions arising from soft real photon contributions (after including both emission and absorption with respect to heat bath), rendering the theory of scalar QED at finite temperature to be IR finite to all orders in perturbation theory.

5.5 Real photon emission to and absorption from the heat bath

The charged scalar particle being present inside the heat bath interacts with the bath via the exchange of the real photons. Hence, at finite temperature in addition to emitting the real photon to the heat bath, the photon can also be absorbed from it. This is in contrast to the zero temperature field theory, where real photons cannot be absorbed from the vacuum. The real photons can be emitted from/absorbed to the either of the p and p'-leg. Hence, the contributions arising from each leg are independent of each other and can be calculated separately. Similar to the virtual photon insertion the real photon can be inserted on a scalar propagator to create a new insertion vertex, or it can also be inserted on an already existing trilinear vertex to form a seagull vertex. The main difference between the virtual and the real photon cases related to the insertion vertices is that there cannot be any tadpole diagrams for the real photon cases (as the real photon actually brings in/out the momenta from the heat bath).

In contrast to virtual photon corrections, the real photon actually carries out or brings in physical momenta. Without loss of any generality, this extra factor of the momenta can be accounted for by adjusting the momentum at hard vertex V and by keeping the momenta associated with the p and p' external legs unchanged. Hence, due to this fact the momenta of scalar propagators which lie in between the new emission/absorption vertex and the hard vertex V gets modified; and all the other scalar propagator momenta is kept unchanged. For an example, if the photon is emitted then the extra additional momentum that the real photon carries out can be taken into account by readjusting the photon momentum at the hard vertex by replacing q to $(q + k)$. Now, if the real photon is emitted with a momentum k from new insertion vertex μ on the p'-leg, where μ vertex is situated at the immediate right to vertex number q (as shown in the first diagram of Fig. 4.8) then, *only* the momentum of the scalar propagators which are in between vertex number $q \leq b \leq V$ will

be modified; and the changed value of the propagator momentum for the left of vertex b on p'-leg is given by $(p' + \sum_{i=1}^{b} l'_i + k)$ for $q \leq b \leq s$. And, if the real photon is emitted with same momentum k from new insertion vertex v on the p-leg, where v vertex is situated at the immediate left to vertex number j (as in the first diagram of Fig. 4.9) then, *only* the momentum of the scalar propagators which are in between vertex number $j \leq a \leq V$ will be modified; and the changed value of the propagator momentum for the left of vertex a on p-leg is given by, $(p + \sum_{i=1}^{a} l_i - k)$ for $j \leq a \leq r$. Note a difference in the signature of additive factor of k between p' and p-leg; while on p'-leg it comes with a *plus* sign, for p-leg it comes with a *minus* sign. The difference of this sign of contribution of photon momentum in scalar propagator is due to the fact that in both the cases real photon is emitted from the emission vertex. Whereas, the corresponding factors of photon momenta k in scalar propagators for new virtual photon insertion, always arose with a *similar* sign (see the discussion above Eq. 3.8 for comparison) in both the legs for the cases of virtual photons, as virtual photons are emitted at one leg and absorbed in the other leg. This difference of sign of additive k term will be of *crucial* importance while we factorize the matrix element squared for real photon case. For an absorption of the real photon, all the above discussion holds true with a flip in the sign of k, *i.e.*, wherever in the above discussion k factor arose now we have to replace that by $-k$ for photon absorption.

Apart from these, as the real photon emission/absorption contributes in the matrix element squared (cross section) level $|\mathcal{M}^{\text{scalar}}|^2$; hence the modification of the phase space factor for the real photons must be included. The thermal phase space for photon with momentum k_i can be written down as in Eq. 4.7 and we mention it here again for completeness and convenience,

$$d\phi_i = \frac{d^4 k_i}{(2\pi)^4} \, 2\pi \delta(k_i^2) \left[\theta(k_i^0) + N_{\text{B}}(|k_i^0|) \right] . \tag{5.44}$$

In the above expression $\theta(k_i^0)$ correspond to the step function (denoting zero temperature analogous part of the phase space). For emission of real photons $k_i^0 > 0$ and for the

absorption of real photon $k_i^0 < 0$.

Hence, the emission of real photon comes with an overall statistical factor of $(N_B + 1)$ in phase space, and for absorption of real photon the corresponding factor is N_B in the phase space at finite temperature. The presence of statistical weight factors in the form of number operator (distribution function) worsens the IR divergence for the cases of real photon emission/absorption from heat bath. The leading IR divergence again become linear as $N_B \sim 1/|k|$ in IR limit.

To incorporate the extension of the GY technique to the thermal case, the real photon polarization sum has to be re-expressed as in Eq. 4.5 and Eq. 4.6 of Chapter 4 in terms of the $\widetilde{K}$ and $\widetilde{G}$ real photon insertions.

5.5.1 Real $\widetilde{K}$ photon emission and absorption

Inclusion of the real $\widetilde{K}$ photon to an nth order diagram is comparatively simpler than the analogous case of K photons for virtual photons. The contribution coming from both the legs can be evaluated independently (and there is no complication related to the double-counting, tadpole diagrams etc). The real photons being physical, can only correspond to the thermal type-1 only whether emitted/absorbed. Hence, the real photon insertion vertices μ and/or ν correspond to thermal vertex type-1 only. This also simplifies the real photon calculation a lot. Here, we will make a note that, the virtual K photon insertion contribution came out to be proportional to D^{11}, which can be seen from Eq. 5.27 and Eq. 5.28. This fact will be crucial to obtain the cancellation of IR divergent factors between virtual and real soft photon cross-sections.

The real $\widetilde{K}$ photon emission contribution calculation follows a similar technique as in virtual K photon case. After using 'Generalized Feynman identity' we again find there is a pairwise term by term cancellation, leaving the contribution of the matrix element including $\widetilde{K}$ photon contribution on p'-leg to be proportional to n^{th} order matrix element $\mathcal{M}_n^{\text{scalar}}$

with contribution of $\widetilde{K}$ photon factored out. The corresponding calculation for the p-leg results in a similar factorization with an extra 'minus' sign with respect to the corresponding analogous virtual photon insertion, making the matrix element to be proportional to $-\mathcal{M}_n^{\text{scalar}}$. Now, the origin of this 'minus' sign is due to the fact that, for both the cases, from the p' and p-leg real photon is emitted and hence carries out momenta k for each case. This also gave rise to different sign of additive k factors in the scalar propagators in the discussion related to Section 5.5 above.

This overall sign is flipped for the real $\widetilde{K}$ photon absorption from heat bath. However, in the matrix element squared level, the contribution coming from p and p'-leg has to be multiplied, giving the *same* factor for both the real photon emission and absorption cases.

Therefore after considering all the possibilities of emission and absorption of $\widetilde{K}$ photons from both the legs and then squaring, the contribution to the $(n+1)^{\text{th}}$ order cross section, obtained by emission/absorption of a real photon form heat bath to the lower order diagram for thermal scalar QED becomes,

$$\left| \mathcal{M}_{n+1}^{\text{scalar}; \widetilde{K}\gamma,\text{tot}} \right|^2 \propto - e^2 \left[\tilde{b}_k(p, p) - 2\tilde{b}_k(p', p) + \tilde{b}_k(p', p') \right] \times \left| \mathcal{M}_n^{\text{scalar}} \right|^2$$

$$\equiv - e^2 \widetilde{J}^2(k) \left| \mathcal{M}_n^{\text{scalar}} \right|^2 . \tag{5.45}$$

While obtaining the above result the inclusion of seagull vertex contributions have also been taken into account. And the result also holds true, if some of the already existing vertices of nth order diagram correspond to virtual photon (K or G) insertion.

5.5.2 Real $\widetilde{G}$ photon emission and absorption

The inclusion of real $\widetilde{G}$ photon to an nth order diagram has a very similar structure related to the inclusion of the virtual G photon inclusion. There are obviously certain differences between both the cases (which we will discuss below), but the fundamental technique to

prove that $\widetilde{G}$ photon contributions are IR finite, have some common similarity with G photon case. Similar to the real $\widetilde{K}$ photon insertion, the computation of $\widetilde{G}$ photon contribution is comparatively simpler; as there are no possibility of double counting or presence of tadpole diagrams. All the other subtleties which we mentioned in Subsection 5.3.1 for G photons also hold for $\widetilde{G}$ photons also.

The main point to notice here, is about the dependence on k due to the inclusion of finite temperature. Due to the construction of $\tilde{b}_k(p_f, p_i)$ the leading IR divergences (linear divergence from thermal part and logarithmic divergence due to zero temperature) cancels in between '$g_{\mu\nu}$ and the $\tilde{b}_k k_\mu k_\nu$' terms of $\widetilde{G}$ photon polarization sum. Hence, the main concern is about potential sub-divergences arising from powers of k in the numerator. As the leading IR divergence was linear in the denominator (which got cancelled), a linear power of k in the numerator will give us logarithmic IR sub-divergence, and terms with quadratic or more powers of k in the numerator are IR finite.

The crucial difference between the virtual G photon and real $\widetilde{G}$ photon contribution is that, the phase space corresponding to the real photon emission/absorption Eq. 5.44 is not symmetric under the exchange of real photon momenta k, *i.e.*, $(k \leftrightarrow -k)$ due to the presence of zero temperature part indicated by step function $\theta(k_i^0)$. But, we have to notice that the finite temperature part of the phase space denoted by number operator is symmetric under photon momenta exchange (*i.e.*, under real photon emission and absorption). Hence, any potential logarithmic sub-divergence arising from the finite temperature part now vanishes under $(k \leftrightarrow -k)$ symmetry as the thermal phase space is symmetric, and the whole integrand is odd under photon momentum integral. Thus, the contribution of real $\widetilde{G}$ photon insertions are IR finite.

Again some of the already existing real photons in n^{th} order diagram, can pose a potential logarithmic sub-divergence when they go soft. Hence, they are the part of controlling momenta regarding IR divergences. And, as analogous to G photon calculations, symmetrizing them (as the thermal part of phase space is symmetric under photon momenta

exchange) with respect to their momenta brings in at-least one or more powers of photon momenta, from the set of controlling momenta in the numerator softening and cancelling all the sub-divergence for $\widetilde{G}$ photon contribution.

Therefore, the contribution of real $\widetilde{G}$ photon emission/absorption are IR finite in the cross section.

5.6   The total cross section for the real photon emission and absorption

We have obtained that the $\widetilde{K}$ photon insertions contain the IR divergences, and $\widetilde{G}$ photon insertions are all IR finite when both the emission and absorption of the real photons are considered together. As a fully real n^{th} order diagram contributes a factor of 'e^{2n}' in the matrix element square level, for those diagrams all the already existing vertices correspond to real photon insertions, and hence the diagram has n number of real photons. Now, to apply the GY rearrangement of polarization sums real photons have to be separated in terms of $\widetilde{K}$ and $\widetilde{G}$ photons, such that in a diagram of nth order, if there are n_K numbers of $\widetilde{K}$ and n_G numbers of $\widetilde{G}$ photon emission/absorption then $n = n_K + n_G$. Such a distinct class of diagrams having n_K numbers of $\widetilde{K}$ and n_G numbers of $\widetilde{G}$ photons can appear in $n!/(n_K!n_G!)$ ways. Here, each real photon brings in/carries out physical momenta k_l to/from the relevant diagram. Due to the presence of identical n number of photons in the final state, we have to divide by a factor $n!$ at this n^{th} order. The expression of the cross-section then becomes,

$$
d\sigma_n^{\text{real}} = \sum_{n_K=0}^{n} \frac{1}{n_K!} \left[\prod_{i=1}^{n_K} \int d\phi_i \left\{ -e^2 \widetilde{J}^2(k_i) \right\} \right] \times \frac{1}{n_G!} \left[\prod_{j=n_K+1}^{n} \int d\phi_j \left\{ -\widetilde{G}_{\mu\nu} \left| \mathcal{M}_{n_G}^{\text{scalar};\mu\nu,\tilde{G}\gamma,tot} \right|^2 \right\} \right] \times
$$
$$
(2\pi)^4 \delta^4 \left(p + q - p' - \sum_{l=1}^{n} (-1)^l k_l \right).
$$

(5.46)

116

In the above expression, the factor $(-1)^l$ in the delta function, corresponds to ± 1; based on the fact that, whether real photon having momentum k_l is emitted to/absorbed from heat bath. The relevant phase space factor of real photon is given by Eq. 5.44 and the factor $\widetilde{J}(k_i)$ which arose from Eq. 5.45 contains the IR divergent pieces. We manipulate the four momentum conserving delta function using the trick shown in Eq. 5.47 to separate out the k_l dependence.

$$(2\pi)^4 \delta^4 \left(p + q - p' - \sum_{l=1}^{n} (-1)^l k_l \right) = \int d^4 x \exp\left[-i(p + q - p') \cdot x \right] \prod_l \exp(\pm i\, k_l \cdot x) \,. $$

(5.47)

In the expression above, the sign of photon momenta k_l in the last bracketed term depends on whether the real photon was emitted to or absorbed from heat bath. We also separate out the contributions of $\widetilde{K}$ photons from this last bracketed term as below,

$$\prod_{l=1}^{n} \exp\left[\pm i\, k_l \cdot x \right] = \prod_{k=1}^{n_K} \exp\left[\pm i\, k_k \cdot x \right] \times \prod_{g=n_K+1}^{n} \exp\left[\pm i\, k_g \cdot x \right] \,. $$

(5.48)

The first set of terms depend on the photon momenta k_k of the $\widetilde{K}$ photon insertions. These factors are hence combined with the common factor for every contribution of $\widetilde{K}$ insertion in Eq. 5.46 (after noting that subscript i and k of photon momenta are dummy indices). The total contribution due to *each* $\widetilde{K}$ photon hence becomes equal to the expression,

$$\widetilde{B}(x) = -e^2 \int \widetilde{J}^2(k_k) d\phi_k \exp\left[\pm i\, k_k \cdot x \right] \,. $$

(5.49)

The complete contribution due to $\widetilde{K}$ for *all* real photons in Eq. 5.46 can now be factored as,

$$d\sigma_n^{\mathrm{real};\,\widetilde{K}\gamma} \propto \sum_{n_K=0}^{n} \frac{1}{n_K!} \left(\widetilde{B}(x) \right)^{n_K} \,. $$

(5.50)

The above expression therefore can be exponentiated as $n \to \infty$. This factor will be used to compute the total cross-section (including real and virtual) for the relevant process to

117

all orders in perturbation theory.

5.7 The total cross section to all orders for thermal scalar QED

Therefore, the all order corrections in perturbation theory related to the tree level cross section of $\gamma^{(*)}\phi \to \phi$, in thermal scalar QED including both the virtual and real (soft emission/absorption) photon contributions, result in an expression of the total cross section for this process as below,

$$
\begin{aligned}
\mathrm{d}\sigma^{\mathrm{tot}} &= \int \mathrm{d}^4 x\, e^{-i(p+q-p')\cdot x} \mathrm{d}\phi_{p'} \exp\left[B + B^*\right] \exp\left[\widetilde{B}\right] \times \\
&\qquad \sigma_G^{\mathrm{virtual}} \sum_{n_G=0}^{\infty} \frac{1}{n_G!} \prod_{j=0}^{n_G} \times \int \mathrm{d}\phi_j e^{\pm i k_j \cdot x} \left[-\widetilde{G}_{\mu\nu} \left|\mathcal{M}_{n_G}^{\mathrm{scalar};\,\mu\nu,\,\tilde{G}\gamma,\,tot}\right|^2\right] , \\
&= \int \mathrm{d}^4 x\, e^{-i(p+q-p')\cdot x} \mathrm{d}\phi_{p'} \exp\left[B + B^* + \widetilde{B}\right] \sigma^{\mathrm{finite}}(x) .
\end{aligned}
\tag{5.51}
$$

In the above expression, the σ^{finite} factor contains *all* the IR finite G and $\widetilde{G}$ photon contributions; arising respectively from both the virtual and real photon contributions. In Eq. 5.51 *all* the IR divergent contributions arising from both the virtual and real photon is found to be exponentiated and *these contributions combine together to produce an IR finite sum*, as can be shown by studying the small - k behaviour of these terms,

$$
\begin{aligned}
(B + B^*) + \widetilde{B} &= e^2 \int \mathrm{d}\phi_k \left[J(k)^2 \left\{1 + 2N_{\mathrm{B}}(|k^0|)\right\} - \widetilde{J}(k)^2 \left\{\left(1 + N_{\mathrm{B}}(|k^0|)\right) e^{ik\cdot x} + N_{\mathrm{B}}(|k^0|)e^{-ik\cdot x}\right\}\right] \\
&\xrightarrow{k\to 0} 0 + O(k^2) .
\end{aligned}
\tag{5.52}
$$

It is to be noted that the cancellation of IR divergence occurs among virtual and real photon contributions *only* when the real photon absorption terms from the heat bath (second term in the squared bracket in Eq. 5.52 above) are also included. Therefore, the scalar QED at

finite temperature is IR finite to all orders in perturbation theory, the proof of which was presented here.

5.8 Summary

The infrared structure of a particular theory at finite temperature is much more intricate than the corresponding theory at zero temperature due to the presence of thermal fluctuations. Here, in this chapter we have particularly focused our attention on the thermal theory of scalar QED. Due to the presence of the thermal photons and thermal scalars the IR structure of the theory becomes highly complicated. The IR divergence associated with the theory, contains both leading linear and sub-leading logarithmic (due to thermal fluctuations) divergences, in addition to already present leading logarithmic (due to quantum fluctuation) divergences.

The presence of both the trilinear and the seagull vertices in scalar QED complicates the situation further. There can be tadpole contributions now in scalar QED for new virtual photon insertions on the same leg. Thus the numbers of diagrams related to a higher order process proliferate extensively. After avoiding the matter related to the double counting of vertices, the similar classes of diagrams were grouped together in particular sets to observe the nature of factorization easily. Both the seagull and tadpole diagrams played a crucial role cancelling respectively linear and quadratic in photon momenta terms in numerator. Although these terms are finite but without cancellation of these terms a neat factorization leading to IR resummation would not have been possible. The seagull insertion and tadpole diagrams were *indispensable* to achieve this neat factorization and resummation.

The virtual K photon contributions were found to contain all the leading linear and sub-leading logarithmic divergences. The virtual G photon contributions were found to be IR finite in thermal field theory, and can be calculated order by order to obtain finite temperature corrections in perturbation theory.

119

As for the real photons in addition to the photon emission, the absorption of the photons from the heat bath also become feasible, and must be included in the calculation. The phase space factor for real photon emission/absorption also gets modified due to finite temperature. The $\widetilde{K}$ photon contributions were found to factorize in the square of matrix element. These $\widetilde{K}$ contributions also contained all the leading linear and sub-leading logarithmic divergence in the case of real photon. The $\widetilde{G}$ photon terms turned out to be IR finite, after considering the symmetric nature of the relevant thermal part of real photon phase space.

All the virtual and real photon contributions were then considered together, to find that all the leading linear and sub-leading logarithmic divergences cancel between virtual K and soft real $\widetilde{K}$ photon contributions, in the cross-section of the processes related to thermal scalar QED to all orders in perturbation theory; implying the theory to be IR finite. *Only with inclusion of both the absorption and the emission of real photons the IR divergence were found to cancel against the virtual photons counterpart.* Therefore, the scalar QED at finite temperature is IR finite to all orders in perturbation theory.

Chapter 6

Infrared finiteness of a theory of dark matter at finite temperature

6.1 Prologue

To explain the results of the precision measurements ranging over a multitude of length-scales related to various astrophysical and cosmological observations, the existence of Dark Matter (DM) is necessitated; which overwhelms the ordinary component of matter in the known Universe. Among the various potential candidates for DM and the production mechanisms, usually the most natural and well studied mechanism to meet the current abundance of DM is through the production of the DM thermally in the post-inflation reheating phase. The ensuing number density of DM is then determined by a set of coupled Boltzmann equations in the expanding Lemaitre-Friedmann-Robertson-Walker Universe. The temperature of the universe decreases with its expansion; resulting in the DM component to fall out of equilibrium, and the number density of DM freezes out. This freeze out of DM happens when interaction rate of DM particles falls below the Hubble expansion rate of the Universe.

With the advent of precision cosmology, this relic density of the DM in the energy fraction of the Universe has been measured by 'WMAP' Ref. [56], followed by 'PLANCK' [57, 58], with extreme precision. Hence, only an order of magnitude prediction of relic densities from theoretical calculations are not any more justifiable. There have been efforts to include the higher order corrections in theoretical calculations [78–85] to the annihilation cross-section of the DM at zero temperature. The higher order (NLO) corrections at zero temperature were found to be non-negligible with respect to the leading order. But, as the DM was in thermal equilibrium with the background plasma until the freeze out; hence the temperature effects can modify the relic density calculations appreciably, and the predictions including the higher order NLO corrections performed at finite temperature are highly desirable. The efforts in this directions were fruitfully discussed in Refs. [86, 87]. Particularly in Ref. [86] Beneke et. al. have performed a relic density calculation in the thermal field theory at NLO. They have obtained the finite thermal correction to relic density due to temperature effects, and have found the IR divergences related to corresponding process to cancel at NLO completely when both the absorption and emission of the particles from the heat bath were allowed. This motivated us to look into an all order IR behaviour of the corresponding theory at finite temperature.

The Lagrangian corresponding to the related model is expressed as,

$$
\begin{aligned}
\mathcal{L} = &- \frac{1}{4} F_{\mu\nu} F^{\mu\nu} + \overline{f} \left(i\slashed{D} - m_f \right) f + \frac{1}{2} \overline{\chi} \left(i\slashed{\partial} - m_\chi \right) \chi \\
&+ \left(D^\mu \phi \right)^\dagger \left(D_\mu \phi \right) - m_\phi^2 \phi^\dagger \phi + \left(\lambda \overline{\chi} P_L f^- \phi^+ + \text{h.c.} \right) .
\end{aligned}
\tag{6.1}
$$

This particular model has been studied extensively in Refs. [100–103] at zero temperature, relating the importance of electroweak bremsstrahlung and lift of helicity suppression at higher order NLO corrections. The relevant part of the Lagrangian as expressed in Eq. 6.1 describes a simplified model of DM, which is an extension of Standard Model (SM) containing left handed SM fermion doublets $f = (f^0, f^-)^T$ along-with additional scalar doublet $\phi = (\phi^+, \phi^0)^T$ which are super-partners of SM fermions f. The model also contains

an $SU(2) \times U(1)$ singlet Majorana fermion χ which is the concerned dark matter candidate. The model is motivated by WIMP (weakly interacting massive particle) paradigm in MSSM (minimal supersymmetric Standard Model), where the DM candidate χ is a bino (bino-like) having a mass of TeV scale, $m_\chi \approx \mathcal{O}$ (0.1–1 TeV), and mass of sfermion ϕ is $m_\phi > m_\chi$. Here, χ is the DM candidate having a mass of TeV scale; the freeze-out happens at a temperature $T_{freeze-out} \approx m_\chi / 20$. Hence, the freeze-out of DM takes place after the electro-weak transition. At this scale, only the electromagnetic interactions are of relevance to treat the IR finiteness of the corresponding theory. The covariant derivative term in Eq. 6.1 will only contain the photon contributions, *i.e.*, $\mathcal{D}_\mu = \partial_\mu + ieA_\mu$. In the concerned Lagrangian, the DM candidate χ interacts with the SM fermions f via the Yukawa interaction term as written in Eq. 6.1. In the interaction term, there should also be interaction terms relating the neutral components, *i.e.*, $\lambda \overline{\chi} P_L f^0 \phi^0$ which allows processes like $\chi + \overline{\chi} \leftrightarrow f^0 + \overline{f}^0$; which we have to certainly include while estimating the inclusive cross-section. But, we have discounted here in Eq. 6.1 any such interaction terms, as neutral components will not receive any electromagnetic corrections at higher order and hence will not be of importance in the discussion of IR resummation.

To observe the IR finiteness of the theory, we will start with the processes,

$$\chi + \overline{\chi} \leftrightarrow f + \overline{f}, \qquad \text{and} \qquad \chi + f \to \chi + f, \qquad (6.2)$$

which are of importance to estimate the relic density of DM candidate, and will consider the higher order electromagnetic corrections to these at finite temperature. A particular diagram representing the annihilation process of Eq. 6.2 at tree level has been shown in Fig. 6.1. In Fig. 6.1 the DM candidate χ is represented by double solid lines, the SM fermion f and the heavy scalar ϕ have been respectively represented by single solid and dashed lines.

We would also like to mention here that, though the Lagrangian of Eq. 6.1 may seem too simplistic, the model actually encapsulates the essence of a wide class of models. More

about this was already discussed in Chapter 1. With the use of this particular Lagrangian Eq. 6.1 we are able to capture all the subtle issues related to IR structure of all those various class of models, while making the way for considerable simplification focusing on the fundamental process of GY factorization leading to IR resummation at finite temperature.
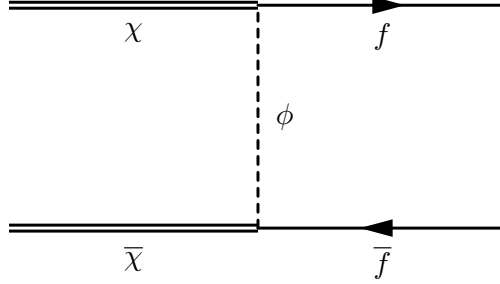
Figure 6.1: *A typical dark matter χ annihilation/scattering process at tree-level.*

To study the IR structure of the corresponding theory of Eq. 6.1 we will start with the effect of adding a virtual/real photon in rearranged polarization sum in all possible ways to the nth order processes related to Eq. 6.2 at finite temperature.

6.2 The nth order diagram and the choice of special vertex

To identify correctly the IR structure of the theory of DM, we will start with an nth order diagram of typical processes Eq. 6.2 involving DM; and will see the effect of insertion of additional photon (virtual or real) to that corresponding process in all possible ways. We will in particular start with an nth order process related to $\chi(q + q')\, f(p) \to \chi(q')\, f(p')$ [1], implying the in-between scalar propagator of the lowest (tree-level) order process has

---

[1] The result of nth order annihilation processes $\chi + \bar{\chi} \to f + \bar{f}$ can be obtained, using simple use of crossing symmetry related to the nth order process of $\chi + f \to \chi + f$. But, we have here chosen to show the proof simply for the latter process, to avoid unnecessary complicated expression due to the presence of extra (-1) form factor in the vertex factors of aniparticles and to avoid different fermion (SM) propagator structure for antiparticles, which may divert us from the main structure of the proof. The crossing symmetry ensures the proof for the annihilation processes, and an explicit calculation relating such annihilation processes also establishes the same fact.

a momentum of $(p - q')$. The schematic diagram for the corresponding n^{th} order process has been shown in Fig. 6.2.
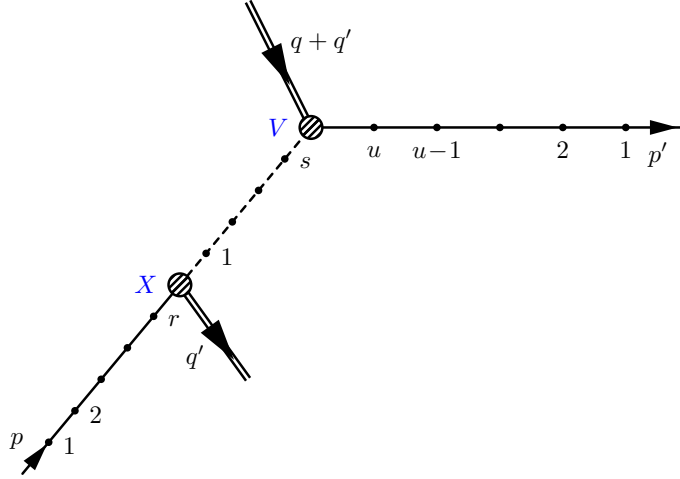
Figure 6.2: *A typical n^{th} order diagram for the process $\chi f \to \chi f$ has been drawn. As now there are two distinct vertices where hard external momenta flows in (vertex V)/out (vertex X); hence any one of those can be chosen as the special vertex to distinguish between initial p and final p'-leg. Here, we have chosen vertex V to be that special vertex. Hence, the final p'-leg (consisting of final fermion line) has u number of vertices. The initial p-leg consists of both the initial fermion line and intermediate scalar line. The number of vertices on initial fermion, intermediate scalar, and full p-leg is respectively given by r, s and $r + s = w$. For an nth order diagram, where all the existing photon insertions are virtual $n \le u + s + r = m \le 2n$.*

Now, here is a difference in this n^{th} order diagram, with respect to all other similar diagrams which we have discussed in the earlier chapters. Now, there are two special vertices where the hard momentum (carried by DM 'χ') flows in (at vertex V) /out (at vertex X). According to GY [12] either of these vertices can be used as the special vertex to distinguish between the initial p and final p'-leg. We will here chose the vertex V to be that special vertex. Hence, all the part of the diagram which comes before the special interaction vertex belongs to initial p-leg; *i.e.*, with our choice, the initial fermion line and the internal scalar line belong to initial p-leg, and all the part of diagram which comes after the special interaction vertex V belongs to the final p'-leg, *i.e.*, the final fermion line makes up the final p'-leg. Now, we could have also chosen X as the special vertex; then in

such case internal scalar would belong to the final p'-leg instead of initial p-leg. It can be shown [12], that the contribution of the diagrams, for which the photons would have ended on internal scalar lines *for a particular diagram* in a higher order would have differed by a finite renormalization; but while considering *all the sets of diagrams* of a particular order all those finite renormalization parts cancels among themselves and vanishes, providing us the same result corresponding to the choice of special vertex being V.

The tree level contribution for the process $\chi(q+q')\,f(p) \to \chi(q')\,f(p')$ would correspond to a matrix element,

$$i\,\mathcal{M}_0 = \left[\bar{u}(p')\Gamma_V u(q+q')\right] \left[iS^{t_V,t_X}_{p-q'}\right] \left[\bar{u}(q')\Gamma_X u(p)\right] . \tag{6.3}$$

Note, the presence of the scalar propagator even for the tree level diagram (producing an extra factor of 'i'). The Γ_V and Γ_X correspond to the vertex factors due to the Yukawa interactions respectively at interaction vertex V and X for this model. The explicit expressions for these vertices involving Majorana fermions can be used from Ref. [124,125], but we will never in our forthcoming discussions use any special explicit form of interaction vertices making the proof as general as possible.

We will start with an nth order diagram related to process $\chi(q+q')\,f(p) \to \chi(q')\,f(p')$, in which all the existing photons are virtual photons (without loss of any generality). This (virtual) n^{th} order diagram contributes a charge factor of 'e^{2n}' in the matrix element, and there are respectively *exactly u* and r number of (trilinear) vertices on the final (p') fermion and initial (p) fermion leg. The number of vertices on the internal scalar (which belong to p-leg) leg are equal to s. Now, as the scalar can have both the trilinear and seagull vertices, hence if all the vertices which are present on the scalar line are trilinear then $s = 2n - u - r$; and if all the vertices on the scalar leg is quadrilinear (seagull vertices or tadpole diagrams) then $s = (2n - u - r)/2$; and s has a value in between these extremes if there is an admixture of trilinear and quadrilinear vertices. Hence, the total number of vertices m of an nth order diagram where all the existing photons are virtual, is given by

$n \leq u + s + r = m \leq 2n$, where the lowest value corresponds to the case where there is no virtual photon insertion on fermion lines, and all the scalar insertion vertex being quadrilinear. The upper limit of m corresponds to the case when all the photon interaction vertices (whether on fermion or scalar) are trilinear.

In accordance with all the notations set up in the previous chapters, (without loss of any generality) the momenta of already existing photons on p'/p-leg are all outgoing/incoming and are denoted by l_i'/l_i. The momentum of fermion propagator to the *left* of the vertex number q on the final p' leg is given by $(p' + \Sigma_{i=1}^{q} l_i') \equiv p' + \Sigma_q$. And a similar fermionic propagator momentum to the *right* of vertex number j on the initial p leg is expressed as $(p + \Sigma_{i=1}^{j} l_i) \equiv p + \Sigma_j$. The momentum of the scalar propagator adjacent (immediately right) to the vertex X on the initial p-leg in Fig. 6.2 is given by $p - q' + \Sigma_r \equiv P$. Hence, the momentum of scalar propagator to the *right* of the vertex number g on the internal scalar line on initial p-leg is expressed as $(P + \Sigma_{i=1}^{g} l_i) \equiv P + \Sigma_g$; with $g = 1, \cdots, s$. The Lorentz indices related to the photon interaction vertices on final fermion p'-leg, initial scalar p-leg and initial fermion p-leg are respectively denoted by μ_i, α_i, ν_i (and this notation will be respected in all upcoming discussions).

After noting all the above notations, the matrix element of nth order diagram as in Fig. 6.2 related to process $\chi(q + q') f(p) \to \chi(q') f(p')$ having all trilinear photon vertices (generalization to a diagram containing arbitrary number of seagull diagrams is trivial as discussed in Chapter 5, and will be discussed here also in upcoming discussions) can be expressed at finite temperature as,

$$
\begin{aligned}
i\mathcal{M}_n = (e)^{2n}(-i)^m(-1)^{\Sigma_{i=1}^{m}(t_i+1)}(i)^{m+1} \times \\
\times \left[\bar{u}_{p'} \gamma_{\mu_1} F_{p'+\Sigma_1}^{t_1,t_2} \gamma_{\mu_2} F_{p'+\Sigma_2}^{t_2,t_3} \cdots \gamma_{\mu_u} F_{p'+\Sigma_u}^{t_u,t_V} \Gamma_V u_{q+q'} \right] \\
\times \left[S_{P+\Sigma_s}^{t_V,t_s} (2P + 2\Sigma_{s-1} + l_s)_{\alpha_s} S_{P+\Sigma_{s-1}}^{t_s,t_{s-1}} \cdots (2P + l_1)_{\alpha_1} S_P^{t_1,t_x} \right] \\
\times \left[\bar{u}_{q'} \Gamma_X F_{p+\Sigma_r}^{t_X,t_r} \gamma_{\nu_r} F_{p+\Sigma_{r-1}}^{t_r,t_{r-1}} \gamma_{\nu_{r-1}} \cdots F_{p+\Sigma_1}^{t_2,t_1} \gamma_{\nu_1} u_p \right] \times \mathcal{D}_{\{t_i\}}^{\mu_1,\cdots,\mu_s;\alpha_s,\cdots,\alpha_1;\nu_r,\cdots,\nu_1} .
\end{aligned} \quad (6.4)
$$

Comparing Eq. 6.4 with a similar expression for thermal scalar QED in Eq. 4.26 we find there is an extra factor of 'i' coming from propagators, due to the presence of an extra scalar propagator in the tree level diagram Eq. 6.3. The above Eq. 6.4 can be symbolically expressed as,

$$\mathcal{M}_n = (e)^{2n}(-1)^{\sum_{i=1}^m (t_i+1)} \times \left[C_u^{\text{fermion } p'}\right] \times \left[C_s^{\text{scalar } p}\right] \times \left[C_r^{\text{fermion } p}\right] \times \mathcal{D}_n ,$$
$$\equiv (e)^{2n}(-1)^{\sum_{i=1}^m (t_i+1)} \times \left[C_u^{\text{fermion } p'}\right] \times \left[C_{s+r}^p\right] \times \mathcal{D}_n , \qquad (6.5)$$

where we have to note that the definitions of $C_u^{\text{fermion } p'}$ and $C_r^{\text{fermion } p}$ referring to the contributions from fermionic part of p' and p leg are little bit different from the similar similar fermionic contributions in Eq. 4.8. Here, we have absorbed factors of $\Gamma_V u_{q+q'}$ / $\bar{u}_{q'}\Gamma_X$ in the expression of $C_u^{\text{fermion } p'}$ / $C_r^{\text{fermion } p}$. This is done to keep the notation simple and not to write each and every time the contribution of DM-scalar-fermion vertex and Majorana fermion spinor factors explicitly in upcoming discussion making the expression untidy. These factors being related to DM particle do not get modified (due to higher order photon insertions) in the higher orders, and merely get carried along as multiplicative factors (until when the final cross section has to be calculated, where sum or average over DM particle polarization sums may need to be performed). The contribution of the scalar initial p-leg is expressed as $C_s^{\text{scalar } p}$ where the scalar leg may or may not have exactly s numbers of dotted interaction vertices on the internal scalar line but always contributes exactly a charge factor of 'e^{2n-u-r}' to the matrix element, irrespective of number of vertices s present.

6.3   Virtual K photon insertion

We will start by inspecting the effect of insertion of an additional K photon in all possible ways to the nth order diagram related to process $\chi(q + q') f(p) \to \chi(q') f(p')$. The new insertion can rise in distinctively three ways. Before venturing into the full fledged cal-

culation for each case, we just list down and summarize the basic technicalities related to each case here.

Insertion of virtual K photon in between final p' and initial p-leg : The insertion of the μ vertex end of the virtual K photon on the final fermionic p'-leg in all possible ways, is analogous to the case of similar insertion for thermal fermionic QED, thus producing a similar result. For each particular insertion of the μ vertex, the other end ν vertex of the virtual K photon has to be inserted in all possible ways to the initial p-leg. As the initial leg now comprises of both the initial fermionic p-leg and internal scalar p-leg, thus there are two distinct class of categories of diagrams, where the ν vertex end of photon is inserted either on fermionic p-leg or internal scalar p-leg.

Due to off-shellness of the internal scalar p-leg, all the contributions of ν vertex insertion on scalar line now will finally reduce to two terms after internal term by term cancellations. One of these terms will then cancel against the total result (a single term) coming from all the contributions of ν vertex insertion on initial fermionic p-leg. Hence there is an observation of non-trivial so called 'double-cancellation' for the contribution from ν vertex insertion on initial p-leg irrespective of the explicit nature of vertex factor Γ_X. The final matrix element will be proportional to lower order matrix element with the K photon contributions factored out.

Both the ends of virtual K photon insertion are on final fermionic p'-leg : This particular case when both the ends of the virtual K photon are on the final fermionic p'-leg is exactly analogous to the case of similar insertion for the thermal fermionic QED case as the initial p-leg does not play any role here. Hence, the result of this case can be evaluated trivially.

Both the ends of virtual K photon insertion are on initial p-leg : This case with both ends of virtual K photon insertion are on the p-leg is the most difficult one, as both initial fermion leg and internal scalar line belong to p-leg in addition to the possibility of tadpole contributions for scalar leg. This case can be categorized into three classes; both the new

virtual K photon ends being on scalar p-leg, both of the virtual photon ends being on fermionic p-leg , and each of the ends being shared between scalar p and fermionic p-leg.

As internal scalar line is involved for both the insertion being on initial p-leg, the numbers of concerned diagrams proliferate immensely for this case. For organizational purposes and to easily track the nature of GY reduction, cancellation of terms and factorization we will group the set of diagrams into sets of diagrams (set I, II, III, IV) as shown in Fig. 6.8 for insertions being solely on scalar leg. We will see complicated cancellation of contributions among the groups, which will be discussed in detail later. The remnant sets of terms from this contribution will cancel against set of terms resulting from initial p leg photon insertions between scalar-fermion legs in an even more non-trivial way irrespective of vertex factor Γ_X, again implying a non-trivial 'double-cancellation'. We will enlighten more about the nature of cancellations in detail in discussions to follow.

As there are possibilities of having one/both the μ and ν vertex insertions on the internal scalar p-leg, hence there are possibilities that the new insertion vertex could turn out be a trilinear one or a seagull one. We will again group the appropriate adjacent trilinear and seagull insertions accordingly to define circled vertices. There will be circled vertices related to one/both of μ and ν insertions. The notations of circled vertices are in accordance with all the previously mentioned chapters (as described in the paragraph below Eq. 4.35) As we will use these expressions of circled vertices on many occasions in upcoming discussions, we will list down the contributions of them here for once and all. The contribution of the circled $_q\mu$ vertex on internal scalar p-leg has an expression,

$$
\begin{aligned}
k_\mu\, C_{s+1}^{\text{scalar }p\,,\,q\,\mu} = {} & (-1)^{(t_\mu+1)}\, S_{P+\Sigma_s}^{t_\nu,t_s}\,(2P+2\Sigma_{s-1}+l_s)_{\alpha_s}\cdots S_{P+\Sigma_{q+1}}^{t_{q+2},t_{q+1}}\,(2P+2\Sigma_q+l_{q+1})_{\alpha_{q+1}} \\
& \times \left[\delta_{t_\mu,t_q}\, S_{P+\Sigma_q}^{t_{q+1},t_q}\,(2P+2\Sigma_{q-1}+l_q)_{\alpha_q} - \delta_{t_\mu,t_{q+1}}\, S_{P+\Sigma_q+k}^{t_{q+1},t_q}\,(2P+2\Sigma_{q-1}+2k+l_q)_{\alpha_q} \right] \\
& \times S_{P+\Sigma_{q-1}+k}^{t_q,t_{q-1}}\,(2P+2\Sigma_{q-2}+2k+l_{q-1})_{\alpha_{q-1}}\cdots, \\
\equiv {} & M_q - M_{q+1}\,, \hspace{4cm} (6.6)
\end{aligned}
$$

where we have used 'Generalized Feynman Identities' Appendix B to obtain the GY reduction resulting in the final expression in Eq. 6.6. We will make note here, that we will always use M_i to denote the contributions from internal scalar leg due to circled μ insertions in following discussions. The ellipses in above expression Eq. 6.6 include the rest of the scalar p-leg contributions which may have k (new photon momentum) dependent terms, depending on the exact location of ν vertex insertion down the p-leg (as according to our notation vertex ν is always placed to the left of μ insertion to avoid double counting, making the new photon momentum k flow through all the propagators which are in between vertices ν and μ). A similar expression can be written for the circled ν vertex insertion on the scalar p-leg, which can be expressed as,

$$
\begin{aligned}
k_\nu C_{s+1}^{\text{scalar } p, \nu_j} = (-1)^{(t_\nu + 1)} \; \cdots \; S_{P+\Sigma_j+k}^{t_{j+1}, t_j} \times & \\
\left[\delta_{t_\nu, t_j} \left(2P + 2\Sigma_{j-1} + l_j\right)_{\alpha_j} S_{P+\Sigma_{j-1}}^{t_j, t_{j-1}} - \delta_{t_\nu, t_{j-1}} \left(2P + 2\Sigma_{j-1} + 2k + l_j\right)_{\alpha_j} S_{P+\Sigma_{j-1}+k}^{t_j, t_{j-1}} \right] \times & \\
\left(2P + 2\Sigma_{j-2} + l_{j-1}\right)_{\alpha_{j-1}} \cdots \left(2P + l_1\right)_{\alpha_1} S_P^{t_1, t_X} , & \\
\equiv N_j - N_{j-1} . & \quad (6.7)
\end{aligned}
$$

Here, in the above expression we note that there is an extra $S_P^{t_1, t_X}$ factor with respect to a similar circled vertex contribution specified on Eq. 4.35, arising as the internal scalar line on p-leg is off-shell (a similar off-shell propagator contribution is also inside the ellipses of Eq. 6.6 and has not been shown explicitly). The notation N_i will always be used to denote the contributions from internal scalar leg due to circled ν vertex insertions in all following discussions. It is also to be noted that, in Eq. 6.6 and Eq. 6.7 the subscripts of M and N terms explicitly refer to the thermal type of vertices after GY reduction captured by the delta function terms in the explicit individual contributions faithfully. In the Eq. 6.7 the ellipses refer to the scalar contribution of the p leg from special vertex V to vertex number $(j+1)$ on scalar leg. This term with ellipses may have k dependence, depending on the exact location of μ vertex. We would also like to mention that, as the vertex X is on the initial p-leg; hence sometimes if needed, the vertex X may be referred to as vertex

number 0 (zero) for discussions involving internal scalar p-leg; and also sometimes can be referred to as vertex number $(r+1)$ for the discussions involving initial fermionic p-leg.

6.4 Virtual K photon insertion between initial p and final p'-leg

We now add a virtual photon in all possible ways to the nth order diagram related to process $\chi(q+q')f(p) \to \chi(q')f(p')$. The corresponding matrix element after using the Eq. 6.5 can be symbolically expressed as,

$$
\mathcal{M}_{n+1}^{p',p} = (e)^{2n+2}(-i)^{m+2}(-1)^{\Sigma_{i=1}^{m}(t_i+1)}(-1)^{(t_\mu+1)}(-1)^{(t_\nu+1)}(i)^{m+2}\times
$$
$$
\left[C_{u+1}^{\text{fermion } p';\mu}\right] \times \left[C_{s+r+1}^{p;\nu}\right] \times \mathcal{D}_{n+1}^{\mu\nu} . \tag{6.8}
$$

In the above expression, μ vertex is inserted on the final p'-leg, and ν vertex is inserted on the initial p-leg. The contribution $C_{u+1}^{\text{fermion } p';\mu}$ from p'-leg being due to fermion line has now (after new photon insertion) exactly $(u+1)$ number of vertices. The same cannot be said about the contribution $C_{s+r+1}^{p;\nu}$ due to the initial p-leg. This contribution may or may not correspomd to having one more number of vertex with respect to C_{s+r}^{p}. If the new ν vertex is on initial fermion line or on scalar line but is a trilinear insertion then the number of vertices will increase by a additive factor of one. If the new vertex is on scalar p-leg and is a seagull vertex then the number of vertices on initial p-leg will remain unchanged. In any case, $C_{s+r+1}^{p;\nu}$ will contribute an additional multiplicative charge factor 'e' to the matrix element than the contribution C_{s+r}^{p}, and hence the notation.

Now, using the definition of the virtual K photon at finite temperature Eq. 4.3, the corre-

sponding K photon contribution related to the matrix element can be expressed as,

$$\mathcal{M}_{n+1}^{K\gamma,\, p',p} = (e)^{2n+2}(-1)^{\sum_{i=1}^{m}(t_i+1)}(-1)^{(t_\mu+1)}(-1)^{(t_\nu+1)}\times$$

$$\int \frac{\mathrm{d}^4 k}{(2\pi)^4} \left[k_\mu\, C_{u+1}^{\text{fermion } p';\mu} \right] \times \left[k_\nu\, C_{s+r+1}^{p;\nu} \right] \times \left[-ib_k(p',p)\, D^{t_\mu,t_\nu} \right] \times \mathcal{D}_n \, . \quad (6.9)$$

From Eq. 6.9 we observe that the contribution of the p and p'-leg due to K photon insertion can be evaluated independently of each other. We will compute these contributions in detail in the following sections.

6.4.1   Insertion of vertex μ on final fermionic p'-leg

The insertion of the μ vertex to the fermionic final p'-leg is analogous to the similar thermal fermionic QED insertions. A particular contribution when new insertion vertex μ is inserted to the right of already existing vertex q on final p'-leg can be expressed as,

$$k_\mu\, C_{u+1}^{\text{fermion } p';\mu \text{ to right of } q} = \bar{u}_{p'} \gamma_{\mu_1} F_{p'+\Sigma_1}^{t_1,t_2} \cdots \gamma_{\mu_{q-1}} \left[F_{p'+\Sigma_{q-1}}^{t_{q-1},t_\mu} \, \slashed{k}\, F_{p'+\Sigma_{q-1}+k}^{t_\mu,t_q} \right] \gamma_{\mu_q} \cdots$$

$$\times F_{p'+\Sigma_{s-1}+k}^{t_{s-1},t_s} \gamma_{\mu_s} F_{p'+\Sigma_s+k}^{t_s,t_V} \Gamma_V\, u_{q+q'} \, . \quad (6.10)$$

The above expression has quite a bit similarity with the expression of Eq. 4.15. After using the generalized Feynman's identity and after a pairwise cancellation of terms all the contributions due to μ vertex insertions in all possible ways on p'-leg reduces to,

$$k_\mu\, C_{u+1}^{\text{fermion } p';\mu} = (-1)^{(t_\mu+1)} \delta_{t_\mu,t_V} \left[\bar{u}_{p'} \gamma_{\mu_1} \cdots \gamma_{\mu_{q-1}} F_{p'+\Sigma_{q-1}}^{t_{q-1},t_q} \cdots (\text{no } k) \cdots F_{p'+\Sigma_s}^{t_s,t_V} \Gamma_V\, u_{q+q'} \right] \, ,$$

$$= (-1)^{(t_\mu+1)} \delta_{t_\mu,t_V}\, C_u^{\text{fermion } p'} \, , \quad (6.11)$$

which is an exact analogue of Eq. 4.18. The higher order contribution due to K photon insertion $k_\mu\, C_{u+1}^{\text{fermion } p';\mu}$ turns out to be proportional to lower order contribution of p'-leg $C_u^{\text{fermion } p'}$ times some multiplicative factors which arose as a result of GY reduction.

6.4.2 Insertion of vertex ν on initial p-leg

The insertion of the new ν vertex on the initial p-leg can arise in two distinct ways. The first way is when ν vertex is inserted on the scalar part of the initial p-leg, and in the second way the new ν vertex is inserted on initial fermionic part of the p-leg. Hence the corresponding K photon contribution related to p-leg can be put together symbolically as,

$$k_\nu C_{s+r+1}^{p;\nu} = \left[k_\nu C_{s+1}^{\text{scalar } p ;\nu} \right] \times \widetilde{C}_r^{\text{fermion } p} + \widetilde{C}_s^{\text{scalar } p} \times \left[k_\nu C_{r+1}^{\text{fermion } p;\nu} \right],$$

$$\equiv k_\nu C_{s+r+1}^{\text{scalar};\nu} + k_\nu C_{s+r+1}^{\text{fermion};\nu} . \tag{6.12}$$

In the above expression, $k_\nu C_{s+1}^{\text{scalar } p ;\nu}$ and $k_\nu C_{r+1}^{\text{fermion } p;\nu}$ respectively denote the contribution of K photon insertion *only* due to ν vertex insertion being on scalar and fermionic part of p-leg. The contributions $\widetilde{C}_r^{\text{fermion } p}$ and $\widetilde{C}_s^{\text{scalar } p}$ respectively denote the remnant part of the fermionic and scalar contribution respectively. As the momentum k of the new K photon flows through all the propagators which are in between ν and μ vertices; hence the momentum k does not flow through any initial fermionic line on p-leg if the ν insertion is on the initial scalar p-leg, *i.e.*,

$$\widetilde{C}_r^{\text{fermion } p} = C_r^{\text{fermion } p} . \tag{6.13}$$

But, when the new ν insertion is on the initial fermionic leg then the photon momentum k flows through all the internal scalar p-leg lines, shifting the momentum flowing through them by a factor k, so their contribution is changed as,

$$\widetilde{C}_s^{\text{scalar } p} = C_s^{\text{scalar } p} (P_i \to P_i + k) . \tag{6.14}$$

Here from Eq. 6.12 we want to again mention that, although the contributing diagrams of $k_\nu C_{r+1}^{\text{fermion } p;\nu}$ have all $(r + 1)$ number of vertices the contributing diagrams to $k_\nu C_{s+1}^{\text{scalar } p ;\nu}$ *may not always* have $(s + 1)$ number of vertices. There are certainly some contributing

diagrams where all the photon interaction vertices are trilinear, which have exactly $(s+1)$ numbers of dotted vertices (on schematic diagram); but this is not generically true for other contributing diagrams which have seagull interaction vertices. But, what is *always true* is that $k_\nu C_{s+1}^{\text{scalar } p\,;\nu}$ has one extra contributing electron charge factor 'e' than the lower order contribution $C_s^{\text{scalar } p}$. We have already discussed in the paragraph just below Eq. 6.5 that the $C_s^{\text{scalar } p}$ contributes a charge factor of e^{2n-u-r}; hence $k_\nu C_{s+1}^{\text{scalar } p\,;\nu}$ or more specifically $C_{s+1}^{\text{scalar } p\,;\nu}$ will contribute a charge factor $e^{2n-u-r+1}$ [2]. The contribution $k_\nu C_{s+r+1}^{\text{fermion};\nu}$ in Eq. 6.12 suggest that the ν vertex has been inserted on the fermionic part of the p-leg (suggesred by $s+r+1$ in subscript), and a similar notation should be understood for $k_\nu C_{s+r+1}^{\text{scalar};\nu}$. As it is obvious from Eq. 6.12, $k_\nu C_{s+1}^{\text{scalar } p\,;\nu}$ and $k_\nu C_{r+1}^{\text{fermion } p;\nu}$ can be evaluated independently of each other, hence we will continue to do so in following discussions.

6.4.3 Insertion of vertex ν on internal scalar p-leg

The ν vertex insertion on the internal scalar p-leg can arise either due to new trilinear or seagull vertices. The appropriate trilinear and seagull vertices can be grouped together to form s number of circled vertices ($j = 1, 2, ... s$) along-with an unpaired trilinear insertion where ν vertex is to left of V (for each fixed choice of vertex μ) and are shown in Fig. 6.3.
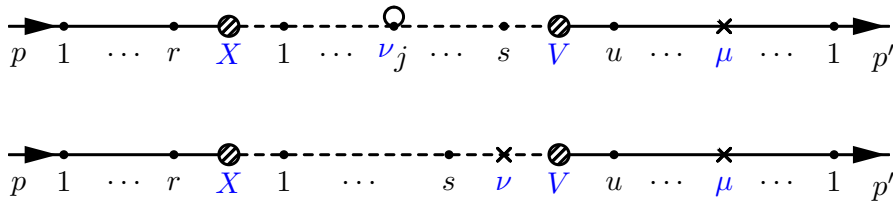

Figure 6.3: *Diagrams contributing to K photon insertion with ν insertion vertex being on the internal scalar p-leg, for each fixed choice of μ vertex insertion (on p'-leg). There are s number of circled vertex diagrams for $j = 1, 2, \cdots, s$ represented in first diagram, and a trinilear insertion diagram in second figure, where ν is situated immediately left to V.*

---

[2]The charge factor can also be derived separately using the fact that, $C_{s+1}^{\text{scalar } p\,;\nu}$ contributes to $(n+1)^{\text{th}}$ order matrix element, and the fermion contributions to charge factors are exactly proportional to the number of trilinear vertices. Hence, the charge factor associated with $C_{s+1}^{\text{scalar } p\,;\nu}$ is $e^{2(n+1)-(u+1)-r} = e^{2n-u-r+1}$ which is another way of getting same charge factor.

The contributions of Fig. 6.3 can be symbolically expressed as,

$$k_\nu C_{s+1}^{p;\nu} = \left[\sum_{j=1}^{s} k_\nu C_{s+1}^{\text{scalar } p \,;\, \nu_j} \right] + k_\nu C_{s+1}^{\text{scalar } p \,;\, \nu \text{ left of } V} . \tag{6.15}$$

A typical contribution of circled ν_j insertion has already been specified in Eq. 6.7. Making use of this equation for all the choices of circled vertices $j = 1, 2, \cdots, s$ and then summing up all those contributions, we can express the squared bracketed term of Eq. 6.15 as,

$$\sum_{j=1}^{s} k_\nu C_{s+1}^{\text{scalar } p \,;\, \nu_j} = (N_1 - N_0) + (N_2 - N_1) + \cdots + (N_s - N_{s-1}) ,$$

$$= N_s - N_0 . \tag{6.16}$$

Here, we have to note that the N_0 term only survives as the internal scalar line is off-shell. The N_0 would have vanished if the scalar line would have been on-shell. We will discuss more about the origin of this term in the paragraph below Eq. 6.18.

The additional single diagram coming from the trilinear insertion on the vertex immediately left of vertex V can be expressed as,

$$k_\nu C_{s+1}^{\text{scalar } p \,;\, \nu \text{ left of } V} = (-1)^{(t_\nu + 1)} \left[S_{P+\Sigma_s+k}^{t_\nu, t_\nu} (2P + 2\Sigma_s + k) \cdot k \, S_{P+\Sigma_s}^{t_\nu, t_s} \right] (2P + 2\Sigma_{s-1} + l_s)_{\alpha_s} \cdots$$

$$(2P + l_1)_{\alpha_1} \, S_P^{t_1, t_X} ,$$

$$= (-1)^{(t_\nu + 1)} \left[\delta_{t_\nu, t_\nu} S_{P+\Sigma_s}^{t_\nu, t_s} - \delta_{t_\nu, t_s} S_{P+\Sigma_s+k}^{t_\nu, t_s} \right] (2P + 2\Sigma_{s-1} + l_s)_{\alpha_s} \cdots$$

$$(2P + l_1)_{\alpha_1} \, S_P^{t_1, t_X} ,$$

$$\equiv N_{s+1} - N_s , \tag{6.17}$$

after using the generalized Feynman's Identity Appendix B. The total contribution due to all the ν vertices insertion on the internal scalar p-leg then can be expressed as (using

results of Eq. 6.16 and Eq. 6.17 and plugging back in Eq. 6.15),

$$k_\nu C_{s+1}^{\text{scalar } p\,;\nu} = N_{s+1} - N_0 \,,$$

$$= (-1)^{(t_\nu+1)} \left[\delta_{t_\nu,t_V} S_{P+\Sigma_s}^{t_V,t_s} \cdots S_{P+\Sigma_1}^{t_2,t_1} (2P + l_1)_{\alpha_1} S_P^{t_1,t_X} \right.$$

$$\left. - \delta_{t_\nu,t_X} S_{P+\Sigma_s+k}^{t_V,t_s} \cdots (2P + 2k + l_1)_{\alpha_1} S_{P+k}^{t_1,t_X} \right] \,. \qquad (6.18)$$

In the above expression the N_0 term proportional to δ_{t_ν,t_X} is only present as the internal scalar line being off-shell, and would have vanished if scalar line were to be on-shell. The origin of this term is from the ν_1 circled insertion. The circled ν_1 insertion consist of a trilinear sub-contribution,

$$k_\nu C_{s+1}^{\text{scalar } p\,;\nu \text{ to the left of } 1} = \cdots (2P + 2\Sigma_1 + 2k + l_2)_{\alpha_2} S_{P+k+\Sigma_1}^{t_2,t_1} (2P + 2k + l_1)_{\alpha_1} \left[S_{P+k}^{t_1,t_\nu} (2P+k) \cdot k \, S_P^{t_\nu,t_X} \right] \,,$$

$$\qquad (6.19)$$

where the square bracketed term in Eq. 6.19 has been simplified using the generalized Feynman's Identity where the $(2P + k) \cdot k$ term is manipulated as,

$$(2P + k) \cdot k = \left[(P + k)^2 - m_\phi^2 \right] - \left[P^2 - m_\phi^2 \right] \,. \qquad (6.20)$$

Eq. 6.20 is used to simplify the squared bracketed term of Eq. 6.19 as in expression below,

$$\left[S_{P+k}^{t_1,t_\nu} (2P + k) \cdot k \, S_P^{t_\nu,t_X} \right] = (-1)^{(t_\nu+1)} \left[\delta_{t_\nu,t_1} S_P^{t_1,t_X} - \delta_{t_\nu,t_X} S_{P+k}^{t_1,t_X} \right] \,. \qquad (6.21)$$

In Eq. 6.21 the last term proportional to δ_{t_ν,t_X} arises *only because* the internal scalar p-leg is off-shell. If the scalar leg were on-shell, then $\left[P^2 - m_\phi^2 \right] = 0$ in Eq. 6.20 making the term proportional to δ_{t_ν,t_X} vanish. As the scalar line is off-shell hence the Eq. 6.19 can be

simplified as,

$$k_\nu C^{\text{scalar } p \,;\, \nu \text{ to the left of } 1}_{s+1} = (-1)^{(t_\nu + 1)} \cdots (2P + 2\Sigma_1 + 2k + l_2)_{\alpha_2} S^{t_2,t_1}_{P+k+\Sigma_1} (2P + 2k + l_1)_{\alpha_1}$$

$$\times \left[\delta_{t_\nu, t_1} S^{t_1, t_X}_{P} - \delta_{t_\nu, t_X} S^{t_1, t_X}_{P+k} \right] , \tag{6.22}$$

where the last term proportional to δ_{t_ν, t_X} is N_0 in Eq. 6.18. The circled vertex ν_1 would also have one seagull sub-contribution expressed as,

$$k_\nu C^{\text{scalar } p \,;\, \nu \text{ at } 1}_{s+1} = (-1)^{(t_\nu + 1)} \cdots (2P + 2\Sigma_1 + 2k + l_2)_{\alpha_2} S^{t_2,t_1}_{P+k+\Sigma_1} \left[\delta_{t_\nu, t_1} (-2k)_{\alpha_1} S^{t_1, t_X}_{P} \right] . \tag{6.23}$$

This term will only cancel an additive $(2k)_{\alpha_1}$ from Eq. 6.22 producing the term N_1. And N_1 has anyway canceled in pairwise cancellation in Eq. 6.16 when all the circled vertices contributions are summed up.

Therefore, the main difference to note here is that, the contribution $k_\nu C^{\text{scalar } p \,;\, \nu}_{s+1}$ turns out to be difference of two terms as in Eq. 6.18; which is in contrast to a similar contribution for scalar QED regarding p-leg insertions (see Eq. 5.11), resulting only a single term proportional to the lower order contribution. Here, in Eq. 6.18 the other extra term proportional to δ_{t_ν, t_X} *only* arises as the internal scalar p-leg is off-shell.

As for the ν insertion being on the internal scalar line, the additional photon momenta k does not flow through the fermionic propagators of initial fermionic p-leg. Therefore the contribution of the initial fermionic p-leg is unchanged and is expressed as,

$$\widetilde{C}^{\text{fermion } p}_r = C^{\text{fermion } p}_r . \tag{6.24}$$

Therefore, with the help of Eq. 6.18 and Eq. 6.24 the total contribution of adding ν vertex

in all possible ways to the internal initial scalar p-leg can be expressed as,

$$
\begin{aligned}
k_\nu C^{\text{scalar};\nu}_{s+r+1} &= \left[k_\nu \, C^{\text{scalar};\nu}_{s+1} \right] \times \widetilde{C}^{\text{fermion } p}_r \, , \\
&= \left[N_{s+1} - N_0 \right] C^{\text{fermion } p}_r \, , \\
&= (-1)^{(t_\nu+1)} \Big[\delta_{t_\nu,t_V} S^{t_V,t_s}_{P+\Sigma_s} \cdots S^{t_2,t_1}_{P+\Sigma_1} (2P + l_1)_{\alpha_1} \, S^{t_1,t_X}_P \\
&\qquad - \delta_{t_\nu,t_X} S^{t_V,t_s}_{P+\Sigma_s+k} \cdots (2P + 2k + l_1)_{\alpha_1} \, S^{t_1,t_X}_{P+k} \Big] \\
&\qquad \times \left\{ \bar{u}_{q'} \Gamma_X F^{t_X,t_r}_{p+\Sigma_r} \gamma_{\nu_r} \cdots (\text{no } k) \, u_p \right\} \, , \tag{6.25}
\end{aligned}
$$

where "no k" refers to the fact that the terms represented by the ellipses are independent of k.

6.4.4 Insertion of vertex ν on initial fermionic p-leg

The insertion of the ν vertex to the initial fermionic p-leg is similar to the analogous fermionic QED case for photon insertions on p-leg. For each particular choice of μ vertex insertion on the final fermionic p'-leg, the ν vertex can be inserted in $(r+1)$ possible ways (generating trilinear vertices) to the initial fermionic p-leg. A typical diagram among the set of $(r+1)$ diagrams has been shown schematically in Fig. 6.4 (where ν corresponds to the newly inserted trilinear photon vertex on fermionic p-leg).
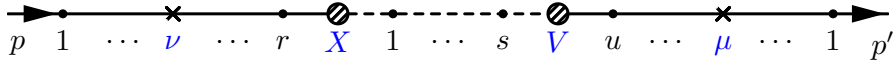

Figure 6.4: *A typical diagram among a set of $(r+1)$ diagrams, contributing to K photon insertion with ν insertion vertex being on the initial fermionic p-leg, for each fixed choice of μ vertex insertion (on p'-leg). We note here that the photon momentum k of newly inserted photon now flows through the entire internal scalar line.*

After applying generalized Feynman's Identities and summing up all the $(r+1)$ sub-contributions, there are again pairwise cancellation of terms between the sub-contributions.

This cancellation provides us with the final expression related to v insertion on initial p-leg, being proportional to a single term which arises from a remnant contribution (after pairwise cancellation), where the new v trilinear vertex is inserted immediately to the left of vertex X. The final total contribution of initial fermion leg can be expressed as in Eq. 6.26 below,

$$
\begin{aligned}
k_v C_{r+1}^{\text{fermion } p;v} &= (-1)^{(t_v+1)} \delta_{t_v,t_X} \bar{u}_{q'} \Gamma_X F_{p+\sum_r}^{t_X,t_r} \gamma_{v_r} \cdots (\text{no } k)\, u_p \\
&= (-1)^{(t_v+1)} \delta_{t_v,t_X} \times \left[C_r^{\text{fermion } p} \right],
\end{aligned}
\tag{6.26}
$$

where the '(no k)' bracketed expression suggest that there is not any k dependence in the above expression. The Eq. 6.26 is an exact analogue of Eq. 4.20, as the higher order contribution due to K photon insertion $k_v C_{r+1}^{\text{fermion } p;v}$ on initial fermionic p-leg becomes proportional to lower order contribution $C_r^{\text{fermion } p}$ times some multiplicative factors which arose as a result of GY reduction.

From Fig. 6.4 it is evident that the photon momentum now flows through the entire internal scalar p leg. Hence, the scalar lines will get this additive photon momentum factor k to their existing momenta, and the whole contribution will get modified as,

$$
\widetilde{C}_s^{\text{scalar } p} = C_s^{\text{scalar } p} \left(P_i \to P_i + k \right).
\tag{6.27}
$$

Using the results of Eq. 6.26 and Eq. 6.27 the total contribution for the v vertex insertion on the fermionic line can be expressed as,

$$
\begin{aligned}
k_v C_{s+r+1}^{\text{fermion};v} &= \widetilde{C}_s^{\text{scalar } p} \times \left[k_v C_{r+1}^{\text{fermion } p;v} \right], \\
&= (-1)^{(t_v+1)} \left[S_{P+\sum_s+k}^{t_V,t_s} \cdots (2P + 2k + l_1)_{\alpha_1} S_{P+k}^{t_1,t_X} \right] \times \\
&\quad \left\{ \bar{u}_{q'} \Gamma_X F_{p+\sum_r}^{t_X,t_r} \delta_{t_v,t_X} \gamma_{v_r} \cdots (\text{no } k)\, u_p \right\},
\end{aligned}
\tag{6.28}
$$

with the first term in square brackets containing k dependence both from the vertex factors

and the propagator terms.

6.4.5 The total contribution of ν vertex insertion on initial p-leg

Using the results of Eq. 6.25 and Eq. 6.28 and plugging those back in Eq. 6.12, the total contribution of the ν vertex insertion on the initial p-leg can be written down as,

$$
\begin{aligned}
k_\nu C^{p;\nu}_{s+r+1} &= k_\nu \left\{ C^{\text{scalar};\nu}_{s+r+1} \right\} + k_\nu \left\{ C^{\text{fermion};\nu}_{s+r+1} \right\} , \\
&= (-1)^{(t_\nu+1)} \left\{ \left[\delta_{t_\nu,t_V} S^{t_V,t_s}_{P+\Sigma_s} \cdots S^{t_2,t_1}_{P+\Sigma_1} (2P+l_1)_{\alpha_1} S^{t_1,t_X}_P \right. \right. \\
&\quad - \left. \delta_{t_\nu,t_X} S^{t_V,t_s}_{P+\Sigma_s+k} \cdots (2P+2k+l_1)_{\alpha_1} S^{t_1,t_X}_{P+k} \right] \times \left[\bar{u}_{q'} \Gamma_X F^{t_X,t_r}_{p+\Sigma_r} \gamma_{\nu_r} \cdots u_p \right] \Big\} \\
&\quad + (-1)^{(t_\nu+1)} \left\{ \left[S^{t_V,t_s}_{P+\Sigma_s+k} \cdots (2P+2k+l_1)_{\alpha_1} S^{t_1,t_X}_{P+k} \right] \times \right. \\
&\quad \left. \left[\bar{u}_{q'} \Gamma_X F^{t_X,t_r}_{p+\Sigma_r} \delta_{t_\nu,t_X} \gamma_{\nu_r} \cdots (\text{no } k) \, u_p \right] \right\} , \\
&= (-1)^{(t_\nu+1)} \left[\delta_{t_\nu,t_V} S^{t_V,t_s}_{P+\Sigma_s} \cdots S^{t_2,t_1}_{P+\Sigma_1} (2P+l_1)_{\alpha_1} S^{t_1,t_X}_P \right] \times \left\{ \bar{u}_{q'} \Gamma_X F^{t_X,t_r}_{p+\Sigma_r} \gamma_{\nu_r} \cdots u_p \right\} .
\end{aligned}
$$
$$(6.29)$$

In the above expression we find that the contribution $k_\nu \left\{ C^{\text{fermion};\nu}_{s+r+1} \right\}$ cancels exactly against a similar and opposite sub-contribution proportional to δ_{t_ν,t_X} from $k_\nu \left\{ C^{\text{scalar};\nu}_{s+r+1} \right\}$ term. The final contribution is again proportional to the lower order contribution coming from p-leg. The interpretation of this cancellation is non-trivial and we will discuss about the nature of the cancellation in more detail in following paragraph.

Nature of the double-cancellation for K photon insertion between p' and p-leg

☞ We have observed a double-cancellation in Eq. 6.29. To appreciate the cancellation, we note that all the possible ways of ν vertex insertions on the initial scalar p-leg result in a pairwise cancellation among the sub-contributions, finally producing two remnant terms which are respectively proportional to δ_{t_ν,t_V} and δ_{t_ν,t_X}. These delta functions respectively result from the remnant terms of the sub-contributions, from ν vertex being inserted on

141

scalar p-leg immediately to the left of V and to the right of X on scalar leg.

All the possible ways of v vertex insertions on the initial fermionic p-leg result in a pair-wise cancellation among the sub-contributions, leaving only a single term proportional δ_{t_v,t_X}. This final contribution for fermionic insertions results from a remnant term of sub-contribution, where v is inserted to the immediate left of the vertex X on fermion line.

Therefore, the full contribution of fermion line (corresponding to remnant term from sub-contribution *left of* vertex X) *exactly* cancels against one of the contributing terms of scalar insertions (corresponding to remnant term from sub-contribution *right of* vertex X). The final total contribution of p-leg therefore, becomes proportional to lower order contribution with multiplicative δ_{t_v,t_v} factor (which resulted from GY reduction). We have to appreciate here that we have obtained a double-cancellation; the sets of scalar insertions themselves, and the same is true for fermionic insertions. The remnant scalar (one of the two remaining terms) and fermionic contributions then cancel against each other *independent of the explicit form of* Γ_X. As we will find in upcoming discussions, without obtaining this kind of a double-cancellation, the proof of IR factorization and resummation for K photon contributions would have been impossible.

☞ The factor Γ_X (Γ_V) is present in all of the sub-contributions representing the relevant factor corresponding to χ-ϕ-f interaction vertex. One may expect the explicit structure of the Γ_X to play a crucial role in the calculation. But, unexpectedly the nature of the cancellation does not depend on the explicit structure of the Γ_X (as we have never used any explicit structure of Γ_X (Γ_V) in above calculation). Therefore the nature of cancellation is generic and is 'blind' to the explicit structure of Γ_X. For example ϕ could have represented a pseudo-scalar field in place of a scalar one; or there could have been explicitly a pseudo-scalar (γ_5) term in addition to CP even terms; or rather there could have been other additional neutral fields at the interaction vertices in some models of non-renormalizable effective theory. The point we want to stress here is that the nature of cancellation is quite generic and is independent of explicit structure of the Γ_X (Γ_V) interaction vertex factors.

6.4.6 Final matrix element for K photon insertion between initial p and final p'-leg

Using the results of Eq. 6.29 and Eq. 6.11 and plugging them back in Eq. 6.9, the final matrix element for the total contribution of inserting virtual K photon turns out to be,

$$
\mathcal{M}_{n+1}^{K\gamma,\,p',p} = (e)^{2n+2}(-i)^{m+2}(-1)^{\sum_{i=1}^{m}(t_i+1)}(-1)^{(t_\mu+1)}(-1)^{(t_\nu+1)}(i)^{m+2} \times \int \frac{\mathrm{d}^4 k}{(2\pi)^4}
$$
$$
b_k(p',p)\left[k_\mu\, C_{u+1}^{\text{fermion }p';\mu}\right] \times \left[k_\nu\, C_{s+r+1}^{p;\nu}\right] \times \left[-iD^{t_\mu,t_\nu}\right] \times \mathcal{D}_n\;,
$$
$$
= (e)^{2n+2}(-1)^{\sum_{i=1}^{m}(t_i+1)}(-1)^{(t_\mu+1)}(-1)^{(t_\nu+1)}\times
$$
$$
\int \frac{\mathrm{d}^4 k}{(2\pi)^4}\, b_k(p',p)\left[(-1)^{(t_\mu+1)}\left\{\bar{u}_{p'}\gamma_{\mu_1}F_{p'+\Sigma_1}^{t_1,t_2}\cdots(\text{no }k)\cdots F_{p'+\Sigma_s}^{t_s,t_V}\,\delta_{t_\mu,t_V}\,\Gamma_V\,u_{q+q'}\right\}\right]
$$
$$
\times \left[(-1)^{(t_\nu+1)}\left\{\delta_{t_\nu,t_V}S_{P+\Sigma_s}^{t_V,t_s}\cdots S_{P+\Sigma_1}^{t_2,t_1}(2P+l_1)_{\alpha_1}S_P^{t_1,t_X}\right\}\times\right.
$$
$$
\left.\left\{\bar{u}_{q'}\Gamma_X F_{p+\Sigma_r}^{t_X,t_r}\gamma_{\nu_r}\cdots(\text{no }k)\,u_p\right\}\right]\times\left[-iD^{t_\mu,t_\nu}\right]\times\mathcal{D}_n\;,
$$
$$
\implies \mathcal{M}_{n+1}^{K\gamma,\,p',p} = -ie^2\int \frac{\mathrm{d}^4 k}{(2\pi)^4}\, b_k(p',p)\left[\delta_{t_\mu,t_V}\,\delta_{t_\nu,t_V}\right]D^{t_\mu,t_\nu}(k)\times\mathcal{M}_n\;. \tag{6.30}
$$

Here, the higher order matrix element turns out to be proportional to the lower order matrix element (after comparing with Eq. 6.4) with all the contributions of the K photon insertions factored out. The delta functions are obtained as a result of GY reduction. We would like to mention here that, as the DM particles are physical and bring in/take out hard physical momenta, thus the thermal type of the vertices V and X are always type-1, *i.e.*, $t_V = t_X = 1$.

6.5 Insertion of both the vertices of virtual K photon on final fermionic p'-leg

The insertion of both the ends of K photon to the final fermionic p'-leg is much more straightforward than the other two cases. This is exactly similar to the analogous case of thermal fermionic QED. After avoiding any possibility of double-counting the higher

order matrix element turns out to be proportional to the lower order matrix element times the contributions of K photon insertions factored out [41]. The final expression for the higher order matrix element hence can be expressed as,

$$\mathcal{M}_{n+1}^{K\gamma,\,p',\,p'} = +ie^2 \int \frac{\mathrm{d}^4 k}{(2\pi)^4} b_k(p',p') \left[\delta_{t_\mu,t_1} \, \delta_{t_\nu,t_1} \right] D^{t_\mu,t_\nu}(k) \times \mathcal{M}_n \, . \qquad (6.31)$$

We have listed this result for the sake of convenience and completeness. The outgoing SM fermions f being physical and carrying hard momenta, the thermal type associated with the outermost vertices are of type-1, *i.e.*, $t_1 = 1$ in the above expression. It is also to be noted that the overall ie^2 factor has a multiplicative positive $(+)$ sign here in contrast to the expression of Eq. 6.30 where ie^2 factor had an overall negative $(-)$ multiplicative sign. This is always true for the cases, where both the photon insertions are on same leg (see Eq. 5.24 of Chapter 5).

6.6 Insertion of both the vertices of virtual K photon on initial p-leg

This case where both the ends of the virtual K photon are inserted on the initial p-leg is the most complicated one. There are distinctively three separate classes among which the insertions can happen. These are particularly,

- Both ends of the new K photon insertion are on the internal scalar leg.

- One end of the new K photon insertion is on the scalar leg whereas the other one is on the initial fermionic leg.

- Both ends of the new K photon insertion are on the initial fermionic leg.

As both the photon ends are inserted on the initial p-leg hence, we have to take care to avoid double-counting. As before we, will do so, by *always* placing ν vertex to the left of

μ vertex insertion. With this understanding, the higher order matrix element after adding a virtual photon on the initial p-leg can be symbolically expressed as,

$$\mathcal{M}_{n+1}^{p,p} = (e)^{2n+2}(-i)^{m+2}(-1)^{\sum_{i=1}^{m}(t_i+1)}(-1)^{(t_\mu+1)}(-1)^{(t_\nu+1)}(i)^{m+2}\times$$
$$\left[C_u^{\text{fermion } p'}\right] \times \left[C_{s+r+2}^{p;\mu\nu}\right] \times \mathcal{D}_{n+1}^{\mu\nu}, \tag{6.32}$$

where, in the above expression all the notations of contributions of corresponding legs are in accordance with all previous discussion. We will note that $C_{s+r+2}^{p;\mu\nu}$ always contributes two extra multiplicative charge factor e^2 to the overall factors of matrix element than the corresponding C_{s+r}^p contribution. Using the definition of K polarization sum (see Eq. 4.3) the corresponding matrix element for the K photon insertion can be written as,

$$\mathcal{M}_{n+1}^{K\gamma,p,p} \sim \int \frac{d^4k}{(2\pi)^4} b_k(p,p) \left[C_u^{\text{fermion } p'}\right] \times \left[k_\mu k_\nu C_{s+r+2}^{p;\mu\nu}\right] \times [-iD^{t_\mu,t_\nu}] \times \mathcal{D}_n. \tag{6.33}$$

The relevant contribution to the matrix element now can be symbolically expressed as,

$$k_\mu k_\nu C_{s+r+2}^{p,\mu\nu} = k_\mu k_\nu \left[C_{s+2}^{\text{scalar } p;\mu\nu} \times C_r^{\text{fermion } p} + C_{s+1}^{\text{scalar};\mu} \times C_{r+1}^{\text{fermion } p;\nu}\right.$$
$$\left. + C_s^{\text{scalar } p} \times C_{r+2}^{\text{fermion } p;\mu\nu}\right]. \tag{6.34}$$

As we have already discussed, there are three distinctive classes of the contribution related to this case. The first term of Eq. 6.34 refers to both the insertions being on the internal scalar p-leg, the second term refers to the contribution with the two K photon ends being on the internal scalar p-leg and initial fermionic p-leg, and the third term refers to both the ends of K photon being inserted on the initial fermionic p-leg. The subscripts associated with the scalar contributions are to be understood according to all the discussions mentioned in previous sections. It is again mentioned here, that the subscripts of scalar contributions may/may not show faithfully the number of concerned vertices in the diagrams of sub-contributions, but they *always* correctly specify the contribution of charge factors to the overall matrix element.

145

6.6.1 Insertion of both the virtual K photon vertices on the internal scalar p-leg

This is the most complicated case among all the three possible distinctive classes. As both the ends of new K photon are inserted on the internal scalar p-leg, hence there is also the possibility of emergence of tadpole diagrams. The scalar line allows both the trilinear and seagull insertions; thus the number of the diagrams proliferate immensely. To avoid double-counting of vertices, the new ν vertex is always inserted to the left of μ vertex. To manage this proliferated numbers of diagrams and to show the nature of factorization and GY reduction clearly, the diagrams are grouped into four sets.

We will show here how the sets have been defined. We will start with a particular case when the new μ vertex is inserted to the immediate left of vertex V on scalar leg, either making a new trilinear vertex (left of vertex number s) or making a seagull vertex (at vertex number s). For each of those fixed μ (trilinear/seagull) vertex we will add the ν vertices in all possible ways to the left of μ vertices.

For all the trilinear new ν vertex insertions, the contributing diagrams are grouped into Fig. 6.5 and symbolically denoted as 'Set A'.

And for all the seagull new ν vertex insertions, the contributing diagrams are grouped into Fig. 6.6 and symbolically denoted as 'Set B'. Note that, for Set B there is also a choice when μ and ν makes a seagull insertion (a tadpole diagram) immediately to the left of special vertex V.

Before simplifying the results of both Set A and Set B, note that all the trilinear ν vertex insertions are collected into the first and seagull ν vertex insertions are collected into the second square bracketed terms for, both Set A and Set B respectively in Fig. 6.5 and Fig. 6.6.

146

Figure 6.5: *The diagrams which contribute to Set A (when both the photon insertions are on internal scalar leg) have been shown here. The diagrams correspond to 'trilinear' ν vertex insertions in all possible ways, when μ insertion is either a fixed trilinear (all the first square bracketed terms) or a fixed seagull insertion (all the second square bracketed terms) situated immediately left of vertex V.*

Figure 6.6: *The diagrams which contribute to Set B (when both the photon insertions are on internal scalar leg) have been shown here. The diagrams correspond to 'seagull' ν vertex insertions in all possible ways, when μ insertion is either a fixed trilinear (all the first square bracketed terms) or a fixed seagull insertion (all the second square bracketed terms) situated immediately left of vertex V.*

147

For both the cases of Set A and Set B, the first $(s-1)$ diagrams inside parentheses from both first and second squared bracketed terms are collected together to form $(s-1)$ terms with $_s\mu$ circled vertex inside the third (final) square bracketed terms.

Actually, to understand clearly which diagrams are collected together (from either Set A or B) the parentheses have been colour coded. The diagrams from same colour coded parentheses are collected together to obtain the final diagrams, which are also inside same colour coded parentheses. From this colour coded parentheses, it is also evident that other two terms from Set A, in the magenta coloured parentheses also group together to form a single circled vertex contribution.

The contributions of Set A and Set B can be symbolically written as in the equations below,

$$\text{Set } A = [\, (A_1 + \cdots + A_{s-1}) + (A') + (A'')\,]\,, \tag{6.35}$$

where, in the above expression, the contributions of the first $(s-1)$ terms from Set A Fig. 6.5 has been collected together and are denoted by $(A_1 + \cdots + A_{s-1})$. The other two remnant terms from Fig. 6.5 have been denoted by respectively (A') and (A''). The terms are again colour coded for easy identification.

Similarly for Set B Fig. 6.5 the first $(s-1)$ terms are collected together and are denoted by $(B_1 + \cdots + B_{s-1})$ and the other two remnant terms from Fig. 6.5 have been denoted by respectively (B') and (B''). Here, also the contributions are colour coded.

$$\text{Set } B = [\, (B_1 + \cdots + B_{s-1}) + (B') + (B'')\,]\,. \tag{6.36}$$

Now, the contributions of Set A and Set B are added together as in Fig. 6.7. There is again scope of simplification among the sub-contributions of Set A and Set B. The first $(s-1)$ terms from Set A and Set B again group together to make v_j circled vertices where, $j = 1, 2, ..., (s-1)$. There is also a simplification between $A'' + B''$ terms making a $_v\mu$ circled vertex term. This $_v\mu$ circled vertex term has also a tadpole contribution.

Figure 6.7: *The contributions from Set A Figs. 6.5 and Set B 6.6 have been added together, to obtain a simplified set of terms.*

The contribution of Set *A* and Set *B* can be symbolically written as,

$$\text{Set } A + \text{Set } B = \left[(A_1 + B_1) + \cdots + (A_{s-1} + B_{s-1})\right] + \left[A'\right] + \left[B'\right] + \left[A'' + B''\right],$$

$$= \text{Set I}_s + \text{Set II}_s + \text{Set III}_s + \text{Set IV}_s. \tag{6.37}$$

Now in above expression Set I_s correspond to the $(s-1)$ number of circled vertices contributions, where ν_j runs from $j = 1, 2, ..., (s-1)$ while $_s\mu$ is at a fixed place.

$$\text{Set I}_s = \left[(A_1 + B_1) + \cdots + (A_{s-1} + B_{s-1})\right]. \tag{6.38}$$

In Eq. 6.37, Set II_s corresponds to a contribution where the trilinear ν vertex is immediately adjacent to circled $_s\mu$ vertex.

$$\text{Set II}_s = \left[A'\right]. \tag{6.39}$$

In Eq. 6.37 Set III_s corresponds to a contribution, where ν makes a seagull vertex at vertex number s and μ is a trilinear insertion situated immediately to the right of the $\nu = s$ seagull vertex, so that

$$\text{Set III}_s = \left[B'\right]. \tag{6.40}$$

In Eq. 6.37, Set IV_s correspond to a contribution where the adjacent trilinear insertion of ν and μ vertices, and the $\nu = \mu$ tadpole diagram combine together to form a $_\nu\mu$ circled

vertex, so that

$$\text{Set IV}_s = \left[A'' + B''\right].\tag{6.41}$$

All the above grouping of terms were performed for a special location of μ vertex insertion namely at s, but this kind of grouping can also be performed for any arbitrary location of μ insertion vertex on p-leg. With this consideration, we can say that all the contributing diagrams, when both ends of the K photon insertions are on the same internal scalar p leg can be grouped into four independent sets, *i.e.*, Set I, Set II, Set III, Set IV. A typical term for each set has been shown in Fig. 6.8.
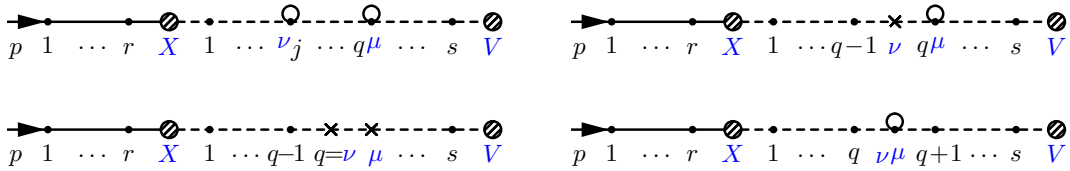
Figure 6.8: *Typical diagrams contributing to Set I, Set II, Set III, Set IV for both the K photon vertices on internal scalar p-leg. Set I at Top-left, Set II at Top-right, Set III at Bottom-left , Set IV at Bottom-right. The final fermionic p'-leg is not shown as that is kept unchanged for initial p-leg insertions.*

- **Set I :** This set has both the ν and μ vertex as circled vertices as shown in the top left diagram of Fig. 6.8. For a particular position of circled vertex $_q\mu$, the circled ν_j vertex can arise in $(q-1)$ ways, *i.e.*, $j = 1, 2, ..., (q-1)$. Now, the circled vertex $_q\mu$ can arise in $(s-1)$ ways corresponding to $q = 2, 3, ..., s$. Therefore Set I consists of a sum of $s(s-1)/2$ number of distinct schematic diagrams, a typical diagram of which is shown as in the top left panel of Fig. 6.8.

- **Set II :** This set has μ circled vertex and ν trilinear vertex. For every $_q\mu$ circled vertex, a trilinear ν vertex is situated immediately to the left of the circled vertex. There are exactly s ways corresponding to $q = 1, 2, ..., s$ in which the circled vertex $_q\mu$ can arise, and hence in this set there are s distinct number of schematic diagrams, a typical diagram of which is shown as in the top right panel of Fig. 6.8.

- **Set III :** This set has ν seagull vertex and μ trilinear vertex. For ν seagull vertex at $q = \nu$ the trilinear μ vertex is situated immediately to the right of the seagull $q = \nu$ vertex. As the seagull $q = \nu$ vertex can arise in s distinct ways corresponding to $q = 1, 2, ..., s$, hence there are s number of distinct schematic diagrams belonging in this set, a typical diagram of which is shown in the bottom left panel of Fig. 6.8.

- **Set IV :** This set comprises of circled $_{\nu}\mu$ vertices. Hence, this set includes all the tadpole diagrams. There are exactly $(s+1)$ distinct terms in this set, corresponding to the $(s + 1)$ number of $_{\nu}\mu$ circled vertex insertions on $(s + 1)$ number of scalar propagators. A typical diagram of this set is shown in the bottom right panel of Fig. 6.8.

Hence, the total contribution due to both ends of the K photon insertion being on the scalar line can be symbolically written down as,

$$k_\mu k_\nu \, C_{s+2}^{\text{scalar } p;\mu\nu} = \left[k_\mu k_\nu \, C_{s+2}^{\text{scalar } p;\mu\nu;I} \right] + \left[k_\mu k_\nu \, C_{s+2}^{\text{scalar } p;\mu\nu;II} \right] +$$
$$+ \left[k_\mu k_\nu \, C_{s+2}^{\text{scalar } p;\mu\nu;III} \right] + \left[k_\mu k_\nu \, C_{s+2}^{\text{scalar } p;\mu\nu;IV} \right] . \quad (6.42)$$

We will continue to evaluate the corresponding contribution of the four sets respectively and then add them to get the full contribution. We will also note that, this is an analogous (but not explicitly same) rearrangement of the terms as in for scalar QED case in Subsection 5.2.3. The rearrangement of sets are little bit different here, to facilitate a more clear cancellation and factorization (as the scalar line is off-shell here, in contrast to scalar QED case where scalar leg was on-shell).

The contribution of the Set I can be expressed as

$$k_\mu k_\nu \, C_{s+2}^{\text{scalar } p\,;\mu\nu;I} = \sum_{q=2}^{s} \sum_{j=1}^{q-1} k_\mu k_\nu \, C_{s+2}^{\text{scalar } p;\, q\mu,\nu_j;\, I} , \quad (6.43)$$

where $k_\mu k_\nu \, C_{s+2}^{\text{scalar } p;\, q\mu,\nu_j;\, I}$ corresponds to the diagram as shown in Fig. 6.9. We have also

drawn the Feynman diagrams related to the schematic diagram.
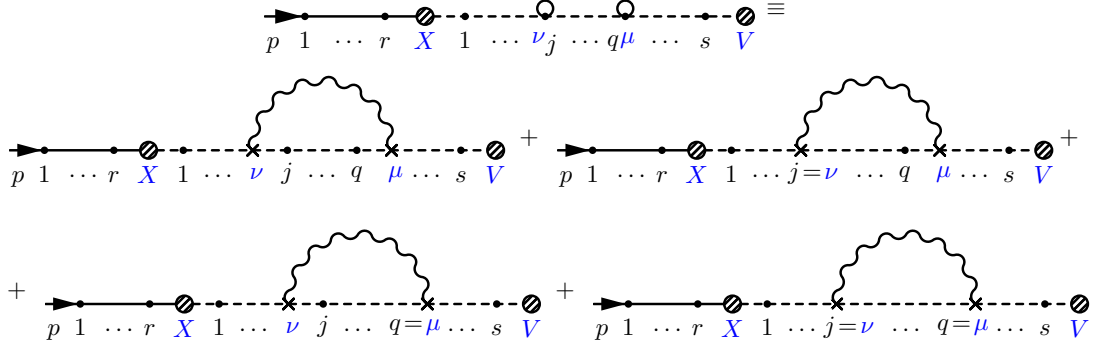
Figure 6.9: *A typical diagram of Set I with contributing Feynman diagrams.*

Using Eq. 6.6 and Eq. 6.7 the contribution of a typical diagram of Set I can be written as,

$$
\begin{aligned}
k_\mu k_\nu\, C_{s+2}^{\text{scalar}\,p\,;\,q\mu;\,\nu_j;\,I} &= (-1)^{(t_\mu+1)}\,(-1)^{(t_\nu+1)}\Big\{ S_{P+\Sigma_s}^{t_V,t_s}\,(2P+2\Sigma_{s-1}+l_s)_{\alpha_s}\cdots S_{P+\Sigma_{q+1}}^{t_{q+2},t_{q+1}} \times \\
&\quad (2P+2\Sigma_q+l_{q+1})_{\alpha_{q+1}}\Big[\delta_{t_\mu,t_q}\,S_{P+\Sigma_q}^{t_{q+1},t_q}\,(2P+2\Sigma_{q-1}+l_q)_{\alpha_q} \\
&\quad -\delta_{t_\mu,t_{q+1}}\,S_{P+\Sigma_q+k}^{t_{q+1},t_q}\,(2P+2\Sigma_{q-1}+2k+l_q)_{\alpha_q}\Big]S_{P+\Sigma_{q-1}+k}^{t_q,t_{q-1}}\cdots\Big\} \\
&\quad \times\Big\{\cdots S_{P+\Sigma_j+k}^{t_{j+1},t_j}\Big[\delta_{t_\nu,t_j}\,(2P+2\Sigma_{j-1}+l_j)_{\alpha_j}\,S_{P+\Sigma_{j-1}}^{t_j,t_{j-1}} \\
&\quad -\delta_{t_\nu,t_{j-1}}\,(2P+2\Sigma_{j-1}+2k+l_j)_{\alpha_j}\,S_{P+\Sigma_{j-1}+k}^{t_j,t_{j-1}}\Big]\times \\
&\quad (2P+2\Sigma_{j-2}+l_{j-1})_{\alpha_{j-1}}\cdots(2P+l_1)_{\alpha_1}\,S_P^{t_1,t_X}\Big\}\,, \\
&\equiv \big\{M_q - M_{q+1}\big\}_\mu\,\big\{N_j - N_{j-1}\big\}_\nu\,, \\
&\equiv \big\{M_{q\mu}\big\}\big\{N_j - N_{j-1}\big\}_\nu\,. \tag{6.44}
\end{aligned}
$$

In the above expression $M_{q\mu}$ corresponds to the expression as defined in Eq. 6.6 and $\big\{N_j - N_{j-1}\big\}_\nu$ arises as a result of using Eq. 6.7. Now summing over all possible $(q-1)$ number of circled ν_j vertices for $j = 1, 2, ..., (q-1)$ we obtain a pairwise cancellation of

terms, resulting in two remnant terms,

$$\sum_{j=1}^{q} k_\mu k_\nu\, C_{s+2}^{\text{scalar } p\,;\,q\mu;\,\nu_j;\,I} = \left\{M_{q\mu}\right\}\left\{(N_{q-1}-N_{q-2}) + (N_{q-2}-N_{q-3}) + \cdots + (N_2-N_1)\right.$$

$$\left. + (N_1 - N_0)\right\},$$

$$= \left\{M_{q\mu}\right\}\left\{N_{q-1} - N_0\right\},$$

$$\equiv C_1^{q\mu;\,I} - C_2^{q\mu;\,I}. \tag{6.45}$$

The complete contribution of Set I, as mentioned in Eq. 6.43, can be obtained after summing over all the $(s-1)$ choices of circled $_q\mu$ vertices, corresponding to $q = 2, 3, ..., s$. But, just from a simple observation of Eq. 6.45 it is obvious that for $q = 1$ the two corresponding terms $C_1^{q\mu;\,I}$ and $C_2^{q\mu;\,I}$ exactly cancel among themselves giving a vanishing contribution. Therefore, we can incorporate this observation by including $q = 1$ also in the limit of the summed contribution of Eq. 6.43 producing a result,

$$k_\mu k_\nu\, C_{s+2}^{\text{scalar } p;\,\mu\nu;\,I} = \sum_{q=1}^{s}\left[C_1^{q\mu;\,I} - C_2^{q\mu;\,I}\right], \tag{6.46}$$

where now the q sum runs from 1 to s. Using the results of Eq. 6.6, Eq. 6.7 and Eq. 6.44 in above Eq. 6.45 we obtain,

$$C_1^{q\mu;\,I} = (-1)^{(t_\mu+1)}\,(-1)^{(t_\nu+1)}\left[S_{P+\Sigma_s}^{t_V,t_s}\,(2P+2\Sigma_{s-1}+l_s)_{\alpha_s}\,S_{P+\Sigma_{s-1}}^{t_s,t_{s-1}}\,\cdots(2P+2\Sigma_q+l_{q+1})_{\alpha_{q+1}}\right]$$

$$\left[\delta_{t_\mu,t_q}\,S_{P+\Sigma_q}^{t_{q+1},t_q}\,(2P+2\Sigma_{q-1}+l_q)_{\alpha_q} - \delta_{t_\mu,t_{q+1}}\,S_{P+\Sigma_q+k}^{t_{q+1},t_q}\,(2P+2\Sigma_{q-1}+2k+l_q)_{\alpha_q}\right]\times$$

$$\left\{\delta_{t_\nu,t_{q-1}}\,S_{P+\Sigma_{q-1}+k}^{t_q,t_{q-1}}\,(2P+2\Sigma_{q-2}+l_{q-1})_{\alpha_{q-1}}\cdots S_P^{t_1,t_X}\right\};$$

$$C_2^{q\mu;\,I} = (-1)^{(t_\mu+1)}\,(-1)^{(t_\nu+1)}\left[S_{P+\Sigma_s}^{t_V,t_s}\,(2P+2\Sigma_{s-1}+l_s)_{\alpha_s}\,S_{P+\Sigma_{s-1}}^{t_s,t_{s-1}}\,\cdots(2P+2\Sigma_q+l_{q+1})_{\alpha_{q+1}}\right]$$

$$\left[\delta_{t_\mu,t_q}\,S_{P+\Sigma_q}^{t_{q+1},t_q}\,(2P+2\Sigma_{q-1}+l_q)_{\alpha_q} - \delta_{t_\mu,t_{q+1}}\,S_{P+\Sigma_q+k}^{t_{q+1},t_q}\,(2P+2\Sigma_{q-1}+2k+l_q)_{\alpha_q}\right]\times$$

$$\left\{\delta_{t_\nu,t_X}\,S_{P+\Sigma_{q-1}+k}^{t_q,t_{q-1}}\,(2P+2\Sigma_{q-2}+2k+l_{q-1})_{\alpha_{q-1}}\cdots(2P+2k+l_1)_{\alpha_1}\,S_{P+k}^{t_1,t_X}\right\}, \tag{6.47}$$

where we notice (see Fig. 6.9) from the above equation that the momentum k of the virtual K photon does not flow beyond right of insertion vertex μ or circled vertex $_q\mu$, hence the

part of the scalar p leg contribution which is in between vertex $(q + 1)$ and V remains unchanged. This unchanged factor which is marked by magenta colour will occur frequently in the following discussion, so we will use the notation $[\mathcal{U}]_{q+1}$ (with $\mathcal{U}$ denoting unchanged) for this unchanged factor as below,

$$[\mathcal{U}]_{q+1} = \left[S_{P+\Sigma_s}^{t_V,t_s} \left(2P+2\Sigma_{s-1}+l_s\right)_{\alpha_s} S_{P+\Sigma_{s-1}}^{t_s,t_{s-1}} \cdots \left(2P+2\Sigma_q+l_{q+1}\right)_{\alpha_{q+1}} \right]. \qquad (6.48)$$

The total contribution of Set II is symbolically expressed as,

$$k_\mu k_\nu \, C_{s+2}^{\text{scalar } p;\,\mu\nu;\,II} = \sum_{q=1}^{s} k_\mu k_\nu \, C_{s+2}^{\text{scalar } p;\,q\mu\nu;\,II}. \qquad (6.49)$$

A typical term of this contribution corresponds to the schematic as shown in Fig. 6.10.

Figure 6.10: *A typical diagram of Set II with contributing Feynman diagrams.*

The contribution of a typical term of Set II is given by

$$
\begin{aligned}
k_\mu k_\nu C_{s+2}^{\text{scalar } p;\,q\mu\nu;\,II} = \ & (-1)^{(t_\mu+1)} (-1)^{(t_\nu+1)} \Big\{ S_{P+\Sigma_s}^{t_V,t_s} \left(2P+2\Sigma_{s-1}+l_s\right)_{\alpha_s} \cdots S_{P+\Sigma_{q+1}}^{t_{q+2},t_{q+1}} \times \\
& \left(2P+2\Sigma_q+l_{q+1}\right)_{\alpha_{q+1}} \Big[\delta_{t_\mu,t_q} S_{P+\Sigma_q}^{t_{q+1},t_q} \left(2P+2\Sigma_{q-1}+l_q\right)_{\alpha_q} \\
& -\delta_{t_\mu,t_{q+1}} S_{P+\Sigma_q+k}^{t_{q+1},t_q} \left(2P+2\Sigma_{q-1}+2k+l_q\right)_{\alpha_q} \Big] \Big\} \\
& \times \Big\{ \left[\delta_{t_\nu,t_q} S_{P+\Sigma_{q-1}}^{t_q,t_{q-1}} - \delta_{t_\nu,t_{q-1}} S_{P+\Sigma_{q-1}+k}^{t_q,t_{q-1}} \right] \left(2P+2\Sigma_{q-2}+l_{q-1}\right)_{\alpha_{q-1}} \cdots S_P^{t_1,t_X} \Big\}, \\
\equiv \ & \left[C_1^{q\mu;\,II} - C_2^{q\mu;\,II} \right] - C_3^{q\mu;\,II}, \qquad (6.50)
\end{aligned}
$$

To obtain Eq. 6.50 the results of Eq. 6.6 and the generalized Feynman's Identities have

been used. The two terms in the first curly bracket are due to a result of using Eq. 6.6 to simplify the circled $_q\mu$ insertion. And the terms in the second curly bracket arise after using generalized Feyman's identities. Here $C_1^{q\mu;\,II} - C_2^{q\mu;\,II}$ arise from multiplication of the first term of the second curly bracket with the whole of the first curly bracket and the $-C_3^{q\mu;\,II}$ is a result of multiplication of second term of the second curly bracket with the whole of the first curly bracket. After using Eq. 6.48 the contribution can be written as,

$$C_1^{q\mu;\,II} - C_2^{q\mu;\,II} = (-1)^{(t_\mu+1)} (-1)^{(t_\nu+1)} [\mathcal{U}]_{q+1} \left[\delta_{t_\mu,t_q} S_{P+\Sigma_q}^{t_{q+1},t_q} (2P+2\Sigma_{q-1}+l_q)_{\alpha_q} \right. $$
$$\left. - \delta_{t_\mu,t_{q+1}} S_{P+\Sigma_q+k}^{t_{q+1},t_q} (2P+2\Sigma_{q-1}+2k+l_q)_{\alpha_q} \right]$$
$$\times \left\{ \delta_{t_\nu,t_q} S_{P+\Sigma_{q-1}}^{t_q,t_{q-1}} (2P+2\Sigma_{q-2}+l_{q-1})_{\alpha_{q-1}} \cdots S_P^{t_1,t_X} \right\} , \qquad (6.51)$$

and the individual contributions can be expressed as,

$$C_1^{q\mu;\,II} = (-1)^{(t_\mu+1)} (-1)^{(t_\nu+1)} [\mathcal{U}]_{q+1} \left[\delta_{t_\mu,t_q} S_{P+\Sigma_q}^{t_{q+1},t_q} (2P+2\Sigma_{q-1}+l_q)_{\alpha_q} \right]$$
$$\times \left\{ \delta_{t_\nu,t_q} S_{P+\Sigma_{q-1}}^{t_q,t_{q-1}} (2P+2\Sigma_{q-2}+l_{q-1})_{\alpha_{q-1}} \cdots S_P^{t_1,t_X} \right\} ,$$
$$= (-1)^{(t_\mu+1)} (-1)^{(t_\nu+1)} \left[\delta_{t_\mu,t_q} \delta_{t_\nu,t_q} \right] [\mathcal{U}]_{q+1} \left[S_{P+\Sigma_q}^{t_{q+1},t_q} (2P+2\Sigma_{q-1}+l_q)_{\alpha_q} \cdots S_P^{t_1,t_X} \right] ;$$
$$(6.52)$$

$$-C_2^{q\mu;\,II} = -(-1)^{(t_\mu+1)} (-1)^{(t_\nu+1)} [\mathcal{U}]_{q+1} \left[\delta_{t_\mu,t_{q+1}} S_{P+\Sigma_q+k}^{t_{q+1},t_q} (2P+2\Sigma_{q-1}+2k+l_q)_{\alpha_q} \right]$$
$$\times \left\{ \delta_{t_\nu,t_q} S_{P+\Sigma_{q-1}}^{t_q,t_{q-1}} (2P+2\Sigma_{q-2}+l_{q-1})_{\alpha_{q-1}} \cdots S_P^{t_1,t_X} \right\} ,$$
$$= -(-1)^{(t_\mu+1)} (-1)^{(t_\nu+1)} \left[\delta_{t_\mu,t_{q+1}} \delta_{t_\nu,t_q} \right] [\mathcal{U}]_{q+1} \left[S_{P+\Sigma_q+k}^{t_{q+1},t_q} \left(2P+2\Sigma_{q-1}+\boxed{2k}+l_q\right)_{\alpha_q} \times \right.$$
$$\left. S_{P+\Sigma_{q-1}}^{t_q,t_{q-1}} \cdots S_P^{t_1,t_X} \right] ; \qquad (6.53)$$

$$-C_3^{q\mu;\,II} = -(-1)^{(t_\mu+1)}(-1)^{(t_\nu+1)}\left[\mathcal{U}\right]_{q+1}\left[\delta_{t_\mu,t_q}\,S_{P+\Sigma_q}^{t_{q+1},t_q}\left(2P+2\Sigma_{q-1}+l_q\right)_{\alpha_q}\right.$$

$$-\delta_{t_\mu,t_{q+1}}\,S_{P+\Sigma_q+k}^{t_{q+1},t_q}\left(2P+2\Sigma_{q-1}+2k+l_q\right)_{\alpha_q}\Bigr]$$

$$\times\left\{\delta_{t_\nu,t_{q-1}}\,S_{P+\Sigma_{q-1}+k}^{t_q,t_{q-1}}\left(2P+2\Sigma_{q-2}+l_{q-1}\right)_{\alpha_{q-1}}\cdots S_P^{t_1,t_X}\right\},$$

$$=-\,C_1^{q\mu;\,I}\,; \tag{6.54}$$

where we note that $-C_3^{q\mu;\,II}$ is exactly opposite of $C_1^{q\mu;\,I}$ of Eq. 6.47 (*i.e.*, $-C_3^{q\mu;\,II} = -C_1^{q\mu;\,I}$) and we will see cancellation between these terms in upcoming discussions.

The total contribution of Set III is symbolically given by,

$$k_\mu k_\nu\,C_{s+2}^{\text{scalar }p;\,\mu\nu;\,III} \;=\; \sum_{q=1}^{s} k_\mu k_\nu\,C_{s+2}^{\text{scalar }p;\,\mu,\,q=\nu;\,III}\,. \tag{6.55}$$

A typical contributing diagram of Set III is schematically and with Feynman diagram shown in Fig. 6.11.

$$p \quad 1 \quad \cdots \quad r \quad X \quad 1 \quad \cdots q{-}1 \quad q{=}\nu \;\; \mu \;\; \cdots \;\; s \quad V \qquad\qquad p \quad 1 \quad \cdots \quad r \quad X \quad 1 \quad \cdots q{-}1 \quad q{=}\nu \;\; \mu \;\; \cdots \;\; s \quad V$$
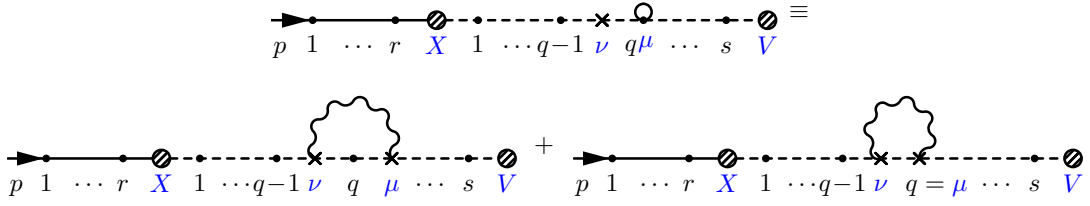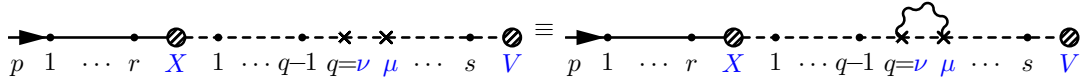
Figure 6.11: *A typical diagram of Set III with contributing Feynman diagram.*

The contribution of the typical diagram is given by,

$$k_\mu k_\nu C_{s+2}^{\text{scalar }p;\,\mu,\,q=\nu;\,III} = (-1)^{(t_\nu+1)}\left[\mathcal{U}\right]_{q+1}\left[S_{P+\Sigma_q}^{t_{q+1},t_\mu}\left(2P+2\Sigma_{q-1}+k\right)\cdot kS_{P+\Sigma_q+k}^{t_\mu,t_\nu}\right]$$

$$\times\left((-2k)_{\alpha_q}\delta_{t_\nu,t_q}\right)S_{P+\Sigma_{q-1}}^{t_q,t_{q-1}}\cdots S_P^{t_1,t_X}\,,$$

$$= (-1)^{(t_\mu+1)}(-1)^{(t_\nu+1)}\left[\mathcal{U}\right]_{q+1}\left[\delta_{t_\mu,t_\nu}S_{P+\Sigma_q}^{t_{q+1},t_q}-\delta_{t_\mu,t_{q+1}}S_{P+\Sigma_q+k}^{t_{q+1},t_q}\right],$$

$$\times\left((-2k)_{\alpha_q}\delta_{t_\nu,t_q}\right)S_{P+\Sigma_{q-1}}^{t_q,t_{q-1}}\cdots S_P^{t_1,t_X}\,,$$

$$\equiv C_1^{q;III} - C_2^{q;III}\,, \tag{6.56}$$

where in the above Eq. 6.56 the individual contribution of the final expression is given by,

$$C_1^{q;III} = (-1)^{(t_\mu+1)}(-1)^{(t_\nu+1)} \left[\delta_{t_\mu,t_q} \, \delta_{t_\nu,t_q} \right] [\mathcal{U}]_{q+1} \left\{ S_{P+\Sigma_q}^{t_{q+1},t_q} \, (-2k)_{\alpha_q} \, S_{P+\Sigma_{q-1}}^{t_q,t_{q-1}} \cdots S_P^{t_1,t_X} \right\},$$

$$-C_2^{q;III} = (-1)^{(t_\mu+1)}(-1)^{(t_\nu+1)} \left[-\delta_{t_\mu,t_{q+1}} \, \delta_{t_\nu,t_q} \right] [\mathcal{U}]_{q+1} \left\{ S_{P+\Sigma_q+k}^{t_{q+1},t_q} \, (-2k)_{\alpha_q} \, S_{P+\Sigma_{q-1}}^{t_q,t_{q-1}} \cdots S_P^{t_1,t_X} \right\}.$$

$$\text{(6.57)}$$

The total contribution of the Set IV can be written symbolically as,

$$k_\mu k_\nu C_{s+2}^{\text{scalar } p\,;\,\mu\nu;\, IV} = \sum_{q=0}^{s} k_\mu k_\nu C_{s+2}^{\text{scalar } p\,;\,\nu\mu;\, q;\, IV}, \tag{6.58}$$

where a typical term of the Set IV now also contains tadpole insertion. A typical contribution has been shown both schematically and with Feynman diagrams in Fig. 6.12.
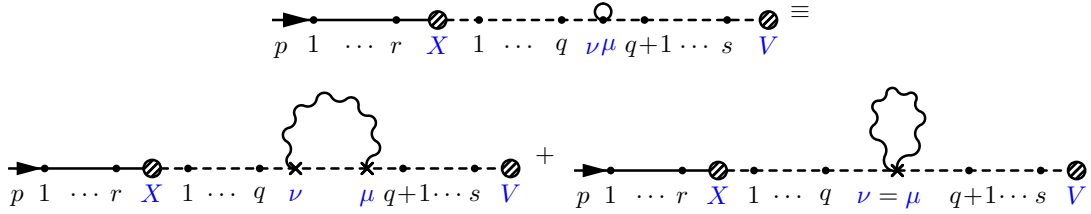
Figure 6.12: A typical diagram of Set IV with contributing Feynman diagrams.

The same contribution of typical diagram Fig. 6.12 can be written symbolically as,

$$k_\mu k_\nu C_{s+2}^{\text{scalar } p\,;\,\nu\mu;\, q;\, IV} = C_{s+2}^{\text{scalar } p\,;\,\nu \text{ left of } \mu;\, q;\, IV} + C_{s+2}^{\text{scalar } p\,;\,\nu=\mu;\, q;\, IV}. \tag{6.59}$$

As the momentum k of the K photon flows from the ν vertex to the μ vertex; hence here in Set IV, when the ν and μ trilinear insertion vertices are adjacent to each other, then this momentum only flows through a single propagator and that propagator is shared by both the ν and μ vertices. Therefore the GY reduction for this case can only happen at a particular vertex. Considering this fact, the contribution due to adjacent trilinear insertions

on scalar leg is given by,

$$
\begin{aligned}
k_\mu k_\nu C_{s+2}^{\text{scalar } p;\nu \text{ left of } \mu; q; IV} &= \cdots (2P+2\Sigma_q + l_{q+1})_{\alpha_{q+1}} \left[S_{P+\Sigma_q}^{t_{q+1},t_\mu} (2P+2\Sigma_q + k) \cdot k \, S_{P+\Sigma_q+k}^{t_\mu,t_\nu} \right] \times \\
&\qquad (2P+2\Sigma_q + k) \cdot k \, S_{P+\Sigma_q}^{t_\nu,t_q} \cdots \\
&= (-1)^{(t_\mu+1)}(-1)^{(t_\nu+1)} \times \Big\{ \cdots (2P+2\Sigma_q + l_{q+1})_{\alpha_{q+1}} \times \\
&\qquad \left[\delta_{t_\mu,t_\nu} S_{P+\Sigma_q}^{t_{q+1},t_\nu} - \delta_{t_\mu,t_{q+1}} S_{P+\Sigma_q+k}^{t_{q+1},t_\nu} \right] \times (2P+2\Sigma_q + k) \cdot k \, S_{P+\Sigma_q}^{t_\nu,t_q} \cdots \Big\}, \\
&= (-1)^{(t_\mu+1)}(-1)^{(t_\nu+1)} \Big\{ \cdots (2P+2\Sigma_q + l_{q+1})_{\alpha_{q+1}} \times \\
&\qquad \Big\{ \delta_{t_\mu,t_\nu} \left[S_{P+\Sigma_q}^{t_{q+1},t_\nu} (2P+2\Sigma_q + k) \cdot k \, S_{P+\Sigma_q}^{t_\nu,t_q} \right] \\
&\qquad - \delta_{t_\mu,t_{q+1}} \left[\delta_{t_\nu,t_{q+1}} S_{P+\Sigma_q}^{t_{q+1},t_q} - \delta_{t_\nu,t_q} S_{P+\Sigma_q+k}^{t_{q+1},t_q} \right] \Big\} \cdots \Big\}, \\
&= (-1)^{(t_\mu+1)}(-1)^{(t_\nu+1)} \Big\{ \cdots (2P+2\Sigma_q + l_{q+1})_{\alpha_{q+1}} \times \\
&\qquad \Big\{ \left[\delta_{t_\mu,t_\nu} S_{P+\Sigma_q}^{t_{q+1},t_\nu} \left((2P+2\Sigma_q) \cdot k + k^2 \right) S_{P+\Sigma_q}^{t_\nu,t_q} \right] \\
&\qquad - \left[\delta_{t_\mu,t_{q+1}} \delta_{t_\nu,t_{q+1}} S_{P+\Sigma_q}^{t_{q+1},t_q} \right] + \left[\delta_{t_\mu,t_{q+1}} \delta_{t_\nu,t_q} S_{P+\Sigma_q+k}^{t_{q+1},t_q} \right] \Big\} \cdots \Big\}, \\
&\equiv \left[C_1^{q;IV} \right] - \left[C_2^{q;IV} \right] + \left[C_3^{q;IV} \right].
\end{aligned}
\tag{6.60}
$$

In Eq. 6.60 the ellipses denote that there is no photon momentum k dependence related to the other parts of scalar contributions. The contribution of the tadpole diagram can be expressed as,

$$
\begin{aligned}
k_\mu k_\nu C_{s+2}^{\text{scalar } p;\nu=\mu; q; IV} &= \cdots (2P+2\Sigma_q + l_{q+1})_{\alpha_{q+1}} S_{P+\Sigma_q}^{t_{q+1},t_\mu} \left(\frac{-2g^{\mu\nu}\delta_{t_\mu,t_\nu}}{2} k_\mu k_\nu \right) S_{P+\Sigma_q}^{t_\mu,t_q} \cdots, \\
&= (-1)^{(t_\mu+1)}(-1)^{(t_\nu+1)} \delta_{t_\mu,t_\nu} \Big\{ \cdots (2P+2\Sigma_q + l_{q+1})_{\alpha_{q+1}} S_{P+\Sigma_q}^{t_{q+1},t_\mu} \left(-k^2 \right) S_{P+\Sigma_q}^{t_\mu,t_q} \cdots \Big\}, \\
&\equiv - C_4^{q;IV},
\end{aligned}
\tag{6.61}
$$

where in Eq. 6.61 we have made use of the fact that $(-1)^{(t_\mu+1)}(-1)^{(t_\nu+1)}\delta_{t_\mu,t_\nu} = \delta_{t_\mu,t_\nu}$, and used proper symmetry factor $1/2$ related to seagull insertion. It is to be noted that the contribution $-C_4^{q;IV}$ exactly cancels the k^2 dependence of $C_1^{q;IV}$ term. And although $O(k^2)$ terms are IR finite, but without their cancellations among themselves the factorization and resummation of IR divergent terms is impossible (as was with pure thermal scalar QED).

The total contribution of the Set IV terms then can be symbolically expressed as,

$$k_\mu k_\nu C_{s+2}^{\text{scalar } p\,;\,\mu\nu;\,IV} = \sum_{q=0}^{s} \left[C_1^{q;IV} - C_2^{q;IV} + C_3^{q;IV} - C_4^{q;IV} \right] . \tag{6.62}$$

The total contribution of the higher $(n+1)^{\text{th}}$ order matrix element due to insertion of virtual K photon to the lower order matrix element, when both of the ends of newly inserted virtual K photon are on the internal scalar p-leg gives rise to a final expression (where, we have used Eq. 6.32 Eq. 6.33, and Eq. 6.34) as shown below,

$$\mathcal{M}_{n+1}^{K\gamma,\,p,p}\big|_{\text{scalar}} = (e)^{2n+2}(-i)^{m+2}(-1)^{\sum_{i=1}^{m}(t_i+1)}(-1)^{(t_\mu+1)}(-1)^{(t_\nu+1)}(i)^{m+2} \int \frac{\mathrm{d}^4 k}{(2\pi)^4} \times$$

$$b_k(p,p)\left[C_u^{\text{fermion } p'}\right] \times \left[k_\mu k_\nu C_{s+2}^{\text{scalar } p\,;\,\mu\nu} \times C_r^{\text{fermion } p}\right]\left[-iD^{t_\mu,t_\nu}\right] \times \mathcal{D}_n\,,$$

$$= (e)^{2n+2}(-i)^{m+2}(-1)^{\sum_{i=1}^{m}(t_i+1)}(-1)^{(t_\mu+1)}(-1)^{(t_\nu+1)}(i)^{m+2} \int \frac{\mathrm{d}^4 k}{(2\pi)^4} \times$$

$$b_k(p,p)\left[C_u^{\text{fermion } p'}\right] \times \left\{ \sum_{q=1}^{s}\left[C_1^{q\mu;\,I} - C_2^{q\mu;\,I}\right] + \sum_{q=1}^{s}\left[C_1^{q\mu;\,II} - C_2^{q\mu;\,II} - C_3^{q\mu;\,II}\right] + \right.$$

$$\left. \sum_{q=1}^{s}\left[C_1^{q;III} - C_2^{q;III}\right] + \sum_{q=0}^{s}\left[C_1^{q;IV} - C_2^{q;IV} + C_3^{q;IV} - C_4^{q;IV}\right] \right\} \times$$

$$\left[C_r^{\text{fermion } p}\right]\left[-iD^{t_\mu,t_\nu}\right] \times \mathcal{D}_n\,, \tag{6.63}$$

In the above expression, the contribution due to final fermionic p'-leg *i.e.*, $C_u^{\text{fermion } p'}$ and initial fermionic p-leg *i.e.*, $C_r^{\text{fermion } p}$ is unchanged; as both the ends of K photon insertion was on the internal scalar p-leg. We also observe that some distinct contributions arising from different sets either fully/partially cancel among themselves. The relevant terms which have a full/partial cancellations among themselves have been colour coded (with same colour) in Eq. 6.63. Here below, we list down our observations of the cancellations.

1. The contributions $C_1^{q\mu;\,I}$ and $C_3^{q\mu;\,II}$ are exactly identical, and fully cancel among themselves.

2. The total s number of contributions of $C_1^{q\mu;\,II}$ exactly cancel against the first s number of contributions of $C_2^{q;IV}$, (when $q = 0\,(\text{or } X), 1, 2, ..., (s-1)$); leaving only the

remnant surviving contribution $C_2^{s;IV}$.

3. The contribution $C_2^{q\mu;II}$, $C_2^{q;III}$ and $C_3^{q;IV}$ have an partial cancellation among themselves leaving behind only a single contribution. The full contribution of $C_2^{q;III}$, Eq. 6.57 (which is proportional to $-(2k)_{\alpha_q}$) cancels exactly against the "boxed" terms of $C_2^{q\mu;II}$ which are proportional to $(2k)_{\alpha_q}$, Eq. 6.53, resulting in a total contribution given by,

$$-\sum_{q=1}^{s} C_2^{q;II+III} \equiv -\sum_{q=1}^{s} \left[C_2^{q\mu;II} + C_2^{q;III} \right] = -\sum_{q=1}^{s} \left[(-1)^{(t_\mu+1)}(-1)^{(t_\nu+1)} \delta_{t_\mu,t_q+1} \delta_{t_\nu,t_q} \right] [\mathcal{U}]_{q+1} \times$$
$$\left[S_{P+\Sigma_q+k}^{t_{q+1},t_q} (2P+2\Sigma_{q-1}+l_q)_{\alpha_q} S_{P+\Sigma_{q-1}}^{t_q,t_{q-1}} \cdots S_P^{t_1,t_X} \right].$$
$$(6.64)$$

The total s number of terms from the contribution $C_2^{q;II+III}$ Eq. 6.64 cancels exactly with the last s number of terms from the contribution $C_3^{q;IV}$ for $q = 1, 2, ..., s$, leaving behind the surviving term, $C_3^{X;IV}$ corresponding to $q = X$ (or 0) term.

4. All the contributions coming from $C_1^{q;III}$, $C_1^{q;IV}$ and $C_4^{q;IV}$ vanish exactly. The k^2 dependent terms from $C_1^{q;IV}$ and $C_4^{q;IV}$ cancel exactly among themselves. The remaining k dependence of $C_1^{q;IV}$ and total k dependence of $C_1^{q;III}$ are linear in k, hence odd in k. All the other terms (arising due to $C_u^{\text{fermion } p'}$ and $C_r^{\text{fermion } p}$, $b_k(p, p)$, photon propagator) in the integrand are even in k. Hence, the total contribution of these terms vanishes upon momentum integration.

With this nature of cancellation of terms, among the contributions coming from the four sets of distinct classes of diagrams, we find that the full contribution of the Set II and Set III vanishes. We get some remaining surviving contributions from Set I and Set IV (after simplification and cancellation of terms among these sets also). The total contribution of the internal scalar p-leg (which can be expressed as a sum of contributions of the four sets) when both the ends of new K photon insertion is on internal scalar leg can be expressed

160

as in Eq. 6.65 below,

$$k_\mu k_\nu \, C_{s+2}^{\text{scalar } p \,;\, \mu\nu} = \left[-\sum_{q=1}^{s} C_2^{q\mu; I}\right]_I + \left[0\right]_{II} + \left[0\right]_{III} + \left[-C_2^{s;IV} + C_3^{X;IV}\right]_{IV} \,,$$

$$= \left[-\sum_{q=1}^{s} C_2^{q\mu; I}\right]$$

$$+ \left[-\left\{\left[(-1)^{(t_\mu+1)}(-1)^{(t_\nu+1)} \delta_{t_\mu, t_V} \, \delta_{t_\nu, t_V}\right] S_{P+\Sigma_q}^{t_{q+1}, t_q} \, \left(2P + 2\Sigma_{q-1} + l_q\right)_{\alpha_q} \cdots S_P^{t_1, t_X}\right\}$$

$$+ \left\{\left[(-1)^{(t_\mu+1)}(-1)^{(t_\nu+1)} \delta_{t_\mu, t_1} \, \delta_{t_\nu, t_X}\right] S_{P+\Sigma_q}^{t_{q+1}, t_q} \, \left(2P + 2\Sigma_{q-1} + l_q\right)_{\alpha_q} \cdots S_{P+k}^{t_1, t_X}\right\}\right] \,,$$

$$\equiv \left\{-\sum_{q=1}^{s} C_1^{q; \text{ss}} - C_2^{\text{ss}} + C_3^{\text{ss}}\right\} \,. \tag{6.65}$$

In the above expression, the notations related to surviving remnant contributions are redefined as; $C_2^{q\mu; I} \equiv C_1^{q; \text{ss}}$, $C_2^{s;IV} \equiv C_2^{\text{ss}}$ and $C_3^{X;IV} \equiv C_3^{\text{ss}}$. The superscript 'ss' of the redefined notations of the contributions imply that these contributions are due to K photon insertions when both the ends of K photon is on internal scalar (*i.e.*, scalar-scalar insertions or 'ss' insertions). It is to be noted that the second term C_2^{ss} is proportional to the lower order contribution and does not have any k dependence. The third term C_3^{ss} has only a single k dependent factor in the propagator $S_{P+k}^{t_1, t_X}$ of the contribution, which arose from the $_\nu\mu$ circled insertion being immediately to the right of the vertex X. The term C_3^{ss} only survives as the internal scalar line is off-shell. The sum of $C_1^{q; \text{ss}}$ terms also have k dependence associated with them. Hence, the contribution when both the ends of K photon are on the internal scalar p-leg does not *independently* factorize as the contribution coming from K photon insertion times the lower order contribution (due to the presence of momentum k dependent contributions). Hence, the contribution of the matrix element corresponding to both the K photon ends being inserted on internal scalar leg can be expressed as,

$$\mathcal{M}_{n+1}^{K\gamma, p, p} \Big|_{\text{scalar}} \sim \int \frac{\mathrm{d}^4 k}{(2\pi)^4} b_k(p, p) \left[C_u^{\text{fermion } p'}\right] \times \left\{-\sum_{q=1}^{s} C_1^{q; \text{ss}} - C_2^{\text{ss}} + C_3^{\text{ss}}\right\}$$

$$\times \left[C_r^{\text{fermion } p}\right] \left[-i D^{t_\mu, t_\nu}\right] \times \mathcal{D}_n \,. \tag{6.66}$$

Here, we have used the results of Eq. 6.65 in the Eq. 6.63 and have suppressed the overall factors of charge and 'i' in the final expression of Eq. 6.66.

6.6.2 Insertion of K photon vertices sharing internal scalar and initial fermionic p-leg

Now we discuss the case when the K photon vertices are equally shared among the internal scalar and initial fermionic p-leg. This type of insertion corresponds to the second term in the square bracket of Eq. 6.34. The relevant part of the matrix element corresponding to the K photon insertions for this case reads,

$$\mathcal{M}_{n+1}^{K\gamma,\,p,p}|_{\text{scalar,fermion}} = (e)^{2n+2}(-i)^{m+2}(-1)^{\sum_{i=1}^{s}(t_i+1)}(-1)^{(t_\mu+1)}(-1)^{(t_\nu+1)}(i)^{m+2}\times$$

$$\int \frac{\mathrm{d}^4 k}{(2\pi)^4} b_k(p,p) \left[C_u^{\text{fermion } p'}\right] \times \left[k_\mu C_{s+1}^{\text{scalar } p;\,\mu}\right] \times \left[k_\nu C_{r+1}^{\text{fermion } p;\,\nu}\right]$$

$$\times \left[-iD^{\,t_\mu,t_\nu}\right] \times \mathcal{D}_n, \qquad (6.67)$$

where we have used the relevant part of Eq. 6.34 in Eq. 6.33 to obtain the above expression. From the above expression, we note that the higher order contributions $k_\mu C_{s+1}^{\text{scalar } p;\,\mu}$ and $k_\nu C_{r+1}^{\text{fermion } p;\,\nu}$ corresponding to respectively higher order internal scalar and initial fermionic contributions are independent of each other and can be evaluated separately.
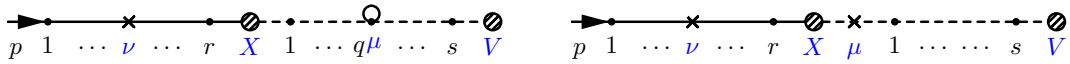
Figure 6.13: *Typical contributing diagrams when ν insertion is on initial fermionic p-leg and μ insertion is on internal scalar p-leg. For, each particular choice of ν insertion, there are s number of circled vertex diagrams $q = 1, 2, ..., s$ and a trilinear insertion of μ vertex on scalar line.*

For each (and every) particular choice of ν vertex insertion on the initial fermionic p-leg, there can be $s+1$ possible (schematically) ways in which the new μ vertex can be inserted

on the internal scalar p-leg. Among these $s + 1$ number of ways, there are s number of ways in which the new μ insertions can be represented by circled vertices for $q = 1, 2, ..., s$ (a typical diagram is shown in left panel of Fig. 6.13); and one trilinear μ vertex insertion (shown in right panel of Fig. 6.13) where the new trilinear μ is inserted immediately to the right of the vertex X.

The contribution of the initial fermionic line from all the possible insertions of the new ν vertices (from K photon) can be evaluated analogously to the case of thermal fermionic QED. After using generalized Feynman's identities, we find the corresponding sub-contributions have pairwise cancellations among themselves, leaving behind a single term which is proportional to the lower order initial fermionic p-leg contribution. The higher order contribution is hence expressed as,

$$
\begin{aligned}
k_\nu\, C_{r+1}^{\text{fermion } p;\, \nu} &= (-1)^{(t_\nu+1)} \delta_{t_\nu, t_X} \left\{ \bar{u}_{q'} \Gamma_X F_{p+\Sigma_r}^{t_X, t_r} \gamma_{\nu_r} \cdots (\text{no } k)\, u_p \right\}\,, \\
&= (-1)^{(t_\nu+1)} \delta_{t_\nu, t_X}\, C_r^{\text{fermion } p}\,.
\end{aligned}
\tag{6.68}
$$

The above Eq. 6.68 is an exact analogue of Eq. 4.20. And, for the insertions of μ vertices on the internal scalar p-leg, using Eq. 6.6 we can write the full contribution of K photon insertion between initial fermionic and internal scalar leg as,

$$
\begin{aligned}
k_\mu k_\nu\, C_{s+1}^{\text{scalar } p;\, \mu}\, C_{r+1}^{\text{fermion } p;\, \nu} &= \left[k_\mu\, C_{s+1}^{\text{scalar } p;\, \mu} \right] \left[(-1)^{(t_\nu+1)} \delta_{t_\nu, t_X}\, C_r^{\text{fermion } p} \right]\,, \\
&= (-1)^{(t_\mu+1)} (-1)^{(t_\nu+1)} \times C_r^{\text{fermion } p} \times \\
&\quad \left[\left\{ \sum_{q=1}^{s} \delta_{t_\nu, t_X} [\mathcal{U}]_{q+1} \left[\delta_{t_\mu, t_q} S_{P+\Sigma_q}^{t_{q+1}, t_q} \left(2P + 2\Sigma_{q-1} + l_q \right)_{\alpha_q} - \right. \right. \right. \\
&\qquad \left. \delta_{t_\mu, t_{q+1}} S_{P+\Sigma_q + k}^{t_{q+1}, t_q} \left(2P + 2\Sigma_{q-1} + 2k + l_q \right)_{\alpha_q} \right] \left\{ S_{P+\Sigma_{q-1}+k}^{t_q, t_{q-1}} \cdots S_{P+k}^{t_1, t_X} \right\} \right\} \\
&\qquad \left. + \left\{ [\mathcal{U}]_{q+1} S_{P+\Sigma_q}^{t_{q+1}, t_q} \cdots (2P + l_1)_{\alpha_1} \left[\delta_{t_\mu, t_X} \delta_{t_\nu, t_X} S_P^{t_1, t_X} - \delta_{t_\mu, t_1} \delta_{t_\nu, t_X} S_{P+k}^{t_1, t_X} \right] \right\} \right]\,, \\
&\equiv \left[\left\{ \sum_{q=1}^{s} C_1^{q;\, \text{sf}} \right\} + \left\{ C_2^{\text{sf}} \right\} - \left\{ C_3^{\text{sf}} \right\} \right] C_r^{\text{fermion } p}\,.
\end{aligned}
\tag{6.69}
$$

In the above expression of Eq. 6.69, the $\sum_{q=1}^{s} C_1^{q;\,\text{sf}}$ correspond to the terms which are inside the first curly braces of second line of Eq. 6.69 and arises due to summing over the sub-contributions of all the circled insertions. The C_2^{sf} and C_3^{sf} represent the terms in the second curly braces of Eq. 6.69 and arise due to the trilinear μ insertion sub-contribution. The particular expressions for C_2^{sf} and C_3^{sf} are respectively given by,

$$C_2^{\text{sf}} = (-1)^{(t_\mu+1)}(-1)^{(t_\nu+1)} \left\{ \left[\delta_{t_\mu, t_X} \delta_{t_\nu, t_X} \right] S_{P+\Sigma_q}^{t_{q+1}, t_q} \left(2P + 2\Sigma_{q-1} + l_q \right)_{\alpha_q} \cdots S_P^{t_1, t_X} \right\},$$

$$-C_3^{\text{sf}} = -(-1)^{(t_\mu+1)}(-1)^{(t_\nu+1)} \left\{ \left[\delta_{t_\mu, t_1} \delta_{t_\nu, t_X} \right] S_{P+\Sigma_q}^{t_{q+1}, t_q} \left(2P + 2\Sigma_{q-1} + l_q \right)_{\alpha_q} \cdots S_{P+k}^{t_1, t_X} \right\}, \quad (6.70)$$

where both in Eq. 6.69 and Eq. 6.70, the 'sf' superscript on the final contributions suggest that these contributions are the result of the two ends of the K photons being shared among internal scalar and initial fermionic p-leg (*i.e.*, scalar-fermion insertions and thus suggesting superscript of 'sf').

Hence, using the results of Eq. 6.69, and plugging the result back in the Eq. 6.67 we find the total higher order matrix element corresponding to the K photon insertion ends on the internal scalar line and initial fermionic p leg can be expressed as,

$$\mathcal{M}_{n+1}^{K\gamma,\,p,p} \big|_{\text{scalar, fermion}} \sim \int \frac{\mathrm{d}^4 k}{(2\pi)^4} b_k(p,p) \left[C_u^{\text{fermion } p'} \right] \times \left\{ \sum_{q=1}^{s} C_1^{q;\,\text{sf}} + C_2^{\text{sf}} - C_3^{\text{sf}} \right\}$$

$$\times \left[C_r^{\text{fermion } p} \right] [-iD^{t_\mu, t_\nu}] \times \mathcal{D}_n . \quad (6.71)$$

Comparing Eq. 6.67 with Eq. 6.63; and also comparing final results of Eq. 6.71 with Eq. 6.66 we find that the same overall factors have been suppressed in the above expression.

We also observe that the total contribution of '$\mathcal{M}_{n+1}^{K\gamma,\,p,p} \big|_{\text{scalar, fermion}}$' of Eq. 6.71 exactly cancels against the '$\mathcal{M}_{n+1}^{K\gamma,\,p,p} \big|_{\text{scalar}}$' contribution of Eq. 6.66. The similar colour coded sub-contributions of these full contributions exactly cancel among themselves. The exact nature of the cancellation is rather intricate and demands a full discussion, which is

elaborated in the following paragraph.

Nature of the double-cancellation for both the ends of K photon being inserted on initial p-leg

☞ The s number of the terms in the contribution $C_1^{q;\mathrm{sf}}$ of Eq. 6.71, exactly cancels against the s number of terms $-C_1^{q;\mathrm{ss}}$ of Eq. 6.66. We have to remind ourselves that, the $-C_1^{q;\mathrm{ss}}$ arose from the sub-contributions which were proportional to $M_{q\mu} \times (-N_0)$ (from Eq. 6.45); suggesting that ν insertion of the K photon insertion was fixed as ν_1 circled vertex (just to the immediately right of vertex X) and all the other possibilities of μ insertions on scalar line as circled vertices were then summed up, leading to the s number of contributions $-C_1^{q;\mathrm{ss}}$. Whereas, the $C_1^{q;\mathrm{sf}}$ has a quite different origin. $C_1^{q;\mathrm{sf}}$ resulted from the contributions for which all the possibilities of the ν vertex insertions on the initial fermionic p-leg were summed up, resulting in pairwise cancellation of terms and producing a remnant surviving term from the ν insertion being immediately to the left of vertex X and is proportional to δ_{t_ν, t_X}. Then all the contributions of possible circled μ insertions on the internal scalar have been summed up leading to $C_1^{q;\mathrm{sf}}$. Therefore, this cancellation actually signifies the cancellation of s set of terms, among which for one set the ν insertion was situated immediately right of vertex X, and for the other set ν insertion was situated immediately left of vertex X. Hence, the cancellation is among the s set of contributing terms from across the vertex X; between the insertions of initial fermionic and internal scalar line. The origin of this cancellation is quite intricate and is *independent of the exact form of the interaction vertex X*.

☞ The C_2^{sf} contribution of Eq. 6.71, exactly cancels against $-C_2^{\mathrm{ss}}$ contribution of Eq. 6.66. Both the terms were proportional to the lower order contribution, but were having very different origin. The C_2^{sf} resulted from a sub-contribution where both the ν (on initial fermionic leg) and μ (on internal scalar line) are trilinear insertions, and are situated immediately adjacent (respectively left and right) of vertex X, producing a term proportional

to $[\delta_{t_\mu,t_X}\delta_{t_\nu,t_X}]$ times lower order matrix element. Whereas, $-C_2^{\rm ss}$ resulted from a surviving sub-contribution, when the $_\nu\mu$ circled vertex was situated immediately left of vertex V, producing a term proportional to $[\delta_{t_\mu,t_V}\delta_{t_\nu,t_V}]$ times lower order matrix element. As both the DM particles are physical and brings in/takes out hard momenta thus the thermal type of vertices V and X can be only of type-1, *i.e.*, $t_V = t_X = 1$. After noting this consideration we find that, $C_2^{\rm sf}$ and $-C_2^{\rm ss}$ exactly cancel between themselves, *irrespective on the exact form of vertex X and V*. This is a very non-trivial case of cancellation, which could not be anyway predicted from either pure fermionic or scalar thermal QED.

☞ The $-C_3^{\rm sf}$ contribution of Eq. 6.71 and the $C_3^{\rm ss}$ contribution of Eq. 6.66 exactly cancel among themselves. Both the terms originated as the internal scalar leg was off-shell and both of these surviving terms came out to be proportional to $\left[\delta_{t_\mu,t_1}\delta_{t_\nu,t_X}\right]$ and exactly cancelling each-other.

☞ All the above mentioned double-cancellations (at first having simplification and cancellation among respective (scalar/fermionic) legs, and then cancellation of the remnant surviving terms from initial fermionic and internal scalar contributions again within themselves) are independent of exact form of either vertex V and X, implying a similar nature of cancellation to hold true for a more general theory of charged scalars, charged fermions and neutrals also.

6.6.3 Insertion of both the virtual K photon vertices on the initial fermionic p-leg

The K photon insertion when both the insertion vertices are on the initial fermionic p-leg correspond to the third term of Eq. 6.34. Using the Eq. 6.34 with the Eq. 6.32 and Eq. 6.33 the higher order matrix element in this case, when both vertices of the K photon insertion are on the initial fermionic p-leg can be symbolically written as

$$\mathcal{M}_{n+1}^{K\gamma, p, p}\big|_{\text{fermion}} = (e)^{2n+2}(-i)^{m+2}(-1)^{\sum_{i=1}^{m}(t_i+1)}(-1)^{(t_\mu+1)}(-1)^{(t_\nu+1)}(i)^{m+2} \times \int \frac{\mathrm{d}^4 k}{(2\pi)^4} \times$$

$$b_k(p, p)\left[C_u^{\text{fermion } p'}\right] \times \left[C_s^{\text{scalar } p}\right] \times \left[k_\mu k_\nu C_{r+2}^{\text{fermion } p;\mu\nu}\right] \times \left[-iD^{t_\mu, t_\nu}\right] \times \mathcal{D}_n \, .$$

$$(6.72)$$

Here, we have to note that as the new K photon is only inserted on the initial fermionic p-leg, hence the contribution of final fermionic p'-leg $C_u^{\text{fermion } p'}$ and contribution of internal scalar p-leg $C_s^{\text{scalar } p}$ is left unchanged. Typical diagrams contributing to $k_\mu k_\nu C_{r+2}^{\text{fermion } p;\mu\nu}$ have been shown in Fig. 6.14.
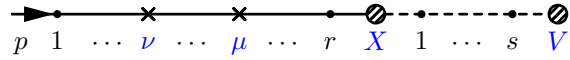
Figure 6.14: *Typical diagram corresponding to both the insertions of K photon being on initial fermionic p-leg. All the set of diagrams, correspond to all the possible insertions of ν and μ vertices, when ν is placed always to the left of μ insertion to avoid double-counting.*

The full contribution of $k_\mu k_\nu C_{r+2}^{\text{fermion } p;\mu\nu}$ would correspond to summing over all the possible diagrams of Fig. 6.14, for all choices of ν and μ, where ν is always situated to the left of μ insertion to avoid double-counting. The effect of photon insertion vertices can be simplified using the generalized Feynman's identities, which will result in a pairwise cancellation of terms, resulting in a final expression proportional to the lower order matrix element (this is exactly analogous to insertion on p-leg for pure fermionic QED, see Ref. [41] and Chapter 4 for details).

But, according to GY Ref. [12] the outermost self-energy diagram on either the initial/final leg has to be removed to account for wave function renormalization. But, as we have not removed any such contribution from final fermionic p'-leg insertions; such contribution of outermost self energy has to be removed from initial (fermionic) p-leg photon insertions.

Taking this into account, the net contribution corresponding to both the ends of K photon being on initial fermionic p-leg turn out to be zero (see Ref. [41] for details),

$$k_\mu k_\nu C_{r+2}^{\text{fermion } p;\mu,\nu} = 0 \; ;$$

$$\text{Hence, } \mathcal{M}_{n+1}^{p,p}|_{\text{fermion}} = 0 \; . \tag{6.73}$$

6.6.4 Final matrix element for both the K photon insertion being on initial p-leg

The total matrix element due to the insertion of the both the ends of the K photon to the initial matrix element hence can be written down as,

$$\mathcal{M}_{n+1}^{K\gamma,\,p,p} = \mathcal{M}_{n+1}^{K\gamma,\,p,p}|_{\text{scalar}} + \mathcal{M}_{n+1}^{K\gamma,\,p,p}|_{\text{scalar,fermion}} + \mathcal{M}_{n+1}^{K\gamma,\,p,p}|_{\text{fermion}} = 0 \; , \tag{6.74}$$

where to obtain the results of Eq. 6.74, we have used the individual results of Eq. 6.66, Eq. 6.71 and Eq. 6.73; and incorporated those in Eq. 6.33 and Eq. 6.32. We have already observed that the contributions $\mathcal{M}_{n+1}^{K\gamma,\,p,p}|_{\text{scalar}}$ and $\mathcal{M}_{n+1}^{K\gamma,\,p,p}|_{\text{scalar,fermion}}$ exactly cancel against each other, from Eq. 6.66 and Eq. 6.71. The contribution $\mathcal{M}_{n+1}^{K\gamma,\,p,p}|_{\text{fermion}}$ also vanishes according to Eq. 6.73. Hence, the total contribution of the matrix element $\mathcal{M}_{n+1}^{K\gamma,\,p,p}$ due to insertion of K photon solely on the initial p-leg turns out to be zero.

We must understand here that this result of $\mathcal{M}_{n+1}^{K\gamma,\,p,p}$ being equal to zero is due to the fact that the outermost self-energy correction from initial (fermionic) p-leg was removed to account for the wave function renormalization rendering $\mathcal{M}_{n+1}^{K\gamma,\,p,p}|_{\text{fermion}}$ to vanish (rather than producing a term being proportional to lower order matrix element), giving rise to results of Eq. 6.74. As in any case, whether the outermost self energy contribution is discounted or not, the contributions of $\mathcal{M}_{n+1}^{K\gamma,\,p,p}|_{\text{scalar}}$ and $\mathcal{M}_{n+1}^{K\gamma,\,p,p}|_{\text{scalar,fermion}}$ would have exactly canceled between themselves; thus discounting the outermost self energy correction plays a major role implying the result of Eq. 6.74.

Now, as neither of the initial p-leg or the final p'-leg is fundamentally more important than the other one, thus the compensation of outer most self energy insertion to account for wave function could have happened for p'-leg (for K photon insertion being solely on final fermionic p'-leg), refraining any such compensation from the initial p-leg. In that case the results of $\mathcal{M}_{n+1}^{K\gamma,p,p}$ Eq. 6.74, and $\mathcal{M}_{n+1}^{K\gamma,p',p'}$ Eq. 6.31 would have switched among themselves (with factor of $b_k(p',p')$ of Eq. 6.31 be replaced by $b_k(p,p)$ in Eq. 6.74).

Therefore it is necessary and convenient to symmetrize the results of both the K photon insertion being on the final p'- leg Eq. 6.31 and the results of both the K photon insertion being on the initial p- leg, Eq. 6.74 among themselves producing the final results,

$$
\begin{aligned}
\mathcal{M}_{n+1}^{K\gamma,p',p'} &= +\frac{ie^2}{2} \int \frac{\mathrm{d}^4 k}{(2\pi)^4} \, \delta_{t_\mu,t_1} \, \delta_{t_\nu,t_1} \, b_k(p',p') \, D^{t_\mu,t_\nu}(k) \, \mathcal{M}_n \, ; \\
\mathcal{M}_{n+1}^{K\gamma,p,p} &= +\frac{ie^2}{2} \int \frac{\mathrm{d}^4 k}{(2\pi)^4} \, \delta_{t_\mu,t_1} \, \delta_{t_\nu,t_1} \, b_k(p,p) \, D^{t_\mu,t_\nu}(k) \, \mathcal{M}_n \, .
\end{aligned}
\tag{6.75}
$$

Note the existence of extra $1/2$ factors in the above expressions resulting from the symmetrization procedure.

6.7 The total contribution due to virtual K photon insertions

Using the results of Eq. 6.30, Eq. 6.75 the total contribution of inserting a K photon in all possible ways to n^{th} order process related to $\chi(q+q') \, f(p) \rightarrow \chi(q') \, f(p')$ can be expressed as,

$$
\begin{aligned}
\mathcal{M}_{n+1}^{K\gamma,\,\text{tot}} &= \frac{ie^2}{2} \int \frac{\mathrm{d}^4 k}{(2\pi)^4} \left\{ \delta_{t_\mu,t_1} \, \delta_{t_\nu,t_1} \, D^{t_\mu,t_\nu}(k) \left[b_k(p',p') + b_k(p,p) \right] \right. \\
&\quad \left. + \, \delta_{t_\mu,t_V} \, \delta_{t_\nu,t_V} \, D^{t_\mu,t_\nu}(k) \left[-2 b_k(p',p) \right] \right\} \mathcal{M}_n \, , \\
&\equiv [B] \, \mathcal{M}_n \, ,
\end{aligned}
\tag{6.76}
$$

169

where in the above expression of Eq. 6.76, all the effects due to K photon insertion containing all the IR divergences have been factorized and collected in B. The expression of B is defined as,

$$
\begin{aligned}
B &= \frac{ie^2}{2} \int \frac{\mathrm{d}^4 k}{(2\pi)^4} \, D^{11}(k) \left[b_k(p', p') - 2b_k(p', p) + b_k(p, p) \right], \\
&\equiv \frac{ie^2}{2} \int \frac{\mathrm{d}^4 k}{(2\pi)^4} \, D^{11}(k) \left[J^2(k) \right].
\end{aligned}
\tag{6.77}
$$

We find B and thus the higher order matrix element $\mathcal{M}_{n+1}^{K\gamma,\,\mathrm{tot}}$ to be proportional to the (11) component of the photon propagator, *i.e.*, being proportional to $D^{11}(k)$. This dependence on $D^{11}(k)$ arose as all the hard/external physically observable particles must be of type-1, constraining '$t_V = t_1 = 1$'. We will see the matrix element $\mathcal{M}_{n+1}^{K\gamma,\,\mathrm{tot}}$ for virtual K photon insertion being proportional to the $D^{11}(k)$ component of thermal photon propagator will play a crucial role in obtaining cancellation of the IR divergent pieces between virtual and real soft photon contributions.

It has to be also noted that, the result of Eq. 6.76 is independent of whether the lower order diagram has one or more already existing K, G or real photon insertions. The result does not also depend on whether the lower order matrix element have already existing quadrilinear (seagull/tadpole) insertions, as those insertions only behave like inert vertices (as we have already discussed in Chapter. 5) and any new K photon would not be able to get inserted at those quadrilinear vertices. Hence, the effect of having quadrilinear vertices will be to having some extra inert multiplicative factors in the matrix element, which will be carried along while performing the factorization, without spoiling any feature of the factorization that we have discussed so far. We can also have some disallowed diagrams on the fermion legs in lower order (according to GY) contribution, which may become allowed diagrams in higher order contribution (analogous to Subsection. 5.2.6 of Chapter 5 but involving fermions). Following an analogous procedure of Chapter 5 but now for the disallowed diagrams being situated on fermionic legs, we find the contributions of those terms to drop off for this case of thermal theory of DM also.

6.8   The total matrix element for the virtual photon insertions

Before moving on to calculating the total matrix element due to the virtual photon insertion, we would like to mention here that the G photon contributions again turn out to be IR finite. The leading IR behaviour of G photons (leading logarithmic due to zero temperature part, and leading linear and sub-leading logarithmic due to finite temperature) are similar for both G photon insertions being on either scalar or fermionic leg or a mixture of scalar and fermion leg. These leading IR behaviour of the G photon contribution vanishes due to choice of b_k at finite temperature as in the Chapter 5 and Chapter 4. Now, we can get additional intricate IR structure due to presence of thermal scalars, and there can be divergent sub-diagrams spanning fermionic, scalar or both scalar and fermionic leg. Analogous to Section. 5.3 at first identifying skeletal graph, and then symmetrizing over the controlling sets of momenta of those skeletal graphs, removes any kind of apparent IR divergences for this case concerning theory of DM also (the whole process proceeds exactly analogous to the process for scalar QED at finite temperature as in Section 5.3, and we have refrained here from discussing same arguments and subtleties to avoid unnecessary repetitions).

We use here the fact that the G photon contributions are IR finite, and all the IR divergences are contained inside K photon insertions. The IR divergent pieces factor out according to Eq. 6.76, and the higher order K photon contribution becomes proportional to the lower order matrix element. A fully virtual n^{th} order diagram contributes a factor of 'α^n' (or 'e^{2n}') at the leading order. Therefore, there are always n number of virtual photons associated with fully virtual diagrams. But, due to GY photon polarization sum rearrangement, all the virtual photons should be re-written in terms of K and G photon polarization sums. Hence, if an nth order diagram consists of n_K number of virtual K photons and n_G number of virtual G photons, then $n = n_K + n_G$. Due to the Bose symmetry related to n number

of photons, each distinct class of diagram (having n_k number of K photon and n_G number of G photon) can arise in $n!/(n_K!\,n_G!)$ ways. Therefore, the full matrix element for virtual photon insertions can be expressed as a summation of all possible individual terms,

$$\frac{1}{n!}\mathcal{M}_n = \sum_{n_K=0}^{n} \frac{1}{n_K!}\frac{1}{n-n_K!}\mathcal{M}_{n_G,n_K}\ . \tag{6.78}$$

Therefore, summing over to all orders, the above expression becomes,

$$\sum_{n=0}^{\infty}\frac{1}{n!}\mathcal{M}_n = \sum_{n=0}^{\infty}\sum_{n_K=0}^{n} \frac{1}{n_K!}\frac{1}{n-n_K!}\mathcal{M}_{n_G,n_K}\ ,$$

$$= \sum_{n_K=0}^{\infty}\sum_{n_G=0}^{\infty} \frac{1}{n_K!}\frac{1}{n_G!}\mathcal{M}_{n_G,n_K}\ . \tag{6.79}$$

Using the fact that the contributions of the K photons factor out according to Eq. 6.76, the expression of Eq. 5.39 can be further simplified as,

$$\sum_{n=0}^{\infty}\frac{1}{n!}\mathcal{M}_n = \sum_{n_K=0}^{\infty} \frac{(B)^{n_K}}{n_K!} \sum_{n_G=0}^{\infty} \frac{1}{n_G!}\mathcal{M}_{n_G}\ ,$$

$$= \mathrm{e}^{B} \sum_{n_G=0}^{\infty} \frac{1}{n_G!}\mathcal{M}_{n_G}\ , \tag{6.80}$$

where all the IR divergent pieces have been exponentiated and resummed in Eq. 6.80.

6.9 The total cross section to all orders for thermal theory of Dark Matter

We will at first discuss about the real photon insertions here briefly, for sake of completeness. The real $\widetilde{K}$ and $\widetilde{G}$ photon insertion results, follow calculations exactly analogous to the cases as mentioned in Section 5.5 and Section 5.6. One of the main differences for real photon cases in the thermal field theory is that, in addition to the emission of real photons into heat bath the real photons can also be absorbed from the heat bath with corresponding

phase space factor,

$$d\phi_i = \frac{d^4 k_i}{(2\pi)^4} \, 2\pi\delta(k_i^2) \left[\theta(k_i^0) + N_{\mathrm{B}}(|k_i^0|) \right] , \tag{6.81}$$

where $N_{\mathrm{B}}(|k_i^0|)$ corresponds to the distribution function for boson (photon) at finite temperature, and $k_i^0 > 0$ correspond to real photon emissions and $k_i^0 < 0$ correspond to cases of real photon absorption. The real photon also brings in/takes out finite photon physical momenta and thus can only be of thermal type-1 only. After taking account of all these facts, the $\widetilde{K}$ photon calculation can be performed with exact analogy of virtual K photon calculation, after writing down the polarizations of emitted or absorbed photons in accordance with GY prescription of Eq. 4.5. But, now the factorization of $\widetilde{K}$ photon occurs only in the square of matrix element level, and in $\tilde{b}_k(p_f, p_i)$, the momenta p_f and p_i correspond to the momenta of the particular leg of nth order diagram, in which the real photon insertions are present respectively in the matrix element, and in the adjoint matrix element. The calculation of $\widetilde{K}$ photon is much simpler than the K photon calculations, as tadpole diagrams cannot be present in the current $\widetilde{K}$ photon (as real photon carries in/takes out physical momenta). Therefore the full contribution of the $\widetilde{K}$ photon insertions can be factorized in the cross section rather than in the matrix element itself and is expressed as,

$$\left| \mathcal{M}_{n+1}^{\widetilde{K}\gamma,\text{tot}} \right|^2 \propto - e^2 \left[\tilde{b}_k(p, p) - 2\tilde{b}_k(p', p) + \tilde{b}_k(p', p') \right] \times \left| \mathcal{M}_n \right|^2$$
$$\equiv - e^2 \widetilde{J}^{\,2}(k) \left| \mathcal{M}_n \right|^2 , \tag{6.82}$$

where all the IR divergences are again factored out in the $\widetilde{J}^{\,2}(k)$ in the above expression. This IR divergent factor then can be exponentiated after manipulation of the momentum conserving delta function,

$$(2\pi)^2 \delta^4 \left(p + q - p' - \sum_{m=1}^{r} (-1)^m k_m \right) , \tag{6.83}$$

in a process analogous to Section. 5.6, producing an exponentiation where the exponent contains the IR divergent term (analogous to Eq. 5.49),

$$\widetilde{B}(x) = -e^2 \int \widetilde{J}^2(k_m) \mathrm{d}\phi_m \exp\left[\pm i\, k_m \cdot x\right] \ . \tag{6.84}$$

In the above expression, the ± signs respectively correspond to real photon emission and absorption. Eq. 6.84 is the real photon analogue of Eq. 6.77 (except that $\widetilde{B}$ arises in the cross section level, but exponentiation of B happens in matrix element level).

The $\widetilde{G}$ photon contribution again turn out to be IR finite after using the fact that the thermal phase space is symmetric in finite temperature, with exact analogy to Subsection 5.5.2 of thermal scalar QED.

Therefore, the all order corrections in perturbation theory related to the tree level cross section of $\chi(q+q')\, f(p) \to \chi(q')\, f(p')$, in thermal theory of dark matter including both the virtual and real (soft emission/absorption) photon contributions, result in an expression of the total cross section for this process as below,

$$
\begin{aligned}
\mathrm{d}\sigma^{\mathrm{tot}} &= \int \mathrm{d}^4 x\, e^{-i(p+q-p')\cdot x} \mathrm{d}\phi_{p'} \exp\left[B+B^*\right] \exp\left[\widetilde{B}\right] \times \\
&\qquad \sigma_G^{\mathrm{virtual}} \sum_{n_G=0}^{\infty} \frac{1}{n_G!} \prod_{j=0}^{n_G} \times \int \mathrm{d}\phi_j\, e^{\pm i k_j \cdot x} \left[-\widetilde{G}_{\mu\nu} \left|\mathcal{M}_{n_G}^{\mu\nu,\tilde{G}\gamma,tot}\right|^2\right] , \\
&= \int \mathrm{d}^4 x\, e^{-i(p+q-p')\cdot x}\, \mathrm{d}\phi_{p'} \exp\left[B+B^*+\widetilde{B}\right] \sigma^{\mathrm{finite}}(x) \ . \tag{6.85}
\end{aligned}
$$

We note here that, symbolically the Eq. 6.85 looks exactly similar to the expression of Eq. 5.51; but we must stress here that, the actual explicit factors corresponding to the IR finite pieces of the matrix elements of Eq. 6.85 and Eq. 5.51 are quite different and explicitly dependent on the relevant interaction Lagrangian for the processes.

In the above expression of Eq. 6.85, the 'σ^{finite}' factor contains *all* the IR finite pieces arising from the virtual G and the real $\widetilde{G}$ photon contributions. In Eq. 6.85 *all* the IR divergent pieces coming from both the virtual and real photon insertion are found to be

exponentiated in the factors '$\exp[B + B^*] \times \exp\left[\widetilde{B}\right]$' and *these contributions combine together to produce an IR finite sum*, as can be shown by studying the small-k behaviour of these terms,

$$
\begin{aligned}
(B + B^*) + \widetilde{B} = e^2 \int \mathrm{d}\phi_k \Bigg[& J(k)^2 \left\{1 + 2N_{\mathrm{B}}(|k^0|)\right\} \\
& -\widetilde{J}(k)^2 \left\{\left(1 + N_{\mathrm{B}}(|k^0|)\right) e^{ik\cdot x} + N_{\mathrm{B}}(|k^0|)e^{-ik\cdot x}\right\} \Bigg] \\
& \xrightarrow{k\to 0} \; 0 + O(k^2) \, .
\end{aligned}
\tag{6.86}
$$

In the above expression, we have inserted the explicit expressions of J^2 and $\widetilde{J}^2$ respectively using the results of Eq. 6.77 and Eq. 6.82, to find that the IR divergent pieces cancel among the virtual and real (soft) photon contributions, making the total cross section IR finite. Both the absorption and the emission of the real photons with respect to heat bath were *necessary* to obtain this IR finite result. We also note that the cancellation resulted as both the final form of matrix element of virtual and real photon contributions turned out to be proportional to thermal type-1 of thermal photons. Here, we have thus demonstrated the proof of IR finiteness of a theory of dark matter interacting with charged fermions and scalars at finite temperature to all orders in perturbation theory.

6.10   Summary

In this chapter, we have focused our attention on a simplified theory of dark matter (DM) interacting with charged scalars and fermions at finite temperature. We have chosen the DM to be a Majorana charge-less particle (bino-like in the context of the minimal super-symmetric model, MSSM) motivated by the WIMP (weakly interacting massive particle) paradigm. The IR structure of this model can be successfully related to the IR structures of other wide-spread relevant models of DM also in the WIMP paradigm.

Particularly, here we assume the DM mass to be in a ballpark so that the freeze-out happens

after the electroweak phase transition, making electromagnetic interactions to be of prime importance while estimating the relic density. To observe the IR structure of the theory of DM, we start by inspecting the effect of adding virtual and real photons in rearranged K and G polarization sums as prescribed by the Grammer and Yennie (GY) procedure, to n^{th} order diagrams related to processes determining relic density. We particularly chose the nth order diagram related to the process $\chi f \to \chi f$ (mediated by an internal heavy charged scalar ϕ) where χ is the DM candidate and f belongs to the Standard Model (SM) fermion doublet.

We identify the special interaction vertex and unambiguously separate out the initial and final leg (to carry out the GY procedure) such that the outgoing SM fermionic leg becomes the final p'-leg; and the incoming SM fermionic and internal scalar line constitute the initial p-leg. We then examine in detail the effect of adding an additional virtual photon, of either K or G type, to the nth order diagram. In each case, we find that the IR divergences are contained in the K photon contributions and they factor out so that they are proportional to the lower (n^{th}) order matrix element. In contrast, the G photon insertions give finite contributions.

The result of K photon insertions, where the ends of virtual photon are solely on final p'-leg follows trivially according to pure fermionic QED results. The K photon insertion, where the two ends of the virtual photon are inserted, one on the p and the other on the p'-leg, is rather non-trivial, and consist of two distinct classes of diagrams (*i.e.*, scalar(p)-fermion(p') and fermion(p)-fermion(p') classes) depending on whether the vertex on the p-leg is inserted on the scalar or initial fermion line. After using the notion of circled vertices, the contributions of these two distinct classes are shown to have a non-trivial double-cancellation of sub-contributions among themselves, finally producing a result proportional to lower the order matrix element. The K photon insertion, where the ends of the virtual photon are solely on the p-leg is the most non trivial one, and consists of three distinct classes of diagrams (*i.e.*, scalar(p)-scalar(p), scalar(p)-fermion(p)

and fermion(p)-fermion(p) classes, since each vertex can be inserted either on the scalar or initial fermion line). Among these three classes the contribution (scalar(p)-scalar(p)) for which both the ends of the K photons are inserted on the internal scalar leg is the most difficult one. In this case the number of diagrams proliferate extensively as the tadpole diagrams are also allowed. After avoiding any potential double counting of the diagrams, the contributions were grouped into four distinct sets Set I, II, III and IV for better management of the IR structure. The different sub-contributions among these sets were found to cancel among themselves, resulting in the total contribution from Set II and Set III to vanish. Only some sub-contributions from Set I and Set IV survive this cancellation, and result in the final expression for scalar(p)-scalar(p) insertion classes. But these remnant contributions were then found to *exactly* cancel against the contributions of scalar(p)-fermion(p) classes of diagrams, via a very intricate double-cancellation. The contribution of fermion(p)-fermion(p) classes of diagrams turn out to be zero, after discounting outermost self energy correction for wave function renormalization. After symmetrizing the results of K photon being inserted on solely the final p'-leg and being inserted solely initial p-leg, the total matrix element turns out to be proportional to the lower order matrix element with all the IR divergent terms resulting due to K photon contribution factorized and exponentiated.

The non-trivial double cancellations mentioned above were found to be independent of any explicit structure of DM-fermion-scalar interaction vertex. This implies the factorization and resummation of the IR divergence were independent of the particular choice of the model, and can be generalized to a full theory of neutrals interacting with charged scalars and fermions.

The seagull and tadpole diagrams again played an *indispensable* role, cancelling respectively the linearly k dependent and quadratic k dependent finite terms. Without cancellation of these terms a neat and *exact* IR factorization for the theory of DM would be impossible.

Again, as in the previous cases of field theories at finite temperature, real photons can both be emitted into and absorbed from the heat bath with different weighted phase space factors. The real $\widetilde{G}$ photon insertion contributions to the cross section also turn out to be IR finite, after considering the concerned thermal part of the phase space being symmetric in real photon exchange. The real $\widetilde{K}$ contributions to the cross section were found to contain all the IR divergent pieces for the real photon insertions just like the virtual K photon contributions. In addition, the IR divergent pieces due to virtual K and real $\widetilde{K}$ photon insertions cancel among each other. *Only after including* both the emission and absorption of real thermal photons from heat bath, this cancellation of IR divergent pieces were found to hold, making the total cross-section of the concerned theory IR finite. Hence the total cross section for the thermal field theory of dark matter interacting with charged scalars and fermions turns out to be IR finite to all orders in perturbation theory.

Chapter 7

Conclusion

This thesis is concerned with the infra-red (IR) behaviour of some field theories at finite temperature. In particular, we focused on the IR behaviour in the context of a model of dark matter (DM), where DM is a bino (bino-like) particle interacting with charged scalars and charged fermions via Yukawa interaction, motivated by the WIMP (weakly interacting massive particle) paradigm. We assume DM was thermally produced in the early universe, and stayed in equilibrium with the background plasma until the 'freeze-out' scenario occurred. Thus, the thermal effects play a crucial role to determine the present day relic density of DM. But, to coherently predict the relic density of DM from the theory, a complete understanding of the IR structure of the corresponding theory at finite temperature is unavoidable. Hence, we proceed to inspect the IR structure of the relevant model of DM at finite temperature. At the temperatures of interest, this involves the study of purely electro-magnetic contributions to processes such as the annihilation or scattering of the dark matter particles, χ, into standard model fermions, such as $\chi\bar{\chi} \leftrightarrow f\bar{f}$ or $\chi f \leftrightarrow \chi f$. For this study, it was important to first study the thermal theory of purely scalar QED (that of fermionic QED is already known) and apply these results to the case of DM. We established that these processes are infra-red finite to all orders in perturbation theory.

After a quick introduction, motivating the general features of field theories at finite tem-

perature, we moved on to discuss the real time formulation of thermal field theory. We briefly discussed the aspects of real time formulation of thermal field theory, necessary for calculations in this thesis. We observed that the IR structures became more intricate and divergent (especially for bosons) for theories at finite temperature. To analyze the IR structure of the corresponding theory we applied the prescription proposed by Grammer and Yennie (GY) [12]. The original technique of GY was proposed for field theories at zero temperature.

After reviewing the technique for zero temperature field theory (particularly for fermionic QED at zero temperature), we proceeded to tame the IR divergences at finite temperature. The IR structure of relevant theories at finite temperature is far more intriguing. Due to the presence of photons (bosons) the leading IR divergence becomes linear at finite temperature in contrast to the leading logarithmic dependence at zero temperature. In addition to this, there are also additional sub-leading logarithmic IR divergences arising from the thermal fluctuations, apart from the original leading logarithmic IR divergences arising from quantum fluctuations. Furthermore, being in the presence of heat bath, now apart from the usual emission of real photons at higher order, the absorption of real photons from the heat bath is also allowed. Both emission to and absorption of the real photons with respect to heat bath occur with different thermal phase space factors. To account for all of these intricacies at finite temperature, the original prescription of GY technique was extended to finite temperature case as in Ref. [41].

After showing that the extension of GY techniques was capable to uniquely and unambiguously capture the IR finite and divergent pieces, the extended technique was used to shed light upon the IR structure of thermal scalar QED, and thermal theory of dark matter. The theory of scalar QED (or for any theory, where charged scalars are involved, be it at zero/finite temperature) is much more difficult to tackle, as the theory now admits, in addition to normal trilinear (scalar-photon-scalar) interaction contributions, quadrilinear contributions (seagull insertions and tadpole diagrams) also. After proving the general-

ization of Feynman identities holding true for thermal theory of scalars, we grouped the trilinear and quadrilinear contributions into 'circled vertices', which helped us to coherently manage the proliferation of numbers of diagrams at higher orders. We used the technique of GY at finite temperature for scalar QED, to find out that all the virtual K photon contribution gets factorized as an IR divergent contribution times the lower order matrix element. The seagull and tadpole contributions played a crucial role to obtain this exact factorization. They particularly cancel some IR finite terms linear and quadratic in photon momentum. Without the exact cancellation of these terms (by virtue of seagull and tadpole contributions) such a neat and exact factorization would be impossible to attain. We found the virtual G photon contributions to be IR finite. The real $\widetilde{K}$ photon contributions also factorized out of the cross section. The $\widetilde{G}$ photon contributions turned out to be IR finite using the symmetric property of thermal part of the phase space. All the IR divergences were found to be contained in virtual K photon and real $\widetilde{K}$ photon contributions. The IR divergences of these virtual and real contributions were found to cancel among themselves while taking the soft limit for photons, to all orders in the theory.

After proving the IR finiteness of the thermal charged scalar QED, and noting down the existing results on the IR finiteness of thermal fermionic QED [41] we proceeded to study the IR finiteness of a theory of DM interacting with charged scalars and fermions at finite temperature. This was motivated by the calculation to NLO of the thermal corrections to the relevant cross sections for DM annihilation in a bino-like theory in Ref. [86]. This is an important process since the experimental evidence in favor of the existence of dark matter has only been perceived through the gravitational effects in different length scales. Thus the estimation of theoretical predictions of relic density of present day DM content in the cosmological scale is of utmost importance, and this has to be in conjunction with the current experimental constraints. In this theory, the DM candidate freezes out after the electro-weak transition (the temperature at freeze-out being of the order of $m_\chi/20$, where m_χ is the DM mass). At this scale, only electromagnetic interactions are of prime importance in the inspection of the IR structure at finite temperature. Hence we studied

the purely electro-magnetic all-order corrections to these DM scattering and annihilation processes, thereby extending the IR-finiteness results obtained to NLO in Ref. [86] to all orders in the theory. Some of the proof details are outlined as follows:

We used the extension of GY technique at finite temperature, to correctly identify the hard vertex separating out the initial and final leg contributions. The GY reduction for the theory of DM, provides us with similar results, where K and $\widetilde{K}$ photon contributions get factored out (respectively at matrix element and cross section level), and contain all the IR divergent pieces. The G and $\widetilde{G}$ photon contributions again turn out to be IR finite. We have to note here that, while performing the IR factorization of the K and $\widetilde{K}$ photon contributions we found some non-trivial 'double-cancellation' among the sub-contributions; some of which cannot by any means be predicted from the individual results of thermal pure scalar or pure fermionic QED. We found these non-trivial 'double-cancellation' leading to factorization and finally resummation of IR divergent pieces, to be blind to (and hence independent of) the exact form of the scalar-DM-fermion interaction vertex (as in none of the calculations in this thesis we have used any particular explicit form of the scalar-DM-fermion interaction vertex to achieve IR factorization and cancellation). This implies the exact nature of the factorization and exponentiation of IR divergent pieces are much more general and can be applied to general classes of theories, such as the scalar be replaced by a pseudo-scalar, or the DM interaction vertex in addition to CP even term may even have CP odd factors also, there could have been more than one number of neutrals also interacting with charged scalar/fermions in some models of non-renormalizable effective theory of DM, etc. That is, the proof of factorization and resummation (and finally the cancellation) of IR divergent pieces is more generic and can be successfully applied to more general theories, where neutrals, charged scalars, and charged fermions are interacting among themselves. We will again mention here, that the seagull and tadpole contributions for the theory of DM, were again indispensable to obtain the neat factorization and resummations of IR divergent pieces. The IR divergent pieces of K and $\widetilde{K}$ photon contributions were found to cancel among themselves after taking the soft limit for photons. Both for

the scalar QED and theory of DM at finite temperature, this cancellation of the IR divergence could be only obtained after taking into account both the emission/absorption of real photons with respect to the heat bath.

We have discussed about the intricate details of the proof regarding IR structure in the paragraph above, and would like to summarize and list down the key findings of this thesis below for the ease of access of readers.

- We have proved, and found the generic form of generalized Feynman identities (Ward identities) that holds true at finite temperature for the theories involving scalars. These generalized Feynman identities were further used to define 'circled' vertices which helped the grouping of trilinear and quadrilinear contributions in a coherent fashion.

- For both the theory of scalar QED and theory of DM at finite temperature, the quadrilinear seagull and tadpole contributions played a crucial role to factor out the IR divergences leading to resummation. The seagull and tadpole contributions canceled some IR finite sub-contributions, which were respectively linear and quadratic in photon momenta. Although these sub-contributions were IR finite, but without obtaining an exact cancellation of these, IR factorization would become impossible. Hence, in this thesis we discover the vital importance of quadrilinear contributions to obtain the proof of all order IR finiteness for corresponding theories involving scalars.

- For the theory of DM, we have found the IR factorization occurs via non-trivial double-cancellations of sub-contributions. We found the process related to the factorization of IR divergent contributions to be independent of the explicit form of the DM-scalar-fermion interaction vertex. This implies, the final result of the cross-section (which is symbolically written) is valid for a general theory of neutrals interacting with charged scalars and fermions at finite temperature. We want to stress here the fact that the IR finite part of the cross-section will certainly be dependent

on the details of the particular theory, and also will depend on particular processes of interest inside same theory. But, the IR divergent term factorization and resummation (and finally cancellation) are universal at finite temperature.

- After using the GY prescription at finite temperature, we found all the leading linear and sub-leading logarithmic IR divergences due to thermal fluctuation, and all the leading logarithmic IR divergences from zero temperature quantum fluctuation were contained totally in K and $\widetilde{K}$ photon contributions. The contributions of G and $\widetilde{G}$ photon insertions were found to be IR finite.

- The closed form expression of the (symbolically written) final total cross-section is an exact expression. That is, to obtain the expression no approximation (such as Eikonal approximation etc) scheme were used. Hence, this expression can be expanded order by order in perturbation theory to obtain higher orders of IR finite pieces of cross-section at finite temperature.

- Both the real photon emission to and absorption from the heat bath played a crucial role to cancel the IR divergent contributions between virtual and real (soft) photon contributions. Therefore, the absorption of real photons must be included (in addition to emission of real photon) at finite temperature to obtain cancellation of IR divergences.

- Due to the nature of IR factorization and presence of hard observable particle, the virtual photon IR divergent contributions came out to be proportional to only (11) component of the thermal photon propagator. The real photon contributions also being proportional to only (11) component of the propagator, resulted in the cancellation of IR divergent pieces between virtual and real (soft) contribution.

- The IR divergences were found to exactly cancel, after taking the soft limit of the total cross-section of the corresponding theory. At any resolvable photon momenta, from the structure of cross-section, we find that the presence of the heat bath will

be perceptible.

- The virtual and real photon contributions consisted of both the zero and finite temperature pieces. Hence, with this explicit proof of IR finiteness of relevant theory at finite temperature we also implicitly proved the IR finiteness of the same theory at zero temperature.

This proof of IR finiteness was found to be independent of the details of the particular interaction of the current model, and can be extended to other models at finite temperature with presence of other abelian gauge theories (other than electromagnetic interaction).

7.1 Future Directions

Let us now discuss about the future prospects related to results obtained and to the related formalism. We have already seen in the current thesis that the IR divergent pieces factorize and exponentiate to finally cancel among the virtual and real (soft) contributions providing us the IR finite cross-section for relevant theory at finite temperature. We will be very much fascinated to compute the IR finite contributions to cross-section at finite temperature using the current formalism. We are extremely intrigued to investigate the IR finite higher order thermal corrections to the relic abundance of theory of bino (bino-like) DM candidate. These thermal corrections have been already calculated to next-to-leading (NLO) order by Beneke et al. Ref. [86]. As the formalism is quite general, we would like to use it to predict the thermal effects related to other physically relevant quantities in cosmology. We also like to mention here that, throughout the thesis it was considered that the charged scalars and fermions are massive. This approximation is quite appropriate for practical purposes, as the quartic self-interaction which we discounted in the discussions of scalars, always contribute to the scalar mass radiatively in higher orders (making scalar massive); and all the known Standard Model fermions which do interact electromagnetically are all massive (and for the theories of DM, the intermediate scalars

are usually always massive). But, from a purely theoretical point of view, we would be extremely curious to know, whether the current formalism of GY prescription can be extended to include massless charged scalars or fermions, taking care of the related collinear divergences, having a soft-collinear factorization at finite temperature (using a further generalization of the current formalism). These are some open questions that are beyond the scope of this thesis.

We are also interested to investigate the IR structure of non-abelian gauge theories using some generalization of current method. As it is already known that, the intricacies of IR structure for the non-abelian gauge theories are rather nontrivial though; due to the complicated group structure of such theories, along with the presence of self interactions. Such theories can have additional collinear divergences in addition to the soft divergences. A soft-collinear factorization is known to occur for non-abelian theories, particularly at eikonal limit within the framework of soft collinear effective theory (SCET) Ref. [37, 38]. A generalization of the similar factorization using an exact analysis (without going into eikonal limit) for both zero and finite temperature is rather challenging and intriguing, but again is beyond the scope of this thesis.

Appendix A

Feynman rules at finite temperature

We list down the Feynman rules of the relevant theories at finite temperature, for ease of accessibility here. All the Feynman rules have been written down using a metric convention, where $g^{\mu\nu} = \eta^{\mu\nu} = diag(1, -1, -1, -1)$. We have used the real time formulation of thermal field theory, with the symmetric choice of contour, to specify the concerned Feynman rules. All the Feynman rules also have been expressed at zero chemical potential. And, the factors t_a, t_b refer to the thermal types of particles at vertex a and b respectively, thus $t_a, t_b = (1, 2)$ depending on the particular thermal type.

A.1 Feynman rules for the propagators

The thermal scalar propagator for a particle of mass m_ϕ and momentum p is given by,

$$iS^{t_a,t_b}(p, m_\phi) = \begin{pmatrix} \Delta(p) & 0 \\ 0 & \Delta^*(p) \end{pmatrix} + 2\pi\delta(p^2 - m_\phi^2)N_B(|p^0|) \begin{pmatrix} 1 & e^{|p^0|/(2T)} \\ e^{|p^0|/(2T)} & 1 \end{pmatrix}, \quad (A.1)$$

where $\Delta(p) = i/(p^2 - m_\phi^2 + i\epsilon)$, and $N_B(|p^0|)$ is the distribution function for bosons,

$$N_B(|p^0|) \equiv \frac{1}{\exp\{|p^0|/T\} - 1} . \quad (A.2)$$

187

The thermal photon propagator in the Feynman gauge can be written down as,

$$i[D^{\mu\nu}]^{t_a,t_b}(k) = -g^{\mu\nu}iD^{t_a,t_b}(k) \tag{A.3}$$

where k is the photon momentum and

$$iD^{t_i,t_j}(k) = \begin{pmatrix} \Delta(k) & 0 \\ 0 & \Delta^*(k) \end{pmatrix} + 2\pi\delta(k^2)N_{\rm B}(|k^0|)\begin{pmatrix} 1 & e^{|k^0|/(2T)} \\ e^{|k^0|/(2T)} & 1 \end{pmatrix}. \tag{A.4}$$

Here $\Delta(k) = i/(k^2 + i\epsilon)$ for the massless photons, and $N_{\rm B}(|k^0|)$ is the distribution function for photons. Therefore,

$$i[D^{\mu\nu}]^{t_i,t_j}(k) = -g^{\mu\nu}iD^{t_i,t_j}(k) = -g^{\mu\nu}iS^{t_i,t_j}(k,0). \tag{A.5}$$

The thermal propagators for fermions with mass m_f and momentum p can be expressed as,

$$iF^{t_a,t_b}(p,m_f) = \begin{pmatrix} F & 0 \\ 0 & F^* \end{pmatrix} - 2\pi F'\delta(p^2 - m_f^2)N_{\rm F}(|p^0|)\begin{pmatrix} 1 & \epsilon(p_0)e^{|p^0|/(2T)} \\ -\epsilon(p_0)e^{|p^0|/(2T)} & 1 \end{pmatrix},$$

$$\equiv (\not{p} + m_f)\begin{pmatrix} F_p^{-1} & G_p^{-1} \\ -G_p^{-1} & F_p^{*-1} \end{pmatrix}, \tag{A.6}$$

where $F = i/(\not{p} - m_f + i\epsilon)$, and $F' = (\not{p} + m_f)$. From the above expression it can be noted that the full fermion propagator is proportional to $(\not{p} + m_f)$. Here, $N_{\rm F}(|p^0|)$ corresponds to the distribution function for the fermion,

$$N_{\rm F}(|p^0|) \equiv \frac{1}{\exp\{|p^0|/T\} + 1}. \tag{A.7}$$

A.2 The interaction vertex factors

All possible allowed insertion vertices for a theory of fermions and scalars interacting with photons have been shown in Fig. A.1. For the fermions, only trilinear (fermion-photon-fermion) insertion is allowed. For the theories involving scalars, in addition to trilinear (scalar-photon-scalar) insertion vertices, quadrilinear seagull (scalar-scalar- photon-photon) insertion vertices are also allowed.
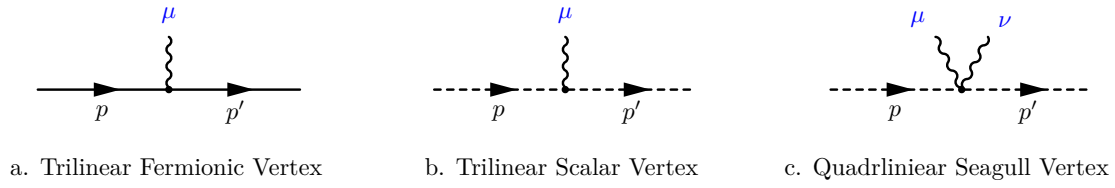

a. Trilinear Fermionic Vertex   b. Trilinear Scalar Vertex   c. Quadrliniear Seagull Vertex

Figure A.1: *All possible allowed insertion vertices for fermions and scalars interacting with photons.*

We note that all particles at a given vertex must be of the same thermal type.

The fermion-photon-fermion trilinear insertion vertex has a contributing factor $(-ie\gamma_\mu)(-1)^{t_\mu+1}$, where $t_\mu = 1, 2$ according to the thermal type (type 1 or 2) of vertices.

The scalar-photon-scalar trilinear insertion vertex has a contributing factor $[-ie(p_\mu + p'_\mu)](-1)^{t_\mu+1}$, where p_μ and p'_μ are the four momenta of the scalar entering and leaving the insertion vertex.

The scalar-scalar-photon-photon quadrilinear seagull insertion vertex has a contributing factor $[+2ie^2 g_{\mu\nu}](-1)^{t_\mu+1}$.

Note the difference in the overall relative sign of the trilinear and quadrilinear interaction vertex contributions.

Appendix B

Generalized Feynman's Identities at finite temperature

The propagator identities: From the propagators expressed in Eq. A.1, Eq. A.4, and Eq. A.6, we observe that,

$$(\not{p} - m_f) \, iF^{\,t_a,t_b}(p, m_f) \equiv (\not{p} - m_f) \, iF_p^{\,t_a,t_b} = i(-1)^{(t_a+1)}\delta_{t_a,t_b} \, ,$$

$$(p^2 - m_\phi^2) \, iS^{\,t_a,t_b}(p, m_\phi) \equiv (p^2 - m_\phi^2) \, iS_p^{\,t_a,t_b} = i(-1)^{(t_a+1)}\delta_{t_a,t_b} \, . \tag{B.1}$$

We have written down the momentum dependence of the propagators in the subscript, which is in accordance with all our previous discussions.

The generalized Feynman identities at finite temperature: We will start with the contribution of nth order process in a relevant theory. According to the GY prescription, after choosing uniquely the special hard vertex which separates out the initial and final leg, suppose the outermost incoming particle on initial leg has momentum p and the outermost outgoing particle on final leg has momentum p' associated with them. All the already existing virtual photon momenta on the $p \, (p')$ legs are considered to be all incoming(outgoing) with momenta $l_i(l_i')$. According to this notation, the momentum of propagator to the *left* of the

q^{th} vertex on the final p' leg becomes $(p' + \Sigma_{i=1}^{q} l'_i) \equiv (p' + \Sigma_q)$; and the momentum of propagator to the *right* of the jth vertex on the initial p leg reads $(p + \Sigma_{i=1}^{j} l_i) \equiv (p + \Sigma_j)$.

Generalized Feynman identities for fermions : For insertion of μ vertex of K photon having momentum k in between $q - 1$ and q vertices on final p'-leg, and of similar ν vertex insertion between $j - 1$ and j vertices on initial p-leg for a fermionic theory we have respectively the generalized Feynman identities

$$F^{t_{q-1},t_\mu}_{p'+\Sigma_{q-1}} \slashed{k} \, F^{t_\mu,t_q}_{p'+\Sigma_{q-1}+k} = \left(-1 \right)^{(t_\mu+1)} \left[\delta_{t_\mu,t_q} F^{t_{q-1},t_q}_{p'+\Sigma_{q-1}} - \delta_{t_\mu,t_{q-1}} F^{t_{q-1},t_q}_{p'+\Sigma_{q-1}+k} \right] .$$

$$F^{t_j,t_\nu}_{p+\Sigma_{j-1}+k} \slashed{k} \, F^{t_\nu,t_{j-1}}_{p+\Sigma_{j-1}} = \left(-1 \right)^{(t_\nu+1)} \left[\delta_{t_\nu,t_j} F^{t_j,t_{j-1}}_{p+\Sigma_{j-1}} - \delta_{t_\nu,t_{j-1}} F^{t_j,t_{j-1}}_{p+\Sigma_{j-1}+k} \right] . \tag{B.2}$$

We produce the explicit derivation of the first generalized Feynman identity as shown below after using Eq. B.1 for fermionic case,

$$F^{t_{q-1},t_\mu}_{p'+\Sigma_{q-1}} \slashed{k} F^{t_\mu,t_q}_{p'+\Sigma_{q-1}+k}$$

$$= F^{t_{q-1},t_\mu}_{p'+\Sigma_{q-1}} \left[\left(\slashed{p}' + \slashed{\Sigma}_{q-1} + \slashed{k} - m_f \right) - \left(\slashed{p}' + \slashed{\Sigma}_{q-1} - m_f \right) \right] F^{t_\mu,t_q}_{p'+\Sigma_{q-1}+k}$$

$$= F^{t_{q-1},t_\mu}_{p'+\Sigma_{q-1}} \left(\slashed{p}' + \slashed{\Sigma}_{q-1} + \slashed{k} - m_f \right) F^{t_\mu,t_q}_{p'+\Sigma_{q-1}+k} - F^{t_{q-1},t_\mu}_{p'+\Sigma_{q-1}} \left(\slashed{p}' + \slashed{\Sigma}_{q-1} - m_f \right) F^{t_\mu,t_q}_{p'+\Sigma_{q-1}+k}$$

$$= F^{t_{q-1},t_\mu}_{p'+\Sigma_{q-1}} \left(-1 \right)^{(t_\mu+1)} \delta_{t_\mu,t_q} - \left(-1 \right)^{(t_\mu+1)} \delta_{t_\mu,t_{q-1}} F^{t_\mu,t_q}_{p'+\Sigma_{q-1}+k}$$

$$= F^{t_{q-1},t_q}_{p'+\Sigma_{q-1}} \left(-1 \right)^{(t_\mu+1)} \delta_{t_\mu,t_q} - \left(-1 \right)^{(t_\mu+1)} \delta_{t_\mu,t_{q-1}} F^{t_{q-1},t_q}_{p'+\Sigma_{q-1}+k}$$

$$= \left(-1 \right)^{(t_\mu+1)} \left[\delta_{t_\mu,t_q} F^{t_{q-1},t_q}_{p'+\Sigma_{q-1}} - \delta_{t_\mu,t_{q-1}} F^{t_{q-1},t_q}_{p'+\Sigma_{q-1}+k} \right] . \tag{B.3}$$

The second identity of Eq. B.2 for insertion on initial p leg also can be evaluated similarly. Now, for the cases of μ insertion being to the right of the vertex number '1' on the final p'-leg, and ν insertion being to the left of the vertex number '1' on the initial p-leg for a theory of fermion, we have,

$$\bar{u}(p') \slashed{k} F^{t_\mu,t_1}_{p'+k} = (-1)^{(t_\mu+1)} \delta_{t_\mu,t_1} \bar{u}(p') ,$$

$$F^{t_1,t_\nu}_{p+k} \slashed{k} u(p) = (-1)^{(t_\nu+1)} \delta_{t_\nu,t_1} u(p) , \tag{B.4}$$

where in the above expression $\not{p}'u(p') = m_f\, u(p')$, and $\not{p}\, u(p) = m_f\, u(p)$ have been applied to obtain the result.

Generalized Feynman identities for scalars : For insertion of μ vertex of K photon having momenta k in between $q-1$ and q vertices on final p'-leg, and of similar ν vertex insertion between $j-1$ and j vertices on initial p-leg for a scalar theory we have respectively the generalized Feynman identities

$$S\,^{t_{q-1},t_\mu}_{p'+\Sigma_{q-1}}\left[\left(2p'+2\Sigma_{q-1}+k\right).k\right]S\,^{t_\mu,t_q}_{p'+\Sigma_{q-1}+k} = \left(-1\right)^{(t_\mu+1)}\left[\delta_{t_\mu,t_q}S\,^{t_{q-1},t_q}_{p'+\Sigma_{q-1}} - \delta_{t_\mu,t_{q-1}}S\,^{t_{q-1},t_q}_{p'+\Sigma_{q-1}+k}\right],$$

$$S\,^{t_j,t_\nu}_{p+\Sigma_{j-1}+k}\left[\left(2p+2\Sigma_{j-1}+k\right).k\right]S\,^{t_\nu,t_{j-1}}_{p+\Sigma_{j-1}} = \left(-1\right)^{(t_\nu+1)}\left[\delta_{t_\nu,t_j}\,S\,^{t_j,t_{j-1}}_{p+\Sigma_{j-1}} - \delta_{t_\nu,t_{j-1}}\,S\,^{t_j,t_{j-1}}_{p+\Sigma_{j-1}+k}\right].$$

$$\text{(B.5)}$$

We produce the explicit derivation of the first generalized Feynman identity as shown below after using Eq. B.1 for scalar case,

$$S\,^{t_{q-1},t_\mu}_{p'+\Sigma_{q-1}}\left[\left(2p'+2\Sigma_{q-1}+k\right).k\right]S\,^{t_\mu,t_q}_{p'+\Sigma_{q-1}+k}$$

$$= S\,^{t_{q-1},t_\mu}_{p'+\Sigma_{q-1}}\left[\left(p'+\Sigma_{q-1}\right)^2 + 2\left(p'+\Sigma_{q-1}\right).k + k^2 - m_\phi^2 - \left(p'+\Sigma_{q-1}\right)^2 + m_\phi^2\right]S\,^{t_\mu,t_q}_{p'+\Sigma_{q-1}+k}$$

$$= S\,^{t_{q-1},t_\mu}_{p'+\Sigma_{q-1}}\left[\left\{\left(p'+\Sigma_{q-1}\right)^2 - m_\phi^2\right\} - \left\{\left(p'+\Sigma_{q-1}\right)^2 - m_\phi^2\right\}\right]S\,^{t_\mu,t_q}_{p'+\Sigma_{q-1}+k}$$

$$= S\,^{t_{q-1},t_\mu}_{p'+\Sigma_{q-1}}\left\{\left(p'+\Sigma_{q-1}\right)^2 - m_\phi^2\right\}S\,^{t_\mu,t_q}_{p'+\Sigma_{q-1}+k} - S\,^{t_{q-1},t_\mu}_{p'+\Sigma_{q-1}}\left\{\left(p'+\Sigma_{q-1}\right)^2 - m_\phi^2\right\}S\,^{t_\mu,t_q}_{p'+\Sigma_{q-1}+k}$$

$$= S\,^{t_{q-1},t_\mu}_{p'+\Sigma_{q-1}}\left(-1\right)^{(t_\mu+1)}\delta_{t_\mu,t_q} - \left(-1\right)^{(t_\mu+1)}\delta_{t_\mu,t_{q-1}}S\,^{t_\mu,t_q}_{p'+\Sigma_{q-1}+k}$$

$$= S\,^{t_{q-1},t_q}_{p'+\Sigma_{q-1}}\left(-1\right)^{(t_\mu+1)}\delta_{t_\mu,t_q} - \left(-1\right)^{(t_\mu+1)}\delta_{t_\mu,t_{q-1}}S\,^{t_{q-1},t_q}_{p'+\Sigma_{q-1}+k}$$

$$= \left(-1\right)^{(t_\mu+1)}\left[\delta_{t_\mu,t_q}S\,^{t_{q-1},t_q}_{p'+\Sigma_{q-1}} - \delta_{t_\mu,t_{q-1}}S\,^{t_{q-1},t_q}_{p'+\Sigma_{q-1}+k}\right]. \qquad\text{(B.6)}$$

The second identity of Eq. B.5 for insertion on initial p leg also can be evaluated similarly. Now, for the cases of μ insertion being to the right of the vertex number '1' on the final p'-leg, and ν insertion being to the left of the vertex number '1' on the initial p-leg for a

theory of scalar, we have,

$$[(2p' + k) \cdot k] \, S^{t_\mu, t_1}_{p'+k} = (-1)^{(t_\mu+1)} \, \delta_{t_\mu, t_1} \, ,$$

$$S^{t_1, t_\nu}_{p+k} \, [(2p + k) \cdot k] = (-1)^{(t_\nu+1)} \, \delta_{t_\nu, t_1} \, , \qquad\qquad \text{(B.7)}$$

where to obtain the above equation $p'^2 = p^2 = m_\phi^2$ has been used.

REFERENCES

[1] T. Aoyama, M. Hayakawa, T. Kinoshita and M. Nio, "Tenth-Order QED Contribution to the Electron $g-2$ and an Improved Value of the Fine Structure Constant," Phys. Rev. Lett. **109** (2012), 111807.

[2] T. Aoyama, M. Hayakawa, T. Kinoshita and M. Nio, "Tenth-Order Electron Anomalous Magnetic Moment: Contribution of Diagrams without Closed Lepton Loops," Phys. Rev. D **91** (2015) no.3, 033006, [erratum: Phys. Rev. D **96** (2017) no.1, 019901].

[3] D. Hanneke, S. F. Hoogerheide and G. Gabrielse, "Cavity Control of a Single-Electron Quantum Cyclotron: Measuring the Electron Magnetic Moment," Phys. Rev. A **83** (2011), 052122.

[4] F. Bloch and A. Nordsieck, "Note on the Radiation Field of the electron," Phys. Rev. **52** (1937), 54-59.

[5] F. E. Low, "Scattering of light of very low frequency by systems of spin 1/2," Phys. Rev. **96** (1954), 1428-1432.

[6] M. Gell-Mann and M. L. Goldberger, "Scattering of low-energy photons by particles of spin 1/2," Phys. Rev. **96** (1954), 1433-1438.

[7] F. E. Low, "Bremsstrahlung of very low-energy quanta in elementary particle collisions," Phys. Rev. **110** (1958), 974-977.

[8] E. Kazes, "Generalized current conservation and low energy limit of photon interactions," Nuovo Cim. **13** (1959), 1226-1239.

[9] K. E. Eriksson, "On radiative corrections due to soft photons," Nuovo Cim. **19** (1961), 1010-1028.

[10] D. R. Yennie, S. C. Frautschi and H. Suura, "The infrared divergence phenomena and high-energy processes," Annals Phys. **13** (1961), 379-452.

[11] S. Weinberg, "The Quantum theory of fields. Vol. 1: Foundations," Cambridge: Cambridge University Press, 1995.

[12] G. Grammer, Jr. and D. R. Yennie, "Improved treatment for the infrared divergence problem in quantum electrodynamics," Phys. Rev. D **8** (1973), 4332-4344.

[13] T. Kinoshita, "Mass singularities of Feynman amplitudes," J. Math. Phys. **3** (1962), 650-677.

[14] T. D. Lee and M. Nauenberg, "Degenerate Systems and Mass Singularities," Phys. Rev. **133** (1964), B1549.

[15] S. Weinberg, "Infrared photons and gravitons," Phys. Rev. **140** (1965), B516-B524.

[16] V. Chung, "Infrared Divergence in Quantum Electrodynamics," Phys. Rev. **140** (1965), B1110-B1122.

[17] T. W. B. Kibble, "Coherent Soft-Photon States and Infrared Divergences. I. Classical Currents," J. Math. Phys. **9** (1968) no.2, 315-324.

[18] T. W. B. Kibble, "Coherent soft-photon states and infrared divergences. II. mass-shell singularities of green's functions," Phys. Rev. **173** (1968), 1527-1535.

[19] T. W. B. Kibble, "Coherent soft-photon states and infrared divergences. III. asymptotic states and reduction formulas," Phys. Rev. **174** (1968), 1882-1901.

[20] T. W. B. Kibble, "Coherent soft-photon states and infrared divergences. IV. the scattering operator," Phys. Rev. **175** (1968), 1624-1640.

[21] J. K. Storrow, "Photons in S-matrix theory," Nuovo Cimento A (1965-1970) **54** (1968), 15-41.

[22] J. K. Storrow, "Photons in S-matrix theory II - Systems with many charged particles," Nuovo Cimento A (1965-1970) **57** (1968), 763-776.

[23] D. Zwanziger, "Reduction formulas for charged particles and coherent states in quantum electrodynamics," Phys. Rev. D **7** (1973), 1082-1099.

[24] P. P. Kulish and L. D. Faddeev, "Asymptotic conditions and infrared divergences in quantum electrodynamics," Theor. Math. Phys. **4** (1970), 745.

[25] G. Giavarini and G. Marchesini, "IR Finite S Matrix in the QCD Coherent State Basis," Nucl. Phys. B **296** (1988), 546-556.

[26] V. Del Duca, L. Magnea and G. F. Sterman, "Collinear Infrared Factorization and Asymptotic Evolution," Nucl. Phys. B **324** (1989), 391-411.

[27] J. Ware, R. Saotome and R. Akhoury, "Construction of an asymptotic S matrix for perturbative quantum gravity," JHEP **10** (2013), 159.

[28] T. He, P. Mitra, A. P. Porfyriadis and A. Strominger, "New Symmetries of Massless QED," JHEP **10** (2014), 112.

[29] T. He, P. Mitra and A. Strominger, "2D Kac-Moody Symmetry of 4D Yang-Mills Theory," JHEP **10** (2016), 137.

[30] A. Strominger, "Asymptotic Symmetries of Yang-Mills Theory," JHEP **07** (2014), 151.

[31] D. Kapec, M. Pate and A. Strominger, "New Symmetries of QED," Adv. Theor. Math. Phys. **21** (2017), 1769-1785.

[32] M. Campiglia and A. Laddha, "Asymptotic symmetries of QED and Weinberg's soft photon theorem," JHEP **07** (2015), 115.

[33] L. Bieri and D. Garfinkle, "An electromagnetic analogue of gravitational wave memory," Class. Quant. Grav. **30** (2013), 195009.

[34] L. Susskind, "Electromagnetic Memory," [arXiv:1507.02584 [hep-th]].

[35] S. Pasterski, "Asymptotic Symmetries and Electromagnetic Memory," JHEP **09** (2017), 154.

[36] M. Pate, A. M. Raclariu and A. Strominger, "Color Memory: A Yang-Mills Analog of Gravitational Wave Memory," Phys. Rev. Lett. **119** (2017) no.26, 261602.

[37] C. W. Bauer, S. Fleming, D. Pirjol and I. W. Stewart, "An Effective field theory for collinear and soft gluons: Heavy to light decays," Phys. Rev. D **63** (2001), 114020.

[38] A. J. Larkoski, D. Neill and I. W. Stewart, "Soft Theorems from Effective Field Theory," JHEP **06** (2015), 077.

[39] M. Gyulassy and X. n. Wang, "Multiple collisions and induced gluon Bremsstrahlung in QCD," Nucl. Phys. B **420** (1994), 583-614.

[40] H. A. Weldon, "Suppression of Bremsstrahlung at nonzero temperature," Phys. Rev. D **49** (1994), 1579-1584.

[41] D. Indumathi, "Cancellation of infrared divergences at finite temperature," Annals Phys. **263** (1998), 310-339.

[42] P. Sen, D. Indumathi and D. Choudhury, "Infrared finiteness of a thermal theory of scalar electrodynamics to all orders," Eur. Phys. J. C **79** (2019) no.6, 532.

[43] P. Sen, D. Indumathi and D. Choudhury, "Infrared finiteness of a complete theory of charged scalars and fermions at finite temperature," Eur. Phys. J. C **80** (2020) no.10, 972.

[44] F. Zwicky, "Die Rotverschiebung von extragalaktischen Nebeln," Helv. Phys. Acta 6 (1933), 110-127.

[45] F. Zwicky, "On the Masses of Nebulae and of Clusters of Nebulae," Astrophys. J. 86 (1937), 217-246.

[46] H. W. Babcock, "The Rotation of the Andromeda Nebula," Lick Obs. Bull. 19 (1939) 1.

[47] V. C. Rubin and W. K. Ford, Jr., "Rotation of the Andromeda Nebula from a Spectroscopic Survey of Emission Regions," Astrophys. J. 159 (1970), 379-403.

[48] M. S. Roberts and R. N. Whitehurst, "The Rotation Curve and Geometry of M31 at LargeGalactocentric Distances," Astrophys. J. 201 (1975), 327-346.

[49] R. Massey, T. Kitching and J. Richard, "The dark matter of gravitational lensing," Rept. Prog. Phys. 73 (2010), 086901.

[50] B. Paczynski, "Gravitational microlensing by the galactic halo," Astrophys. J. 304 (1986), 1-5.

[51] P. Tisserand *et al.* [EROS-2], "Limits on the Macho Content of the Galactic Halo from the EROS-2 Survey of the Magellanic Clouds," Astron. Astrophys. 469 (2007), 387-404.

[52] D. Clowe, M. Bradac, A. H. Gonzalez, M. Markevitch, S. W. Randall, C. Jones and D. Zaritsky, "A direct empirical proof of the existence of dark matter," Astrophys. J. Lett. 648 (2006), L109-L113.

[53] S. W. Allen, A. E. Evrard and A. B. Mantz, "Cosmological Parameters from Observations of Galaxy Clusters," Ann. Rev. Astron. Astrophys. 49 (2011), 409-470.

[54] J. D. Simon, "The Faintest Dwarf Galaxies," Ann. Rev. Astron. Astrophys. 57 (2019) no.1, 375-415.

[55] P. Salucci, "The distribution of dark matter in galaxies," Astron. Astrophys. Rev. **27** (2019) no.1, 2.

[56] E. Komatsu *et al.* [WMAP], "Seven-Year Wilkinson Microwave Anisotropy Probe (WMAP) Observations: Cosmological Interpretation," Astrophys. J. Suppl. **192** (2011), 18.

[57] P. A. R. Ade *et al.* [Planck], "Planck 2015 results. XIII. Cosmological parameters," Astron. Astrophys. **594** (2016), A13.

[58] N. Aghanim *et al.* [Planck], "Planck 2018 results. VI. Cosmological parameters," Astron. Astrophys. **641** (2020), A6.

[59] E. W. Kolb and M. S. Turner, "The Early Universe," Front. Phys. **69** (1990), 1-547.

[60] M. Milgrom, "A Modification of the Newtonian dynamics as a possible alternative to the hidden mass hypothesis," Astrophys. J. **270** (1983), 365-370.

[61] S. Bharadwaj and S. Kar, "Modeling galaxy halos using dark matter with pressure," Phys. Rev. D **68** (2003), 023516.

[62] G. Jungman, M. Kamionkowski and K. Griest, "Supersymmetric dark matter," Phys. Rept. **267** (1996), 195-373.

[63] G. Bertone, D. Hooper and J. Silk, "Particle dark matter: Evidence, candidates and constraints," Phys. Rept. **405** (2005), 279-390.

[64] J. L. Feng, "Dark Matter Candidates from Particle Physics and Methods of Detection," Ann. Rev. Astron. Astrophys. **48** (2010), 495-545.

[65] V. A. Bednyakov, "Is it possible to discover a dark matter particle with an accelerator ?," Phys. Part. Nucl. **47** (2016) no.5, 711-774.

[66] G. Arcadi, M. Dutra, P. Ghosh, M. Lindner, Y. Mambrini, M. Pierre, S. Profumo and F. S. Queiroz, "The waning of the WIMP ? A review of models, searches, and constraints," Eur. Phys. J. C **78** (2018) no.3, 203.

[67] H. Baer, K. Y. Choi, J. E. Kim and L. Roszkowski, "Dark matter production in the early Universe: beyond the thermal WIMP paradigm," Phys. Rept. **555** (2015), 1-60.

[68] S. Tremaine and J. E. Gunn, "Dynamical Role of Light Neutral Leptons in Cosmology," Phys. Rev. Lett. **42** (1979), 407-410.

[69] L. Randall, J. Scholtz and J. Unwin, "Cores in Dwarf Galaxies from Fermi Repulsion," Mon. Not. Roy. Astron. Soc. **467** (2017) no.2, 1515-1525.

[70] E. Armengaud, N. Palanque-Delabrouille, C. Yèche, D. J. E. Marsh and J. Baur, "Constraining the mass of light bosonic dark matter using SDSS Lyman-α forest," Mon. Not. Roy. Astron. Soc. **471** (2017) no.4, 4606-4614.

[71] M. Nori, R. Murgia, V. Iršič, M. Baldi and M. Viel, "Lyman α forest and non-linear structure characterization in Fuzzy Dark Matter cosmologies," Mon. Not. Roy. Astron. Soc. **482** (2019) no.3, 3227-3243.

[72] B. Bozek, D. J. E. Marsh, J. Silk and R. F. G. Wyse, "Galaxy UV-luminosity function and reionization constraints on axion dark matter," Mon. Not. Roy. Astron. Soc. **450** (2015) no.1, 209-222.

[73] H. Y. Schive, T. Chiueh, T. Broadhurst and K. W. Huang, "Contrasting Galaxy Formation from Quantum Wave Dark Matter, ψDM, with ΛCDM, using Planck and Hubble Data," Astrophys. J. **818** (2016) no.1, 89.

[74] E. O. Nadler, V. Gluscevic, K. K. Boddy and R. H. Wechsler, "Constraints on Dark Matter Microphysics from the Milky Way Satellite Population," Astrophys. J. Lett. **878** (2019) no.2, 32, [erratum: Astrophys. J. Lett. **897** (2020) no.2, L46].

[75] M. A. Monroy-Rodríguez and C. Allen, "The end of the MACHO era- revisited: new limits on MACHO masses from halo wide binaries," Astrophys. J. **790** (2014) no.2, 159.

[76] T. D. Brandt, "Constraints on MACHO Dark Matter from Compact Stellar Systems in Ultra-Faint Dwarf Galaxies," Astrophys. J. Lett. **824** (2016) no.2, L31.

[77] B. Audren, J. Lesgourgues, G. Mangano, P. D. Serpico and T. Tram, "Strongest model-independent bound on the lifetime of Dark Matter," JCAP **12** (2014), 028.

[78] N. Baro, F. Boudjema and A. Semenov, "Full one-loop corrections to the relic density in the MSSM: A Few examples," Phys. Lett. B **660** (2008), 550-560.

[79] N. Baro, F. Boudjema, G. Chalons and S. Hao, "Relic density at one-loop with gauge boson pair production," Phys. Rev. D **81** (2010), 015005.

[80] A. Chatterjee, M. Drees and S. Kulkarni, "Radiative Corrections to the Neutralino Dark Matter Relic Density - an Effective Coupling Approach," Phys. Rev. D **86** (2012), 105025.

[81] P. Ciafaloni, D. Comelli, A. De Simone, E. Morgante, A. Riotto and A. Urbano, "The Role of Electroweak Corrections for the Dark Matter Relic Abundance," JCAP **10** (2013), 031.

[82] J. Harz, B. Herrmann, M. Klasen, K. Kovarik and Q. L. Boulc'h, "Neutralino-stop coannihilation into electroweak gauge and Higgs bosons at one loop," Phys. Rev. D **87** (2013) no.5, 054031.

[83] B. Herrmann, M. Klasen and K. Kovarik, "Neutralino Annihilation into Massive Quarks with SUSY-QCD Corrections," Phys. Rev. D **79** (2009), 061701.

[84] B. Herrmann, M. Klasen and K. Kovarik, "SUSY-QCD effects on neutralino dark matter annihilation beyond scalar or gaugino mass unification," Phys. Rev. D **80** (2009), 085025.

[85] B. Herrmann, M. Klasen, K. Kovarik, M. Meinecke and P. Steppeler, "One-loop corrections to gaugino (co)annihilation into quarks in the MSSM," Phys. Rev. D **89** (2014) no.11, 114012.

[86] M. Beneke, F. Dighera and A. Hryczuk, "Relic density computations at NLO: infrared finiteness and thermal correction," JHEP **10** (2014), 045, [erratum: JHEP **07** (2016), 106].

[87] M. Beneke, F. Dighera and A. Hryczuk, "Finite-temperature modification of heavy particle decay and dark matter annihilation," JHEP **09** (2016), 031.

[88] S. P. Martin, "A Supersymmetry primer," Adv. Ser. Direct. High Energy Phys. **18** (1998), 1-98.

[89] M. Drees, "An Introduction to supersymmetry," [arXiv:hep-ph/9611409 [hep-ph]].

[90] M. Drees, R. Godbole and P. Roy, "Theory and phenomenology of sparticles: An account of four-dimensional N=1 supersymmetry in high energy physics," World Scientific, Singapore (2005).

[91] I. J. R. Aitchison, "Supersymmetry and the MSSM: An Elementary introduction," [arXiv:hep-ph/0505105 [hep-ph]].

[92] H. Baer and X. Tata, "Weak scale supersymmetry: From superfields to scattering events," Cambridge University Press, 2006.

[93] J. R. Ellis, J. S. Hagelin, D. V. Nanopoulos, K. A. Olive and M. Srednicki, "Supersymmetric Relics from the Big Bang," Nucl. Phys. B **238** (1984), 453-476.

[94] K. Griest, "Cross-Sections, Relic Abundance and Detection Rates for Neutralino Dark Matter," Phys. Rev. D **38** (1988), 2357, [erratum: Phys. Rev. D **39** (1989), 3802].

[95] J. R. Ellis and R. A. Flores, "Prospects for neutralino detection with a Ge-73 + Ge-76 detector," Phys. Lett. B **300** (1993), 175-182.

[96] A. Bottino, V. de Alfaro, N. Fornengo, G. Mignola and M. Pignone, "On the neutralino as dark matter candidate. 1. Relic abundance.," Astropart. Phys. **2** (1994), 67-76.

[97] T. Falk, K. A. Olive and M. Srednicki, "Heavy sneutrinos as dark matter," Phys. Lett. B **339** (1994), 248-251.

[98] V. A. Bednyakov, H. V. Klapdor-Kleingrothaus and S. G. Kovalenko, "Possible constraints on SUSY model parameters from direct dark matter search," Phys. Lett. B **329** (1994), 5-9.

[99] V. A. Bednyakov, H. V. Klapdor-Kleingrothaus and S. G. Kovalenko, "Superlight neutralino as a dark matter particle candidate," Phys. Rev. D **55** (1997), 503-514.

[100] Q. H. Cao, E. Ma and G. Shaughnessy, "Dark Matter: The Leptonic Connection," Phys. Lett. B **673** (2009), 152-155.

[101] N. F. Bell, J. B. Dent, T. D. Jacques and T. J. Weiler, "W/Z Bremsstrahlung as the Dominant Annihilation Channel for Dark Matter," Phys. Rev. D **83** (2011), 013001.

[102] N. F. Bell, J. B. Dent, T. D. Jacques and T. J. Weiler, "Dark Matter Annihilation Signatures from Electroweak Bremsstrahlung," Phys. Rev. D **84** (2011), 103517.

[103] P. Ciafaloni, M. Cirelli, D. Comelli, A. De Simone, A. Riotto and A. Urbano, "On the Importance of Electroweak Corrections for Majorana Dark Matter Indirect Detection," JCAP **06** (2011), 018.

[104] T. Matsubara, "A New approach to quantum statistical mechanics," Prog. Theor. Phys. **14** (1955), 351-378.

[105] K. c. Chou, Z. b. Su, B. l. Hao and L. Yu, "Equilibrium and Nonequilibrium Formalisms Made Unified," Phys. Rept. **118** (1985), 1-131.

[106] J. I. Kapusta and C. Gale, "Finite-temperature field theory: Principles and applications," Cambridge University Press, (2006).

[107] M. L. Bellac, "Thermal Field Theory," Cambridge University Press, Cambridge, (1996).

[108] A. K. Das, "Finite Temperature Field Theory,", World scientific, Singapore (1997).

[109] A. K. Das, "Topics in finite temperature field theory," Quantum field theory: A 20th century profile, 383-411, [arXiv:hep-ph/0004125 [hep-ph]].

[110] N. P. Landsman and C. G. van Weert, "Real and Imaginary Time Field Theory at Finite Temperature and Density," Phys. Rept. **145** (1987), 141.

[111] J. S. Schwinger, "Brownian motion of a quantum oscillator," J. Math. Phys. **2** (1961), 407-432.

[112] L. V. Keldysh, "Diagram technique for nonequilibrium processes," Zh. Eksp. Teor. Fiz. **47** (1964), 1515-1527, Sov. Phys. JETP **20** (1965) 1018.

[113] A. J. Niemi and G. W. Semenoff, "Thermodynamic Calculations in Relativistic Finite Temperature Quantum Field Theories," Nucl. Phys. B **230** (1984), 181-221.

[114] R. L. Kobes and G. W. Semenoff, "Discontinuities of Green Functions in Field Theory at Finite Temperature and Density," Nucl. Phys. B **260** (1985), 714-746.

[115] R. J. Rivers, "Path Integral Methods in Quantum Field Theory," Chapter 15 ,Cambridge University Press, Cambridge, (1987).

[116] A. J. Niemi and G. W. Semenoff, "Finite Temperature Quantum Field Theory in Minkowski Space," Annals Phys. **152** (1984), 105.

[117] I. Ojima, "Gauge Fields at Finite Temperatures: Thermo Field Dynamics, KMS Condition and their Extension to Gauge Theories," Annals Phys. **137** (1981), 1.

[118] H. Matsumoto, Y. Nakano, H. Umezawa, F. Mancini and M. Marinaro, "Thermo Field Dynamics in Interaction Representation," Prog. Theor. Phys. **70** (1983), 599-602.

[119] H. Umezawa, H. Matsumoto and M. Tachiki, "Thermo Field Dynamics and Condensed States," North-Holland Publishing Company, Amsterdam (Netherlands), (1982), ISBN 0444863613.

[120] Y. Takahashi and H. Umezawa, "Thermo field dynamics," Int. J. Mod. Phys. B **10** (1996), 1755-1805.

[121] H. Umezawa, "Advanced field theory: Micro, macro, and thermal physics," AIP press, New York (1995).

[122] R. Kubo, "Statistical mechanical theory of irreversible processes. 1. General theory and simple applications in magnetic and conduction problems," J. Phys. Soc. Jap. **12** (1957), 570-586.

[123] P. C. Martin and J. S. Schwinger, "Theory of many particle systems. 1.," Phys. Rev. **115** (1959), 1342-1373.

[124] A. Denner, H. Eck, O. Hahn and J. Küblbeck, "Compact Feynman rules for Majorana fermions," Phys. Lett. B **291** (1992), 278-280.

[125] A. Denner, H. Eck, O. Hahn and J. Kublbeck, "Feynman rules for fermion number violating interactions," Nucl. Phys. B **387** (1992), 467-481.

[126] S. Gupta, D. Indumathi, P. Mathews and V. Ravindran, "Bloch-Nordsieck thermometers: One loop exponentiation in finite temperature QED," Nucl. Phys. B **458** (1996), 189-214.

[127] J. F. Donoghue, B. R. Holstein and R. W. Robinett, "Quantum electrodynamics at finite temperature," Annals Phys. **164** (1985), 233, [erratum: Annals Phys. **172** (1986), 483].

[128] R. P. Feynman, "Space - time approach to quantum electrodynamics," Phys. Rev. **76** (1949), 769-789.

[129] J. D. Bjorken and S. D. Drell, "Relativistic quantum fields," McGraw-Hill, New York, (1965).

[130] M. E. Peskin and D. V. Schroeder, "An Introduction to quantum field theory," Reading, MA: Addison-Wesley, (1995).

[131] G. F. Sterman, "An Introduction to quantum field theory," Cambridge: Cambridge University Press, (1993).

[132] E. Bagan, M. Lavelle and D. McMullan, "Soft dynamics and gauge theories," Phys. Rev. D **57** (1998), 4521-4524.

[133] R. Horan, M. Lavelle and D. McMullan, "Asymptotic dynamics in quantum field theory: When does the coupling switch off?," [arXiv:hep-th/0002206 [hep-th]].

[134] L. Matsson, "Generalized recoil theorem for soft quantum emission including photon-pair correlations to infinite order in the coupling constant," Phys. Rev. D **9** (1974), 2894-2904.

[135] L. Matsson, "Correlation expansion in scalar electrodynamics," Phys. Rev. D **10** (1974), 2027.

[136] L. Matsson, "Infrared Divergence Enforces a Rearranged Perturbation Expansion. 1. Scalar Electrodynamics," Nuovo Cim. A **39** (1977), 604.

[137] H. Lehmann, K. Symanzik and W. Zimmermann, "On the formulation of quantized field theories," Nuovo Cim. **1** (1955), 205-225.